Late Cretaceous paleoenvironmental evolution and sea-level history of the Tarfaya Basin, SW Morocco: Evidence from XRF scanner-derived elemental records, benthic and planktonic foraminifera and bulk carbonate stable isotopes

Dissertation

Zu Erlangung des Doktorgrades

Der Mathematisch-Naturwissenschaftlichen Fakultät

Der Christian-Albrechts-Universität zu Kiel

Vorgelegt von

Mohamed Aquit

Kiel, 2014

Referent: Prof. Dr. Wolfgang Kuhnt
Koreferent: Prof. Dr. Karl Stattegger
Tag der mündlichen Prüfung: 15.07.2014
Zum Druck genehmigt: 25.03.2015
Der Dekan: Prof. Dr. Wolfgang J. Duschl

Declaration

I affirm in lieu of oath that up to this date I have not finally failed any dissertation procedures neither at Christian-Albrechts-Universität zu Kiel nor at any other institution of higher education and that I am not currently in any such procedures. I further declare that the thesis was prepared following the Rules of Good Scientific Practice of the German Research Foundation (Information sheet on the publication of dissertations of the Faculty of Mathematics and Natural Sciences, no. 4d).

Kiel, June 2014

Aquit Mohamed

Contents

List of Figures

Figure 3: Comparison of Tarfaya Basin depositional sequences to the eustatic record from the New Jersey margin (Miller et al., 2003, 2004; Mizintseva et al., 2009). Foraminiferal zonation follows Robaszynski and Caron (1995), except for the base of the *G. concavata* Zone due to the later occurrence of *G. concavata* in the Tarfaya Basin. Nannoplankton zonation UC from Burnett et al. (1998); CC zonation is compiled from Bergen, 1994 and Bralower et al., 1995 in the GT012 timescale. Red dashed lines correspond to the unconformities (U1-3) in cores Tarfaya SN°1 and 2 observed in lithology, gray dashed lines correspond to unconformities based on log((Al+Ti+Fe+K+Si)/Ca). Sant.: Santonian; L. Tu.: late Turonian; N. Z.: nannoplankton Zone; F. Z. foraminiferal Zone.

Figure 4: Cross-plots of carbon- and oxygen isotope values of newly drilled cores (Tarfaya SN°1 and 2).

Figure 5: Correlation of bulk carbon isotope ($\delta^{13}C$) from the composite section (cores Tarfaya SN°1 and 2) to the $\delta^{13}C$ records of the Niobrara Formation, US Western Interior Seaway (Locklair et al., 2011) and stacked curves from Wendler (2013). Blue line corresponds to 5pt smoothed curve. Blue arrows indicate positive shifts in $\delta^{13}C$ in the middle Coniacian and at the Santonian-Campanian boundary. N. Z.: nannoplankton Zone; F. Z. foraminiferal Zone; Sant.: Santonian.

Figure 6: Composite geochemical and biostratigraphic records of cores Tarfaya SN°1 and 2. **a**) Elemental log of (Al+Ti+Fe+K+Si)/Ca, gray arrows indicate increasing terrigenous flux, blue arrows indicate increases in carbonate flux in the Tarfaya Basin; **b**) Elemental log of Zr/Rb, blue arrows indicate decreases in grain size, black arrow indicates increase in grain size; **c**) Elemental log of V/Ca, blue arrows indicate increases in carbonate flux; **d**) Elemental log of Br/Ca, blue arrow indicates increases in carbonate flux; **e**) Elemental log of Mn/S, red arrow indicates increasing oxygenation at the sea-floor in the Tarfaya Basin. Red dashed lines correspond to the major unconformities (U1-3) in cores Tarfaya SN°1 and 2, black dashed lines correspond to unconformities based on log((Al+Ti+Fe+K+Si)/Ca). Late Cretaceous (UC) nannoplankton Zones from Burnett et al. (1998). N. Z.: nannoplankton Zone; F. Z. foraminiferal Zone; Sant.: Santonian; L. Tu.: late Turonian.

Figure 7: Composite geochemical, line-scan and biostratigraphic records at the Santonian/Campanian boundary in the Tarfaya Basin. **a**) Green arrow indicates an increase in light reflectance (L*); **b**) Bulk carbon isotope data ($\delta^{13}C$); **c**) Bulk oxygen isotope data ($\delta^{18}O$); **d-e**) Elemental log of Al/Ca and Ti/Ca, black arrows indicate increasing terrigenous flux; **f)** Elemental log of K/Al indicates variation of illite and kaolinite in sediments during the Santonian/Campanian boundary; **g)** Elemental log of Zr/Rb indicates distance of the clastic source and grain size variation in the sediments.

Figure 8: Age-depth plot of main carbon isotope events in the Tarfaya SN°1-2 composite section, following the chronology of Wendler (2013).

Chapter IV. XRF core scanning techniques and its application in the Tarfaya Basin

Figure 1: a) Schematic overview of excitation geometry of the X-ray fluorescence analysis of the elements Si, Ca, and Fe by the XRF core scanner after Richter et al., 2006. Elements in the sediment are ionized by the primary X-rays and emit an element-specific fluorescence radiation, which is registered by the detector. **b)** Schematic overview of excitation of atoms by the X-ray fluorescence analysis.

Figure 2: XRF core scanner spectra of 10, 30 and 50 kV run and the element intensities as area in yellow at position 10 cm in section 15 (segment 1) at Tarfaya SN°1.

Figure 3: XRF core scanner spectra of 10, 30 and 50 kV run and the element intensities as area in yellow at position 10 cm in section 25 (segment 1) at Tarfaya SN°2.

Figure 4: Cross-plots of elements in the Tarfaya SN°2 core with linear trend lines. a) Cross-plot of $CaCO_3$ content (%) vs Ca counts (XRF); b) Cross-plot of Corg (%) vs log((Mn+220)/S) (XRF); c) Cross-plot of Corg (%) vs log(V/Ca) (XRF); d) Cross-plot of TS (%) vs log((Mn+220)/S) (XRF); e) Cross-plot of Corg (%) vs $\delta^{13}C$ (‰ vs. VPDB). $CaCO_3$ content (%), Total Sulfur (%) and Total Organic Carbon (%) are used as reference from Sachse et al. (2012).

Figure 5: Composite geochemical and paleontological records in newly drilled core Tarfaya SN°1. Log-ratios of elements (Al, Ti, Mn, S, Br, Ba and P against Ca) were derived from X-ray fluorescence scanning. Black arrows indicate decrease in terrigenous flux in the Tarfaya Basin and light blue arrows indicate vice-versa. Dark blue arrows indicate increse in oxygenation in the Tarfaya Basin.

Figure 6: Composite geochemical and paleontological records in newly drilled core Tarfaya SN°1. Log-ratios of elements (Ti, Mn, S, Br, Ba and P against Fe) were derived from X-ray fluorescence scanning.
Figure 7: Composite geochemical and paleontological records in newly drilled core Tarfaya SN°2. Log-ratios of elements (Al, Ti, Mn, S, Br, Ba and P against Ca) were derived from X-ray fluorescence scanning. Black arrows indicate decrease in terrigenous flux in the Tarfaya Basin and light blue arrows indicate vice-versa. Dark blue arrows indicate increase in oxygenation in the Tarfaya Basin.
Figure 8: Composite geochemical and paleontological records in newly drilled core Tarfaya SN°2. Log-ratios of elements (Ti, Mn, S, Br, Ba and P against Fe) were derived from X-ray fluorescence scanning.
Figure 9. Composite geochemical and paleontological records in newly drilled cores Tarfaya SN°1 and 2 (composite core). $CaCO_3$ content (%), Total Sulfur (%) and Total Organic Carbon (%) were interpolated from Sachse et al. (2012) records.
Figure 10: Core photograph and log(Al/Ca) and Ca (counts) of idealized sequence in the Tarfaya cores. LS-lowstand sediments, TST-transgressive systems tract, HST-highstand systems tract, RST-regressive systems tract, SB-sequence boundary (transgressive surface of erosion), although sequence boundaries are still marked by erosional unconformities.
Figure 11: Core photograph and l*, a* and b* from line Scan of idealized sequence in the Tarfaya cores.

Chapter V. Organic geochemical characterization of Santonian to early Campanian organic matter-rich marls (Sondage No 1 cores) as related to OAE3 from the Tarfaya Basin, Morocco
Figure 1: Overview of the geology of Tarfaya Basin and adjacent areas including well Tarfaya Sondage No. 1 and previous investigated well Sondage No. 2 (Sachse et al., 2012).
Figure 2: Elemental analysis data of Corg, CaCO3, TS and TS/Corg plotted versus depth for (a) the whole Sondage No. 1; (b) 1st interval (92-97 m) with focus on early Campanian samples and (c) 2_{nd} interval (155-170 m) showing the transition between early Campanian and Santonian samples.
Figure 3: TS and Corg values for the early Campanian and Santonian samples.
Figure 4: Rock-Eval pyrolysis data for the well samples: (a) HI vs. Tmax, (b) S2 vs. C_{org}, and (c) S1 vs. C_{org}.
Figure 5: Maturity parameters plotted versus depth: (a) VRr; (b) Tmax and (c) PI (S1/S1+S2) for the well samples.
Figure 6: Microscopic observations in incident light fluorescence mode (a-d) and in reflected white light (e, f). Photograph a, c, d and e show a Santonian sample, b and f present the amorphous OM, pyrite and foraminifera in an early Campanian sample.
Figure 7: Chromatogram showing distribution of n- and iso- alkanes.
Figure 8: Pr/nC17 vs. Ph/nC18 for well samples indicating oxygen depleted but anoxic environment during deposition (after Shanmugam, 1985).
Figure 9: Characteristic ion spectra for steranes.
Figure 10: Relative composition of C27, C28 and C29 steranes in early Campanian and Santonian samples.
Figure 11: Original sediment compositions of early Campanian and Santonian samples. The lower part of the Santonian drilled in well Sondage No.2 has clearly higher organic matter content than the younger units drilled in well Sondage No.1.
Figure 12: Anoxic parameters: (a) TS/Corg ratio vs. HI (mg/g C_{org}) and (b) TS (%) vs. S2 (mg/g rock).
Figure 13: Stratigraphic ages plotted vs (a) Corg content for all samples of Sondage No. 1 and Sondage No. 2 and (b) temperature evolution against stratigraphic age based on Haq et al., 1987 and c) the eustatic sea level curve (Haq et al., 1987).
Figure 14: Temperature depending oxygen solubility for different pressure ranges in sea water, based on Geng and Duan, 2010.

List of Tables

Acknowledgements

First of all I am deeply grateful to my advisor Prof. Dr. Wolfgang Kuhnt for having offered me this position and for having guided, advised and supported me during my entire PhD program. For the same reasons, I would like to thank Dr. Ann Holbourn who has been available at any moment of those years for giving me particularly precious work direction, improving the quality of my writing, as well as for encouraging me or sometimes persuading me to relax a bit. I am grateful to Prof. Dr. El Hassane Chellai for his supervision, support and guidance throughout my studies. Further, I would like to thank Prof. Dr. Karl Stattegger for his support and guidance during fieldwork in March-April, 2009. Apart from that, my supervisors are very friendly and enthusiastic that I felt easily to be used with the European life. I would like to thank RWE Dea and SFB 754 (TP A7) for funding this project. In particular, Dr. Oliver Kluth, Dr. Torge Schumann from RWE Dea and Dr. Haddou Jabour from ONHYM are acknowledged for cross-reading various parts of the manuscript. I would also like to thank ONHYM for their logistic support and accompanying the field campaign in March-April, 2009 and drilling in September-December, 2009. I would like to thanks Dr. Nils Anderson for his contribution during geochemical data analysis. Furthermore I would like to thank all the people who helped me in my work: Dr. Marcus Regenberg, Dr. Dieter Garbe-Schönberg, Brigitte Salomon. I would like to thank my friends at the University of Kiel. Those I have come to know best are Sven Balmer, Nicholas Fraser, Marfasran Hendrizan, Elena Lo Giudice Cappelli, Karlos Guilherme Diemer Kochhann, Jan Frederik Schröder, Janne Lorensen, Sebastian Beil, Dr. Anke Dürkop, Dr. Rina Zuraida Dr. Jian Xu, and of course all members of the HIWI team. I thank them for their assistance in the lab, their answer to my frequent calls for help with the English language and their understanding and thoughtfulness during difficult times.

My name is on this manuscript, but it would have never been possible to do it without all those persons. I am particularly grateful to my friends Dr. Nabil Khelifi and Dr. Sajid Ali who have been supporting me since the first moment and improving the quality of my writing. I will always keep in mind the fruitful and pleasant atmosphere at the institute. Last but not least I thank my dear parents for their love, support, encouragement and standing by me during my Ph.D. studies.

Abstract

Lithological evidence, benthic foraminiferal census counts, and high-resolution X-ray fluorescence (XRF) scanner-derived elemental data were integrated with planktonic foraminiferal biostratigraphy and bulk carbonate stable isotopes to retrace the Turonian to early Campanian paleoenvironmental evolution and sea-level history of the Tarfaya Atlantic coastal basin (SW Morocco).

The lower Turonian is characterized by impoverished benthic foraminiferal assemblages, which reflect an impingement of the oxygen minimum zone on the shelf during a sea-level highstand. The appearance of low-oxygen tolerant benthic foraminiferal assemblages in the middle to upper Turonian indicates an improvement in bottom water oxygenation, probably linked to offshore retraction of the oxygen minimum zone during a regressive phase. From the late Turonian to Santonian, the presence of benthic foraminiferal with low diversity suggests relatively impoverished oxygenation in bottom water along the shelf. Three long-term oscillations in the abundance of terrigenous elements (increase of Al, Ti, K, Si and Fe normalized against Ca) are shown during the Coniacian and Santonian. This interval, which roughly corresponds to the Coniacian-Santonian Anoxic Event (OAE-3), is characterized by overall oxygen depleted to anoxic conditions at the sea-floor (indicated by the high organic carbon content, the presence of laminations and by low manganese/sulphur, high vanadium/calcium and bromine/calcium ratios in XRF scanning records). The lower Campanian transgression, only recorded in the southern part of the Tarfaya Basin, coincided with substantial deepening, enhanced accumulation of fine-grained clay-rich hemipelagic sediments and improved oxygenation at the sea-floor (highest diversity and abundance of benthic foraminiferal assemblages and low values of log(Mn/S)).

The sea-level changes reconstructed in the Tarfaya Basin are correlated to the global eustatic changes. Two major unconformities (U1/U2 and U3), which punctuate the upper Turonian to lower Campanian succession in Tarfaya SN°1 and 2, are correlative to the base of the Merchantville III and Magothy III sequence boundaries of Miller et al., (2004) and Mizintseva et al. (2009), respectively.

Stable isotope data of bulk carbonates (outcrop sections and composite cores) are correlated to the English Chalk, the Niobrara Formation (US Western Interior Seaway) and to the stacked carbon isotope reference curve of Wendler (2013). The Tarfaya carbon isotope curve reveals in particular the Navigation Event in the Coniacian, the Haven Brow, the Horseshoe Bay and the Buckle Events in the Santonian as well as the Santonian/Campanian Boundary Event.

Zusammenfassung

Lithologische Charakteristika, die Analyse benthischer Foraminiferenvergesellschaftungen und Variationen chemischer Elemente gemessen mit einem hochauflösenden Röntgenfluoreszenz (XRF) Scanner wurden mit der Biostratigraphie planktonischer Foraminiferen und stabilen Isotopendaten der Karbonatgesteine kombiniert, um eine Paläoumwelt-Rekonstruktion durchzuführen und Meeresspiegelschwankungen im atlantischen Tarfaya-Becken (SW-Marokko) für den Zeitraum Turon bis oberes Campan zu untersuchen.

Das untere Turon ist charakterisiert durch eine verarmte Vergesellschaftung benthischer Foraminiferen, welche zurückzuführen ist auf das Übergreifen der Sauerstoffminimumzone auf den Schelf während eines Meeresspiegelhochstandes. Das Auftreten von Foraminiferen mit Toleranz gegenüber niedrigen Sauerstoffgehalten im mittleren und oberen Turon weist auf eine bessere Durchlüftung der Bodenwässer hin, was wahrscheinlich auf das Zurückweichen der Sauerstoffminimumzone infolge einer regressiven Phase zurückzuführen ist. Vom oberen Turon bis zum Santon zeigt die Vergesellschaftung benthischer Foraminiferen eine geringe Diversität, was auf eine Verschlechterung der Sauerstoffsättigung der Bodenwässer des Schelfes hindeutet. Während des Coniacs und Santons wurden drei langfristige Oszillationen in den Konzentrationen terrigener Elemente (Al, Ti, K, Si und Fe normalisiert gegen Ca) identifiziert. Dieser Intervall, welcher mit dem Anoxischen Event 3 (OAE3) korrespondiert, ist gekennzeichnet durch sauerstoffarme bis anoxische Bedingungen am Meeresboden (hoher Gehalt an organischem Kohlenstoff, Laminationen und niedrige Mangan/Schwefel-, hohe Vanadium/Kalzium- und hohe Brom/Kalzium-Verhältnisse gemessen durch XRF-Scans. Die Transgression des unteren Campans, welche nur das südliche Tarfaya-Becken erfasste, wurde begleitet von einer signifikanten Tiefenzunahme, einer verstärkten Ablagerung von feinkörnigen, tonreichen, hemipelagischen Sedimenten und einer verbesserten Durchlüftung der Bodenwässer (die Vergesellschaftung benthischer Foraminiferen weist die höchste Diversität und Individuenzahl simultan zu erniedrigten log(Mn/S)-Verhältnissen auf).

Die Meeresspiegelschwankungen des Tarfaya-Beckens korrelieren mit globalen, eustatischen Meeresspiegeländerungen. Zwei ausgeprägte Diskordanzen (U1/U2 und U3) in den Sedimentabfolgen des oberen Turons bis unteren Campans der Bohrkerne Tarfaya SN°1 und 2 korrelieren mit den Sequenzgrenzen Merchantville III und Magothy III von Miller et al., (2004) und Mizintseva et al., (2009). Die Ergebnisse der Messung Stabiler Isotopen der Karbonatgesteine der

Aufschluss-Sektionen und der korrelierten Bohrkerne (SN°1 und 2) wurden mit der Englischen Kreide, der Niobrara Formation (US Western Interior Seaway) und der kompilierten Kohlenstoff-Isotopenkurve von Wendler (2013) korreliert. Eindeutig identifizierbar waren im Tarfaya Becken das Navigation-Event im Coniac, das Horseshoe Bay und Buckle-Event im Santon und das Santon/Campan-Event.

Chapter I. Introduction

1. Location and geological overview of the study area

The Tarfaya Basin extends along the southern coast of Morocco between 28° N and 24° N. It stretches over more than 1000 km along the western margin of the Sahara (Hafid et al., 2008). The basin is limited by the Anti-Atlas Mountains in the north, the Reguibat Basin in the east, the Mauritanides in the south and the Atlantic Ocean in the west. Figure 1 provides the locations of the outcrop sections and cores studied in the Tarfaya Basin.

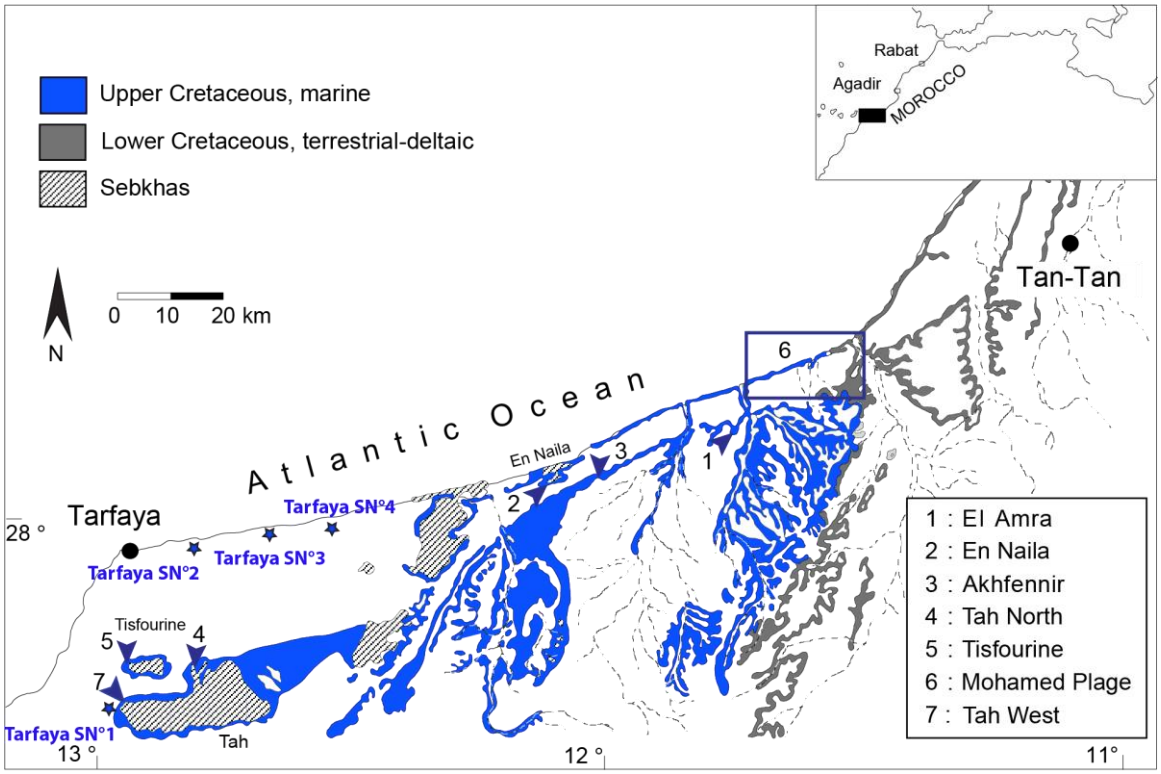

Figure 1: Location of newly drilled Tarfaya SN°1, 2, 3 and 4 cores and outcrop sections in the Tarfaya Basin, which form the base for a composite Albian to early Campanian stratigraphic log. Sections 1-5 were newly logged and sampled, section 6 (Albian-Cenomanian) was previously studied by Kuhnt et al. (2009) and section 7 (lower Campanian) by Holbourn et al. (1999). Geology adapted from Choubert et al. (1966).

The basin is situated at the tectonically stable western margin of the Saharan Platform. The evolution of the Tarfaya Basin is tightly connected with the geological history of the African Craton, controlled by the Late Triassic–Jurassic break-up of the supercontinent Pangaea (Baudin, 1995), resulting in the opening of the Atlantic (Rank et al., 1982). The initial break-up of Pangaea may have been associated with widespread volcanic activity on the Atlantic Ocean and known as the Central Atlantic Magmatic Province (Olsen, 1999). The basement of the basin is composed of folded

Precambrian and Paleozoic rocks, which are uncomformably overlain by Mesozoic and Cenozoic deposits.

During Triassic times, a synrift continental megasequence (1000 m) was deposited in the basin. The sediments include evaporite horizons followed by sills of dolerite basalts. The post rift phase started with the Jurassic marine transgression, which only affected the northern part of the basin (Nzoussi-Mbassani et al., 2005). The post-Triassic extensional structures and subsidence of the basin are related to the opening of the Atlantic Ocean (Wiedmann et al., 1982). Important is the activation of the Zemmour fault that separates the Anti-Atlas and the Tindouf basin to the east (Choubert et al., 1966). With the activation of the fault, steady subsidence of the Tarfaya basin commenced in the Triassic followed by stepwise subsidence in the Jurassic and the Cretaceous.

The Early to Middle Jurassic marine carbonates characterized by silty sandstones, limestones, dolomitic limestones and dolomites transgressed onto the Triassic rift sediments and/or evaporites. The Late Jurassic neritic marly limestones and calcarenites, intercalated with marls, shales and sandstones (formation of Puerto Cansado) are overlying the Early to Middle Jurassic marine carbonates (Choubart et al., 1966; Abou Ali et al., 2005).

A thick deltaic sequence, of the Early Cretaceous age, accumulated during and after a major global Valanginian regression (Vail et al., 1977a). According to Ratschiller (1970), the shallow-marine deposit from the Upper Cretaceous to the Eocene unconformably overlies the continental Lower Cretaceous formations. The upper Albian to lower Cenomanian sequence consists of claystone, marl, siltstone and dolomitic limestone (Wiedmann et al., 1982). The upper Cenomanian–Turonian and Coniacian strata contain deeper-water shales and limestones, followed by shallower-water oyster shell beds present in the Santonian (Freneix, 1972). The Campanian contains also deeper-water shales and limestones. The Maastrichtian only appears in the southern (El Aayun) part of the basin, south of the Sebkha Tah and is mainly composed of greenish marginal marine claystones.

During the Tertiary the sea retreated, although minor transgressions occurred during the late Paleocene to Eocene. Deposits consist mainly of phosphatic and silty marls and dolomites (Butt, 1982). During the Eocene and the Oligocene, the basin sediments were uplifted and folded, suggesting regional epirogenesis and inter-regional Alpine orogenesis related to extensive crustal shortening and subduction in the Tethys region (Dewey et al., 1973). Late Oligocene to early Miocene basin development shows an erosional hiatus because of the coincidence of a major

regression with intensified slumping, canyon incision, and bottom water circulation (Arthur et al., 1979), with only little continental deposition taking place. After this long period of non-deposition or erosion, Miocene-Pliocene sediments unconformably overlay the Lower Cretaceous (Tan Tan Formation), Upper Cretaceous (NE part of the basin), Eocene and Oligocene (SW part of the basin) deposits. Following the Miocene-Pliocene, siliciclastic sediments once again started to be deposited both on- and off-shore with uplift events in the Atlas system (Frizon de Lamotte et al., 2009; Ruiz et al., 2010).

2. Previous work and motivation

The NW African margin represents an excellent model demonstrating syndepositional tectonics of a passive margin in the North Atlantic. The Tarfaya Basin, which comprises the southernmost Atlantic marginal basin of Morocco (latitudes 28° N and 24° N), contains around 700 m of Upper Cretaceous laminated organic carbon-rich biogenic sediments covered by clastic Paleogene and Neogene deposits. This basin provides an excellent location to reconstruct the Late Cretaceous depositional history due to minimal regional tectonic influences (Choubert et al., 1966). In recent years, the Tarfaya basin has been primarily targeted for the study of Upper Cretaceous (Cenomanian-Turonian) laminated organic carbon-rich sediments to understand the intensity of anoxia, the magnitude and nature of the bulk carbonate $\delta^{13}C$ excursions, the biotic effects of anoxia on benthic and planktonic foraminifera, regional patterns of appearance and extinction of marine species and the relation of the regional paleo-environmental evolution to climate and eustatic sea-level changes (e.g. El Albani et al., 1999a and b; Kuhnt et al., 1995, 1997, 2005a, 2009; Kolonic et al., 2005; Mort et al., 2007, 2008; Keller et al., 2008, Gertsch et al., 2010a, Aquit et al., 2013).

In this study, I present detailed sedimentary logging, photographic documentation, sequence stratigraphic interpretation as well as micropaleontological and geochemical analysis of the Upper Cretaceous sedimentary successions studied during five field expeditions of the Kiel Micropaleontology Group in 1997, 1998, 2000, 2003 and 2009 in addition to two cores drilled in fall 2009. During these field expeditions five new outcrop sections El Amra, En Naila, Akhfennir, Tah North and Tisfourine were logged bed-by-bed and sampled in intermediate-high resolution. The main challenge of this study was the detailed stratigraphic correlation of these outcrop sections. (e,g., the correlation of the Coniacian in the El Amra and Akhfennir sections and also the relationship between

the top of the Santonian in the Tah North section and the earliest Campanian in the Tisfourine section). This Santonian/early Campanian transition corresponds to a major sequence boundary at the top of the Santonian (Choubert et al., 1966), which is difficult to investigate in outcrop section due to an intense coverage of this part of the sedimentary succession by sand dunes in the Sebkha Tah. To resolve this enigma, drill cores Tarfaya SN°1 and 2 were recovered with the help of ONHYM (National Office of Hydrocarbons and Mines of Morocco) during October-December 2009. Two additional cores (Tarfaya SN°3 and 4 were drilled further to the northeast to recover the older part of the Tarfaya Upper Cretaceous sedimentary succession down to the initial transgressive deposits of the upper Albian. Figure 1 provides an overview of all sections studied and the locations of the four drill cores Tarfaya SN°1, 2, 3 and 4.

The drilling was carried out along the SW flank of the Sebkha Tazra Anticline in the central part of the Tarfaya Basin. The axis of this anticline is striking NNE-SSW and intersects the main road between Tan-Tan and Tarfaya approx. 10 km SE of the Shell quarry. The W-SW flank of this anticline is then continuously dipping to the W until the eastern margin of the Sebkha Tah in the Southwest (Fig. 2) (Leine, 1986; Fig. 3). This anticline was formed by uplifting and folding of the Cretaceous sedimentary succession during the early Miocene (Leine, 1986**)**. The result of this anticline is uplift of Albian deposits to the surface in the centre of the anticline and Campanian deposits at the southern margin (Sebkha Tah and Tisfourine). Later erosion truncated the Upper Cretaceous sediments, followed by deposition of a relatively thin sequence of Pliocene-Pleistocene clastic sediments, belonging to the Moghrabian Formation (Choubert et al., 1966).

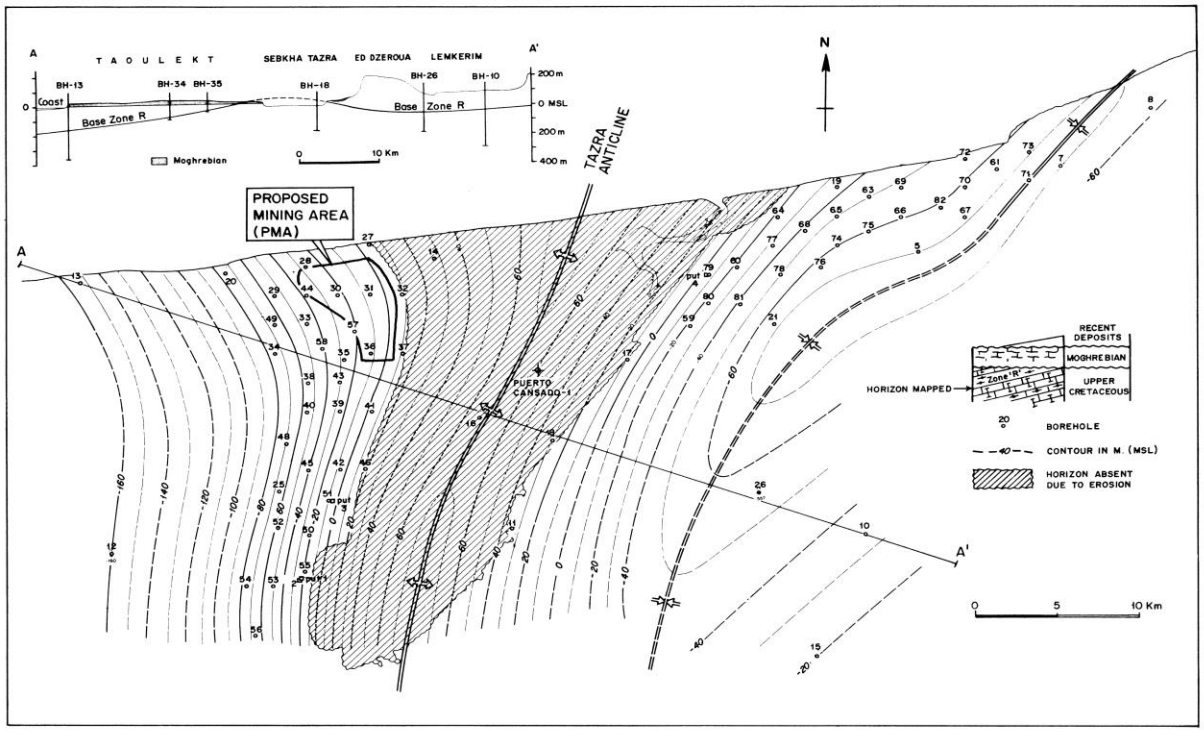

Figure 2: Map showing the location of the Tazra anticline in the Tarfaya Basin, SW Morocco. After Leine (1986).

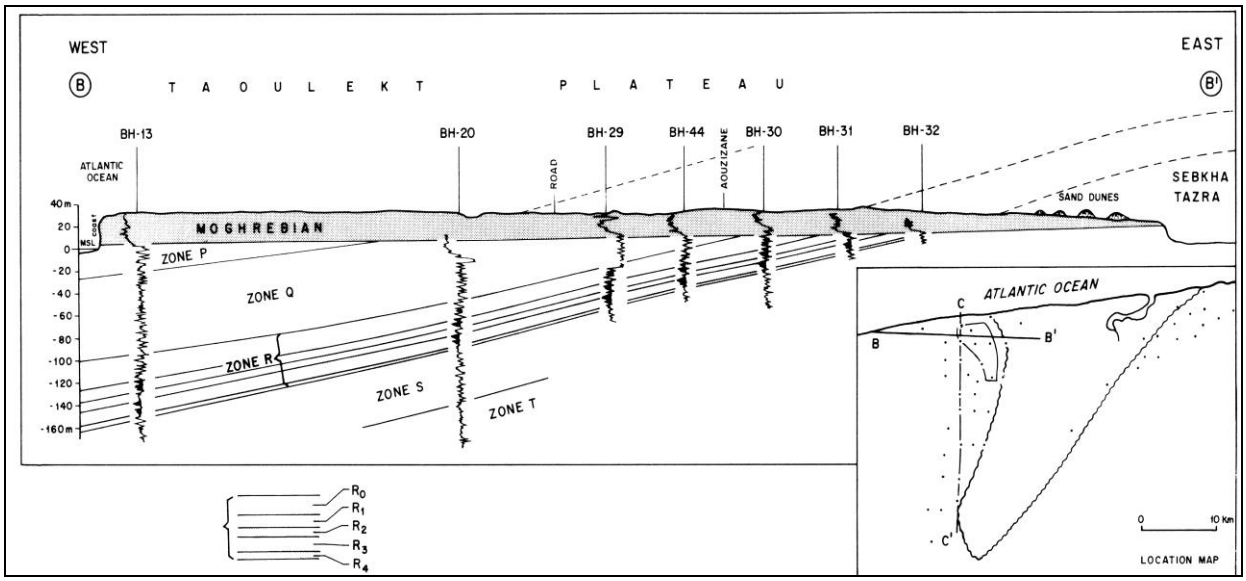

Figure 3: Cretaceous structure of southern flank of the Sebkha Tazra anticline in the Tarfaya Basin, SW Morocco. After Leine (1986).

For obtaining a complete record of the Upper Cretaceous succession in the Tarfaya Basin a drilling campaing was carried out along a transect across the SW flank of the Sebkha Tazra Anticline. Four cores were drilled in the Tarfaya area, which recovered a complete stratigraphic sequence from

the Albian to the Campanian and the Moghrebian Formation at the top of each core. The oldest Cretaceous deposits (early Turonian to Albian) were recovered in core Tarfaya SN°4 close to center of the Sebkha Tazra Anticline. Youngest Cretaceous deposits (early Campanian) were recovered in Tarfaya SN°1 core close to Sebkha Tah. Tarfaya SN°2 and 3 cores were positioned between Tarfaya SN°1 and 4 cores to recover the entire succession with enough overlap to reliably correlate the cores using wireleine logging records. A total of 1100 meters of sediment was recovered with a Longyear L44 hydraulic drilling system "WD3500" (Fig. 4) (350 m at Tarfaya SN°1, 200 m at Tarfaya SN°2, 200 m at Tarfaya SN°3 and 350 m at Tarfaya SN°4), which completely cover the entire ~700 m succession of the Upper Cretaceous, covered by approx. 20-30 m of Moghrabien lumachelle with sandstone beds. Wireline logging (e.g. Natural Gamma Ray with 1 cm resolution) was lowered into the drill hole a few weeks after the drilling was completed (Fig. 5). Cutting of the core in work (Kiel) and archive (ONHYM) halves was carried out with a high precision Kaufmann-Titan diamond rock saw (Fig. 6). Each segments was cleaned with sandpaper before spectrophotometric and XRF-scanner based geochemical analyses. Figures 7 and 8 illustrate the segments before and after cleaning. The geochemical analyses (X-ray fluorescence scanner with 1 cm resolution (Fig. 9), carbonate and oxygen isotopes with 20 and 40 cm resolution), lithological description and micropaleontological investigations (planktonic and benthic foraminifera) were carried out in Kiel using polished sediment slabs and discrete samples.

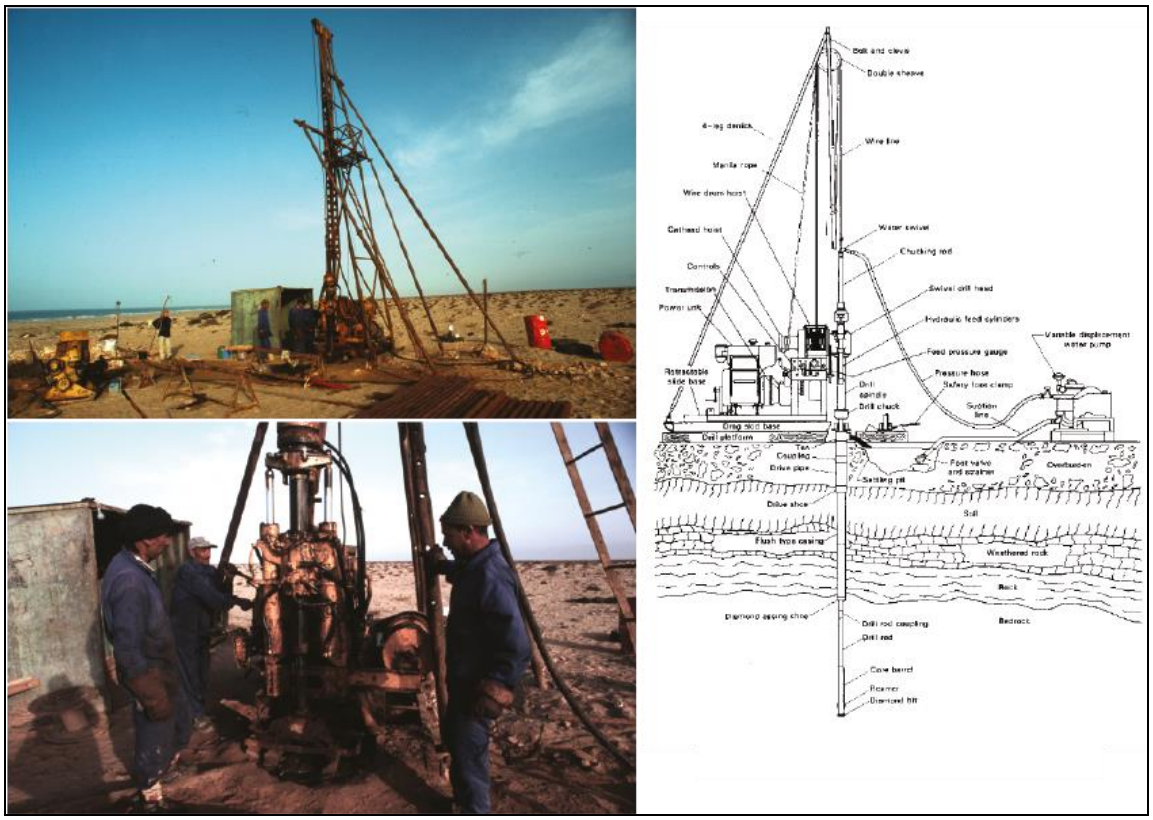

Figure 4: Schema and photograph of Longyear L44 hydraulic drilling system "Sondeuse hydraulique WD3500" used in the Tarfaya drilling.

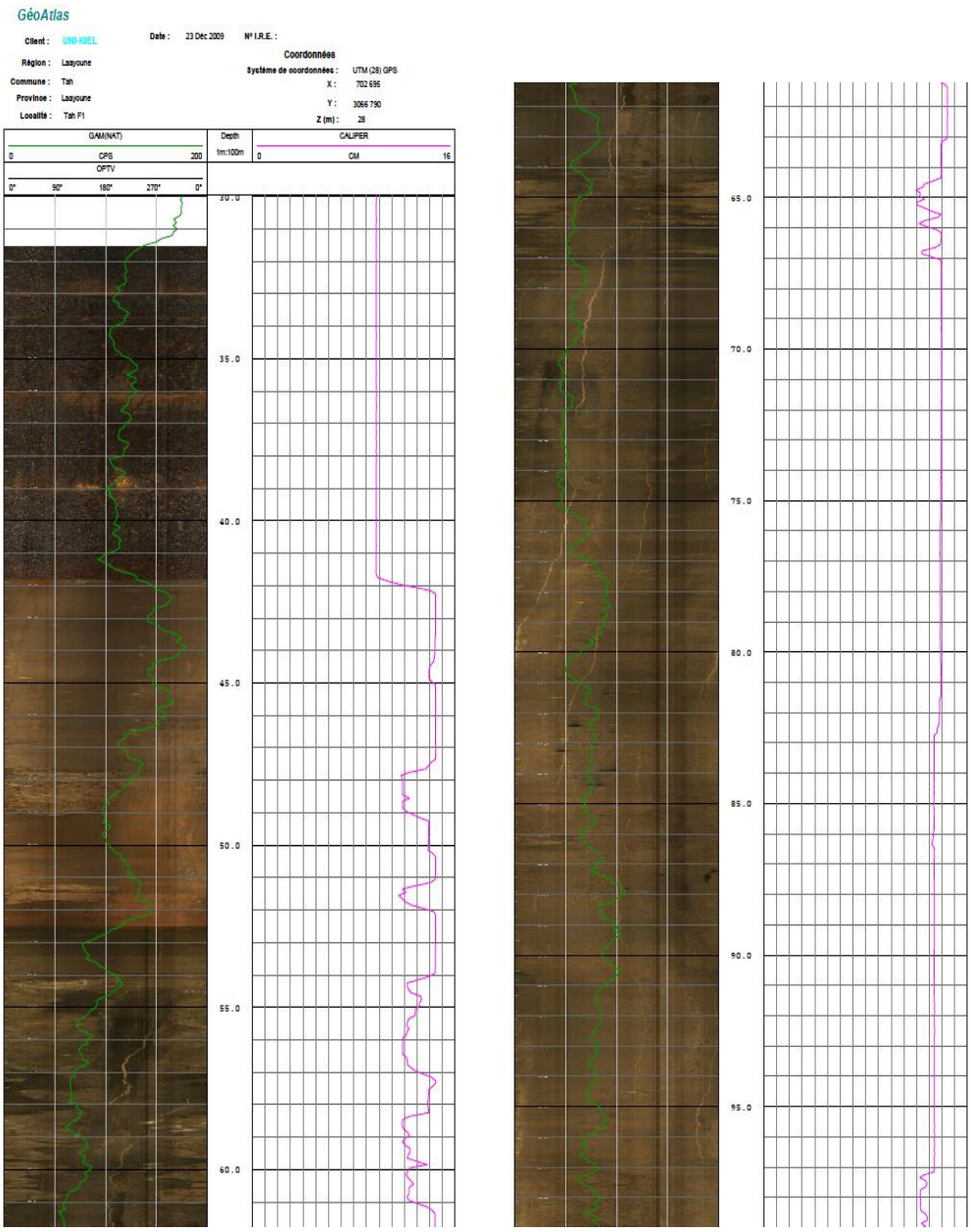

Figure 5: Well downhole photograph and wire-line logging data carried out for Tarfaya SN°1 by the Geoatlas Laayoune Company.

Figure 6: Splitting into archive and working halves with a high precision Kaufmann-Titan diamond rock saw.

Figure 7: Photographs of segment before and after cleaning for analysis.

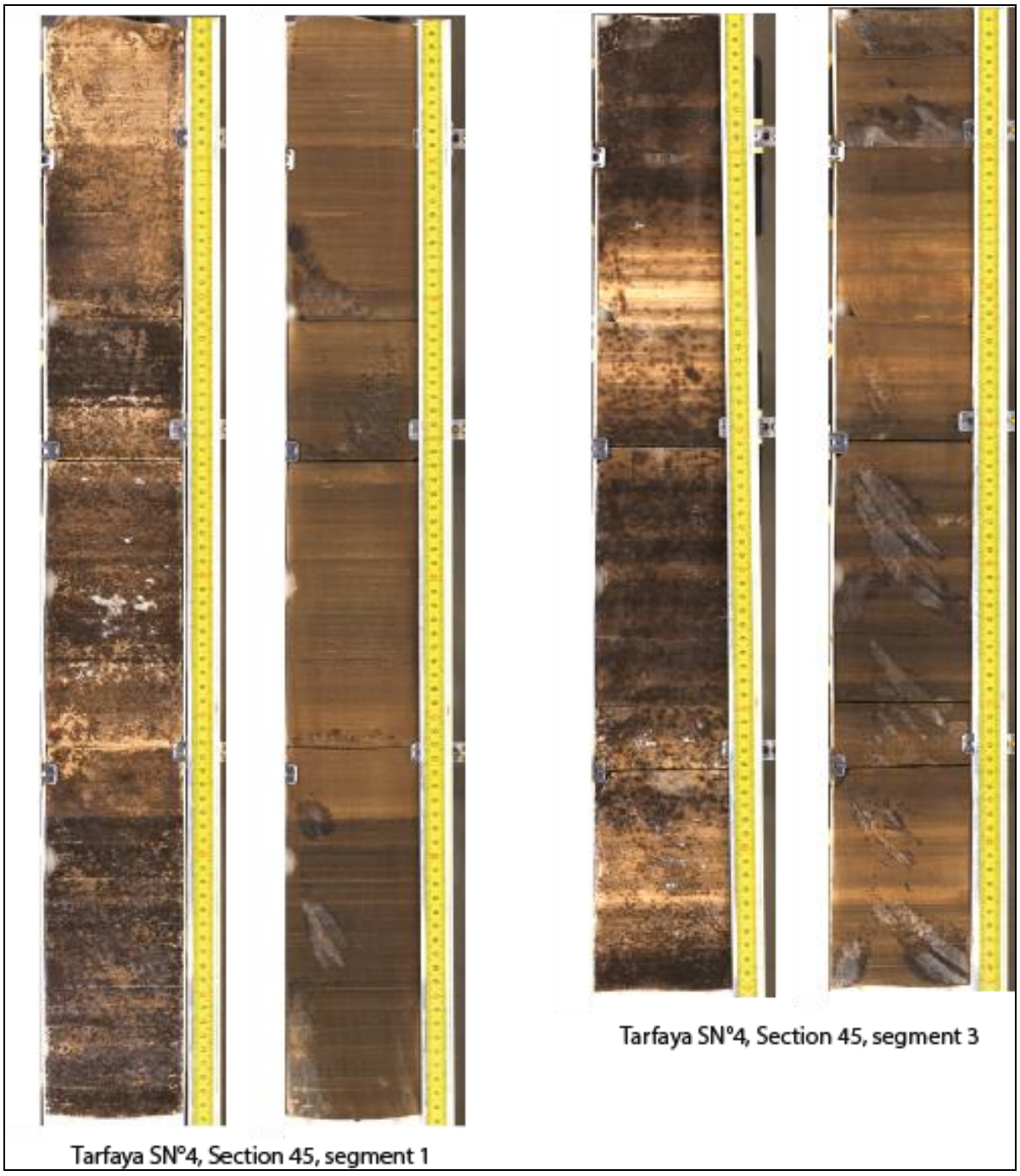

Figure 8: Photographs of segment before and after cleaning for analysis.

Figure 9: X-ray fluorescence core scanner at the Institute of Geosciences, Kiel.

3. Objectives

The principal objectives of this work are: (1) to reconstruct the paleoenvironmental evolution and sea-level changes of the Tarfaya coastal basin during the Turonian to early Campanian, based on wireline-logging, visual core description, bulk carbonate stable isotopes and X-ray fluorescence scanner derived high resolution elemental distribution data (2) to obtain high resolution correlation of Upper Cretaceous organic-rich deposits from outcrop sections with the newly drilled cores from the Tarfaya Basin (3) to date and correlate observed sequence boundaries in the Tarfaya Basin to the global sequences (Hardenbol et al., 1998; Miller et al., 2004) and (4) to investigate the possible influence of orbital insolation changes and eustatic sea-level flucations on the sedimentation in the Tarfaya Basin.

Chapter II. Late Cretaceous paleoenvironmental evolution of the Tarfaya Atlantic coastal Basin, SW Morocco

Mohamed Aquit[1], Wolfgang Kuhnt[1], Ann Holbourn[1], El Hassane Chellai[2], Karl Stattegger[1], Oliver Kluth[3], Haddou Jabour[4],

[1]Institute of Geosciences, Christian-Albrechts-University, D-24118 Kiel, Germany (ma@gpi.uni-kiel.de, wk@gpi.uni-kiel.de, ah@gpi.uni-kiel.de, kst@gpi.uni-kiel.de)

[2]Department of Geology, Faculty of Sciences Semlalia, Cadi Ayyad University–Marrakech, Morocco (chell@ac.ma)

[3]RWE Dea AG, Hamburg, Germany (Oliver.Kluth@rwe.com)

[4]ONHYM, Rabat, Morocco (jabour@onhym.com)

This article is published in Cretaceous Research Journal, Volume 45, October 2013, Pages 288–305.

Abstract

Lithological evidence, benthic foraminiferal census counts, and X-ray fluorescence (XRF) scanner-derived elemental data were integrated with planktonic foraminiferal biostratigraphy and bulk carbonate stable isotopes to retrace the Turonian to early Campanian paleoenvironmental evolution and sea-level history of the Tarfaya Atlantic coastal basin (SW Morocco). The lower Turonian is characterized by laminated organic-rich deposits, which contain impoverished benthic foraminiferal assemblages, reflecting impingement of the oxygen minimum zone on the shelf during a sea-level highstand. This highstand level is correlated to the global transgressive pulse above the sequence boundary Tu1. The appearance of low-oxygen tolerant benthic foraminiferal assemblages dominated by *Gavelinella* sp. in the middle to upper Turonian indicates an improvement in bottom water oxygenation, probably linked to offshore retraction of the oxygen minimum zone during a regressive phase. This interval is marked by major regressive events expressed by a series of erosional truncations associated with the prominent sequence boundaries Tu3 and/or Tu4. Dysoxic-anoxic conditions recorded in the upper Santonian of the Tarfaya Basin coincide with the eustatic sea-level rise prior to Sa3 sequence boundary. The lower Campanian transgression, only recorded in the southern part of the Tarfaya Basin, coincided with substantial deepening, enhanced accumulation of fine-grained clay-rich hemipelagic sediments and improved oxygenation at the sea-floor (highest diversity and abundance of benthic foraminiferal assemblages). Stable isotope data from bulk carbonates are tentatively correlated to the English Chalk carbon isotope reference curve, in particular the Hitch Wood Event in the upper Turonian, the Navigation Event in the lower Coniacian, the Horseshoe Bay Event in the Santonian and the Santonian/Campanian Boundary Event.

Key words: benthic foraminifera, XRF scanning, stable isotopes, Upper Cretaceous, sea-level change, Tarfaya Basin

Introduction

The Tarfaya Basin extends along the west coast of Africa at latitudes 28-24°N, and is limited by the Anti-Atlas Mountains in the north, the Reguibat Basin in the east, the Mauritanides in the south and the Atlantic Ocean in the west. The evolution of the Tarfaya Basin is tightly connected with the geological history of the African Craton and the opening of the Atlantic (Rank et al., 1982). The basement is composed of folded Precambrian and Paleozoic rocks, which are uncomformably overlain by Mesozoic and Cenozoic deposits. The post-Triassic extensional structures and subsidence of the basin are related to the opening of the Atlantic Ocean (Wiedmann et al., 1982). An important evolutionary feature was the activation of the Zemmour fault that separated the basin from the Anti-Atlas and Tindouf Basin (Choubert et al., 1966), and played an important role in the subsidence history of the basin during the Jurassic and Cretaceous. Detailed structural studies of the Tarfaya Basin were previously published by Wiedmann et al. (1982), El Khatib et al. (1995, 1996) and El Albani et al. (1999 a, b).

Expanded sedimentary successions of Cretaceous age were deposited at the northwestern margin of the stable Sahara platform close to the original coastline of the Tarfaya Basin. These rocks are unconformably overlain by relatively thin sequences of Cenozoic proximal marine deposits. On a broad regional scale, the Lower Cretaceous successions are composed of detrital deposits of deltaic or fluvial origin, whereas the Upper Cretaceous deposits consist of limestones and marls, which are rich in organic matter. Previous investigations of Cretaceous and Cenozoic sections exposed close to the coast and around coastal salt flats (Sebkhas) and desiccated river beds in the Tarfaya Basin are listed in Table 1. Whereas recent work concentrated on the Cenomanian-Turonian black shale successions, corresponding to Ocean Anoxic Event 2 (OAE 2), this study focuses on the Turonian to Campanian sections outcropping in the northwestern part of the basin (Fig. 1). Our main objectives are 1) to correlate Upper Cretaceous successions within the Tarfaya Basin and 2) to reconstruct the paleoenvironmental evolution of the coastal marginal basin, based on analysis of lithological units, benthic and planktonic foraminiferal distribution, bulk carbonate stable isotopes and X-ray fluorescence scanner data.

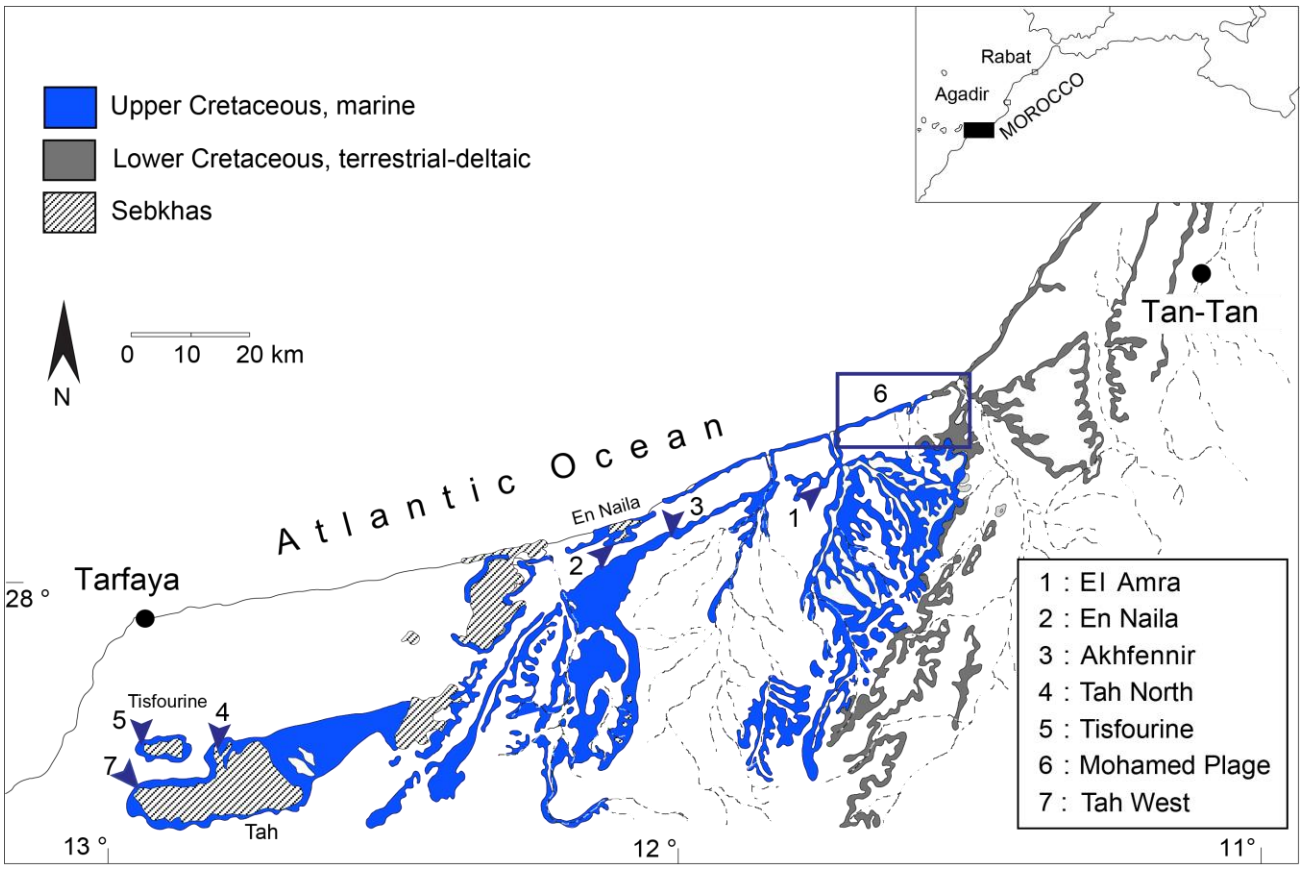

Figure 1: Location of outcrop sections in the Tarfaya Basin, which form the base for a composite Albian to Campanian stratigraphic log. Sections 1-5 were newly logged and sampled, section 6 (Albian-Cenomanian) was previously studied by Kuhnt et al. (2009) and section 7 (lower Campanian) by Holbourn et al. (1999). Geology adapted from Choubert et al. (1966).

Location	Data	Time interval	References
Sebkha Tazra	Petrography, chemical composition and mineralogy of oil shale deposits	Upper Cretaceous (Cenomanian-Campanian)	Leine, 1986
Core S13	Microfossil assemblages and organic matter accumulation rates	Cenomanian-Turonian	Kuhnt et al., 1986, 1990
Cap Juby	Reflection seismic data	Triassic to Miocene	El Khatib et al., 1995
Cores S5, S13, S20, S21, S25, S75,	Cyclostratigraphy of organic-carbon-rich deposits	Cenomanian-Turonian	Kuhnt et al., 1997, 2004
Core S75 Sebkha Tah (Tah West) Oued Amma Fatma	Benthic foraminiferal and clay mineral assemblages	Turonian (Amma Fatma and Core S75) Campanian (Sebkha Tah)	Holbourn et al., 1999
Sebkha Tah Akhfenir Oued Amma Fatma Sebkhat Tazra	Lithology, microfacies and clay mineral assemblages	Cenomanian-Campanian	El Albani et al., 1999a
Tassegdelt El Amra Mohamed Plage	Lithology and microfacies	Cenomanian-Turonian	El Albani et al., 1999b
Mohamed Plage Core S 13	Benthic foraminiferal assemblages	Cenomanian	Gebhardt et al., 2004
Ifni/Tan-Tan margin	Basement structure and seismostratigraphy	Pre-Triassic basement Triassic-Liassic rift	Abou Ali et al., 2005
Cores S13, S57, S75	Carbon isotopes and organic carbon accumulation	Cenomanian-Turonian	Kolonic et al., 2005
Core S13 Mohamed plage	Lithology, stable isotopes and sequence stratigraphy	Cenomanian	Kuhnt et al., 2009

Table 1: Overview of Cretaceous and Cenozoic outcrop successions and drilled cores investigated in the Tarfaya Basain.

1. Material and Methods

During five field expeditions in 1997, 1998, 2000, 2003 and 2009 detailed sedimentary logging, sequence stratigraphic analyses and photographic documentation as well as micropaleontological and geochemical sampling of Cretaceous to Neogene sedimentary successions were undertaken in the northern Tarfaya Basin. Previously published data from selected outcrop sections were integrated with data from five new sections: El Amra, En Naila, Akhfennir, Tah North and Tisfourine that were investigated during the most recent fieldwork. Figures 1-2 and Table 1 provide an overview of all sections studied.

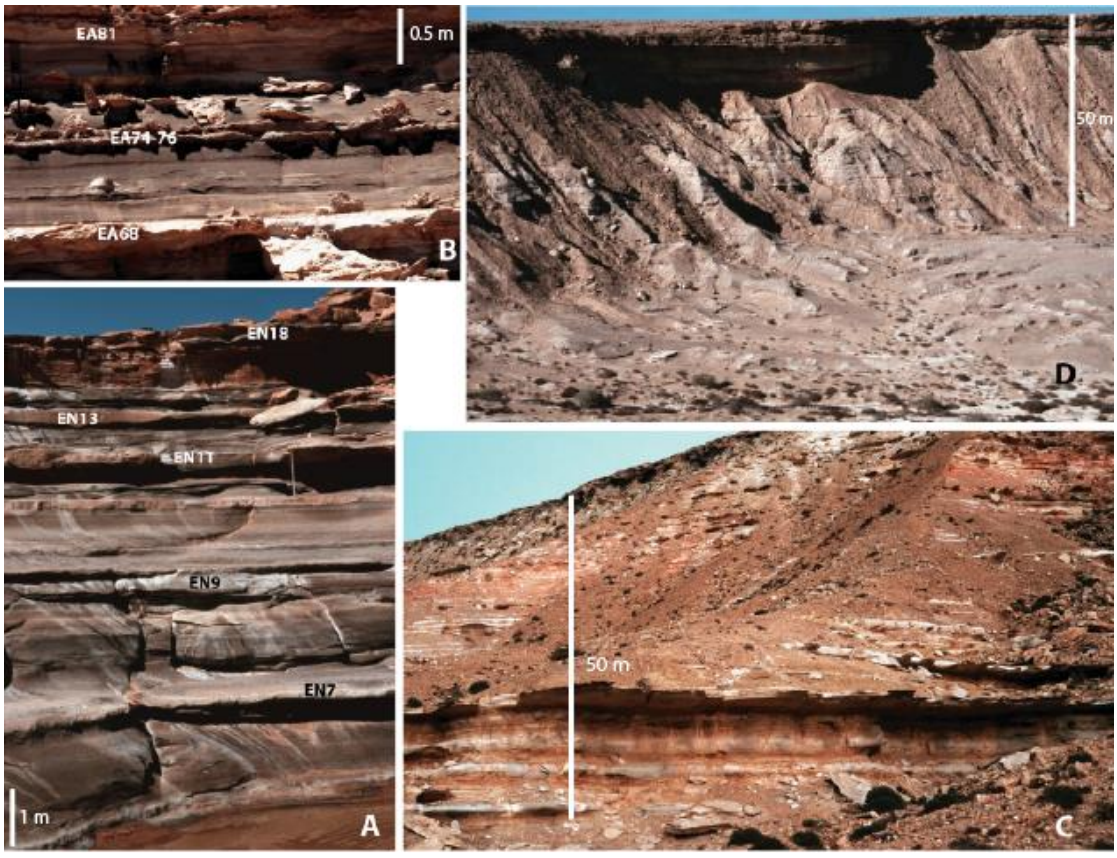

Figure 2: (A) Overview of the lower part of the En Naila section, key beds are labelled; **(B)** uppermost Turonian succession in the El Amra section, key beds are labelled; **(C)** overview of the Akhfennir section (early Santonian); **(D)** overview of the Tah North section (upper Santonian).

1.1. Paleoenvironmental analyses of benthic foraminiferal assemblages

A total of 280 micropaleontological samples from organic rich clay intervals in the El Amra, En Naila, Akhfennir, Tah North and Tisfourine sections of the Tarfaya Basin were dry weighed and processed using an alcoholic solution of anionic tensides (REWOQUAT by REWO-Chemie, Steinau, Germany), which helped to break down indurated samples of organic rich laminated chalk. Benthic foraminifera were quantitatively picked from splits of the 250-630 µm fractions and numbers per 100 g of sample were calculated. Benthic foraminifera were additionally picked from splits of the 125-250 µm fractions in 32 selected samples to complement census counts of the larger size fractions and to ensure that smaller taxa were not overlooked. Key index taxa were determined and documented with scanning electron micrographs. Planktonic foraminifera from splits of the 250-630 µm fractions were picked, planktonic-benthic ratios determined, and a biostratigraphic zonation based on planktonic foraminifera was established. Planktonic foraminifera occur throughout the investigated sections, except in 20 samples of the El Amra section. Planktonic foraminifera are generally well preserved, exhibiting no evidence of dissolution; thus, the lack or low abundance of benthic foraminifera in some intervals was not considered to reflect diagenesis but original changes in the composition of assemblages. Benthic foraminiferal distribution was quantitatively monitored using the following indices:

(1) Shannon-Weaver information function (Shannon and Weaver, 1949), which provides an index of diversity:

$$H(S)=-\sum_{i=1}^{S} P_i \ln p_i$$

where S is the number of species and p_i is the proportion of the ith species (p = total count of one species divided by total count of benthic specimens).

(2) percentage of benthic foraminiferal specimens in the total number of foraminifera: B% = (B/(P+B))*100 where P represents the number of planktonic foraminifera and B the number of benthic foraminifera.

1.2. Stable isotope analysis of bulk carbonate

A total of 255 samples (80 samples from El Amra, 46 samples from En Naila, 25 samples from Akhfennir, 28 from Tisfourine and 76 samples from Tah North) were measured for stable

isotopes of bulk carbonates. Measurements were made with a Finnigan MAT 251 mass spectrometer at the Leibniz Laboratory for Radiometric Dating and Stable Isotope Research at the Christian-Albrechts University in Kiel. The instrument is coupled online to a Carbo-Kiel device for automated CO_2 preparation of carbonate samples. Samples were reacted by individual acid addition. The system has an accuracy (on the delta scale) of ± 0.05‰ for carbon and ± 0.08‰ for oxygen isotopes. The results were calibrated using the National Institute Bureau of Standards and Technology (Gaithersburg, Maryland) carbonate isotope standard NBS 20, internal standards and NBS 19 and are reported as $\delta^{13}C_{carb}$ on the PeeDee belemnite (PDB) scale.

1.3. X-ray fluorescence (XRF)-scanning

XRF measurements were carried out with an Avaatech X-ray fluorescence core scanner at the Institute of Geosciences, Christian-Albrechts-University in Kiel. Scanning was performed (at 1 cm interval) on polished slabs (6 to 8 cm in length) of homogeneous, oriented samples with flat and smooth surface. 10 kv and 30 kv (tube voltage settings) were used to identify the following elements: Ti, Al, Ca, Mg, Fe, K (Table 2).

Tube voltage (kv)	Filter	Elements analysed
10	None	Al, Si, P, S, Cl, K, Ca, Ti, Mn, Fe, Cu, Zn
30	Pd thick	Br, Rb, Sr, Zr,

Table 2: Instrumental settings of the Avaatech XRF core scanner for specific sets of elements (Richter et al., 2006) used in the analyses of discrete rock samples fromoutcrop sections in the Tarfaya Basin.

1.4. Planktonic foraminiferal biostratigraphy and carbon isotope stratigraphy

The planktonic foraminiferal biostratigraphy is based on the zonation of Robaszynski and Caron (1995). Based on the biostratigraphic framework, carbon isotope events were tentatively correlated to the English Chalk carbon isotope reference curve of Jarvis et al. (2006), which provides a robust framework for Late Cretaceous carbon isotope stratigraphy.

2. Results

2.1. Lithostratigraphy

2.1.1. El Amra section

The ~99 m thick El Amra section (28° 09.211´N, 11° 46.075´W) is located a few kilometers inland from the coast, ~110 km northeast of the town of Tarfaya. Three major lithological units were recognized, based on bed to bed logging (Supplementary Fig. 1):

Unit 1 (~23 m thickness, lower Turonian) at the base of the section is mainly composed of dark-brown laminated shale beds (up to ~120 cm thickness) alternating with lighter limestone layers. Two types of limestones occur: nodular limestones (~20 cm thickness) and bioclastic limestones (10-40 cm thickness) with erosive bases, hummocky cross stratifications and horizontal laminations, which are prominent in the upper part of the unit.

Unit 2 (~53 m thickness, middle Turonian to Coniacian) in the middle of the section consists of three lithological subunits. Subunit 1 (23.54-34.20 m), composed of laminated shale beds (15-40 cm thickness) intercalated with nodular limestone layers (~10 cm), is separated from subunit 2 by thin shell beds containing *Crassatella* spp. ("astarte-lumachelle" marker beds of Choubert et al. 1967). Subunit 2 (34.20-50.15 m) consists of laminated shale intercalated with sparitic limestone beds (~10 cm thickness) exhibiting oblique laminations. A distinctive laminated sparitic bed occurs at the top of subunit 2. Subunit 3 (50.15-75.50 m) consists of laminated shales and calcareous marls.

Unit 3 (~23 m thickness, Coniacian) is dominated by laminated shale alternating with marly limestone layers (15-30 cm thickness). Sparitic limestone beds (~20 cm thickness) with oblique laminations characterize the upper part of this unit.

2.1.2. En Naila section

This ~11 m thick section (28° 03.074´N, 12° 07.630´W) is situated in a shallow dry sebkha a few kilometers inland from the coast, ~70 km northeast of Tarfaya. The succession is mainly composed of black laminated shales alternating with limestones of varying thickness (Supplementary Fig. 2). Two types of limestones are present: marly, cross-laminated limestone with wavy base containing shells debris and rare ammonites, and nodular massive limestone containing shell fragments.

2.1.3. Akhfennir section

This ~69 m thick section (28° 04.0´N, 12° 01.3´W) is located a few kilometers inland from the village of Akhfennir, ~80 km northeast of Tarfaya. Two main lithological units are distinguished (Supplementary Fig. 3):

Unit 1, corresponding to the basal and middle part of the section, is mainly composed of marls alternating with bioclastic limestones or nodular limestones (20-40 cm thickness). The limestones at the base of the section show oblique laminations.

Unit 2, corresponding to the upper part of the section, is dominated by marly limestones alternating with calcareous marls (10-25 cm thickness). At the top of the section, the marly limestones evolve into limestones containing shells fragments (inoceramids), which show a characteristic yellow weathering.

2.1.4. Tah North section

This ~47 m thick section (27° 44.110´N, 12° 48.350´W) is located along the western edge of the Sebbka Tah, ~35 km southeast of Tarfaya. It is composed predominantly of laminated marls intercalated with marly limestones of varying thickness (Supplementary Fig. 4). The laminated marls in the lower part of the section (0-15 m) are rich in invertebrate fossils (inoceramids, small oysters and bivalves) and fish teeth. The uppermost 8 m of the Cretaceous succession (37-45 m) consist of thin-bedded marly limestones within dark-gray calcareous marls.

2.1.5. Tisfourine section

This ~21 m thick section (26° 40.148´N, 13° 40.744´W) is located along the southern edge of the Sebbka Tisfourine, ~30 km south of Tarfaya. The lower part of the section (0-8 m) is composed of homogenous dark-gray olive to black, clay-rich marls, followed by intensely bioturbated dar brown marls between 8 and 9 m. The upper part of the Cretaceous succession is composed of weathered homogeneous olive gray marls (Supplementary Fig. 2). The Tisfourine section is considered as the proximal equivalent of the more expanded Tah West section, which is located ~5 km to the South and was previously described by Holbourn et al. (1999).

2.2. Micropaleontology

2.2.1. Planktonic foraminiferal biostratigraphy

The zonation of Robaszynski and Caron (1995) was adapted and additional local zonal boundaries and "subzones" were defined to obtain a more detailed stratigraphic subdivision of the Upper Cretaceous in the Tarfaya Basin. Six global planktonic foraminiferal zones were identified (Table 3; Fig. 3). The following definitions of zones and "subzones" are used:

The ***Whiteinella archaeocretacea* Zone** ranges from the extinction of *Rotalipora cushmani* to the first appearance of *Helvetoglobotruncana helvetica*. In the Tarfaya Basin it can be subdivided using the first appearance of marginotruncanids (*Marginotruncana* ex gr. *renzi*) and *Helvetoglobotruncana praehelvetica*. Correlation to the nannoplankton biostratigraphy (first appearance of *Quadrum gartneri)* and carbon isotope stratigraphy (Kolonic et al., 2005; Kuhnt et al., 2005a) indicates that the chronostratigraphic range of the *W. archaeocretacea* Zone is extended in the Tarfaya basin and includes most of the lower Turonian.

The base of the ***Helvetoglobotruncana helvetica* Zone** is defined with the first appearance of *H. helvetica* (Wonders, 1980). In the Tarfaya sequence, a transitional interval is observed at the base of the *H. helvetica* Zone. This interval is transitional in two aspects: (1) taxonomically due to occurrence of forms transitional between *H. praehelvetica* and *H. helvetica*; (2) quantitatively by the extreme rarity of typical *H. helvetica* in the lowermost part of the zone, which may bias the definition of the lower zonal boundary (depending on the richness and preservation of the faunal assemblages). For local biostratigraphic correlation, the first common occurrence of typical *H. helvetica* is used as the base of the *H. helvetica* Zone. Preliminary correlation with ammonite events in the Tarfaya basin (Wiedmann and Kuhnt, 1996) indicates a chronostratigraphic position in the lower part of the *Mammites nodosoides* ammonite Zone (top of the lower Turonian) for the base of the *H. helvetica* acme Zone.

The lower boundary of the ***Marginotruncana sigali* Zone** is defined by the last appearance of *H. helvetica* and the first appearance of the zonal marker together with *Marginotruncana schneegansi, M. coronata* and *M. marginata*. Additional datum levels in the uppermost part of this zone are defined by the first appearances of *M. sinuosa, M. undulata* and the genus *Falsotruncana*. The base of the *M. sigali* Zone was correlated to the middle part of the *Collignoniceras woollgari*

ammonite Zone (lower part of the middle Turonian) by Amedro et al. (1978) and Robaszynski and Caron (1995). A *Dicarinella primitiva* subzone was initially used in the Tarfaya Basin to characterize the upper part of the *M. sigali* Zone. However, the zonal marker appears as an intermediate form between *M. schneegansi* and *Dicarinella concavata* (Wonders, 1980). Thus, the lower boundary of the *D. primitiva* subzone is ambiguous in the Tarfaya Basin and is not used for stratigraphic correlation.

The lower boundary of the ***Dicarinella concavata* Zone** is well defined by the first appearance of *D. concavata*, which is easily recognized. However, the first occurrence of *D. concavata* in the Tarfaya basin appears somewhat later than its global first appearance. In the Tarfaya basin, *D. concavata* first occurs above the "astarte-lumachelle" marker beds, associated with early Coniacian ammonites (Choubert et al., 1966; Wiedmann et al., 1978), while the base of the *D. concavata* Zone in other subtropical pelagic sections is in the late Turonian (Robaszynski and Caron, 1995; Gradstein et al., 2012). A delayed first occurrence of *D. concavata* in the Tarfaya basin is also supported by correlation to the calcareous nannofossil zonation (Jackie Lees, pers. comm., 2013), which indicates that the base of the *D. concavata* Zone is above the first occurrence of *M. staurophora* within nannoplankton zone UC10 (early to middle Coniacian). The upper boundary of the *D. concavata* Zone is defined by the first appearance of *Dicarinella asymetrica* at the top of the Coniacian

The base of the ***Dicarinella asymetrica* Zone** is generally correlated to the Coniacian/Santonian boundary (Robaszynski and Caron, 1995; Gradstein et al., 2012). However, it is somewhat arbitrary due to the continuous evolution from *D. concavata* into *D. asymetrica* and the relatively rare occurrence of *D. asymetrica* in the early part of its range. To overcome this difficulty, the base of this zone is defined by the first occurrence of typical specimens of *D. asymetrica* with five or more chambers in the last whorl, a wide umbilicus and distinct umbilical ridges (Plate 1).

The base of the ***Globotruncanita elevata* Zone** is defined by the first appearance of *G. elevata* and *G. stuartiformis* at the base of the Campanian. As reported in earlier studies of the Tarfaya basin (Choubert et al., 1966; Wiedmann et al., 1978), there may be a small hiatus in the uppermost Santonian. The top of the *G. elevata* zone is not reached in Cretaceous marine successions north of the Sebkha Tah.

The planktonic foraminiferal zones identified in outcrop sections of the Tarfaya Basin are given in Table 3. Although the Tah North and upper part of the Akhfennir sections are both assigned to the *D.*

asymetrica zone, the Tah North section is considered to be slightly younger in age (late Santonian) on account of its stratigraphically higher position, when correlated across the basin to the Akhfennir section.

Section	Foraminiferal zone	Age
El Amra Section (99 m thickness)	*Helvetoglobotruncana helvetica* zone (0 to 23.36 m)	Early to middle Turonian
	Marginotruncana sigali zone (23.36 to 75.69 m)	Middle to late Turonian
	Dicarinella concavata zone (75.69 to 99 m)	Coniacian
En Naila section (12 m thickness)	*Helvetoglobotruncana helvetica* zone	Early Turonian
Akhfennir section (69 m thickness)	*Dicarinella concavata* and *Dicarinella asymetrica* zone	Coniacian-Santonian
Tah North section (45 m thickness)	*Dicarinella asymetrica* zone	Late Santonian (see text)
Tisfourine section (17 m thickness)	*Globotruncanita elevata* zone	Early Campanian

Table 3: Planktonic foraminiferal zones identified in outcrop sections of the Tarfaya Basin

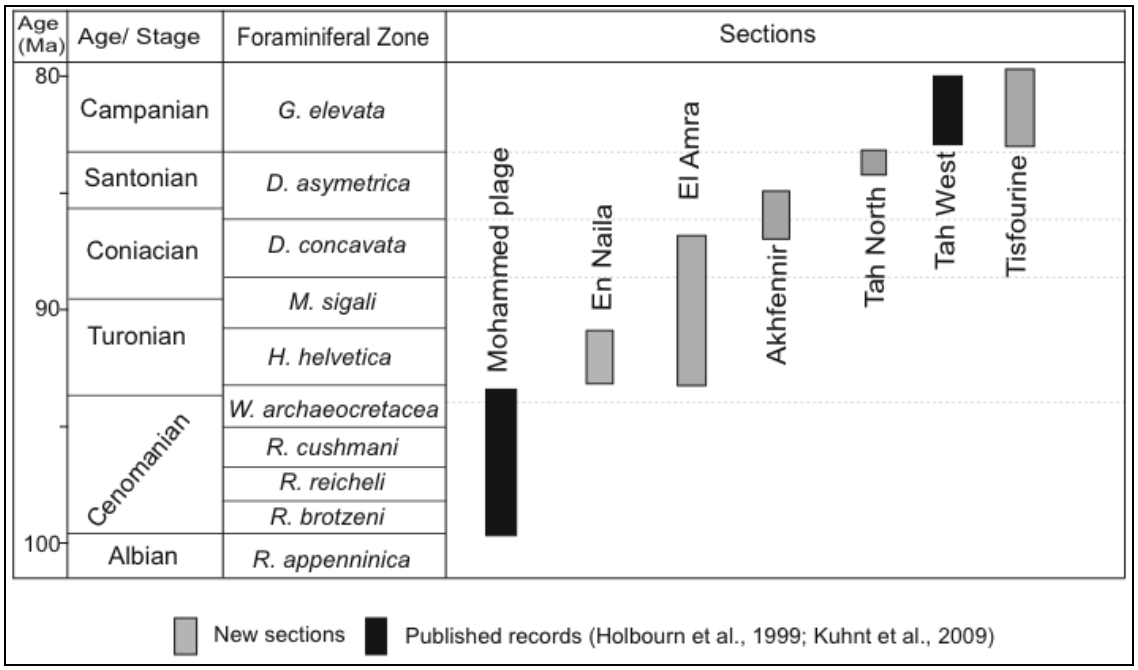

Figure 3: Biostratigraphic correlation of Upper Cretaceous sections in the Tarfaya Basin.

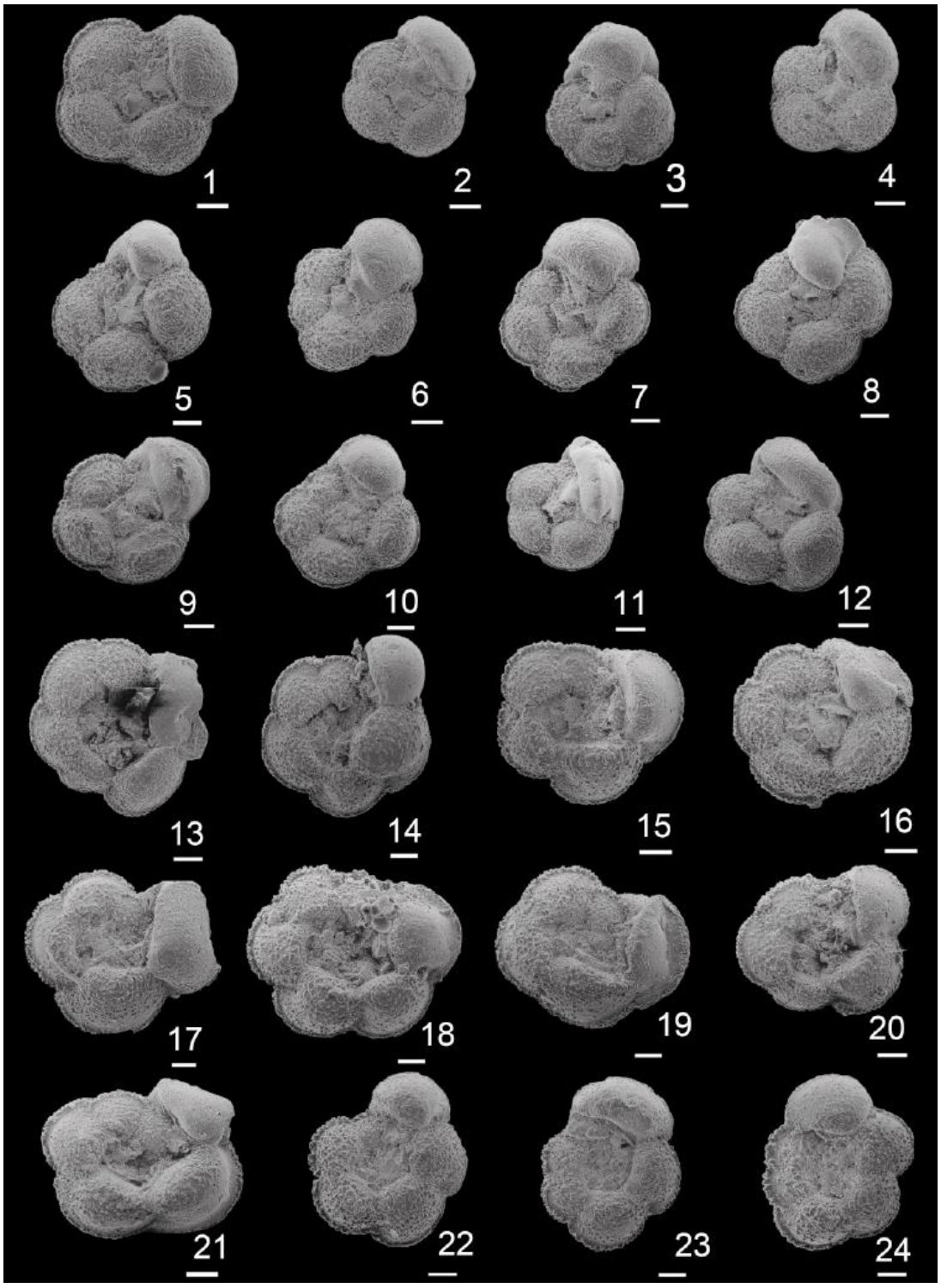

Plate 1: Figs. 1-12: Variability of *Dicarinella concavata* in the uppermost *D. concavata* Zone in the Akhfennir section (Sample T71). Umbilical views of typical specimens and intermediate forms to *Dicarinella asymetrica* (Figs. 7 and 9), which show weak development of umbilical ridges with number of chambers (4-5) in the last whorl and relatively narrow umbilicus typical of *D. concavata*. **Figs. 13-24:** Variability of *Dicarinella asymetrica* in the lowermost *D. asymetrica* Zone in the Akhfennir section. Note still weakly developed umbilical ridges but wider umbilicus and more than 5 chambers in the last whorl in specimens from sample T51 (Figs. 22-24; base of *D. asymetrica* Zone). Typical forms (Figs. 15-16 and 18; Sample T32) possess distinct umbilical ridges, a wider umbilicus and 6 chambers in the last whorl. All scale bars are equal to 100 μm.

2.2.2. Benthic foraminiferal distribution

A total of 30 benthic foraminiferal taxa were identified in 280 samples from the five newly investigated outcrop sections in the Tarfaya Basin. Assemblages exhibit considerable temporal variability both in abundance and diversity. In the El Amra section, the lack or low abundances of benthic foraminifera in Unit 1 and the lower part of Unit 2 corresponds to the dysoxic-anoxic zone identified by Kuhnt and Wiedmann (1995). In the upper part of Unit 2 and in Unit 3 (upper Turonian to Coniacian), benthic foraminifera show low diversity (diversity index: 0–1) and higher abundances (255-11066 specimens/100g (>250 µm) and 6623-107708 specimens/100g (>125 µm). Five dominant taxa were identified: *Neobulimina* sp., *Pyramidina szajnochae*, *Textularia* sp., *Gavelinella* sp. and *Flabellina* sp. (Fig. 4; Plate 2; Supplementary Tables 1 and 2).

The En Naila section (lower Turonian, *H. helvetica* Zone) is virtually devoid of benthic foraminifera within the dominant black shale lithology, except for samples EN17 and EN18, which contain *Gabonita* spp. (Supplementary Table 3).

The Akhfennir section (Coniacian to lower Santonian) is characterized by low diversity (diversity index: 0-1) and highly fluctuating abundances of benthic foraminifera (122-60695 specimens/100g (>250 µm) and 9790-207069 specimens/100g (>125 µm). The assemblages are generally dominated by *Gavelinella* sp., but also include *Neobulimina* sp., *Textularia* sp. and *Flabellina* sp. (Fig. 4; Plate 2; Supplementary Tables 2 and 4).

The Tah North section (middle to upper Santonian) is characterized by low benthic diversity (diversity index: 0-1) and highly fluctuating abundances (554-19536 specimens/100g (>250 µm) and 7753-102873 specimens/100g (>125 µm), except in the upper part of the succession (>32 m), where abundances decrease markedly. The assemblages are generally dominated by *Gavelinella* sp., *Neobulimina* sp., *Textularia* sp., *Lenticulina articulata* and *Flabellina* sp. (Fig. 4; Plate 2; Supplementary Tables 2 and 5).

In the Tisfourine section (lower Campanian), benthic foraminifera exhibit the highest diversity (diversity index: 1.33-2.12) and highest abundances (456-2469 specimens/100g (>250 µm) and 13638-78529 specimens/100g (>125 µm). Twenty-nine taxa were identified including *Gavelinella dakotensis*, *Lingulogavelinella* sp., *Gyroidinoides nitidus*, *Lenticulina articulata* and *Flabellina* sp., which occur frequently throughout the section (Fig. 4; Plate 2; Supplementary Tables 2 and 6).

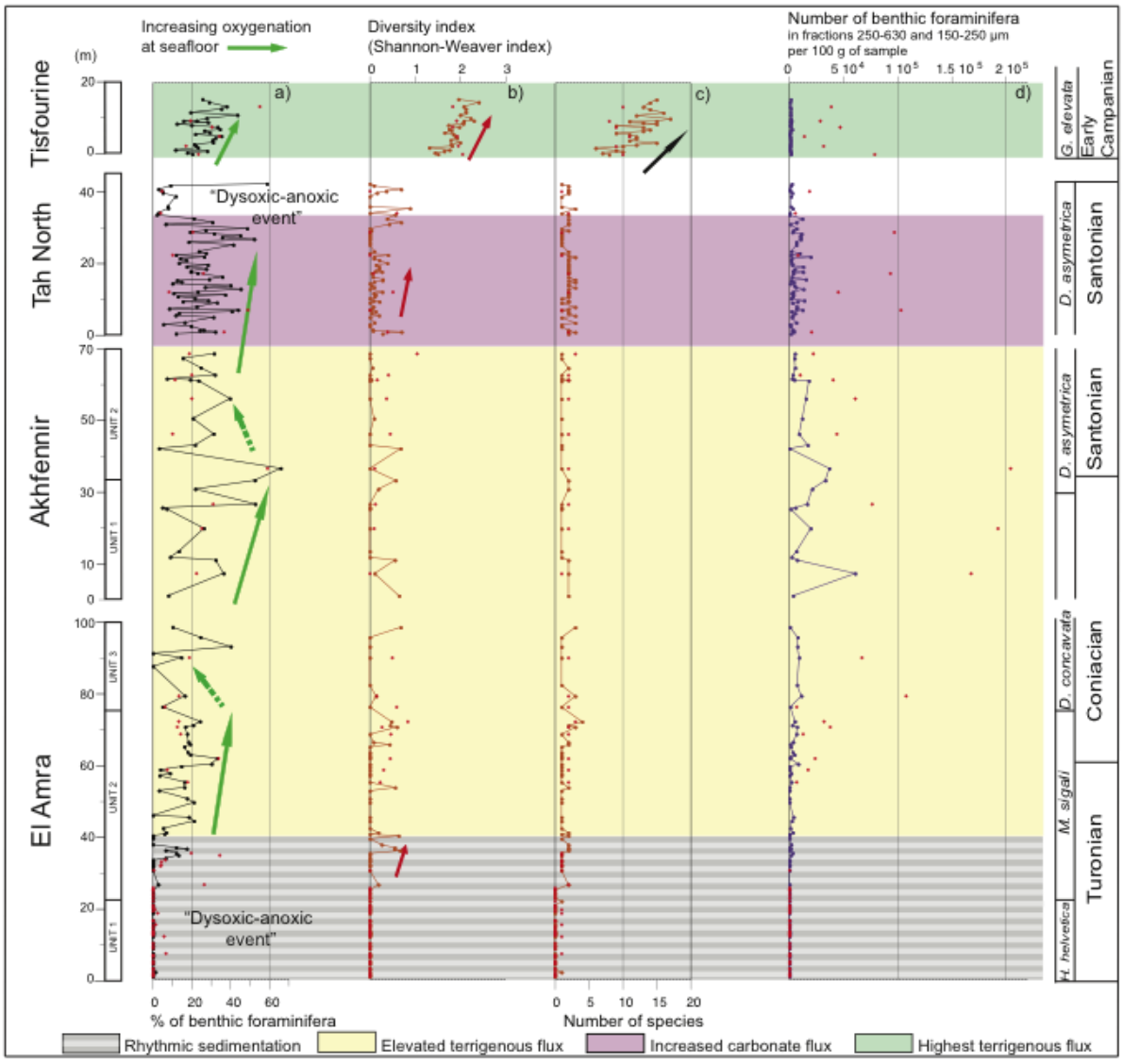

Figure 4: Benthic foraminiferal distribution (size fractions 250-630 and 125-250 µm) in newly logged outcrop sections of the Tarfaya Basin. **a)** %benthic versus planktonic foraminifera, green arrows indicate increasing and decreasing oxygenation at the sea-floor; **b)** Diversity index (Shannon-Weaver index), red arrows indicate marked increase in benthic foraminiferal diversity during the early Campanian; **c)** Number of species, black arrow indicates marked increase in species number during the early Campanian; **d)** Benthic foraminiferal abundance per 100 g of sample. Note: Red dots indicate complementary benthic foraminiferal data from the 125-250 µm fractions. No benthic foraminifera were found in the En Naila samples studied.

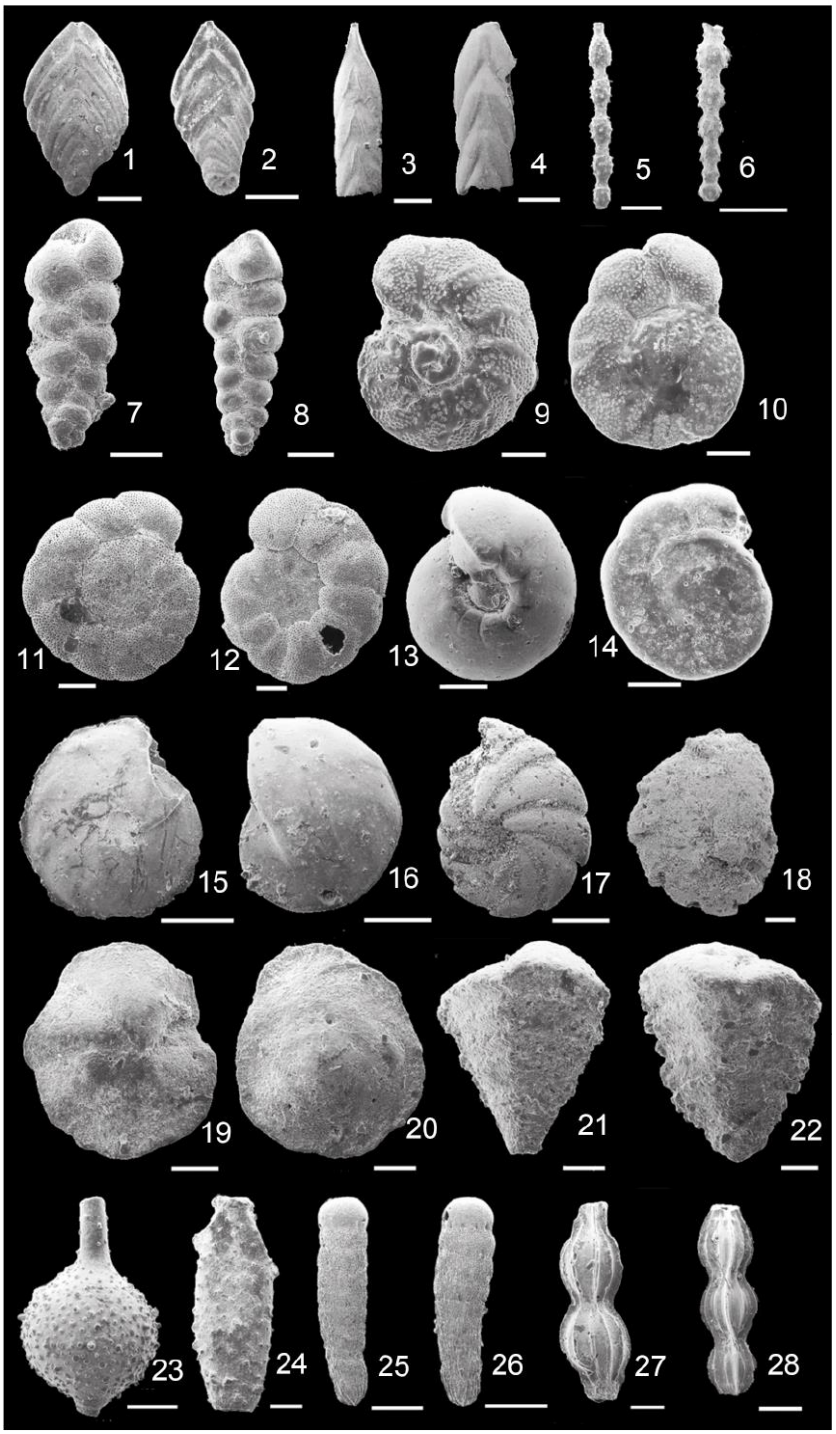

Plate 2: Environmentally significant Late Cretaceous benthic foraminifera in the Tarfaya Basin: **1-2.** *Flabellina* sp 1., sample El Amra 50; **3-4.** *Frondicularia lanceola* (Perner, 1892), sample Tisfourine 13; **5-6.** *Stilostomella alexanderi* (Cushman, 1936), sample Tisfourine 4; **7-8**. *Neobulimina* sp., sample Akhfenir 83; **9-10.** *Gavelinella dakotensis* (Fox, 1954), umbilical and spiral views, sample Tisfourine 15; **11-12**. *Gavelinella* sp., umbilical and spiral views, sample Akhfenir 83; **13-14.** *Gyroidinoides nitidus* (Reuss, 1844), umbilical and spiral views, sample Tisfourine 25; **15-16.** *Lenticulata articulata* (Reuss, 1863), sample Tisfourine 25; **17-18.** *Lenticulina* sp., sample Tisfourine 28; **19-20.** *Osangularia cordieriana* (Hermanni, 1962), umbilical and spiral views, sample Tisfourine 23; **21-22.** *Spiroplectammina cretosa* (Cushman, 1936), sample Tisfourine 22; **23-24.** *Ramulina* sp., sample Tisfourine 18; **25-26.** *Siphogenerinoides* sp., sample Tisfourine 21; **27-28.** *Pyramidulina* sp., sample Tisfourine 21. Scale bars are equal to 300 µm for Figs. 1-6, 15-17, 25-26, and 28, and equal to 100 µm for Figs. 7-14, 18-25, and 27.

2.3. Isotope stratigraphy

Bulk carbonate $\delta^{13}C$ values range between 0.5 and -4‰ in the lower Turonian to lower Campanian successions investigated in the Tarfaya outcrop sections. Values below -4‰, which were measured in cemented carbonate beds and nodules, indicate diagenetic overprint. Maximum values are generally ~2 to 2.5‰ lower than maximum values in the English Chalk and the Italian Scaglia at Gubbio (Jarvis et al., 2006), which is probably due to the higher nutrient content of upwelling water masses in the Tarfaya Basin.

Bulk isotope analysis of 80 samples in the El Amra section (Fig. 5 and 6) reveals an overall decrease in $\delta^{13}C$ from 0.5‰ to values below -1.0‰ from the base to the top of Unit 1. The boundary between Units 1 and 2 (23 m), which corresponds to the boundary between the *H. helvetica* and *M. sigali* zones, is marked by a negative excursion with values dropping below -3‰. Values then fluctuate around -2.0‰ until ~40 m. Above this level, values become enriched, reaching -1.0‰ between 40 and 63 m in an interval, where marginotruncanids occur and benthic foraminifera increase in abundance. This level may correspond to the Hitch Wood Event identified in the Upper Cretaceous of England (Jarvis et al., 2006). From 68 m to the top of the section, values show a sustained decline from -2.0 to -4.5‰. This marked $\delta^{13}C$ decrease may be correlated to the Navigation Event (Jarvis et al., 2006). The $\delta^{18}O$ curve shows no distint trend in the lower 70 m of the section (Turonian). A decrease from -4 to <-6‰ occurs in the upper part of the succession (upper Turonian to lower Coniacian).

The En Naila $\delta^{13}C$ curve (lower Turonian, *H. helvetica* Zone) is characterized by high-amplitude variations with values oscillating between 1.7 and -2.2‰ (Supplementary Fig. 5). Maximum values (>1.5‰) occur in the lower part of the section between 0 and 3 m. Two main decreasing trends are evident between 3 and 6 m (from 1 to -1‰) and between 7 m and the top of the section (from 1 to -2‰).

In the lower part of the Akhfennir section (0 to ~40 m, Coniacian to lower Santonian), the $\delta^{13}C$ curve, based on 25 samples, shows fluctuations between -2 and 0‰. Above 40 m, $\delta^{13}C$ values exhibit a decreasing trend, reaching minimum values <-3.5‰ between 50 and 55 m (lower Santonian). The uppermost samples of the Akhfennir section (above ~55 m) are characterized by marked fluctuations between ~-1.5 and ~3.5‰ (Fig. 6). The $\delta^{18}O$ curve fluctuates between -3 and -6,

showing no distint long-term trend. These marked fluctuations are probably due to diagenetic cementation in the more carbonate-rich intervals.

The $\delta^{13}C$ curve from Tah North (middle to upper Santonian) is characterized by an overall decreasing trend from ~0 to -3.0‰ (Fig. 6). The highest values (~ 0‰) at the base of the section probably correspond to the middle Santonian Horshoe Bay Event in the Upper Cretaceous of England (Jarvis et al., 2006). The $\delta^{18}O$ curve shows no long-term trend and fluctuations are of lower amplitude than in the Akhfennir section, probably reflecting the more homogeneous marly sediment composition.

$\delta^{13}C$ values are highest, remaining close to 0‰, in the lower part of the Tisfourine section (0-8 m), which probably corresponds to Santonian/Campanian Boundary Event. $\delta^{13}C$ values then exhibit a sustained decline from 0.4 to -1.4‰ in the upper part of the section (Fig. 6). The $\delta^{18}O$ curve exhibits a clear trend towards heavier values, related to the global climate cooling in the early Campanian (Clarke and Jenkyns, 1999; Huber et al., 2002).

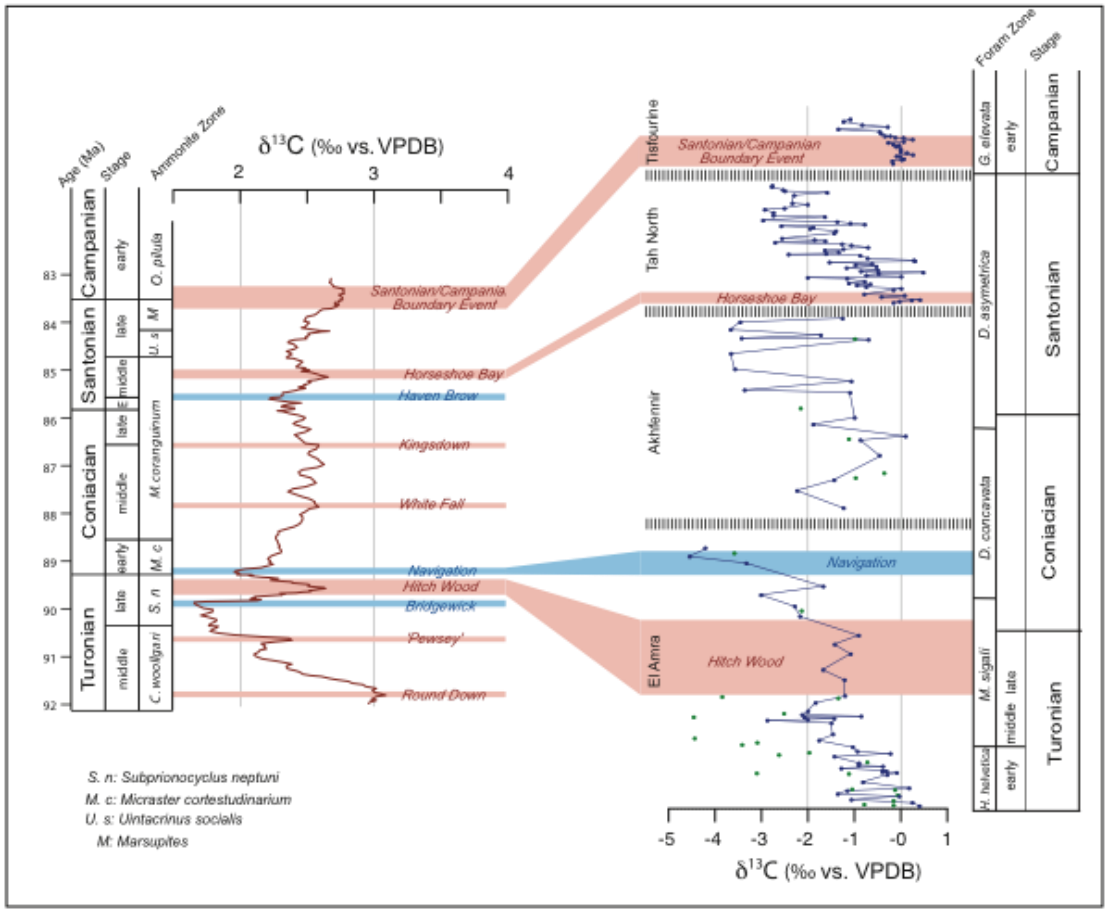

Figure 5: Correlation of bulk carbon isotope ($\delta^{13}C$) from newly investigated outcrop sections of the Tarfaya Basin to the English Chalk carbon isotope reference curve (Jarvis et al., 2006).

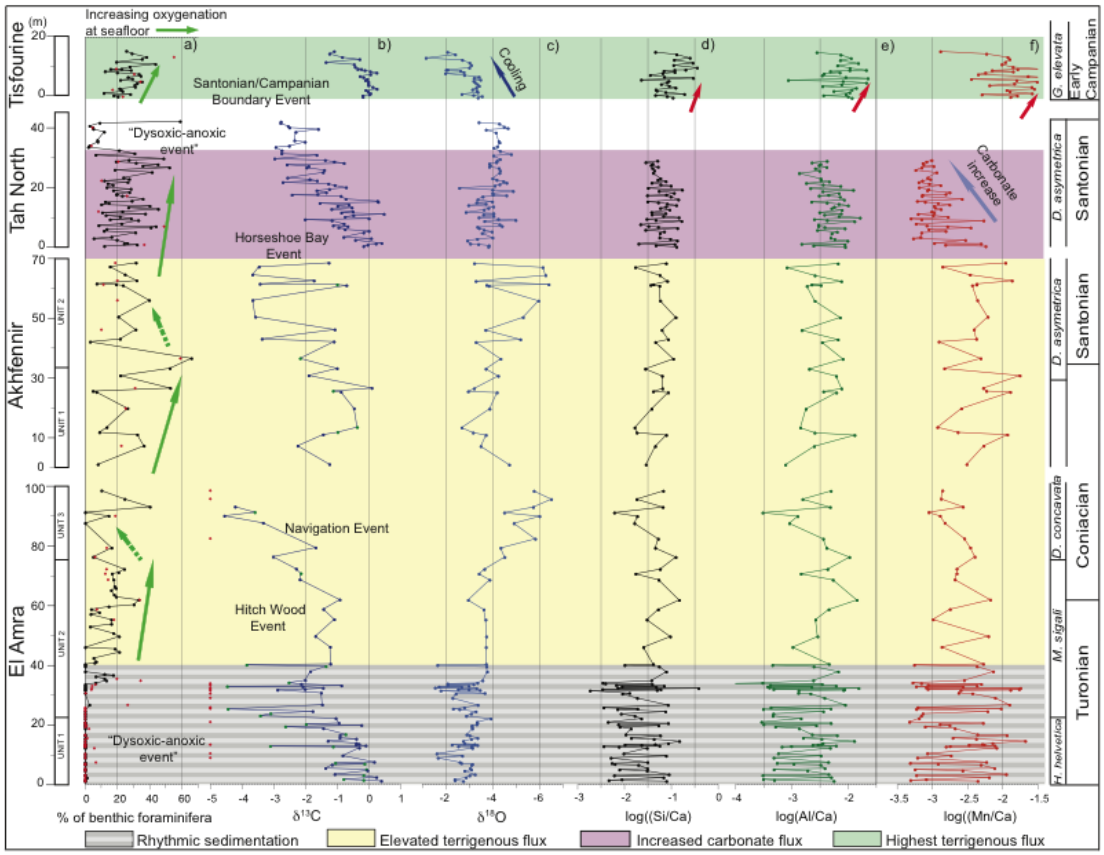

Figure 6: Composite geochemical and paleontological records in newly logged outcrop sections of the Tarfaya Basin. **a)** %benthic versus planktonic foraminifera, green arrows indicate increasing and decreasing oxygenation at the sea-floor; **b)** Bulk carbon isotope data ($\delta^{13}C$) and tentative correlations to the English Chalk carbon isotope reference curve of Jarvis et al. (2006), Green dots indicate limestones, red dots indicate diagenetically altered limestones with $\delta^{13}C$ value below -5%; **c)** Bulk oxygen isotope data ($\delta^{18}O$), blue arrow indicates cooling during the early Campanian; **d-f)** Elemental log-ratios of Si/Ca, Al/Ca and Mn/Ca, red arrows indicate increases in terrigenous flux in the Tisfourine section (Santonian/Campanian boundary); light blue arrow indicates an increase in carbonate flux in the Tah North section (upper Santonian); the En Naila section replicates the lowermost part of the El Amra section, En Naila records are shown is Supplementary Fig. 1.

2.4. Geochemistry (XRF scanning data)

Variations in the abundance of the major elements Fe, Ti, Si and Al present in marine sediment cores have been used to reconstruct changes in terrigenous input into the basins (Peterson et al., 2000; Haug et al., 2001; Jaeschke et al., 2007; Mulitza et al., 2008; Tisserand et al., 2009; Govin et al., 2011). In the Tarfaya Basin, lowstands are characterized by an increase in carbonate-rich rocks (higher Ca), as the elements Si, Al, Fe, Mg, S and Ba become exported into deeper parts of the basin as fine terrigenous clastic material (clay and silt) due to stronger bottom current activity on the shelf. In contrast during highstands, impingement of the oxygen minimum zone onto the shelf and prevalence of deeper, quieter bottom water conditions lead to deposition of Si, Al, Fe, Mg, S and Ba. The log-ratios of Mn/Ca additionally provide information about deep-water oxygenation, as the

sedimentary Mn content in organic-rich environments is almost entirely dependent upon redox conditions. Minerals containing reduced Mn are rare in marine sediments (Calvert and Pedersen, 1996; Tribovillard et al., 2006) and modern and Cretaceous upwelling deposits are commonly depleted in Mn (Brumsack, 1986), thus higher log(Mn/Ca) indicates better oxygenated bottom waters.

At El Amra (lower Turonian to Coniacian), the log(Si/Ca) and log(Al/Ca) curves show strong fluctuations in the lower part of the section (0-40 m), where benthic foraminifera are scarce or absent (Fig. 6). In this interval, values oscillate between -1 and -2.5 for log(Si/Ca) and between -2 and -3.5 for log(Si/Ca). Above ~40 m, values initially fluctuate close to -1 for log(Si/Ca) and -2 for log(Al/Ca), then decrease between 76 and 91 m to -2.5 for log(Si/Ca) and -3.5 for log(Al/Ca), finally showing a small rebound in the uppermost part of the section (91-99 m). The log(Mn/Ca) curve exhibits relatively similar trends with values ranging between -1.7 and -3.3 in the lower part of the section (0-40 m). Values oscillate around -2.5 until ~ 76 m, then decrease to -3 between 76 and 91 m and oscillate between -2.5 and -3 in the uppermost part of the section (91-99 m).

At En Naila (lower Turonian), the log(Si/Ca) and log(Al/Ca) curves show marked fluctuations with values between -1 and -2 for log(Si/Ca) and between -2 and -3.5 for log(Al/Ca), whereas log(Mn/Ca) values oscilate between -2 and -3.2 (Supplementary Fig. 5).

At Akhfennir (Coniacian to lower Santonian), the log(Si/Ca), log(Al/Ca) and log(Mn/Ca) curves exhibit no overall distinct trend with average values fluctuating around -1.1 for log(Si/Ca), -2.4 for the log(Al/Ca) and with values varying between -1.8 and -3.0 for log(Mn/Ca) (Fig. 6).

At Tah North (middle to upper Santonian), the log(Si/Ca) and log(Al/Ca) curves are characterized by low-amplitude fluctuations with values between -1 and -1.5 for log(Si/Ca) and between 2 and -5.5 for log(Al/Ca) (Fig. 6). The log(Mn/Ca) values exhibit an overall decrease from -2.3 to -3.2 from the base of the section to ~27 m, with lowest values and small amplitude variability above ~12 m.

At Tisfourine (lower Campanian), the log(Si/Ca) and log(Al/Ca) curves exhibit no distinct trend. Values range from -1 to -0.5 for log(Si/Ca) and from -2.3 to -1.9 for log(Al/Ca), decreasing towards -1.5 and -2.5, respectively in the uppermost part of the section (Fig. 6). The log(Mn/Ca) values show marked fluctuations from 0 to 13 m, oscillating between -1.5 and -2.5. Towards the top of the section (last two samples), the log(Mn/Ca) values decrease to -2.9.

3. Discussion

3.1. Benthic foraminifera as indicators of paleoproductivity and basin oxgenation

The composition of benthic foraminiferal assemblages is strongly dependent on the productivity of surface waters, the oxygenation of bottom waters, and the rate of export organic carbon flux to the sea-floor (Gooday et al., 1994; van der Zwaan et al., 1999; den Dulk et al., 2000). For instance modern assemblages from intense oxygen minimum zones generally exhibit lower diversity with dominance of species that are more tolerant of oxygen depletion (den Dulk et al., 2000). Thus, changes in the composition of benthic foraminiferal assemblages can be used to monitor temporal variations in organic export flux and bottom water oxygenation. Although species distribution differed considerably during the Cretaceous, benthic foraminifera have been shown to provide powerful proxies for reconstructing the paleoenvironmental evolution of coastal basins (Gebhardt et al., 2004; Holbourn et al., 1999, 2001).

The relatively diverse shelf assemblages from the Mohammed Plage section reflect an overall deepening trend during the Cenomanian (Gebhardt et al., 2004). However, intensification of the oxygen minimum zone probably inhibited a diverse benthic foraminiferal community from becoming established on the shelf in the latest Cenomanian to early Turonian. The absence or low abundance of benthic foraminifers (>250 microns) at the base of El Amra and En Naila sections within laminated strata indicate dysoxic-anoxic bottom waters in the early Turonian, previously linked to the intensification of upwelling along the margin of the Tarfaya Basin (Kuhnt et al., 1990; Holbourn et al., 1999). The presence of relatively well preserved planktonic foraminifera throughout the section supports that the scarcity of benthic foraminifera does not reflect poor preservation in these intervals. The appearance of shelf benthic foraminifera tolerant of low-oxygen conditions at ~35 m in the El Amra section (middle Turonian) marks a slight improvement in bottom water oxygenation, possibly related to a seaward shift and/or decrease in the intensity of the oxygen minimum zone.

From the late Turonian to Santonian, benthic foraminiferal abundances increased, although diversity remained generally low with dominance of *Gavelinella* spp. at El Amra, Akhfennir and Tah North, suggesting relatively impoverished oxygenation at the sea-floor along the shelf. The higher variability of the Tah North record points to considerable temporal fluctuations in bottom water oxygenation. However, the marked decline in abundance and diversity in the upper part of the Tah North section points to an intensification and/or expansion of the oxygen minimum zone, possibly

related to the late Santonian transgressive event below sequence boundary Sa3. However, the correlation of this short interval of anoxia in the upper part of the Tah North succession to a more widespread global event is difficult to ascertain, as the upper part of the section is truncated by an unconformity (Fig. 4). The early Campanian assemblages from the Tisfourine and Tah West sections exhibit high diversity and abundance (Fig. 4; Holbourn et al., 1999), indicating an overall improvement in oxygenation at the sea-floor. However, the high abundance of buliminids and bolivinids together with the elevated marine organic matter content at Tah West point to an elevated organic export flux and vigorous upwelling along the margin of the basin (Holbourn et al., 1999).

3.2. Tarfaya Basin sea-level history and correlation to Cretaceous eustatic sequences

Sea-level was substantially higher than at present and exhibited considerable long- and short-term variability in the Cretaceous greenhouse world (Miller et al., 2005; Müller et al., 2008). Long-term eustatic sea-level changes were probably controlled by plate tectonics. Explanations include higher sea-floor spreading rates, due to hotter oceanic crust displacing sea water and causing long term flooding of continents (Kominz, 1984) or/and breakup of the supercontinent Pangaea, which may have led to overall subsidence of continents relative to the oceans during the Jurassic to Cretaceous. Miller et al., (2003; 2005) suggested that Late Cretaceous sea-level changes, which were relatively large (>25 m) and rapid (<1 m.y.), were glacioeustatic and probably driven by the periodic waxing and waning of ephemeral ice sheets in Antarctica, paced by Milankovitch forcing.

As the Tarfaya Basin remained tectonically stable during most of the Cretaceous, it provides an ideal location to reconstruct regional and global sea-level changes, based on the evolution of marginal marine sequences deposited along the basin edge. Lithological data, XRF derived terrigenous flux estimates, geochemical and micropaleontological estimates of bottom water oxygenation together with planktonic to benthic foraminiferal ratios were integrated to retrace the Cenomanian to Campanian sea-level history of the Tarfaya Basin. This reconstruction leads us to propose a tentative correlation of regional sea-level signals to eustatic changes and sequences suggested by Hardenbol et al. (1998).

3.2.1. Cenomanian to Campanian sea-level history of the Tarfaya Basin

In the Cenomanian succession of Mohammed plage, Kuhnt et al. (2009) identified two main transgressive cycles, separated by a regressive interval characterized by lagoonal lowstand deposits

indicating a transient sea-level fall of >30 m within a main transgressive trend. This long-term global sea-level rise led to major circulation and productivity changes and to the installation of an intensified oxygen minimum zone on the platform of the Tarfaya Basin during the late Cenomanian (Kuhnt and Wiedmann 1995; Kuhnt et al., 1997). Dysoxic-anoxic conditions at the peak of the transgression in the latest Cenomanian/early Turonian are marked by the absence of benthic foraminifera and enhanced preservation of organic matter. However, bioclastic limestone beds displaying hummocky cross-stratification, oblique lamination and erosive bases indicate that major storm events occurred during transient sea-level lowstands (El Albani et al., 1999b; Kuhnt et al., 2009).

In the En Naila section and at base of the El Amra section (Unit 1), the intercalation of lowstand limestone packages and highstand black shales corresponds to marked fluctuations in the XRF-scanner derived elemental composition of laminated organic rich (high Si, Fe and Al) and carbonate-rich (high Ca) deposits (Fig. 6 and Supplementary Fig. 5). These intervals, which are generally impoverished in benthic foraminifera (>250 μm), can be correlated to the last transgressive pulse of the early Turonian within the *H. helvetica* Zone (Fig. 6). In the later part of the Turonian (El Amra section, Unit 2), the basin experienced a major regressive phase with overall advance of the coastline, mainly indicated by generally higher abundances of benthic foraminifera and an increase in the ratio of benthic to planktonic foraminifera (Figs. 4 and 6).

The Coniacian to Santonian interval was marked by successive transgressive and regressive events, which are poorly resolved in the Akhfennir and El Amra (Unit 3) successions. Lumachelle layers (sparitic limestones with numerous shell fragments), which often have erosive basal contacts, can be interpreted as tempestites characterizing lowstands. However, the last transgressive pulse within the *D. asymetrica* zone in the latest Santonian relatively is well constrained in the Tah North section, where sample density and temporal resolution are substantially higher. The scarcity of benthic foraminifera in the upper part of the section points to an intensification of the oxygen minimum zone on the shelf of the Tarfaya Basin, possibly related to peak of the late Santonian transgression. The lower Campanian (*G. elevata* Zone) in the Tisfourine and Tah West sections (Holbourn et al., 1999) is characterized by planktonic and benthic assemblages indicating an outer shelf to upper bathyal environment, significantly deeper than during the Coniacian and most of the Santonian. The presence of marly deposits with increased log (Si/Ca) and log (Al/Ca) in the XRF-scanner data (Fig. 6) indicates a substantial increase in terrigenous flux, potentially linked to climatic

changes in the hinterland and/or tectonic movements at the margins of the basin during an initial phase of basin uplift, which continued during the Cenozoic (El Khatib et al., 1995).

3.2.2. Correlation to Cretaceous eustatic sequences

The prominent early Turonian highstand within the *H. helvetica* Zone, detected in the En Naila succession and at the base of the El Amra succession (Fig. 7), is most likely correlative to the sea-level highstand below the sequence boundary Tu1 of Hardenbol et al. (1998). In contrast, the higher abundances of benthic foraminifera and the presence of erosive bases in the upper Turonian (Unit 2 at El Amra, Fig. 7) indicate a shift of the oxygen minimum zone towards the open ocean associated with a lowering of the sea-level. This regressive phase probably corresponds to the major regressions associated with sequence boundaries Tu3 and Tu4 in Hardenbol et al. (1998).

The latest Turonian to early Coniacian decrease in $\delta^{13}C$ at the top of the El Amra section (starting within the *M. sigali* Zone at ~62 m in the El Amra Section and reaching a minimum within the lower part of the *D. concavata* Zone at ~90 m (15 m above the FO of *D. concavata*) may correspond to the Navigation Event in the Upper Cretaceous English chalk succession (Jarvis et al., 2006). Based on the delayed first occurrence of *D. concavata* in the Tarfaya basin (close to or above the Tu-Co boundary), the $\delta^{13}C$ minimum falls well into the Coniacian and clearly above the Tu4 sequence boundary. This event is associated with very variable conditions on the Tarfaya shelf, including dysoxic environments as shown by the relatively low abundance and diversity of benthic foraminifera and decrease in log(Mn/Ca). This interval probably reflects transgressive pulses associated with the sea-level highstand below the sequence boundary Co1. However, this transgressive trend is punctuated by carbonate-rich intervals characterized by oblique lamination as well as low log(Si/Ca) and log(Al/Ca), which may indicate transient regressive pulses. Similar oscillations close to the Navigation Event are indicated in the sea-level reconstruction of the Russian platform (Sahagian et al., 1996, Jarvis et al., 2006)

The early and middle Santonian sea-level history is poorly constrained in the Akhfennir outcrop section (Fig. 7). The overall increase in carbonate (decrease in log(Mn/Ca), log(Al/Ca), log(Si/Ca)) in the Tah North section may be related to a relative sea-level fall during the late Santonian, possibly corresponding with the eustatic sequence boundary Sa2. One of the most striking events in the sedimentary succession of the Tarfaya Basin is the prevalence of dysoxic-anoxic conditions in the latest Santonian as indicated by the absence or the low abundance and diversity of

benthic foraminiferal assemblages. This "dysoxic-anoxic event" is tentatively related to a major transgressive event in the latest Santonian, prior to the Sa3 sequence boundary in the Hardenbol et al. (1998) scheme.

Following the Sa-3 sequence boundary, which is represented by a hiatus in the Tarfaya sedimentary succession, high diversity benthic foraminiferal assemblages including bathyal species indicate a significant deepening of the sea-floor and somewhat improved oxygenation of bottom waters in the early Campanian, although productivity and organic carbon flux remained high (Holbourn et al., 1999). Enhanced fine-grained terrigenous sediment supply (increased log(Al/Ca) and log(SiCa)) and an increase in bulk carbonate $\delta^{18}O$ and $\delta^{13}C$ are probably related to the onset of global climate change at the Santonian-Campanian boundary (Ando et al., 2011). Although the deepening of the Tarfaya Basin in the early Campanian probably reflect local tectonic activity, it may also relates to several eustatic transgressive events, which occurred within the early Campanian *G. elevata* Zone.

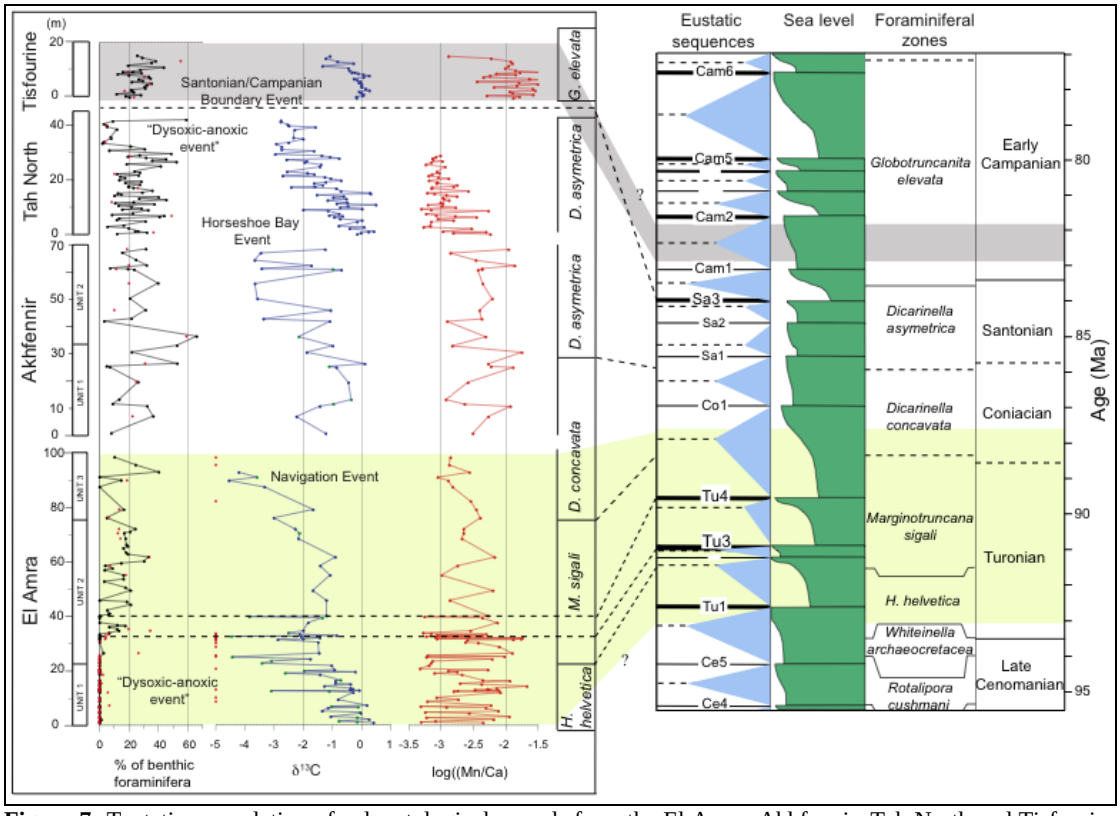

Figure 7: Tentative correlation of paleontological records from the El Amra, Akhfennir, Tah North and Tisfourine sections to eustatic sequences and sea-level history after Hardenbol et al. (1998). **a)** %benthic versus planktonic foraminifera; **b)** Bulk carbon isotope ($\delta^{13}C$); **c)** log (Mn/Ca). Foraminiferal zonation follows Robaszynki and Caron (1995), except for the base of the *G. concavata* Zone due to the later occurrence of *G. concavata* in the Tarfaya Basin. Green and blue shadings mark stratigraphic position of the El Amra and Tisfourine sections.

4. Conclusion

Lithological, paleontological, and geochemical data in five marginal marine successions were integrated to retrace the paleoenvironmental evolution and sea-level history of the Tarfaya Basin from the early Turonian to early Campanian. A global transgression during the early Turonian (En Naila and base of El Amra sections) led to the installation of an oxygen minimum zone on the platform of the Tarfaya Basin, resulting in increased deposition of organic matter and unfavourable conditions at the sea-floor for benthic foraminifera. In the middle Turonian, the appearance of low-oxygen tolerant benthic foraminiferal assemblages dominated by *Gavelinella* sp. (El Amra section, Unit 2) marks an improvement in water oxygenation at the sea-floor, probably associated with retraction of the oxygen minimum zone further offshore during a regressive phase. The late Santonian "dysoxic-anoxic event", only recorded in the Tah North section, may be related to a general intensification and expansion of the oxygen minimum zone in the eastern North Atlantic prior to the Santonian-Campanian boundary. High benthic foraminiferal diversity during the early Campanian (Tisfourine section) indicates a marked improvement in oxygenation at the sea-floor, although organic carbon export flux remained high, as shown by the marine organic matter content.

Bulk carbonate isotope data are tentatively correlated to the English Chalk carbon isotope reference curve of Jarvis et al. (2006), in particular the Hitch Wood Event in the late Turonian, the Navigation Event in the early Coniacian, the White Fall and the Horseshoe Bay Event in the Santonian and the Santonian/Campanian Boundary Event. Our results further suggest that the prominent early Turonian highstand corresponds to the last transgressive pulse below the sequence boundary Tu1 and that the regressive phase during the late Turonian is related to the major regression associated with sequence boundaries Tu3 and Tu4. The late Santonian "dysoxic-anoxic event" recorded in the upper part of the Tah North section possibly coincides with the eustatic sea-level rise prior to the Sa3 sequence boundary. The early Campanian transgressive event follows the Sa3 sequence boundary.

Further investigation will focus on two sedimentary cores (Tarfaya SN°1 and SN°2), newly drilled in the Tarfaya Basin, which provide a continuous and expanded record of shelf sedimentation from the Turonian to the Campanian. High resolution XRF core scanning data and bulk stable isotopes will allow to closely track short- and long-term variations in elemental composition and in

$\delta^{13}C$ and $\delta^{18}O$, thus providing an essential dataset to better understand the paleoceanographic evolution and the sea-level history of this marginal shelf basin during the Turonian to Campanian.

Acknowledgements

This research was funded by RWE-DEA and ONHYM in the framework of the Atlantic Margin Integrated Basin Analysis Project. We thank Colonel Jamal Balagh and Commandant Goto of the Moroccan Army for enabling access to remote outcrop sections during field expeditions. We thank Dr. Nils Andersen (Leibniz Laboratory for Radiometric Dating and Stable Isotope Research) for stable isotope measurements, Dr. Dieter Garbe-Schönberg for advice with the XRF scanner and Wolfgang Reimers, Samuel Müller and Moritz Kuest for technical help. We are also very grateful to Prof. Eduardo Koutsoukos for constructive editorial comments and to Prof. Mark Leckie and one anonymous reviewer for in depth reviews that helped us to improve the manuscript.

Supplementary Material of Chapter II. Late Cretaceous paleoenvironmental evolution of the Tarfaya Atlantic coastal Basin, SW Morocco

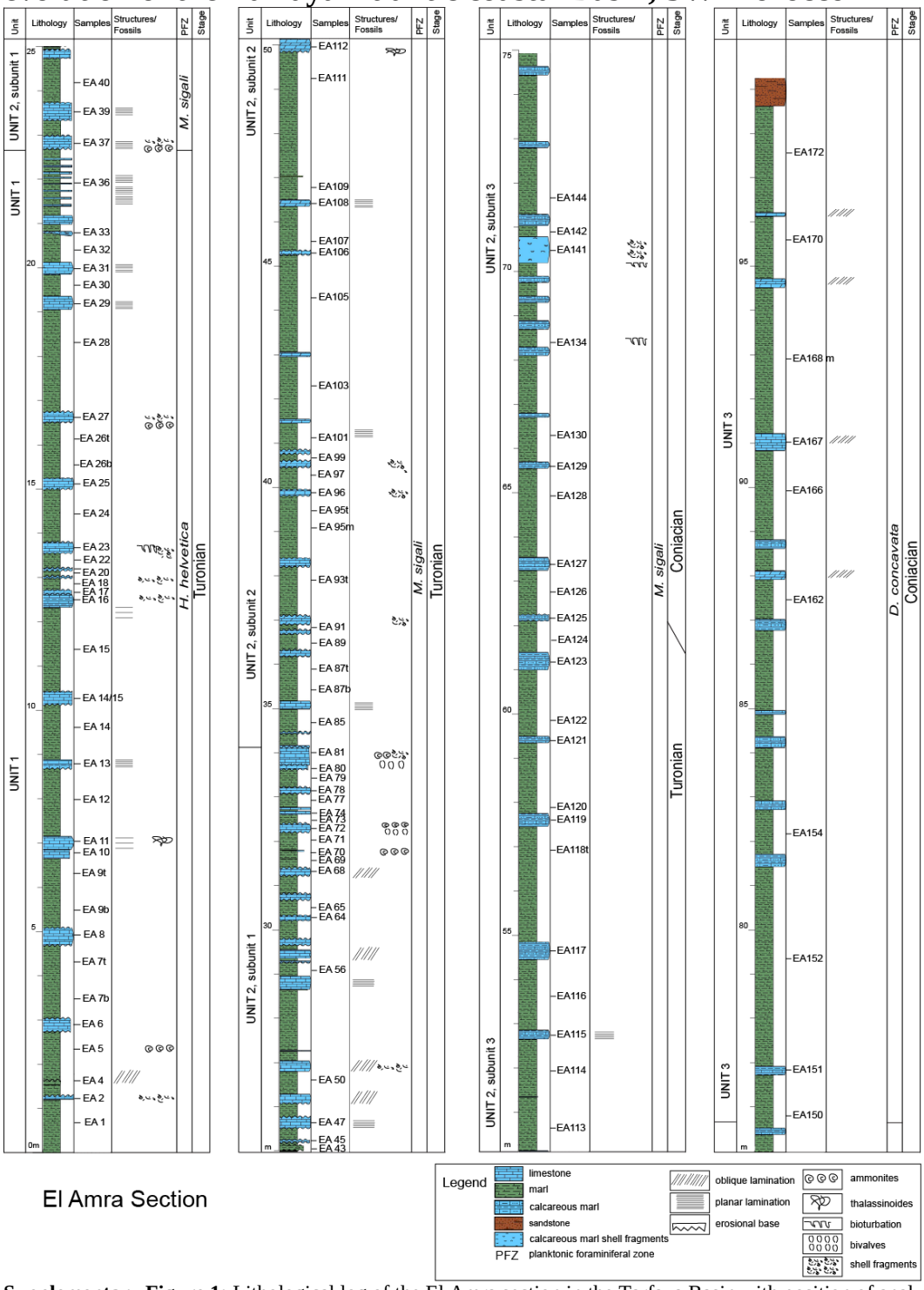

Supplementary Figure 1: Lithological log of the El Amra section in the Tarfaya Basin with position of analyzed samples.

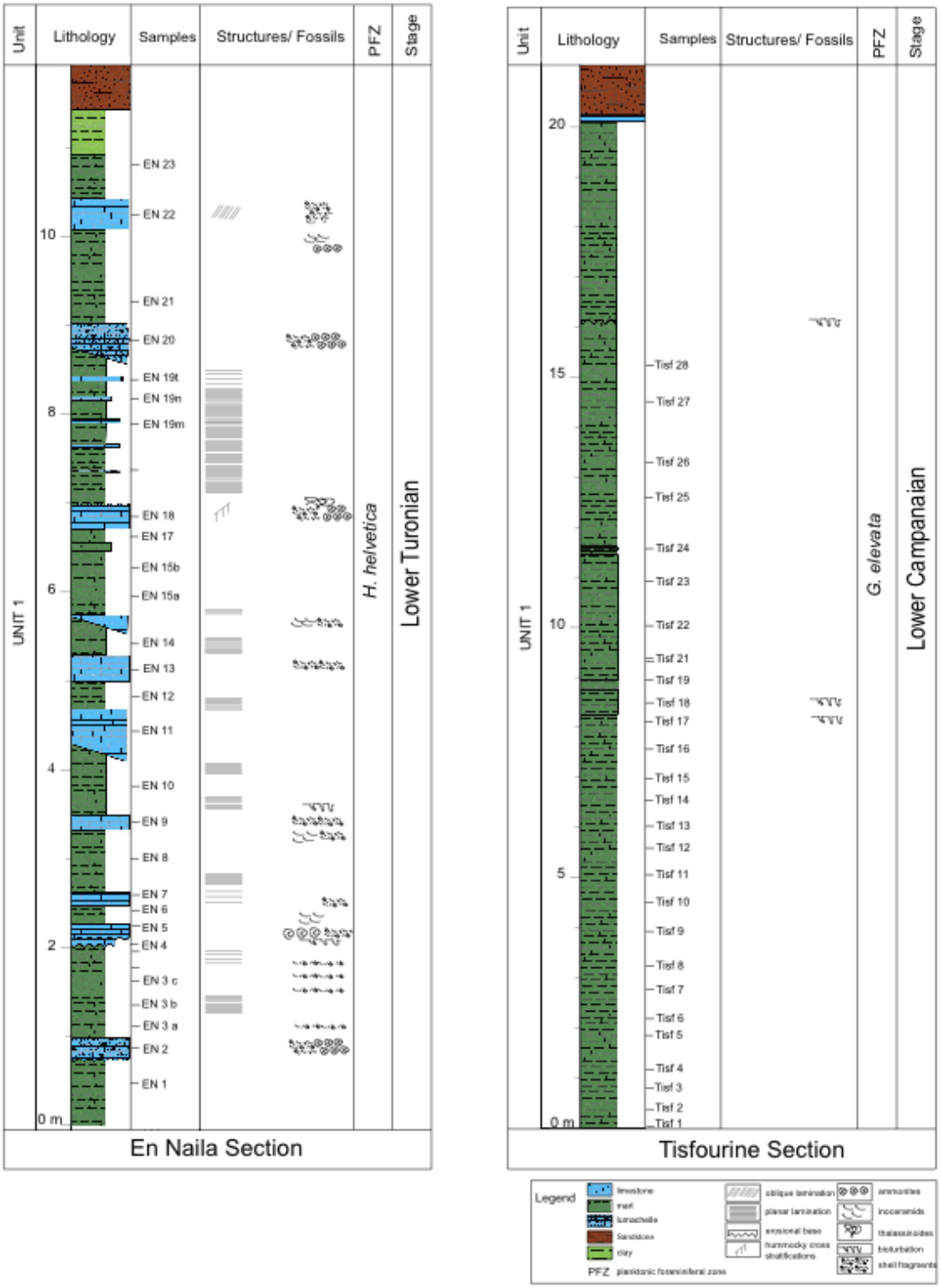

Supplementary Figure 2: Lithological log of the En Naila and Tisfourine sections in the Tarfaya Basin with position of analyzed samples.

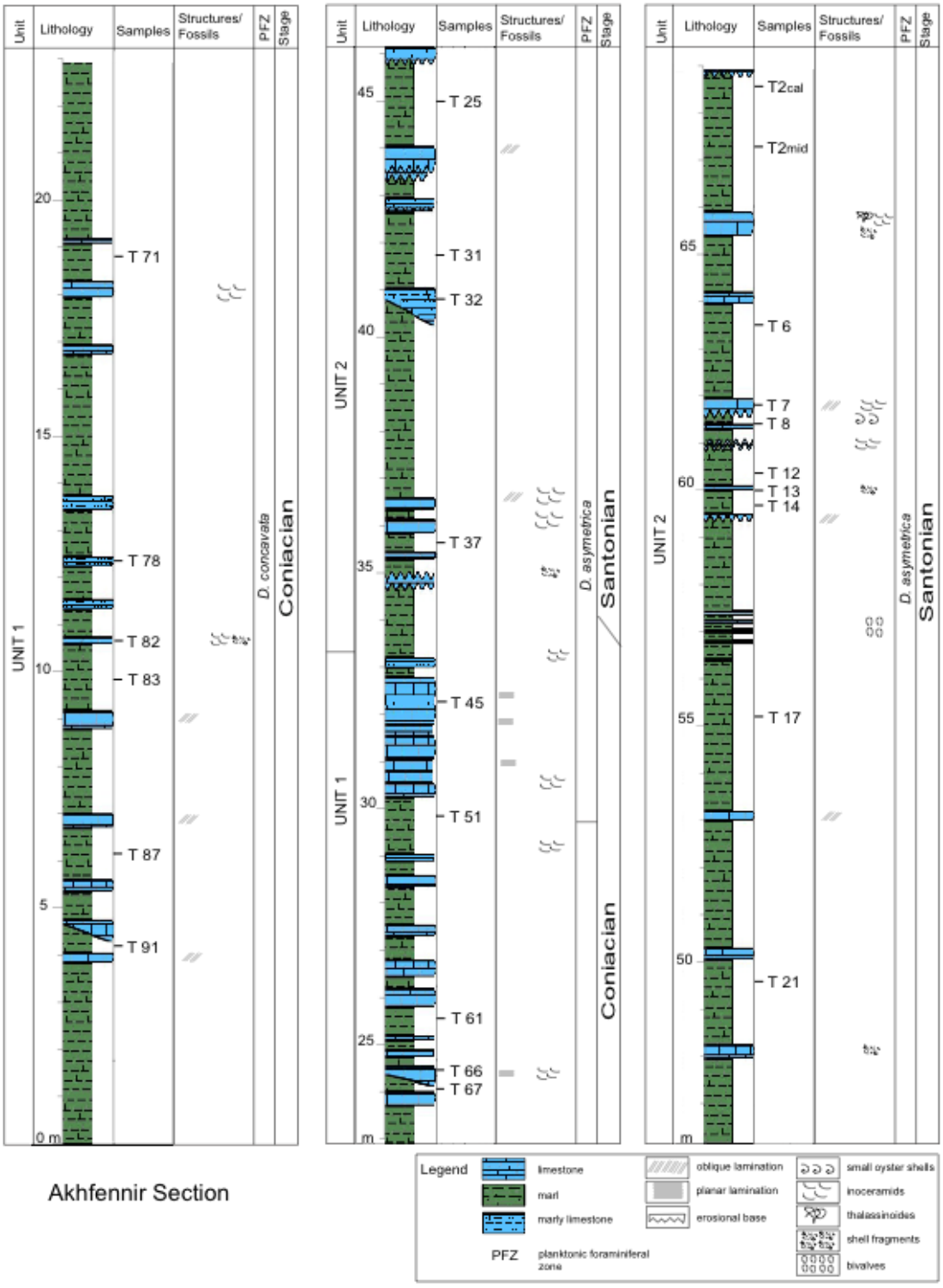

Supplementary Figure 3: Lithological log of the Akhfennir section in the Tarfaya Basin with position of analyzed samples.

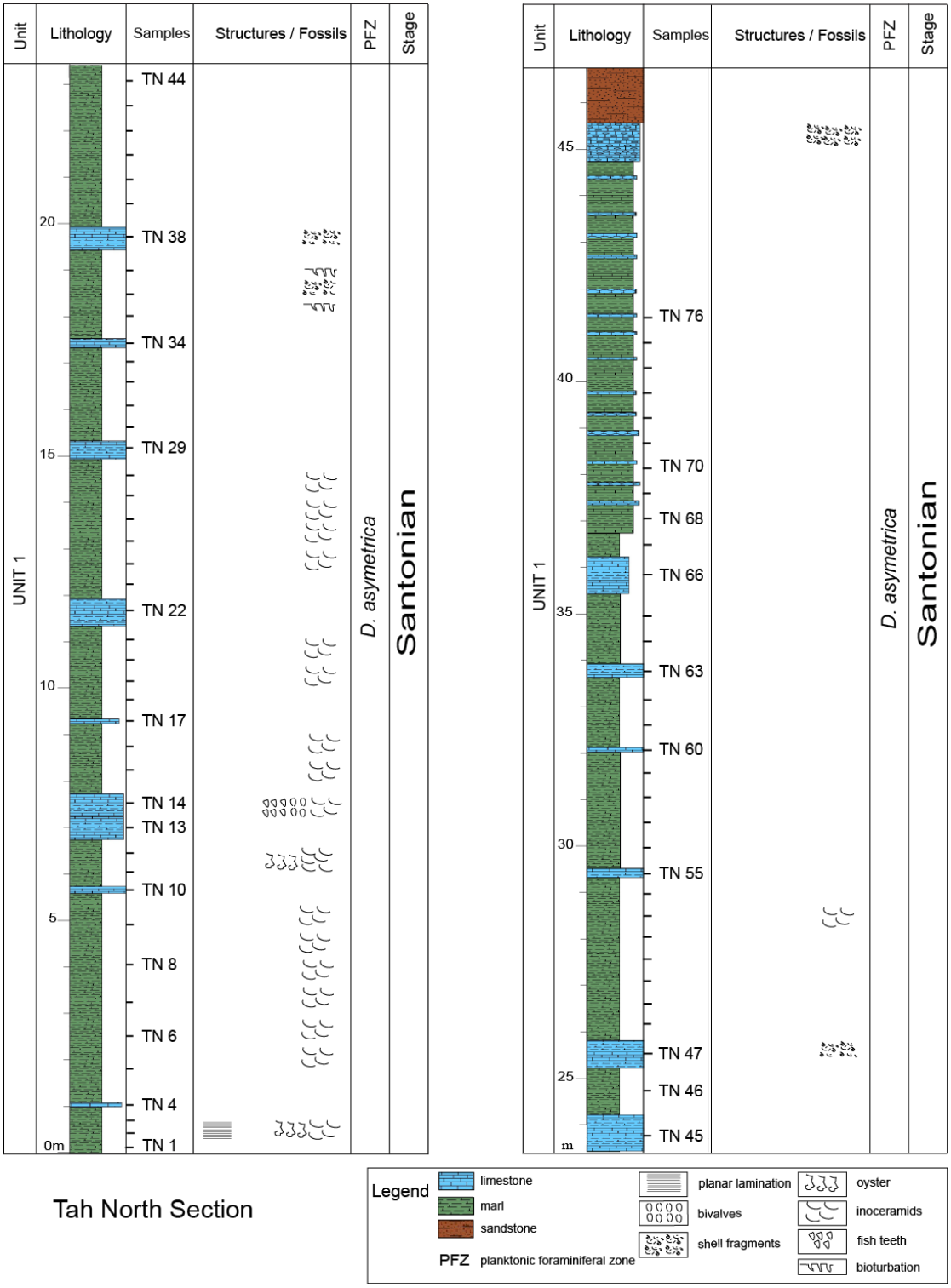

Supplementary Figure 4: Lithological log of the Tah North section in the Tarfaya Basin with position of analyzed samples.

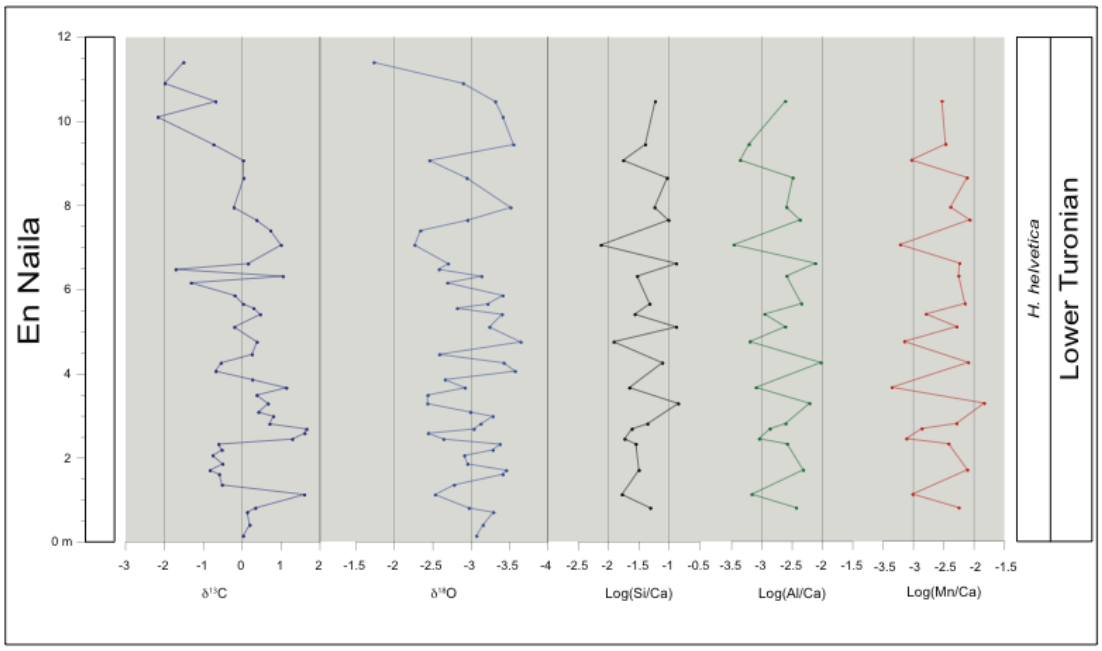

Supplementary Figure 5: Geochemical records in the En Naila section in the Tarfaya Basin based on isotope stratigraphy and log-ratios of elements (Si/Ca, Al/Ca and Mn/Ca) derived from X-ray fluorescence scanning.

Samples / species	Benthic Foraminifera						Number of benthic foraminifera picked in fraction 250-630 µm	Split	Reconverted total of benthic foraminifera from fraction 250-630 µm	Number of benthic foraminifera in fraction 250-630 µm per 100 g of unwashed sample	Diversity index (Shannon-Weaver index)	Number of species	%of benthic foraminifera
	Gavelinella sp.	*Flabellina* sp.	*Lenticulina articulata*	*Textularia* sp.	*Pyramidina szajnochae*	Indeterminate Taxa							
EA 172 top	37	1		15			53	1/8	424	412	0.683	3	10.20
EA 170	174						174	1/64	11136	7509	0.000	1	24.54
EA 168 mid	203						203	1/32	6496	7385	0.000	1	40.16
EA 167							0	0	0	0	0.000	0	0.00
EA 166	194						194	1/32	6208	8804	0.000	1	14.66
EA 162							0	0	0	0	0.000	0	0.00
EA 154	321						321	1/8	2568	6941	0.000	1	15.21
EA 152	445	10	2				457	1/32	14624	11066	0.133	3	16.45
EA 150	77						77	1/8	616	885	0.000	1	4.91
EA 144	77			3	424	1	505	1/16	2020	5008	0.476	4	24.30
EA 142	119				24		143	1/8	1144	2491	0.452	2	20.80
EA 141	182	4				51	237	1/32	7584	6936	0.602	3	16.69

EA 134	387						387	1/16	6192	6567	0.000	1	17.70
EA 130	65	1					66	1/16	1056	3345	0.079	2	18.30
EA 129	58	11					69	1/4	276	797	0.439	2	19.11
EA 128	71						71	1/8	568	1243	0.000	1	16.20
EA 127	144						144	1/8	1152	2880	0.000	1	18.03
EA 126	85						85	1/16	1360	4748	0.000	1	19.30
EA 125	23						23	1/16	368	902	0.000	1	20.50
EA 124	146						146	1/2	292	498	0.000	1	33.13
EA 123	99						99	1/32	3168	8050	0.000	1	30.30
EA 122	14					1	15	1/16	240	624	0.245	2	20.21
EA 121	12						12	1/8	96	375	0.000	1	14.70
EA 120	84						84	1/4	336	255	0.000	1	3.81
EA 119	54						54	1/16	864	1714	0.000	1	8.81
EA 118 top	4						4	1/8	32	75	0.000	1	3.46
EA 118					213		213	1/8	1704	1757	0.000	1	16.27
EA 116	1			3			4	1/4	16	57	0.562	2	16.24
EA 115		1					1	1/4	4	11	0.000	1	3.10
EA 113				4			4	1/16	64	151	0.000	1	17.60
EA 111	1						1	1	1	2	0.000	1	21.06
EA 107							0	0	0	0	0.000	0	0.00
EA 106	93						93	1/16	1488	3740	0.000	1	18.50
EA 105	104						104	1/8	832	2113	0.000	1	21.18
EA 103	36						36	1/8	288	809	0.000	1	5.29
EA 101	40		2				42	1/16	672	3100	0.191	2	6.84
EA 99	7						7	1/4	28	76	0.000	1	5.89
EA 97	1		2				3	1/2	6	23	0.637	2	0.01
EA 95 top	1						1	1/4	4	16	0.000	1	0.00
EA 95 mid	2						2	1/8	16	60	0.000	1	0.00
EA 93 top	12						12	1/8	96	275	0.000	1	0.00
EA 91	50	16					66	1/4	264	353	0.554	2	12.02
EA 89	23	7					30	1/8	240	1191	0.543	2	17.49
EA 87 top	8	5					13	1/2	26	68	0.666	2	6.53
EA 87 base	146						146	1/8	1168	2917	0.000	1	12.00
EA 85	104						104	1/4	416	1212	0.000	1	13.20
EA 81							0	0	0	0	0.000	0	6.53
EA 80							0	0	0	0	0.000	0	
EA 79	3						3	1/2	6	15	0.000	1	0.00
EA 78							0	0	0	0	0.000	0	
EA 77	2						2	1/2	4	17	0.000	1	0.00
EA 74							0	0	0	0	0.000	0	
EA 73							0	0	0	0	0.000	0	0.00
EA 72							0	0	0	0	0.000	0	
EA 71	2						2	1/2	4	16	0.000	1	0.00
EA 70 nod							0	0	0	0	0.000	0	
EA 70	3						3	1/2	6	15	0.000	1	0.00
EA 69							0	0	0	0	0.000	0	0.00
EA 68							0	0	0	0	0.000	0	

EA 65	3						3	1/2	6	9	0.000	1	0.00
EA 64							0	0	0	0	0.000	0	
EA 56							0	0	0	0	0.000	0	
EA 50	2	40					42	1/2	84	75	0.191	2	2.76
EA 47							0	0	0	0	0.000	0	
EA 45							0	0	0	0	0.000	0	
EA 43							0	0	0	0	0.000	0	
EA 40							0	0	0	0	0.000	0	0.00
EA 39							0	0	0	0	0.000	0	0.00
EA 37							0	0	0	0	0.000	0	0.00
EA 36	3						3	1/2	6	17	0.000	1	0.00
EA 33							0	0	0	0	0.000	0	
EA 32							0	0	0	0	0.000	0	0.00
EA 31							0	0	0	0	0.000	0	0.00
EA 30							0	0	0	0	0.000	0	0.00
EA 29							0	0	0	0	0.000	0	
EA 28							0	0	0	0	0.000	0	0.00
EA 27							0	0	0	0	0.000	0	
EA 26 top							0	0	0	0	0.000	0	0.00
EA 26 base							0	0	0	0	0.000	0	0.00
EA 25							0	0	0	0	0.000	0	0.00
EA 24							0	0	0	0	0.000	0	0.00
EA 23							0	0	0	0	0.000	0	
EA 22							0	0	0	0	0.000	0	0.00
EA 21							0	0	0	0	0.000	0	
EA 20							0	0	0	0	0.000	0	0.00
EA 18							0	0	0	0	0.000	0	0.00
EA 17							0	0	0	0	0.000	0	0.00
EA 16							0	0	0	0	0.000	0	0.00
EA 15							0	0	0	0	0.000	0	0.00
EA 14/15							0	0	0	0	0.000	0	0.00
EA 14							0	0	0	0	0.000	0	0.00
EA 13							0	0	0	0	0.000	0	
EA 12 base							0	0	0	0	0.000	0	
EA 11							0	0	0	0	0.000	0	0.00
EA 10							0	0	0	0	0.000	0	0.00
EA 9 top							0	0	0	0	0.000	0	0.00
EA 9 base							0	0	0	0	0.000	0	0.00
EA 8							0	0	0	0	0.000	0	
EA 7 top							0	0	0	0	0.000	0	0.00
EA 7 base							0	0	0	0	0.000	0	0.00
EA 6							0	0	0	0	0.000	0	
EA 5		4					4	1/2	8	16	0.000	1	1.23
EA 4							0	0	0	0	0.000	0	0.00
EA 2							0	0	0	0	0.000	0	
EA 1							0	0	0	0	0.000	0	0.00

Supplementary Table 1: Benthic foraminiferal census counts in the El Amra outcrop section, Tarfaya Basin (250-630 µm size fractions).

Samples / species	Benthic Foraminifera												Number of benthic foraminifera picked in fraction 150-250 µm	Split	Reconverted total of benthic foraminifera from fraction 150-250 µm	Number of benthic foraminifera in fraction 150-250 µm per 100 g of unwashed sample	Diversity index (Shannon-Weaver index)	Number of species
	Gavelinella sp.	Buliminids	*Lenticulina articulata*	*Gyroidinoides nitidus*	*Pyramidulina* sp.	*Flabellina* sp.	*Stilostomella alexanderi*	*Globulina* spp.	*Ramulina* sp.	*Spiroplectammina cretosa*	*Siphogenerinoides* sp.	Indeterminate Taxa						
Tisf 26	17	4	18	36	11			6	2	2	2	2	100	1/512	51200	38463	1.831	10
Tisf 21	16		8	9	5			17	6	4		3	68	1/512	34816	28292	1.917	8
Tisf 16	40	8	6	5	11		3	16	7			3	99	1/512	50688	46605	1.828	9
Tisf 11	38	4	12	8	6	2	1	10	5	2		6	94	1/128	12032	13638	1.931	11
Tisf 6	14		16	22	7		4	28	14		2	4	111	1/256	28416	31394	1.956	9
Tisf 1	17	11	10	12	11		2	25	2	4		4	98	1/1024	100352	78529	2.053	10
TN 2	46											7	53	1/128	6784	20366	0.390	2
TN 12	148												148	1/256	37888	102873	0.000	1
TN 22	27	7											34	1/512	17408	45040	0.508	2
TN 32	62	1											63	1/512	32256	93172	0.082	2
TN 42	16												16	1/256	4096	7753	0.000	1
TN 52	136												136	1/256	34816	96738	0.000	1
TN 62	5	2											7	1/256	1792	5238	0.598	2
TN 72	15												15	1/512	7680	18422	0.000	1
T 2 m	21	9										16	46	1/256	11776	21864	1.044	3
T 8	12	2											14	1/1024	14336	9790	0.410	2
T 13	25	1											26	1/1024	26624	40248	0.163	2
T 17	44	6											50	1/1024	51200	60721	0.367	2
T 25	25	5											30	1/1024	30720	43630	0.451	2
T 37	131	3											134	1/1024	137216	204069	0.107	2
T 61	38	1											39	1/1024	39936	76272	0.119	2
T 71	101	2											103	1/512	52736	192327	0.096	2
T 87	84												84	1/2048	172032	167509	0.000	1
EA 166	37	9											46	1/1024	47104	66805	0.494	2
EA 152	134	5											139	1/1024	142336	107708	0.155	2
EA 150	13	5											18	1/256	4608	6623	0.591	2
EA 144	3	17										5	25	1/512	12800	31738	0.839	3

EA 141	37	3											40	1/1024	40960	37461	0.266	2
EA 134	19	4											23	1/512	11776	12490	0.462	2
EA 124	45	9											54	1/128	6912	23566	0.451	2
EA 120	20	2											22	1/256	5632	17080	0.305	2
EA 118	3	47											50	1/1024	51200	6598	0.227	2
EA 89																		1
EA 87 t																		1
EA 87 b																		1
EA 85																		1
EA 81													0	0	0	0	0.000	0
EA 80																		
EA 79																		1
EA 78																		
EA 77																		1
EA 74																		
EA 73																		1
EA 72													0	0	0	0	0.000	0
EA 71																		1
EA 70 n																		
EA 70													0	0	0	0	0.000	0
EA 69													0	0	0	0	0.000	0
EA 68																		
EA 65													0	0	0	0	0.000	0
EA 64																		
EA 56																		
EA 50																		2
EA 47																		
EA 45																		
EA 43																		
EA 40													0	0	0	0	0.000	0
EA 39													0	0	0	0	0.000	0
EA 37													0	0	0	0	0.000	0
EA 36													0	0	0	0	0.000	0
EA 33																		
EA 32													0	0	0	0	0.000	0
EA 31													0	0	0	0	0.000	0
EA 30													0	0	0	0	0.000	0
EA 29													0					
EA 28													0	0	0	0	0.000	0
EA 27																		
EA 26 t													0	0	0	0	0.000	0
EA 26 b													0	0	0	0	0.000	0
EA 25													0	0	0	0	0.000	0
EA 24													0	0	0	0	0.000	0
EA 23													0					
EA 22													0	0	0	0	0.000	0
EA 21													0					

EA 20													0	0	0	0	0.000	0
EA 18													0	0	0	0	0.000	0
EA 17													0	0	0	0	0.000	0
EA 16													0	0	0	0	0.000	0
EA 15													0	0	0	0	0.000	0
EA 14/15													0	0	0	0	0.000	0
EA 14													0	0	0	0	0.000	0
EA 13													0					
EA 12 base																		
EA 11													0	0	0	0	0.000	0
EA 10													0	0	0	0	0.000	0
EA 9 top													0	0	0	0	0.000	0
EA 9 base													0	0	0	0	0.000	0
EA 8																		
EA 7 top													0	0	0	0	0.000	0
EA 7 base													0	0	0	0	0.000	0
EA 6																		
EA 5													0	0	0	0	0.000	0
EA 4													0	0	0	0	0.000	0
EA 2																		
EA 1													0	0	0	0	0.000	0

En 24													-	-	-	-	-	-
En 23													-	-	-	-	-	-
En 22													-	-	-	-	-	-
En 21 a													-	-	-	-	-	-
En 21													-	-	-	-	-	-
En 20													-	-	-	-	-	-
En 19 top													-	-	-	-	-	-
En 19 mid													-	-	-	-	-	-
En 19 45cm													-	-	-	-	-	-
En 19 a													-	-	-	-	-	-
En 18													-	-	-	-	-	-
En 16													-	-	-	-	-	-
En 15 b													-	-	-	-	-	-
En 15													-	-	-	-	-	-
En 15 a													-	-	-	-	-	-
En 14 b													-	-	-	-	-	-
En 14													-	-	-	-	-	-
En 14 a													-	-	-	-	-	-
En 13													-	-	-	-	-	-
En 12													-	-	-	-	-	-
En 11													-	-	-	-	-	-
En 10 c													-	-	-	-	-	-
En 10													-	-	-	-	-	-
En 10 b													-	-	-	-	-	-
En 10 a													-	-	-	-	-	-

En 9													-	-	-	-	-	-
En 8 c													-	-	-	-	-	-
En 8													-	-	-	-	-	-
En 8 b													-	-	-	-	-	-
En 8 a													-	-	-	-	-	-
En 7													-	-	-	-	-	-
En 6													-	-	-	-	-	-
En 6 a													-	-	-	-	-	-
En 5													-	-	-	-	-	-
En 4													-	-	-	-	-	-
En 3 e													-	-	-	-	-	-
En 3 d													-	-	-	-	-	-
En 3 c													-	-	-	-	-	-
En 3													-	-	-	-	-	-
En 3 b													-	-	-	-	-	-
En 3 a													-	-	-	-	-	-
En 2													-	-	-	-	-	-
En 1													-	-	-	-	-	-
En 1 b													-	-	-	-	-	-
En 1 a													-	-	-	-	-	-
En 1 base													-	-	-	-	-	-

Supplementary Table 2: Benthic foraminiferal census counts in the El Amra, Akhfennir, Tah North, Tisfourine and En Naila outcrop sections, Tarfaya Basin (125-250 µm size fractions).

Samples / species	Benthic Foraminifera	Number of benthic foraminifera picked in fraction 150-250 µm	Split	Reconverted total of benthic foraminifera from fraction 150-250 µm	in fraction 150-250 µm per 100 g of unwashed sample	Diversity index (Shannon-Weaver index)	Number of species
En 24	-	-	-	-	-	-	-
En 23	-	-	-	-	-	-	-
En 22	-	-	-	-	-	-	-
En 21 a	-	-	-	-	-	-	-
En 21	-	-	-	-	-	-	-
En 20	-	-	-	-	-	-	-
En 19 top	-	-	-	-	-	-	-
En 19 middle	-	-	-	-	-	-	-
En 19 45 cm	-	-	-	-	-	-	-

En 19 a	-	-	-	-	-	-	-
En 18	-	-	-	-	-	-	-
En 16	-	-	-	-	-	-	-
En 15 b	-	-	-	-	-	-	-
En 15	-	-	-	-	-	-	-
En 15 a	-	-	-	-	-	-	-
En 14 b	-	-	-	-	-	-	-
En 14	-	-	-	-	-	-	-
En 14 a	-	-	-	-	-	-	-
En 13	-	-	-	-	-	-	-
En 12	-	-	-	-	-	-	-
En 11	-	-	-	-	-	-	-
En 10 c	-	-	-	-	-	-	-
En 10	-	-	-	-	-	-	-
En 10 b	-	-	-	-	-	-	-
En 10 a	-	-	-	-	-	-	-
En 9	-	-	-	-	-	-	-
En 8 c	-	-	-	-	-	-	-
En 8	-	-	-	-	-	-	-
En 8 b	-	-	-	-	-	-	-
En 8 a	-	-	-	-	-	-	-
En 7	-	-	-	-	-	-	-
En 6	-	-	-	-	-	-	-
En 6 a	-	-	-	-	-	-	-
En 5	-	-	-	-	-	-	-
En 4	-	-	-	-	-	-	-
En 3 e	-	-	-	-	-	-	-
En 3 d	-	-	-	-	-	-	-
En 3 c	-	-	-	-	-	-	-
En 3	-	-	-	-	-	-	-
En 3 b	-	-	-	-	-	-	-
En 3 a	-	-	-	-	-	-	-
En 2	-	-	-	-	-	-	-
En 1	-	-	-	-	-	-	-
En 1 b	-	-	-	-	-	-	-
En 1 a	-	-	-	-	-	-	-
En 1 base	-	-	-	-	-	-	-

Supplementary Table 3: Benthic foraminiferal census counts in the En Naila outcrop section, Tarfaya Basin (250-630 µm size fractions).

Sample / species	Benthic Foraminifera				Number of benthic foraminifera picked in fraction 250-630 µm	Split	Reconverted total of benthic foraminifera from fraction 250-630 µm	Number of benthic foraminifera in fraction 250-630 µm per 100 g of unwashed sample	Diversity index (Shannon-Weaver index)	Number of species	%of benthic foraminifera
	Gavelinella sp.	*Neobulimina* sp.	*Flabellina* sp.	*Textularia* sp.							
T 2 melk	335				335	1/8	2680	4975	0.000	1	31.53
T 2 cal	140				140	1/32	4480	4630	0.000	1	15.40
T 6	193		2		195	1/32	6240	5274	0.057	2	24.69
T 7	22				22	1/8	176	462	0.000	1	28.71
T 8	141				141	1/32	4512	3081	0.000	1	31.96
T 12	84				84	1/32	2688	2347	0.000	1	7.17
T 13	182		1		183	1/16	2928	4426	0.034	2	19.26
T 14	283				283	1/64	18112	17944	0.000	1	23.51
T 17	398				398	1/32	12736	15103	0.000	1	39.80
T 21	310				310	1/16	4960	11659	0.096	1	20.63
T 25	195				195	1/32	6240	8861	0.000	1	31.33
T 31	147				147	1/128	18816	16846	0.000	1	21.70
T 32	14				14	1/8	112	122	0.683	1	3.16
T 37	387				387	1/64	24768	36835	0.000	1	65.87
T 45	280	100			380	1/128	48640	33168	0.576	2	52.50
T 51	448			22	470	1/32	15040	21002	0.189	2	21.87
T 61	267				267	1/32	8544	16316	0.000	1	52.79
T 66	66				66	1/32	2112	5363	0.000	1	4.86
T 67	83				83	1/8	664	1143	0.000	1	7.14
T 71	334				334	1/16	5344	19484	0.000	1	26.33
T 78	115				115	1/16	1840	6352	0.000	1	13.39
T 82	35				35	1/32	1120	1963	0.000	1	8.89
T 83	255	83			338	1/16	5408	6998	0.557	2	32.42
T 87	476	11			487	1/128	62336	60695	0.108	2	36.46
T 91	45	85			130	1/16	2080	3370	0.645	2	7.90

Supplementary Table 4: Benthic foraminiferal census counts in the Akhfennir outcrop section, Tarfaya Basin (250-630 µm size fractions).

Sample / species	Benthic Foraminifera						Number of benthic foraminifera picked in fraction 250-630 µm	Split	Reconverted total of benthic foraminifera from fraction 250-630 µm	Number of benthic foraminifera in fraction 250-630 µm per 100 g of unwashed sample	Diversity index (Shannon-Weaver index)	Number of species	%of benthic foraminifera
	Gavelinella sp.	*Flabellina* sp.	*Neobulimina* sp.	*Textularia* sp.	*Frondicularia lanceola*	*Lenticulina articulata*							
TN 76	96						96	4/16	384	2119	0.000	1	58.81
TN 75	54					1	55	2/16	440	1193	0.091	2	8.99
TN 74	5						5	1/16	80	249	0.000	1	2.68
TN 73	2	2					4	1/16	128	311	0.693	2	2.88
TN 72	15		2				17	1/16	272	757	0.362	2	4.73
TN 71	26		1				27	1/16	864	2487	0.158	2	5.02
TN 70	14					1	15	1/16	480	1287	0.245	2	5.66
TN 69	56						56	2/16	448	1465	0.000	1	11.74
TN 68	50						50	1/16	800	2993	0.000	1	7.48
TN 67	42						42	2/16	336	1202	0.000	1	10.02
TN 66	5						5	2/16	40	144	0.000	1	3.49
TN 65	40						40	2/16	320	1218	0.000	1	7.60
TN 64	24	7	6				37	1/16	592	3161	0.891	3	7.83
TN 63	2						2	1/16	32	91	0.000	1	2.01
TN 62	10						10	4/16	40	216	0.000	1	2.68
TN 61	3		1				4	2/16	32	134	0.562	2	2.01
TN 60	5						5	2/16	40	88	0.000	1	1.71
TN 59	117	17					134	1/16	4288	11953	0.380	2	21.04
TN 58	120						120	1/16	1920	3927	0.000	1	23.96
TN 57	57		63				120	1/16	1920	6434	0.692	2	30.68
TN 56	22	4					26	2/16	208	656	0.429	2	6.60
TN 55	32						32	1/16	512	1425	0.000	1	23.20
TN 54	117						117	1/16	1872	6525	0.000	1	48.64
TN 53	172		1				173	2/16	1384	3712	0.036	2	27.15
TN 52	128						128	2/16	1024	2845	0.000	1	19.19
TN 51	131						131	1/16	4192	11129	0.000	1	31.51
TN 50	340						340	1/16	5440	9989	0.000	1	45.05
TN 49	95						95	1/16	3040	10261	0.000	1	35.71
TN 48	122						122	1/16	3904	10378	0.000	1	52.22
TN 47	101						101	1/16	1616	6433	0.000	1	18.40
TN 46	217						217	1/16	3472	6355	0.000	1	41.50
TN 45	26						26	1/16	832	1695	0.000	1	20.20
TN 44	49		1				50	1/16	800	1681	0.098	2	23.71
TN 43	149						149	1/16	4768	9379	0.000	1	27.32
TN 42	55		9				64	2/16	512	1298	0.406	2	11.87

TN 41	182	1	2				185	1/16	5920	19536	0.093	3	26.46
TN 40	54		1				55	2/16	440	1995	0.091	2	14.05
TN 39	53		3				56	2/16	448	1420	0.209	2	17.22
TN 38	47		7				54	1/16	864	2074	0.386	2	13.43
TN 37	66		2				68	1/16	1088	2640	0.133	2	28.28
TN 36	182		10				192	1/16	6144	12715	0.205	2	17.45
TN 35	109		6				115	1/16	1840	4961	0.205	2	27.49
TN 34	73		2				75	1/16	1200	3137	0.123	2	19.55
TN 33	136		11				147	1/16	4704	12534	0.266	2	19.44
TN 32	141	1					142	2/16	1136	3471	0.042	2	22.99
TN 31	96		1				97	2/16	776	3313	0.057	2	25.26
TN 30	75	1					76	2/16	608	2139	0.070	2	35.78
TN 29	168	4	8				180	1/16	5760	15110	0.287	3	29.00
TN 28	46	4					50	2/16	400	1526	0.279	2	12.43
TN 27	125	1	1				127	2/16	1016	3973	0.092	3	14.73
TN 26	19						19	2/16	152	756	0.000	2	10.07
TN 25	189		1				190	2/16	1520	4488	0.033	2	40.09
TN 24	173	2	1				176	2/16	1408	5844	0.097	3	26.87
TN 23	258						258	1/16	4128	12973	0.000	2	45.27
TN 22	58		5				63	1/16	1008	3297	0.277	2	23.05
TN 21	60		1				61	2/16	488	2076	0.084	2	10.60
TN 20	103		3				106	2/16	848	3578	0.129	2	37.32
TN 19	129	3					132	2/16	1056	2896	0.108	2	12.85
TN 18	53						53	2/16	424	1355	0.000	1	21.66
TN 17	137		2				139	1/16	4448	13725	0.075	2	28.58
TN 16	122		7				129	1/16	2064	7434	0.211	2	15.42
TN 15	88						88	2/16	704	2610	0.000	1	33.03
TN 14	218	1	2				221	2/16	1768	6906	0.080	3	22.59
TN 13	128				1		129	1/16	2064	6351	0.045	2	8.37
TN 12	229						229	1/16	3664	12056	0.000	1	43.94
TN 11	135	4					139	4/16	556	1743	0.130	2	40.75
TN 10	156	1					157	2/16	1256	5294	0.039	2	13.38
TN 9	46	1	1				48	1/16	768	2695	0.202	3	11.66
TN 8	31						31	1/16	496	2202	0.000	1	31.19
TN 7	106	1	1				108	1/16	1728	6348	0.105	3	16.41
TN 6	29						29	4/16	116	554	0.000	1	5.35
TN 5	34						34	2/16	272	995	0.000	1	19.69
TN 4	88	1					89	2/16	712	2623	0.062	2	26.24
TN 3	70	1					71	1/16	1136	3655	0.074	2	24.22
TN 2	59	3		20			82	2/16	656	3918	0.702	3	32.17
TN 1	23	2					25	1/16	400	1181	0.279	2	11.87

Supplementary Table 5: Benthic foraminiferal census counts in the Tah North outcrop section, Tarfaya Basin (250-630 µm size fractions).

Samples / species		Tisf 28	Tisf 27	Tisf 26	Tisf 25	Tisf 24	Tisf 23	Tisf 22	Tisf 21	Tisf 20	Tisf 19	Tisf 18
Benthic Foraminifera	*Gavelinella dakotensis*	12	11	32	22	8	5	3	10	2	7	15
	Lingulogavelinella sp.	45	20	25	15	13	26	29	23	6	31	8
	Gyroidinoides nitidus	33	16	22	24	8	17	16	30	14	2	2
	Lenticulina articulata				44	15	18	8	15	14	17	29
	Globulina prisca				2			3				
	Flabellina sp.	4	6	1	5	1		3	1	2	4	1
	Pyramidulina sp.	3	7	2	8			1	3		2	3
	Stilostomella alexanderi	1	3	3		3	2	2	15	7	5	2
	Osangularia cordieriana		5	4		20	27					
	Lenticulina sp.	30	11	12								
	Frondicularia lanceola	1	2		3	1		1	1			1
	Siphogenerinoides sp.	2	6	11		1	8	11	10	5	14	4
	Marginulinopsis curvisepta										1	
	Marginulina bullata	3	3		1	1		3		1		2
	Spiroplectammina cretosa	4		5	38	26	26	32	17	8	2	4
	Ramulina sp.	3	3	6	4	1	1	2	5	1	11	4
	Pseudonodosaria humilis	1			3							
	Laevidentalina spp.				8			3	3	2	1	
	Lingulonodosaria sp.											1
	Pleurostomella subnodosa											1
	Pseudoclavulina sp.	2				1	1	8	3			
	Siphonodosaria sp.											1
	Marginulinopsis subrecta						1		1			
	Praebulimina sp.								4			
	Laevidentalina soluta					1		1				
	Pyramidulina obscura					1		1				
	Globulina spp.	3	5		1							
	Pyramidulina obsolescens			1								
	Indeterminate Taxa		3	1		1	1				2	
Number of benthic foraminifera picked in fraction 250-630 µm		147	101	125	178	102	133	127	141	62	99	78
Split		1/8	1/8	1/8	1/8	1/16	1/8	1/8	1/16	1/8	1/16	1/16
Reconverted total of benthic foraminifera from fraction 250-630 µm		1176	808	1000	1424	1632	1064	1016	2256	496	1584	1248
Number of benthic foraminifera in fraction 250-630 µm per 100 g of sample		1195	633	715	1267	1000	1053	1158	1781	694	1309	1257
Diversity index (Shannon-Weaver index)		1.959	2.409	2.072	2.123	2.123	1.998	2.231	2.303	2.077	2.063	2.062
Number of species		15	14	13	14	16	12	17	15	11	13	15
% of benthic foraminifera		25.59	28.93	38.04	35.31	19.36	43.63	27.64	22.52	15.73	28.41	12.32

Tisf 17	Tisf 16	Tisf 15	Tisf 14	Tisf 13	Tisf 12	Tisf 11	Tisf 10	Tisf 9	Tisf 8	Tisf 7	Tisf 6	Tisf 5	Tisf 4	Tisf 3	Tisf 2	Tisf 1
8	16	50	26	8	4	18	25	25	38	52	25	30	20	38	24	42
16	48	82	55	30	4	38	44	42	4		2	4	15	23		22
	34	68	30	30	21	18	3	8	14	10	17	3	1	5	20	
26	30	47	36	29	26	38	26	29	33	18	27	22	12	18	22	21
	5	2		1			2		1	1	1		1	6	1	11
6	4	6	5	5	3	9	7	6	6	11	4	2	7	3	1	2
	2	2	1		2	6	8	2	2	1	2		1			1
	1		4				3		2	6			5	1		
			3				13	6	33	15	14	4				
4		2	1	3	2	3	2		2	2				1	5	
4	8															
1					1	1										
	3					1		1								
	14	7	2	2	9				1					1		
2	1	4	1		1	4	1	4	6	1	3		2	1	1	1
		1	1						2	1						
1	1	1	3			1		1								
		1							1							
				1	3	1	2	1		3						
		1														
						0			2		2					2
68	167	274	168	109	76	138	136	125	147	121	97	65	64	97	74	102
1/8	1/8	1/8	1/8	1/8	1/2	1/4	1/4	1/8	1/8	1/4	1/8	1/8	1/16	1/8	1/16	1/16
544	1336	2192	1344	872	152	552	544	1000	1176	484	776	520	1024	776	1184	1632
456	1228	2469	936	734	183	613	764	1097	1138	599	936	569	733	949	1342	1277
1.735	1.980	1.748	1.804	1.654	1.846	1.885	1.927	1.787	1.998	1.796	1.816	1.316	1.762	1.642	1.436	1.507
9	13	14	13	9	11	12	12	11	15	12	10	6	9	10	7	8
19.85	33.30	34.54	26.51	29.30	21.77	35.23	32.19	30.72	31.04	21.31	22.24	23.20	11.55	27.99	17.65	20.37

Supplementary Table 6: Benthic foraminiferal census counts in the Tisfourine outcrop section, Tarfaya Basin (250-630 µm size fractions).

Chapter III. A complete archive of late Turonian to Campanian sedimentary deposition in newly drilled cores from the Tarfaya Basin, SW Morocco

Mohamed Aquit[1], Wolfgang Kuhnt[1], Ann Holbourn[1], El Hassane Chellai[2], Jacqueline A. Lees[3], Karl Stattegger[1], Oliver Kluth[4] and Haddou Jabour[5]

[1]Institute of Geosciences, Christian-Albrechts-University of Kiel, Germany

[2]Geology Department, Faculty of Sciences Semlalia, Cadi Ayyad Marrakech University, Morocco

[3]Department of Earth Sciences, University College London, Gower Street, London

[4]RWE Dea AG, Hamburg, Germany

[5]ONHYM, Rabat, Morocco

This paper is in preparation for submission in Geological Society of America Bulletin Journal.

Abstract

The upper Turonian to Campanian organic-rich successions, deposited in the continuously subsiding Tarfaya Atlantic coastal basin (SW Morocco), allow detailed reconstruction of depositional environments at the upper edge of an oceanic oxygen minimum zone impinging on a broad continental shelf. We present high-resolution X-ray fluorescence (XRF) scanning, bulk carbon and oxygen isotope records from two newly drilled sediment cores in the Tarfaya Basin (Tarfaya SN°1 (27° 57´ 43.1´´N, 12° 48´ 37.0´´W) and Tarfaya SN°2 (27° 42´ 36.6´´N, 12° 56´ 39.0´´W), which recovered a continuous upper Turonian to Campanian sedimentary succession of ~290 m thickness. The XRF core scanning records show three long-term oscillations in the abundance of terrigenous elements (increase of Al, Ti, K, Si and Fe normalized against Ca) during the Coniacian and Santonian. This interval, which roughly corresponds to the Coniacian-Santonian Anoxic Event (OAE-3), is characterized by overall oxygen depleted to anoxic conditions at the sea-floor (indicated by the high organic carbon content, the presence of laminations and by low manganese/sulphur, high vanadium/calcium and bromine/calcium ratios in XRF scanning records). A major change in environmental conditions during the early Campanian is reflected by enhanced accumulation of fine-grained carbonate and clay-rich hemipelagic sediments, indicating a substantial improvement in bottom water ventilation. Two major unconformities (U1/U2 and U3), which punctuate the upper Turonian to lower Campanian succession in Tarfaya SN°1 and 2, are correlative to the base of the Merchantville III and Magothy III sequence boundaries of Miller et al., (2004) and Mizintseva et al. (2009), respectively. Stable isotope data of bulk carbonates are correlated to the English Chalk, the Niobrara Formation (US Western Interior Seaway) and to the stacked carbon isotope reference curve of Wendler (2013). The Tarfaya carbon isotope curve reveals in particular the Navigation Event in the Coniacian, the Haven Brow, the Horseshoe Bay and the Buckle Events in the Santonian as well as the Santonian/Campanian Boundary Event. The early Campanian $\delta^{13}C$ record exhibits two long-term cycles (~2 – 2.4 Myr), which are probably related to variations in the Earth's eccentricity and are associated with a long-term trend of cooling and improving deep-water ventilation in the Tarfaya Basin.

Key words: Late Cretaceous, Tarfaya Basin, bulk carbon and oxygen isotopes, high-resolution X-ray fluorescence (XRF) scanning, oceanic anoxic event, sea-level.

1. Introduction

The Late Cretaceous was characterized by several Oceanic Anoxic Events (OAEs), marked by the widespread deposition of organic-rich black shales in coastal and open ocean areas (Schlanger and Jenkyns, 1976). These events have been associated with periods of rising sea-level and positive carbon isotope ($\delta^{13}C$) excursions related to global enhanced burial of ^{12}C-enriched organic matter (OM) (Arthur et al., 1990; Calvert and Pedersen, 1993). The paleoenvironmental conditions during these episodes of organic-rich deposition as well as the causes and consequences of attendant perturbations in biogeochemical cycles have been the subject of intense, and partly controversial, debate over the last decades (e.g., Gautier, 1987; Arthur et al., 1988; Arthur and Sageman, 1994; Brumsack, 2006). Unresolved issues include the global character of anoxic events, their sensitivity/response to orbital climate forcing, the frequency and amplitude of associated sea-level fluctuations, the possible triggering mechanisms such as voluminous volcanic CO_2 release and the nature of subsequent perturbations in the weathering and nutrient cycles.

Reconstructions of eustatic sea-level changes during the Cretaceous were initially based on global syntheses of sequence-stratigraphic data, which are still widely used as an exploration and first-order global correlation tool (Haq et al., 1988; Hardenbol et al., 1998; Haq, 2014). Eustatic curves were derived from the analyses and correlation of local and regional relative sea-level changes along the world's continental margins and resulted in the identification of as many as 58 third-order eustatic events in the Cretaceous (Haq, 2014). These potentially eustatic fluctuations are mainly expressed as relative rapid and large amplitude sea-level falls and most of them are documented in several basins, although the precise stratigraphic correlation of many events remains ambiguous (Miall, 2009; Haq, 2014). The causes for such rapid sea-level falls during the largely ice-free Cretaceous remain a matter of vigorous discussion. However, the buildup of transient ice sheets in Antarctica has been proposed as the most likely explanation (Miller et al., 2005; Flögel et al., 2011; Haq, 2014).

The expanded succession of organic-rich marlstones and limestones within the Tarfaya Basin provides an excellent opportunity to reconstruct climate evolution and sea-level changes through the late Turonian to early Campanian. This marginal basin along the East Atlantic passive continental margin was continuously subsiding during the late Albian to early Campanian, resulting in deposition of a ~700 m thick series of hemipelagic marlstones and limestones in the distal part of the basin close

to the present day coastline near the town of Tarfaya (Choubert et al., 1966; Wiedmann et al., 1978; Aquit et al., 2013). The sedimentary succession can be subdivided in a hierarchy of lithological units, from lithological units with thicknesses of several tens of meters, bedding in the scale of decimeter to meters to fine lamination on the millimeter scale. Several Upper Cretaceous sequences (unconformity-bounded units) were discriminated in outcrop sections (Choubert et al., 1966; Aquit et al., 2013), and excellent age control can be achieved with abundant planktonic foraminifers, ammonites and calcareous nannoplankton in partly excellent preservation (Choubert et al., 1966; Lehman et al., 1966; Wiedmann et al., 1978; Kuhnt et al., 1995, 1997, 2004, 2009). Previous studies mainly focused on the intensity of anoxia, the magnitude and nature of the $\delta^{13}C$ excursion, the biotic effects on benthic and planktonic foraminifera, biostratigraphic records and paleo-environmental evolution during the Cenomanian/Turonian OAE-2 event (e.g., El Albani et al., 1999 a, b; Holbourn et al., 1999; Kuhnt et al., 1997, 2005, 2009; Kolonic et al., 2002, 2005; Mort et al., 2007, 2008; Gertsch et al., 2010; Aquit et al., 2013).

Here, we analyse a 290 m composite record of late Turonian to early Campanian sedimentation from two drill cores, recovered in 2009 in the central part of the Tarfaya Basin close to the Sebkha Tah and the town of Tarfaya. Our main objectives are (1) to reconstruct the paleoenvironmental evolution and sea-level changes of the Tarfaya coastal basin during the late Turonian to early Campanian, based on visual core description, bulk carbonate stable isotopes and X-ray fluorescence scanner derived elemental distribution data; (2) to correlate Upper Cretaceous successions in the newly drilled cores with more proximal outcrop sections (Aquit et al., 2013); (3) to date and correlate observed unconformities (based on carbon isotope and elemental ratio fluctuations and inferred sequence boundaries) to unconfomities in other sedimentary basins, and (4) to compare the local sea-level record to other sea-level curves (Hardenbol et al., 1998; Miller et al., 2004; Haq, 2014) in order to investigate the influence of eustatic sea-level fluctuations on the sedimentation in the Tarfaya Basin.

2. Material and Methods

2.1. Drilling of Cores Tarfaya SN°1 and 2

The East Atlantic passive continental margin and in particular the Tarfaya Basin, with its rapid subsidence during the Late Cretaceous provides an excellent location to recover Cretaceous deposits, which are affected by minimal regional tectonic influences (Choubert et al., 1966). Two

drill cores Tarfaya SN°1 and 2 (approximately 30 km apart) were recovered with the help of ONHYM (National Office of Hydrocarbons and Mines of Morocco) during October-December 2009 (Fig. 1). Core Tarfaya SN°1 is located relatively close to the Sebkha Tah, about 30 km south-east of the town of Tarfaya (27° 42´ 36.6´´N, 12° 56´ 39.0´´W). Core Tarfaya SN°2 is located relatively close to the coastline, about 10 km East of the town of Tarfaya (27° 57´ 43.1´´N, 12° 48´ 37.0´´W). A total of 550 meters of sediment was recovered with a Longyear L44 hydraulic drilling system "Sondeuse hydraulique WD3500" from these two drill sites (350 m at Tarfaya SN°1 and 200 m at Tarfaya SN°2). Metal core barrels (3.05 m long) were used with a diameter of 8.8 cm in the upper part of each hole (from 0 to 147 m for core Tarfaya SN°1 and from 0 to 57.3 m for core Tarfaya SN°2) and with a diameter of 6.8 cm in the lower part of each hole. Individual drilled sections of 3.05 m were divided into segments (~80 cm), which were inserted into plastic sleeves and sealed to avoid desiccation of shales and stored in wooden boxes for transport. Segments were split into archive and working halves with a high precision Kaufmann-Titan diamond rock saw. The cores consist of Cretaceous laminated marlstones and bituminous limestones with high organic matter content, overlain by poorly consolidated Moghrabien lumachelle and sandstone beds. The depth scale of each core is based on the cumulative length of core barrels. Detailed core descriptions made on oriented working half segments prior to x-ray fluorescence scanning (XRF) are presented in the Supplementary Material (Suppl. Figs. 1a, b and 2a, b).

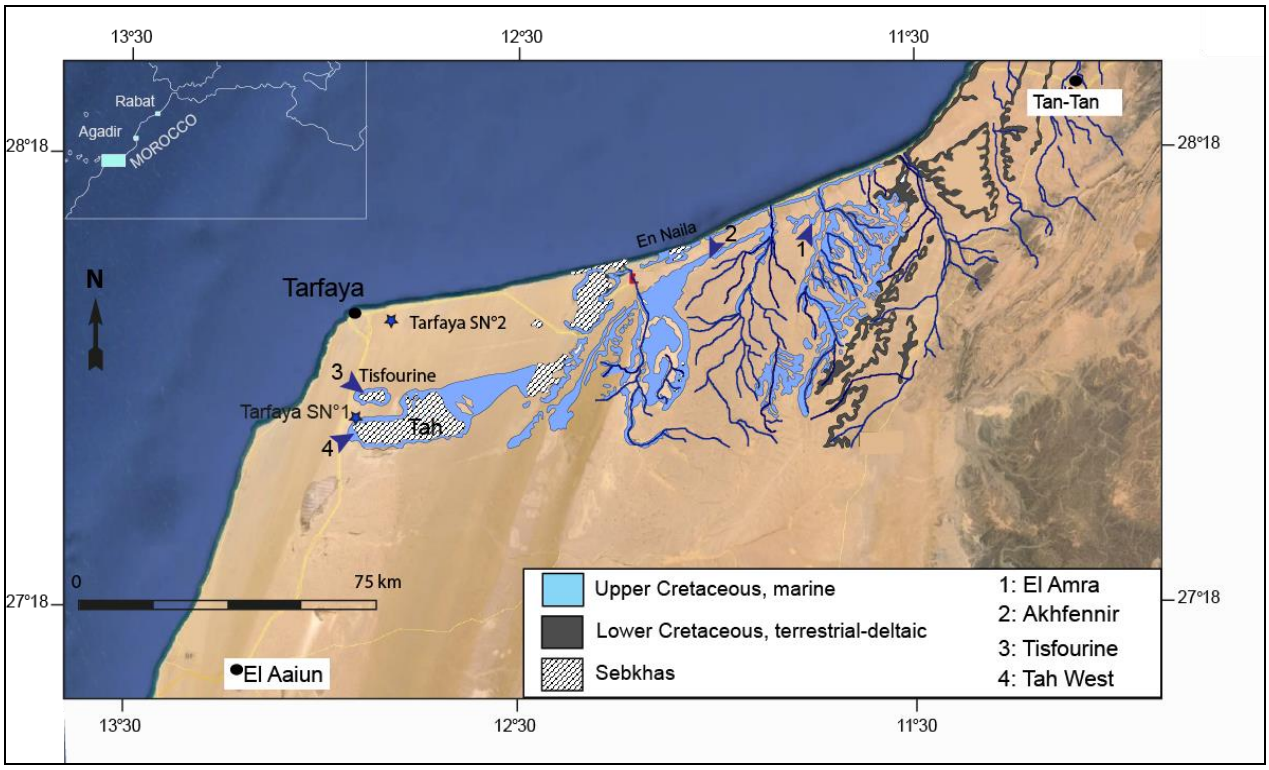

Figure 1: Location of the Tarfaya SN°1 and 2 cores and outcrop sections in the Tarfaya Basin, which form the base for a composite late Turonian to early Campanian stratigraphic log. Sections 1, 2 and 3 (Coniacian to Santonian and early Campanian, respectively) were previously studied by Aquit et al. (2013) and section 4 (early Campanian) by Holbourn et al. (1999). Geological map modified after Choubert et al. (1966).

2.2. Micropaleontology

A total of 73 (42 samples from core Tarfaya SN°1 and 31 samples from core Tarfaya SN°2) micropaleontological samples from bituminous marls with high organic matter content were crushed and processed using an alcoholic solution of anionic tensides (REWOQUAT by REWO-Chemie, Steinau, Germany), which helped to break down indurated samples. Around 50 g of dry sediments from each sample were washed and sieved into 150, 250 and 630 µm fractions. Planktonic foraminifera from the 250-630 µm fraction were picked and a biostratigraphic zonation of planktonic foraminifera was established, based on the zonation of Robaszynski and Caron (1995). A total of 18 subsamples were taken for nannofossil investigation to support and refine the biostratigraphy, using the Late Cretaceous (UC) zonation of Burnett et al. (1998).

2.3. Line-scanning and core photography

Line scan measurements and photographs were acquired with a Ja CVL 1073 CCD color line scan camera with 3 sensors of 2048 pixels and Dichroic RGB beam splitter prism (RGB channels at 630 nm, 535 nm and 450 nm) at the Institute of Geosciences, Christian-Albrechts-University in Kiel. Color measurement in L*a*b* units are from RGB digital images. Scanning was performed (resolution of 143 pixel per 1 centimeter) on the polished surface of oriented cores.

2.4. X-ray fluorescence (XRF) core scanning

Elemental composition of the sediment was analyzed on the working half core surfaces, using the second generation Avaatech X-ray fluorescence core scanner at the Institute of Geosciences, Kiel University. The core surface was covered with 4 μm thickness Ultralene plastic film to avoid contamination and to protect the detector. Measurements were taken continuously over the entire spliced core length at 1 cm intervals with a downcore slit size of 10 mm over a 1 cm^2 area. A few short intervals, mainly in the clay-rich upper part of SN°1, which were too disturbed to obtain smooth surfaces, could not be scanned and appear as gaps in the plots. Tube voltage settings of 10, 30 and 50 kV were used with a sampling time of 10 s to analyze the following elements: Al, Si, Ti, Fe, Mn, S, K, Ba, Zr, Sr, Br and Ca. Raw data spectra were processed by the analysis of X-ray spectra with the iterative least square software (WIN AXIL) package from Canberra Eurisys. Results are reported in the logarithms of elemental ratios, which provide the most easily interpretable signals of relative changes in chemical composition downcore and minimize the risk of measurement artifacts from variable signal intensities and matrix effects (Weltje and Tjallingii, 2008).

Variations in the abundance of the major elements K, Fe, Ti, Si and Al are commonly used to reconstruct abundance changes in the terrigenous component of marine sediments (Peterson et al., 2000; Haug et al., 2001; Jaeschke et al., 2007; Mulitza et al., 2008; Tisserand et al., 2009; Govin et al., 2012). We normalized these records against Ca, mainly derived from the biogenic carbonate of marine organisms and expressed the ratio of terrestrial derived elements vs. marine carbonate as log((Al+Ti+Fe+K+Si)/Ca).

We used the relative abundance of vanadium (expressed as log(V/Ca)) as a proxy for enhanced organic matter accumulation and reducing conditions in the sediments, since V is commonly associated with organic matter in marine sediments either by direct incorporation in

organic complexes or absorption on particulate organic matter during scavenging (Lewan and Maynard, 1982; Prange and Kremling, 1985). Vanadium in deposited particulate organic matter is also more stable under anoxic conditions and, thus, indicates not only enhanced accumulation of organic matter but also oxygen-depleted conditions at the sea-floor making V a useful paleoredox proxy (Shaw et al., 1990; Tribovillard et al., 2006).

Log(Mn/S) additionally provides information about deep-water oxygenation, as the sedimentary Mn content in organic-rich environments is almost entirely dependent upon redox conditions. Minerals containing reduced Mn are rare in marine sediments (Calvert and Pedersen, 1996; Tribovillard et al., 2006) and modern and Cretaceous upwelling deposits are commonly depleted in Mn (Brumsack, 1986). Sulfur can be used to evaluate the degree of pyritization in sediments, which is related also to the TOC content. Low pyritization associated with low TOC content indicates well oxygenated conditions during sedimentation (Rachold and Brumsack, 2001), thus higher log(Mn/S) indicate more oxygenated bottom waters.

Log(Zr/Rb) is related to the distance of the clastic source and grain size variation in the sediments. Liu et al., 2004 and Chen et al., 2006 were using the Zr/Rb-ratio as grain size proxy in the Loess sequence in China. Zirconium is bound to zircon, a heavy mineral, generally transported over short distances, whereas Rb represents a light element derived from biotite and transported in clay minerals over long distances. High log(Zr/Rb) values indicate an increase in grain size and/or a proximal source and sediment transport over a reduced distance.

2.5. Stable isotope analysis of bulk carbonate

A total of 800 samples (500 samples from core Tarfaya SN°1 and 300 samples from core Tarfaya SN°2) were analyzed for stable isotopes of bulk carbonates. Measurements were made with a Finnigan MAT 251 or MAT 253 mass spectrometer at the Leibniz Laboratory for Radiometric Dating and Stable Isotope Research at the Christian-Albrechts University in Kiel. The instruments are coupled online to a Carbo-Kiel device for automated CO_2 preparation of carbonate samples. Samples were reacted by individual acid addition. The system has an accuracy (on the delta scale) of ± 0.05‰ for carbon and ± 0.08‰ for oxygen isotopes. The results were calibrated using the National Institute Bureau of Standards and Technology (Gaithersburg, Maryland) carbonate isotope standard NBS 20, internal standards and NBS 19 and are reported as $\delta^{13}C_{carb}$ on the PeeDee belemnite (PDB) scale.

3. Results

3.1. Chronostratigraphy

The chronostratigraphy of cores Tarfaya SN°1 and 2 is primarily based on plankton foraminiferal zonation, which was supplemented by calcareous nannoplankton datums. We adapted the zonation of Robaszynski and Caron (1995), which defines the four global planktonic foraminiferal zones between the early Campanian to late Turonian that can be clearly discriminated in cores Tarfaya SN°1 and SN°2 (Fig. 2):

1. *Globotruncanita elevata* Zone (lower Campanian)
2. *Dicarinella asymetrica* Zone (late Coniacian to the Santonian/Campanian boundary)
3. *Dicarinella concavata* Zone (early Coniacian to late Coniacian)
4. *Marginotruncana sigali* Zone (late Turonian to early Coniacian)

The top of the *G. elevata* zone is not reached in SN°1, as the youngest sediment was deposited in calcareous nannoplankton Zone UC15c. The first occurrence of typical lower Campanian planktonic foraminiferal assemblages with *Globotruncanita elevata* and *G. stuartiformis* in SN°1 is observed at 158.24 mcd, the last occurrence of *D. asymetrica* is at 158.80 m, the first occurrence of *G. elevata* (in association with *D. asymetrica*) at 159.03 mcd, and the last sample without early Campanian *Globotruncanita* and common *D. asymetrica* is at 159.41 mcd, which places the Santonian-Campanian boundary between 159.03 mcd and 159.41 mcd. This position of the Santonian-Campanian boundary, as defined by the FO of *G. elevata*, is located in the upper part of the positive carbon isotope shift, at or very close to a distinct sediment change at approx. 159.20 mcd (Fig. 2). On the basis of nannoplankton zones this interval lies within Zone UC14a, which corresponds to the early Campanian. Based on calcareous nannoplankton, the Santonian-Campanian boundary, placed at the base of nannoplankton Zone UC13, is located around 179.30 mcd in the Tarfaya cores, ~20 m deeper than the base of the *G. elevata* Zone (Fig. 2). This discrepancy may have two possible explanations: (1) a delayed first occurrence of the deep-dwelling *G. elevata* in the Tarfaya Basin, in analogy to similar late occurrences of *H. helvetica* and *D. concavata* or (2) inconsistencies in the existing correlation of Tethyan planktonic foraminiferal zones and boreal calcareous nannoplankton zones at the base of the Campanian (Gale et al., 1995).

The base of the *Dicarinella asymetrica* Zone is commonly used to define the Coniacian/Santonian boundary (Robaszynski and Caron, 1995; Gradstein et al., 2012). However, the

exact placement of this event may vary due to the continuous evolution from *D. concavata* into *D. asymetrica* and the relatively rare occurrence of *D. asymetrica* in the early part of its range. We previously defined the base of this zone by the first occurrence of typical specimens of *D. asymetrica* with five or more chambers in the last whorl, a wide umbilicus and distinct umbilical ridges (Aquit et al., 2013). However, these typical *D. asymetrica* are very rare in the lower part of the *D. asymetrica* Zone, where *D. concavata* and intermediate forms between *D. concavata* and *D. asymetrica* dominate the assemblages of umbilicoconvex *Dicarinella*. Using the first rare occurrences of *D. asymetrica*, the base of the *D. asymetrica* Zone in cores Tarfaya SN°1 (204.38 m) and SN°2 (57.20 m = 210.45 mcd) falls into the nannoplankton zone UC11a, above the base of *L. grillii*, which corresponds to a late Coniacian age. We placed the Coniacian/Santonian boundary above this datum.

The lower boundary of the *Dicarinella concavata* Zone is well defined by the first appearance of *D. concavata* at 104.16 m in core Tarfaya SN°2. However, the first occurrence of *D. concavata* in the Tarfaya Basin appears somewhat later than its global first appearance in the late Turonian. In outcrop sections of the Tarfaya Basin, *D. concavata* first occurs above the early Coniacian "astarte-lumachelle" marker beds (Aquit et al., 2013), which were dated by ammonites as early Coniacian (Choubert et al., 1966; Wiedmann et al., 1978). An early Coniacian first occurrence of *D. concavata* in the Tarfaya Basin is supported by our correlation to the calcareous nannofossil zonation, which indicates that the base of the *D. concavata* Zone is above the first occurrence of *M. staurophora* within nannoplankton Zone UC10 (lower to middle Coniacian).

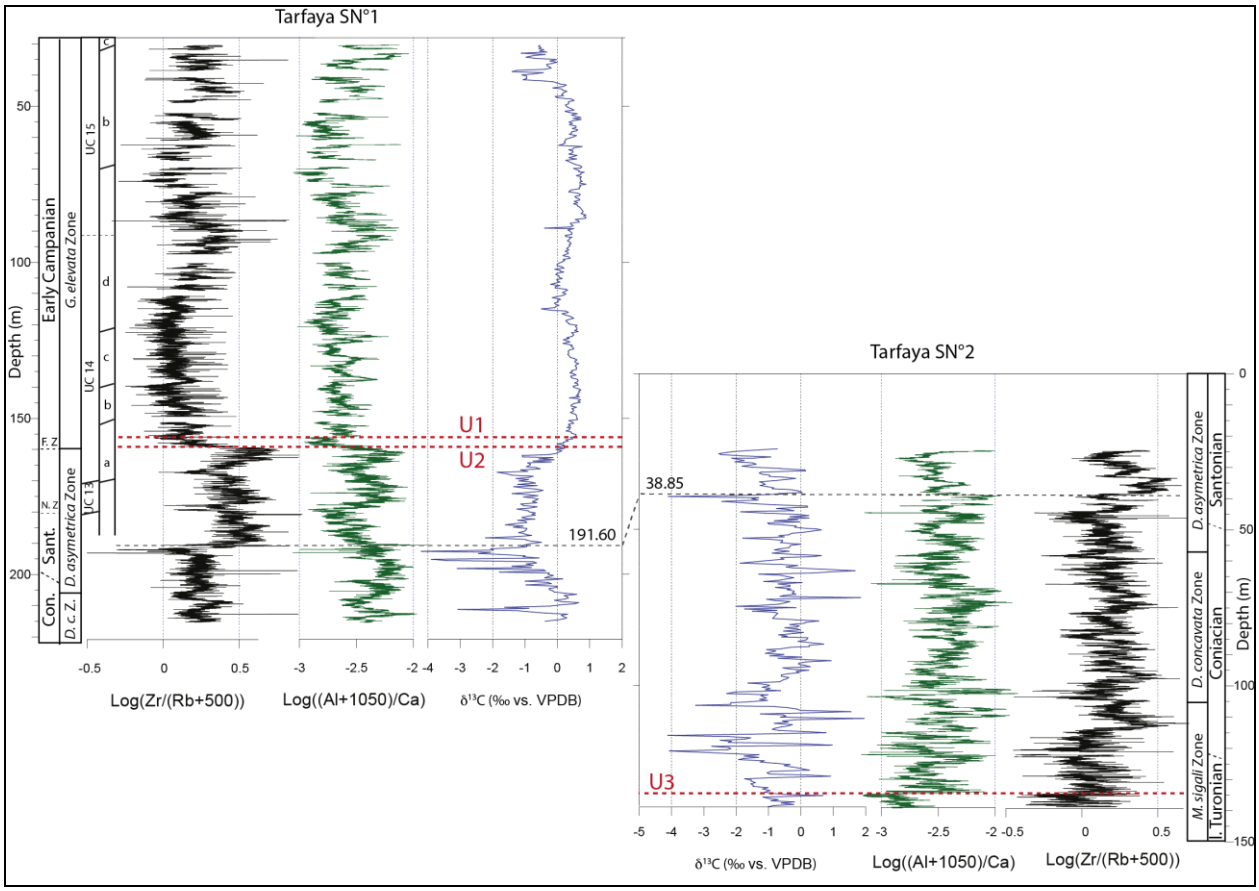

Figure 2: Correlation of the Tarfaya SN°1 and 2 cores based on bulk carbon isotope ($\delta^{13}C$), XRF-scanning Al/Ca and Zr/Rb and planktonic foraminiferal biostratigraphy. Red dashed lines correspond to the unconformities in cores Tarfaya SN°1 and 2, black dashed line corresponds to the tie point for correlation at 191.6 m in Tarfaya SN°1 and at 38.85 m in Tarfaya SN°2. Late Cretaceous (UC) nannoplankton Zones from Burnett et al., (1998). N. Z.: nannoplankton Zone; F. Z. foraminiferal Zone; *D.c.* Z.: *D. concavata* Zone; Sant.: Santonian.

3.2. Correlation of cores Tarfaya SN°1 and SN°2

The correlation of cores Tarfaya SN°1 and SN°2 is based on elemental ratios Al/Ca and Zr/Rb derived from XRF scanning, lithological descriptions, line-scan records, bulk carbonate stable isotopes and planktonic foraminiferal biostratigraphy (Fig. 2 and Suppl. Fig. 3). We define the tie point for correlation at 191.6 m in Tarfaya SN°1 and at 38.85 m in Tarfaya SN°2. This corresponds to a lithological change from laminated black shale with nodular limestones to light brown marlstones in both cores. This correlation is further supported by a decrease in lightness (L*), a major increase in Zr/Rb and a long-term decrease in Al/Ca, at the base of the *D. asymetrica* Zone in both cores. The negative excursion in the bulk carbonate stable isotopes at 39.49 m in core Tarfaya SN°2 is further correlated to the first negative excursion at 192.73 m in core Tarfaya SN°1, supporting the lithological correlation. Both negative excursions have values ~ -4‰.

We constructed a composite depth scale (referred to as mcd) for the two cores using the depth scale of core Tarfaya SN°1 for the upper 191.6 m and the part below 38.85 m in core Tarfaya SN°2 for the lower part of the composite section. Thus, composite depths in core Tarfaya SN°2 can be calculated as:

Composite depth (mcd) = depth in SN°2 (m) - 38.85 m + 191.6 m.

The total composite length of the two cores is 290 mcd. Downcore depths are given as mcd, when referring to the composite section between the two cores, whereas downcore depths in individual cores are given in m.

3.3. Lithology and regional unconformities

Cores Tarfaya SN°1 and 2 are divided into lithological units, based on visual core descriptions and XRF-derived elemental data. Detailed lithological descriptions are provided in the supplementary material (Suppl. Figs. 1 and 2). The upper 14 m in core Tarfaya SN°1 and the upper 24.6 m in core Tarfaya SN°2 consist of Plio-Pleistocene ("Moghrabien") sediments, including sandstones, limestones and lumachelles along with shell fragments. Core Tarfaya SN°1 is not described between 14 and 30 m due to intense fragmentation.

Based on the XRF-scanning Al/Ca and Zr/Rb and line-scan records (L*) as well as on lithological changes, three major unconformities are identified at 156.6 m (U1), 158.8 m (U2) in core Tarfaya SN°1 and at 134 m (U3) in core Tarfaya SN°2. These unconformities occur at 156.6 mcd (U1), 158.8 mcd (U2) and 286.75 mcd (U3) in the composite record. Detailed lithological logs showing the position of the unconformities are provided in Suppl. Figs. 1-2 and 4. Unconformities U1 to 3 occur in the lowermost *G. elevata* Zone (early Campanian, U1), at the boundary between the *D. asymetrica* and *G. elevata* Zones (Santonian-Campanian boundary, U2) and in the uppermost *M. sigali* Zone (latest Turonian, U3), respectively.

Unconformities U1 and U2 correspond to an abrupt lithological change from brown shale to gray marl with heavy bioturbation, an increase in lightness (L*) and a decrease in Al/Ca and Zr/Rb (Suppl. Figs. 1, 2 and 4). In contrast, unconformity U3 in core Tarfaya SN°2 forms an erosive horizon at the base of a light olive green siltstone, characterized by oblique laminations (Suppl. Fig. 4). This unconformity occurs above an interval with alternating laminated black shales and nodular

limestones. Unconformity U3 in core Tarfaya SN°2 is characterized by a marked increase in lightness (L*), a major decrease in Al/Ca and a slight decrease in Zr/Rb.

3.4. Bulk carbonate $\delta^{18}O$ curve

Stable oxygen isotope values ($\delta^{18}O$) of 800 upper Turonian to lower Campanian bulk carbonate samples from Tarfaya SN°1 and SN°2 range largely between –2‰ and –5‰ (Fig. 3). Oxygen isotope data overall reflect Late Cretaceous sea surface temperatures with a robust cooling trend in the lower Campanian (mean -4.19‰, standard deviation 0.59 for the upper Turonian-Santonian below 160 m, mean -3.12‰, standard deviation 0.83 for the lower Campanian, 28.5 – 160 m). Cross-plots of carbon and oxygen isotope values do not show any significant correlation (Fig. 4), which would indicate the addition of a late diagenetic cement to the primary skeletal calcite. We estimated sea surface temperatures from the bulk (mainly coccolith) $\delta^{18}O$ using the equation of Epstein et al. (1953):

$$T\ (°C) = 16.5 - 4.3\ (\delta^{18}O_{calcite} - \delta^{18}O_{water}) + 0.14\ (\delta^{18}O_{calcite} - \delta^{18}O_{water})^2$$

where $\delta^{18}O_{calcite}$ is the oxygen isotopic composition on the PDB-scale and $\delta^{18}O_{water}$ the isotope composition of the water, in which the calcite was secreted, using a $\delta^{18}O_{water}$ of -1‰ (SMOW) for an ice-free world (Shackleton and Kennett, 1975), which corresponds to -1.27‰ on the PDB scale used in the paleotemperature equation. The resulting sea surface paleotemperature estimates of ~30°C (36°C) for the late Turonian to Santonian and ~25°C (30°) for the early Campanian (values in brackets include vital effect corrections for coccolith $\delta^{18}O$ by subtracting 1.1‰ for the vital effect of coccolithophorid calcite formation (Dudley et al., 1986; Ennyu et al., 2002) are largely in agreement with expected sea surface environmental conditions, indicating little influence of burial diagenesis or late diagenetic cementation on the isotope record.

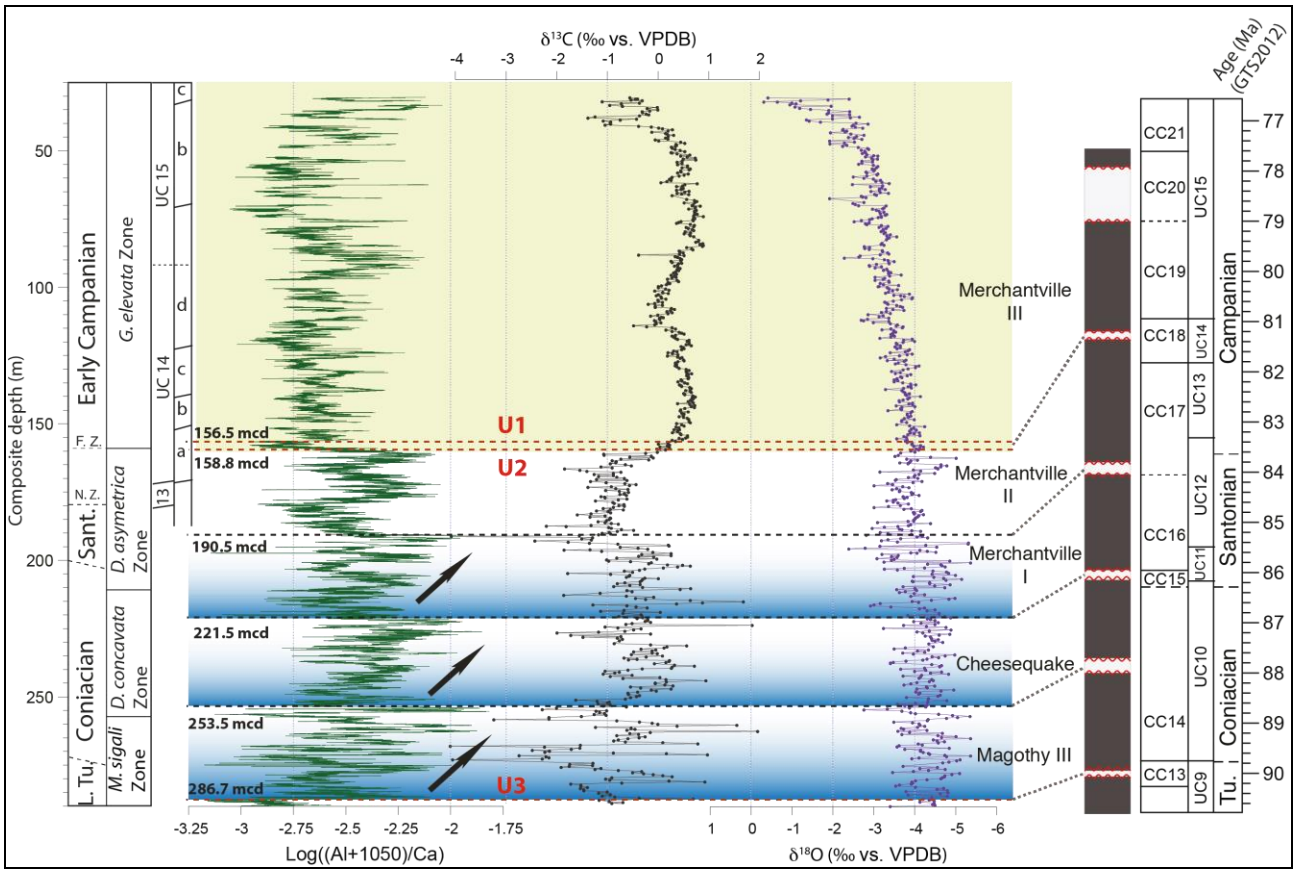

Figure 3: Comparison of Tarfaya Basin depositional sequences to the eustatic record from the New Jersey margin (Miller et al., 2003, 2004; Mizintseva et al., 2009). Foraminiferal zonation follows Robaszynski and Caron (1995), except for the base of the *G. concavata* Zone due to the later occurrence of *G. concavata* in the Tarfaya Basin. Nannoplankton zonation UC from Burnett et al. (1998); CC zonation is compiled from Bergen, 1994 and Bralower et al., 1995 in the GT012 timescale. Red dashed lines correspond to the unconformities (U1-3) in cores Tarfaya SN°1 and 2 observed in lithology, gray dashed lines correspond to unconformities based on log((Al+Ti+Fe+K+Si)/Ca). Sant.: Santonian; L. Tu.: late Turonian; N. Z.: nannoplankton Zone; F. Z. foraminiferal Zone.

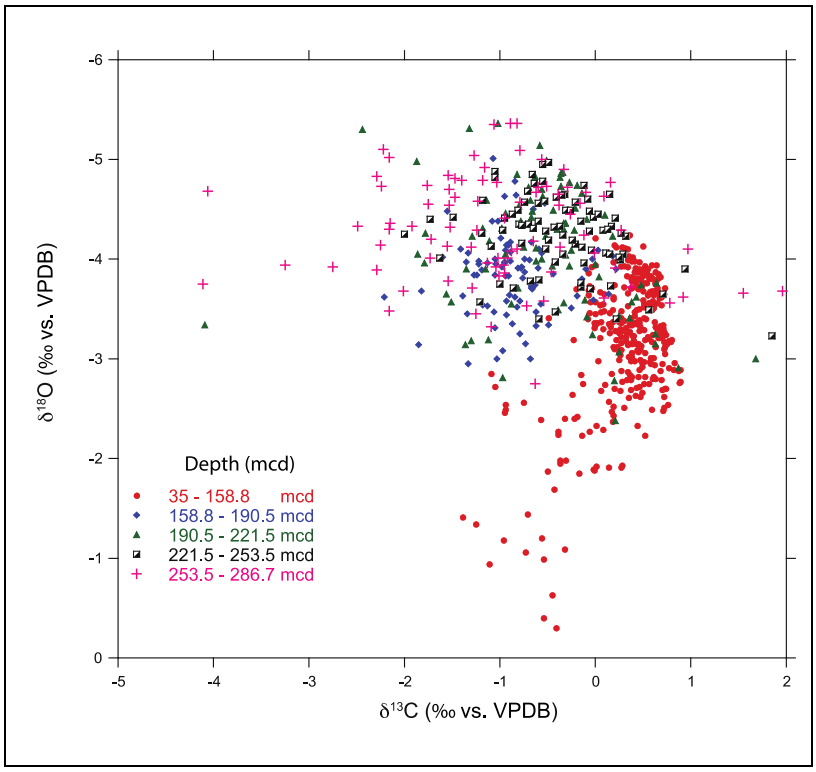

Figure 4: Cross-plots of carbon- and oxygen isotope values of newly drilled cores (Tarfaya SN°1 and 2).

3.5. Bulk carbonate $\delta^{13}C$ curve

Stable oxygen isotope values of 800 upper Turonian to lower Campanian bulk carbonate samples from Tarfaya SN°1 and SN°2 range largely between +1.7‰ and -2.4‰ (Fig. 5). In the upper part of the composite section (28.5 - 160 m, early Campanian), mean $\delta^{13}C$ values (0.28‰, 0.46 standard deviation) are lower than in European reference sections (Jarvis et al., 2006) but comparable to sections in the Eastern Tethys (Li et al., 2006, Wendler et al., 2009, 2013) or at Demerara Rise (MacLeod, 2006). The unusually low values (mean -0.77‰) and high scatter (standard deviation 0.94) of $\delta^{13}C$ below 160 m suggest either presence of secondary calcite with a remineralized organic carbon component in a large number of samples or growth of biogenic (mainly coccolith) calcite in unusually nutrient rich and $\delta^{13}C$ depleted water masses upwelling from an expanded and intensified oxygen minimum zone.

Previous studies of Turonian and Coniacian outcrop sections in the Tarfaya Basin have shown that $\delta^{13}C$ is considerably lowered to values as low as -11‰ within calcareous nodular concretions (El Albani et al., 2001). We avoided these lithologies when sampling cores Tarfaya SN°1 and SN°2 for bulk isotopes, and focused sampling on intervals with relatively high clay mineral content. The

composite carbon isotope record of cores Tarfaya SN°1 and SN°2 is characterized by a series of five low amplitude positive carbon isotope excursions with wavelengths in the range of 30 to 70 m, which are separated by transient high amplitude negative excursions. We identify a first maximum (labelled 1 in Fig. 5) at ~75 mcd. The second maximum at ~155 mcd (labelled 2 in Fig. 5) occurs close to the Santonian-Campanian boundary, the third poorly developed maximum with significantly lower values at ~175 mcd (labelled 3 in Fig. 5) in the middle Santonian, the fourth maximum at ~215 mcd (labelled 4 in Fig. 5) in the late Coniacian and the fifth maximum at ~245 mcd (labelled 5 in Fig. 5) in the middle Coniacian.

The most salient features in the SN°1-2 carbon isotope records are two consistent positive shifts in $\delta^{13}C$ 1) in the middle Coniacian starting at 260 mcd and reaching a first peak at 243 mcd and 2) at the Santonian-Campanian boundary starting at 168 m and reaching a maximum at 153 m. These positive excursions appear also as robust features in other Late Cretaceous $\delta^{13}C$ records (i.e. corresponding to the $\delta^{13}C$ increase between the Buckle/Foreness and the Santonian-Campanian Boundary Event and between the East Cliff to White Fall Events in the English chalk records, Jarvis et al., 2006). The amplitude of these events exceeds 1.5 ‰ in the SN°1-2 records, which is more than double that in the English chalk and the Niobrara Formation of the US Western Interior (Locklair and Sageman, 2008), but similar to records from the eastern Tethys margin in Tibet (Li et al., 2006; Wendler et al., 2009; 2013).

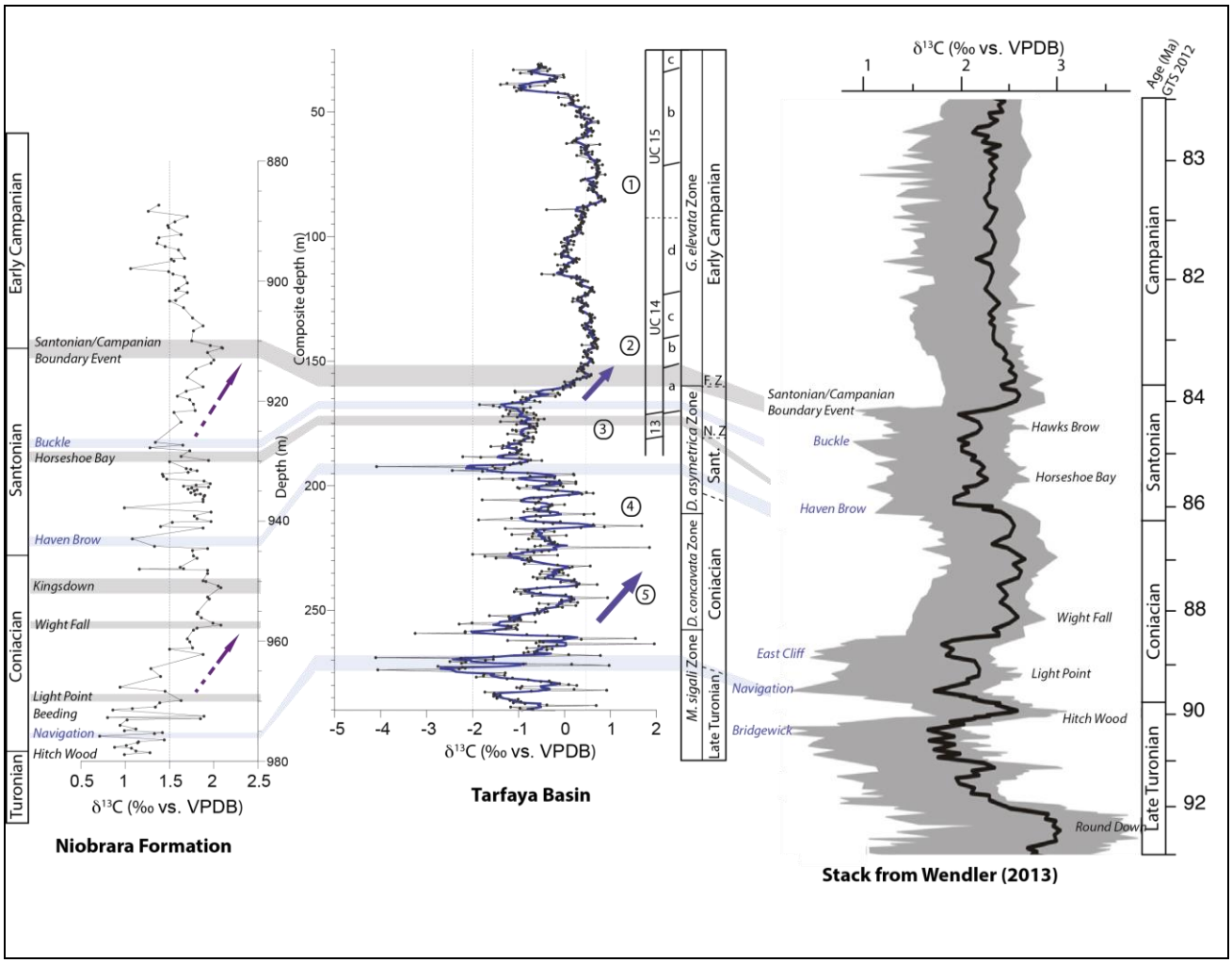

Figure 5: Correlation of bulk carbon isotope ($\delta^{13}C$) from the composite section (cores Tarfaya SN°1 and 2) to the $\delta^{13}C$ records of the Niobrara Formation, US Western Interior Seaway (Locklair et al., 2011) and stacked curves from Wendler (2013). Blue line corresponds to 5pt smoothed curve. Blue arrows indicate positive shifts in $\delta^{13}C$ in the middle Coniacian and at the Santonian-Campanian boundary. N. Z.: nannoplankton Zone; F. Z. foraminiferal Zone; Sant.: Santonian.

3.6. XRF-scanning elemental distribution

3.6.1. Ratio of terrigenous elements to marine carbonate: Log((Al+Ti+Fe+K+Si)/Ca)

The ratio of terrigenous elements to Ca derived from marine carbonate is highest in the Santonian to Coniacian interval of the succession (158.8 - 286.7 mcd) (mean -0.99, standard deviation 0.23) and lowest in the upper Turonian between 286.7 and 290 mcd (mean -1.58) (Fig. 6). This interval is also characterized by the highest variability in terrigenous elements (standard deviation 0.35). The lower Campanian exhibits intermediate values (mean -1.22) with comparatively low variability (standard deviation 0.19). A peculiar feature of the log((Al+Ti+Fe+K+Si)/Ca) curve are three sequences of stacked carbonate-poor and carbonate-rich intervals, each exhibiting an overall

increasing trend in terrigenous elements between 190.5 and 221.5 mcd, between 221.5 and 253.5 mcd and between 253.5 and 286.7 mcd (Fig. 6).

3.6.2. Proximity of the clastic source and sorting during transport: Log(Zr/Rb)

A salient feature of the log(Zr/Rb) curve are considerably higher values in the middle and late Santonian (mean 0.48, standard deviation 0.13), which indicate either a more proximal sediment source or intense winnowing of fine-grained clastic sediment (clay minerals) on the Tarfaya shelf (Fig. 6). Both possibilities are compatible with a significant and persistent lowering of sea-level associated with the sequence boundary at 190.5 m in the lower-middle Santonian. Lowest log(Zr/Rb) values occur in the upper Turonian between ~ 268 mcd and 290 mcd (mean 0.02, standard deviation 0.13) probably associated with a distant sediment source and/or reduced fluvial sediment discharge. Intermediate values of log(Zr/Rb) prevail in the uppermost lower Campanian (28.5 to 158.8 mcd, Sedimentary Unit I) (mean 0.15, standard deviation 0.13) and between ~ 268 and 190.5 mcd in the Coniacian and lower Santonian (Fig. 6).

3.6.3. Geochemical indicators of organic matter accumulation and bottom water oxygenation: Log(Mn/S) and Log(V/Ca)

The lower Campanian interval exhibits the highest log(Mn/S) values (mean -1.33, standard deviation 0.23), indicating improved bottom water ventilation, also evident from benthic foraminiferal assemblages in outcrop sections (Aquit et al., 2013). Between 190.5 and 158.8 mcd (middle to upper Santonian) log(Mn/S) increases from an average of -1.6 to -1.25 in the lower Campanian (Fig. 6). The lower Santonian to upper Turonian is characterized by generally low but highly variable log(Mn/S) indicating overall oxygen depleted to anoxic conditions at the sea-floor punctuated by short ventilation events (mean -1.61, standard deviation 0.18). The most prominent of these ventilation events were associated with facies changes that indicate massive regressions in the latest *D. concavata* Zone (above the SB at 221.5 mcd).

The log(V/Ca) curve generally exhibits an inverse relationship to the log(Mn/S), which reflects the affinity of V to accumulated organic matter and concomitant decrease in bottom water oxygenation. Lowest values characterize the lower Campanian interval of the section (mean -3.31, standard deviation 0.17). The Santonian interval between 158.8 and 190.5 mcd exhibits intermediate

values (mean -3.03, standard deviation 0.17) (Fig. 6). Extremely high values occur in the lower Santonian to upper Turonian (mean -2.86, standard deviation 0.32), with maxima in the highstand sediments below the sequence boundaries at 190.5, 221.5 and 253.5 mcd. The entire interval shows high amplitude fluctuations with peaks of high (log(V/Ca)>-2.5) V accumulation in laminated black shale intervals.

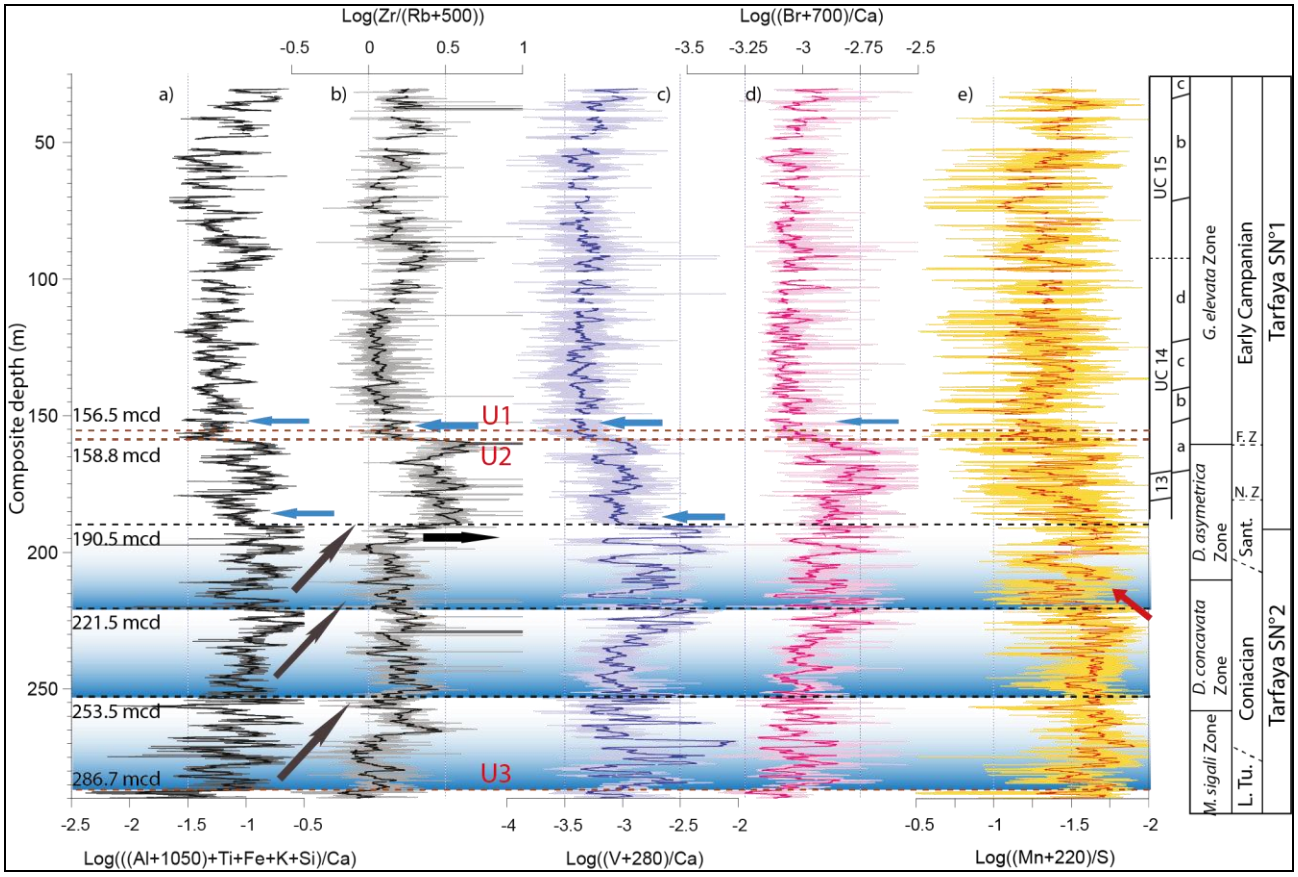

Figure 6: Composite geochemical and biostratigraphic records of cores Tarfaya SN°1 and 2. **a**) Elemental log of (Al+Ti+Fe+K+Si)/Ca, gray arrows indicate increasing terrigenous flux, blue arrows indicate increases in carbonate flux in the Tarfaya Basin; **b**) Elemental log of Zr/Rb, blue arrows indicate decreases in grain size, black arrow indicates increase in grain size; **c**) Elemental log of V/Ca, blue arrows indicate increases in carbonate flux; **d**) Elemental log of Br/Ca, blue arrow indicates increases in carbonate flux; **e**) Elemental log of Mn/S, red arrow indicates increasing oxygenation at the sea-floor in the Tarfaya Basin. Red dashed lines correspond to the major unconformities (U1-3) in cores Tarfaya SN°1 and 2, black dashed lines correspond to unconformities based on log((Al+Ti+Fe+K+Si)/Ca). Late Cretaceous (UC) nannoplankton Zones from Burnett et al. (1998). N. Z.: nannoplankton Zone; F. Z. foraminiferal Zone; Sant.: Santonian; L. Tu.: late Turonian.

4. Discussion

4.1. Latest Turonian to early Campanian sedimentary environments of the Tarfaya Basin

4.1.1. Processes controlling sedimentation of organic-rich and carbonate-rich deposits

The Upper Cretaceous sediments of the Tarfaya Basin were deposited on an open marine shelf, in water depth of ~100 - 150 m (Wiedmann et al., 1978; El Albani et al., 1999a; Kuhnt et al., 2009). Following the depositional concept used for the analysis of Cenomanian sequences in the Tarfaya Basin (Kuhnt et al., 2009), lowstands and sequence boundaries are characterized by carbonate rich sediments, including redeposited shallow water carbonate sands and pebbles. In contrast, transgressive system tracts coincide with the onset of organic-rich sediments, which are commonly laminated, relatively low in carbonate and enriched in Al, K, S and Si (partly biogenic). The episodic occurrence of organic matter-rich sediments has been explained by the impingement of an expanded and intensified oxygen minimum zone onto the shelf during transgressive system tracts and maximum flooding (Kuhnt et al., 2009). This pattern of relatively coarse-grained lowstand carbonates and organic-rich fine clastic transgressive and highstand sedimentation bears similarities to modern "shaved shelf" depositional models (James et al., 1994, Brachert et al., 2003). These models, developed for modern high productivity temperate carbonate shelves such as the Great Australian Bight, indicate that carbonate-rich sediments form during sea-level lowstands, when the wave abrasion depth intersect with the sea-floor. Wave abrasion during lowstands then winnow and export the fine terrigenous clastic material (clay minerals) into deeper parts of the basin. Thus, the residual coarser material on the shelf mainly consists of carbonate grains (foraminiferal tests, shell fragments, calcareous dinoflagellate cysts).

Sediments rich in organic matter were recovered in cores Tarfaya SN°1 and 2 as laminated or homogeneous black, brown or gray marlstones. In the XRF-scanner records, these intervals are characterized by high log(V/Ca) and log(Br/Ca) and low log(Mn/S). These elemental ratios exhibit significant correlation (Suppl. Fig. 5) to sulfur and total organic carbon weight percentages analyzed in core Tarfaya SN°2 (Sachse et al., 2012). The organic matter is mainly derived from marine primary producers (phytoplankton and marine algae) with very small contribution from terrestrial particles (e.g. vitrinite and inertinite) (Sachse et al., 2012). These intervals of organic matter and pyrite-rich, commonly laminated sediments point to oxygen-depleted bottom water conditions with enhanced flux and preservation of organic matter, reflecting episodic encroachment of an expanded

and intensified oxygen minimum zone on the middle to outer shelf of the Tarfaya Basin during intervals of rising and high sea-level. During these transgressive phases and highstands, fine-grained terrigenous sediments were remobilized close to the coastline, transported across the shelf, finally accumulating on the middle-outer shelf. Intervals of laminated organic-rich sediments prominently occur near the top of stratigraphic sequences, in particular below carbonate-rich lowstand sediments near sequence boundaries at 286.7, 253.5, 221.5, 190.5 and 158.8 mcd (Fig. 6, Suppl. Fig. 4).

The most prominent examples of carbonate-rich intervals, which are depleted in terrigenous elements, occur above the unconformity at 286.7 mcd (U3) in the uppermost Turonian. The carbonates are characterized by low log(Al/Ca), log((Al+Ti+Fe+K+Si)/Ca) and log(Zr/Rb) (Fig. 6, Suppl. Fig. 4), intense bioturbation and high log(V/Ca) and log(Mn/S), indicating improved oxygenation at the sea-floor (Fig. 6). Sediment structures (inverse grading, cross lamination) indicate the influence of storm induced bottom currents or storm wave-currents. We relate these limestone beds, which rest unconformably over organic-rich, fine-grained black shales to major regressive events, which brought the sea-floor of the central part of the Tarfaya shelf into the wave abrasion zone for the first time since the Cenomanian-Turonian sea-level maximum.

4.1.2. Evolution of depositional environments

The depositional environment in the Tarfaya Basin changed during the Late Cretaceous, following a major regressive event in the latest Turonian. This regression corresponds to unconformity U3, associated with the regional sea-level fall. The uppermost Turonian to lower Santonian is generally characterized by oxygen depleted to anoxic conditions at the sea-floor, punctuated by short-lived ventilation events (low log(Mn/S) episodes). The impinging of an expanded and intensified oxygen minimum zone on the shelf exhibits a periodic pattern with three cycles of increasing organic matter and clay to carbonate ratios (286.7 - 253.5 mcd, 253.5 - 221.5 mcd and 221.5 - 190.5 mcd) (Fig. 6). This period of organic rich sedimentation on the Tarfaya shelf corresponds in a very broad sense to the Coniacian-Santonian Anoxic Event (OAE-3), which marks an important transition in the long-term global climate evolution from Cretaceous greenhouse conditions, characterized by extremely high temperature and reduced equator-to-pole thermal gradient, to the Late Cretaceous–Paleogene cooling (Wagner et al., 2004). During OAE-3, several marginal basins along the Atlantic margin maintained intense oxygen minimum zones, whereas the

deep basins were already well oxygenated (Arthur et al., 1990; Ly and Kuhnt, 1994; Holbourn et al., 1999; Wagreich, 2012).

A major environmental change occurred at the Santonian-Campanian boundary (unconformities U1 and U2) in the Tarfaya Basin. The early Campanian sedimentary environment is characterized by enhanced accumulation of fine-grained carbonate and clay-rich hemipelagic sediments. Benthic foraminiferal assemblages in outcrop sections close to core Tarfaya SN°1 indicate a depositional environment well below storm wave base (Holbourn et al., 1999; Aquit et al., 2013). Although the deepening of the Tarfaya Basin in the early Campanian probably reflects local tectonic activity, it may also relate to eustatic transgressive events. The increased water depth is also reflected in an improvement of the oxygenation at the sea-floor (increase in log(Mn/S)) and high diversity and abundance of benthic foraminiferal assemblages (Holbourn et al., 1999; Aquit et al., 2013). The end of the Cretaceous sedimentary succession in the Sebkha Tah and Tisfourine sections as well as in Tarfaya SN°1 is marked by a major hiatus, which comprises the entire latest Cretaceous (middle Campanian - Maastrichtian) and Paleogene.

4.2. Comparison of Tarfaya Basin depositional sequences to the eustatic record from the New Jersey margin

Sea-level during the Cretaceous greenhouse world was substantially higher than the present and exhibited considerable long- and short-term variability (Miller et al., 2005; Müller et al., 2008). Long-term eustatic sea-level changes were probably controlled by plate tectonics. In contrast, relatively rapid variations in the order of tens of meters, remain difficult to explain without assuming glacio-eustasy and the presence of ephemeral ice sheets punctuating periods of extreme warmth (Matthews, 1984; Stoll and Schrag, 2000; Miller et al., 2003; Kominz et al., 2008; Kuhnt et al., 2009). The Tarfaya Basin provides a rare opportunity for sea-level reconstruction with its combination of minimal tectonic overprint at the margin of a stable craton, consistent subsidence and continuous deposition of a ~700 m undisturbed Upper Cretaceous sedimentary succession in an open marine shelf setting (Leine et al., 1986). The 290 mcd thick composite succession recovered in cores Tarfaya SN°1 and 2 allows to discriminate five sedimentary sequences from the latest Turonian to early Campanian with boundaries mainly discriminated by XRF data (log(Al/Ca)) (Fig. 6). These sedimentary sequences were correlated to the New Jersey Margin (Miller et al., 2003, 2004;

Mizintseva et al., 2009) based on biostratigraphy and carbon isotope stratigraphy. A correlation of the Tarfaya Basin to the global sea-level is illustrated in figure 7.

The sequence boundary at 286.7 mcd (unconformity U3 in SN°2) marks the base of the Magothy III sequence of Miller et al. (2004) (Fig. 3) in Zone CC13 within the latest Turonian. This sequence boundary separates sediments deposited above the storm wave base following the late Cenomanian-Turonian sea-level highstand. As, this part of the Tarfaya Basin remained in an open marine middle to outer shelf setting throughout this period, a clear effect of lowered sea-level is not evident on the depositional environment, except for the occurrence of common lumachelle beds in the earliest Coniacian, probably related to the action of storm waves.

During the Coniacian, three distinct cycles are recognized in the XRF elemental data (e.g. log(Al/Ca)). Sequence boundaries are placed at the abrupt change from organic carbon-rich laminated sediments to coarser, carbonate rich sediments at 253.5, 221.5 and 190.5 mcd, which form the base of stacked cycles. According to its stratigraphic position, the sequence boundary at 253.5 mcd in Tarfaya SN°2 corresponds to the base of the Cheesequake Sequence of Miller et al. (2004) and Mizintseva et al. (2009) in Zone CC14 within the lower Coniacian (Fig. 3). The sequence boundary at 221.5 mcd can be correlated to the boundary between the Cheesequake and Merchantville Formations (Miller et al., 2004; Mizintseva et al., 2009) in Zone CC15 close to the Coniacian/Santonian boundary. The sequence boundary at 190.5 mcd is traced by XRF data (log(Al/Ca)) at 40 m in core Tarfaya SN°2 (Fig. 2) but could not be clearly discerned in core Tarfaya SN°1. This boundary corresponds to a regressive phase within the late Santonian and is possibly the equivalent of the base of the Merchantville II Formation of Miller et al. (2004) and Mizintseva et al. (2009) (base of Zone CC17).

The stratigraphically highest sequence boundaries at 158.8 and 156.5 mcd in Tarfaya SN°1 (unconformities U1 and 2) are dated as earliest Campanian. These sequence boundaries correspond to repetitive regression phases before the major Campanian transgression phase and are correlative to the base of the Merchantville III Sequence of Miller et al. (2004) and Mizintseva et al. (2009) in Zone CC18 (Fig. 3). A marked increase in carbonate and related decrease in the concentration of terrigenous elements and log(Zr/Rb) occurs in the lower Campanian interval of core Tarfaya SN°1 at 84.5 mcd. This sedimentary change is also reflected by a $\delta^{13}C$ maximum, similar to the $\delta^{13}C$ maximum at the base of the Campanian.

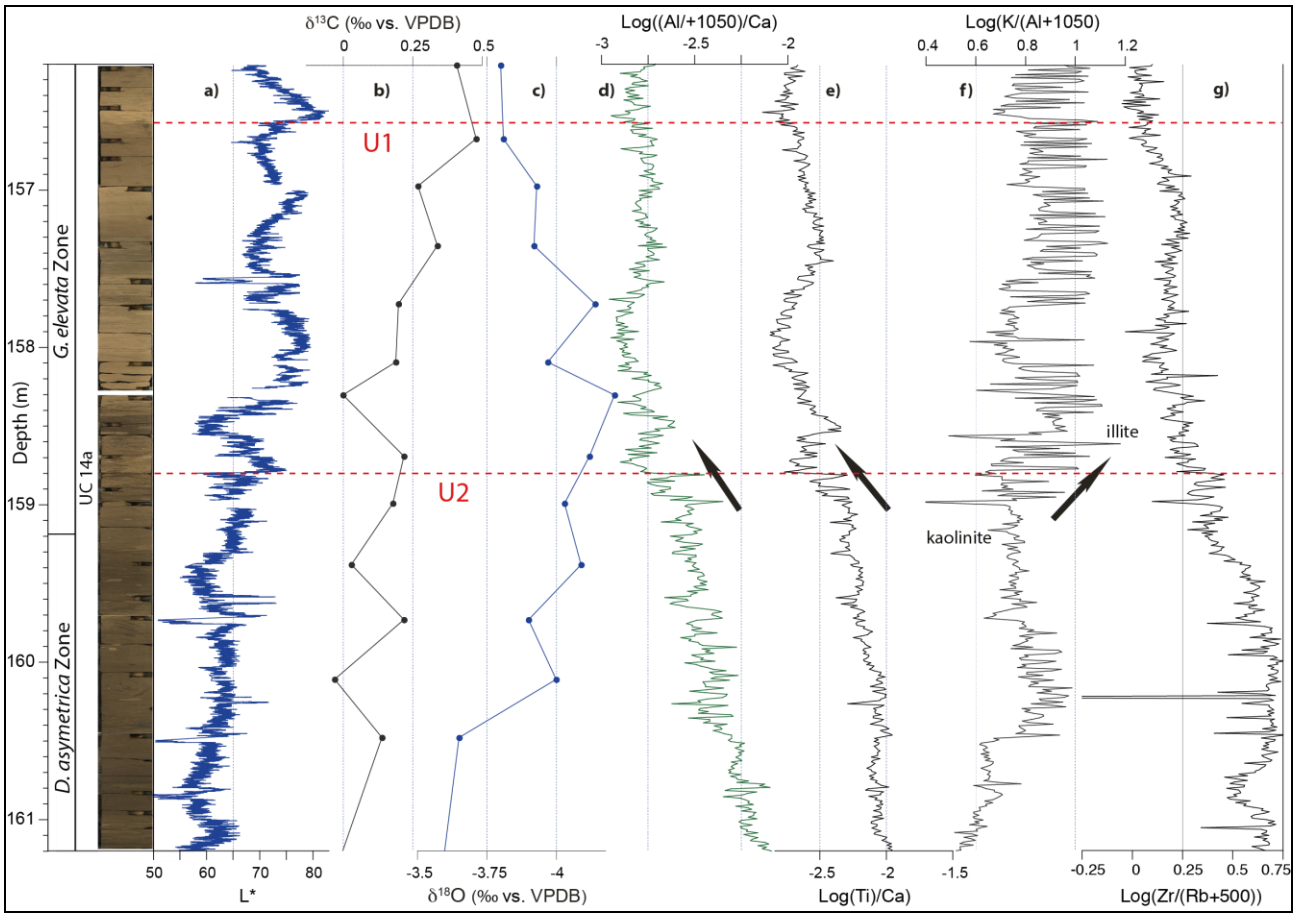

Figure 7: Composite geochemical, line-scan and biostratigraphic records at the Santonian/Campanian boundary in the Tarfaya Basin. **a**) Green arrow indicates an increase in light reflectance (L*); **b**) Bulk carbon isotope data ($\delta^{13}C$); **c**) Bulk oxygen isotope data ($\delta^{18}O$); **d-e**) Elemental log of Al/Ca and Ti/Ca, black arrows indicate increasing terrigenous flux; **f)** Elemental log of K/Al indicates variation of illite and kaolinite in sediments during the Santonian/Campanian boundary; **g)** Elemental log of Zr/Rb indicates distance of the clastic source and grain size variation in the sediments.

4.3. Correlation to the global carbon isotope curve

4.3.1. Variability of the $\delta^{13}C$ record: primary signal or early diagenesis ?

The general shape of the bulk carbonate $\delta^{13}C$ curve exhibits marked differences to other high resolution Late Cretaceous $\delta^{13}C$ curves (Wendler, 2013), which show overall higher $\delta^{13}C$ values and lack the rapid high amplitude fluctuations, characterizing the upper Turonian and Coniacian in Tarfaya. These high frequency $\delta^{13}C$ fluctuations are reflected by lithologic changes, as high $\delta^{13}C$ generally occurs within organic carbon-depleted intervals, when no upwelling related oxygen minimum zone was impinging on the outer shelf. In contrast, low $\delta^{13}C$ characterizes laminated organic rich intervals, when nutrient-rich water masses upwelled to the sea surface (Fig. 3).

A recent compilation of Late Cretaceous $\delta^{13}C$ records (Wendler, 2013) indicates differences in the amplitude of bulk carbonate for late Turonian and Coniacian $\delta^{13}C$ events in the range 1-2‰ between the English chalk reference section, the US Western Interior Niobrara Formation and Eastern Tethys sections in Tibet, which nevertheless all preserve the general pattern of the major carbon isotope variations. Interbasinal and latitudinal differences in the amplitude of Cretaceous $\delta^{13}C$ variations are likely related to locally different upwelling of nutrient-rich and $\delta^{13}C$ depleted water masses, productivity regimes and efficiency of the biological pump. For example, productivity- and pCO_2-dependent large latitudinal differences in the amplitude of carbon isotope excursion in the range of 1 to 4‰ have been recorded in biomarkers for photosynthetic algae during the OAE-2 carbon isotope excursion (Van Bentum et al., 2012). Today, in a well ventilated ocean, the dissolved inorganic carbon of nutrient-rich upwelling water masses can be depleted by more than 1‰ in $\delta^{13}C$ (Berger and Killingley, 1977) and this value may have been significantly higher in the Late Cretaceous Atlantic, when intermediate water masses where strongly depleted in oxygen and enriched in nutrients and ^{12}C. We, thus, regard the generally lower $\delta^{13}C$ in the Tarfaya Basin largely as a primary signal related to the upwelling of strongly nutrient-enriched and $\delta^{13}C$ depleted intermediate water masses.

4.3.2. Carbon isotope stratigraphy

The positive shifts in $\delta^{13}C$ in the middle Coniacian (starting at 260 mcd and reaching a first peak at 243 mcd) and at the Santonian-Campanian boundary (starting at 168 mcd and reaching a maximum at 153 mcd) are correlated to the globally recognized $\delta^{13}C$ increases between the Buckle/Foreness and the Santonian-Campanian Boundary Event and between the East Cliff to White Fall Events in the English chalk records (Jarvis et al., 2006). Based on these anchoring points, the remaining succession of broad $\delta^{13}C$ maxima can be tentatively correlated to main positive isotope events in the English Chalk carbon isotope reference curve (Fig. 5). We relate the second maximum at ~155 mcd to the Santonian-Campanian Boundary Event (SCBE), the third maximum at ~175 mcd to the Horseshoe Bay Event, the fourth maximum at ~215 mcd to the Kingsdown Event and the fifth maximum at ~245 mcd to the Wight Fall Event. In addition, the negative excursions at ~167 mcd, ~193 mcd and ~270 mcd correspond to the Buckle, Haven Brow and Navigation Events, respectively.

The correlation of the outcrop sections in the Tarfaya Basin (Aquit et al., 2013) to the continuous $\delta^{13}C$ records from the Tarfaya SN°1 and 2 cores allows to improve this stratigraphic assignment within the Late Cretaceous. The Tisfourine section (early Campanian) corresponds to the upper part (~30 to 50 mcd) of core Tarfaya SN°1. The Akhfennir (~35 m of Santonian) and Tah North (~40 m of Santonian) are found to strongly overlap, resulting in a total thickness of ~ 45 m. The strong negative excursion within the *D. concavata* Zone, originally correlated to the Navigation Event in the El Amra Section (Aquit et al., 2013), appears stratigraphically slightly younger and probably correlates to the East Cliff Event in the English Chalk succession (Fig. 5).

The global positive carbon isotope shift of the SCBE (Scholle and Arthur, 1980; Jarvis et al., 2006) is well developed between ~168 mcd and 156 mcd in core Tarfaya SN°1 (Fig. 7). The total amplitude of the shift (~1.5‰) from average background values of -1‰ at the base (168 - 170 mcd) to 0.5‰ above the shift (average between 156 and 150 mcd) is substantially higher than in the English Chalk (0.6‰) and in the Scaglia limestone at Gubbio, Italy (0.4‰). The expanded succession in core Tarfaya SN°1 allows a detailed reconstruction of the $\delta^{13}C$ curve across this interval, which reveals a negative excursion with an amplitude of ~1‰ at the onset of the event (168.5 to 167.5 mcd) and a second short-lived negative excursion between 162.5 and 162 mcd (0.9‰ amplitude). In general, the variability of the $\delta^{13}C$ is considerably higher in the lower part (168 to 162 mcd) than in the upper part (162 to 156 mcd) of the excursion.

The similarity of the Tarfaya $\delta^{13}C$ record with the record of the Niobrara Formation in the US Western Interior Seaway (Locklair et al., 2011), which has an orbitally tuned chronology (Locklair and Sageman, 2008) and global carbon isotope stack of Wendler (2013), which was correlated to the GT012 timescale using planktonic foraminiferal zonation, allows a direct integration of the main isotopic events into the geological timescale. A comparison of the depth/age relationship for the main carbon isotope events in the Niobrara Formation, the global carbon isotope stack and Tarfaya is given in Figure 8. According to this compilation, average sedimentation rates in Tarfaya SN°1 and 2 are ~2.1 cm/kyr in the Coniacian, ~1.6 cm/kyr in the Santonian, and ~2.1 cm/kyr in the early Campanian (base of UC15c around 31.6 mcd). In contrast, late Turonian rates are difficult to estimate since the only potential tie point is the base of Magothy III sequence at ~90.2 Ma in the GT012 timescale. According to this age, late Turonian sedimentation rates would be ~5 cm/kyr.

The upper part of the stable carbonate isotope record (between 158.8 and 34 mcd) exhibits two distinct cycles corresponding to the 2 – 2.4 Myr eccentricity cycle, bearing similarity to long

eccentricity cycles in Mesozoic greenhouse sequences (Boulila et al., 2011) and in the third-order sequence record of the New Jersey Margin (Miller et al., 2003, 2004, 2005; Van Sickel et al., 2004; Browning et al., 2008; Kominz et al., 2008; Mizintseva et al., 2009).

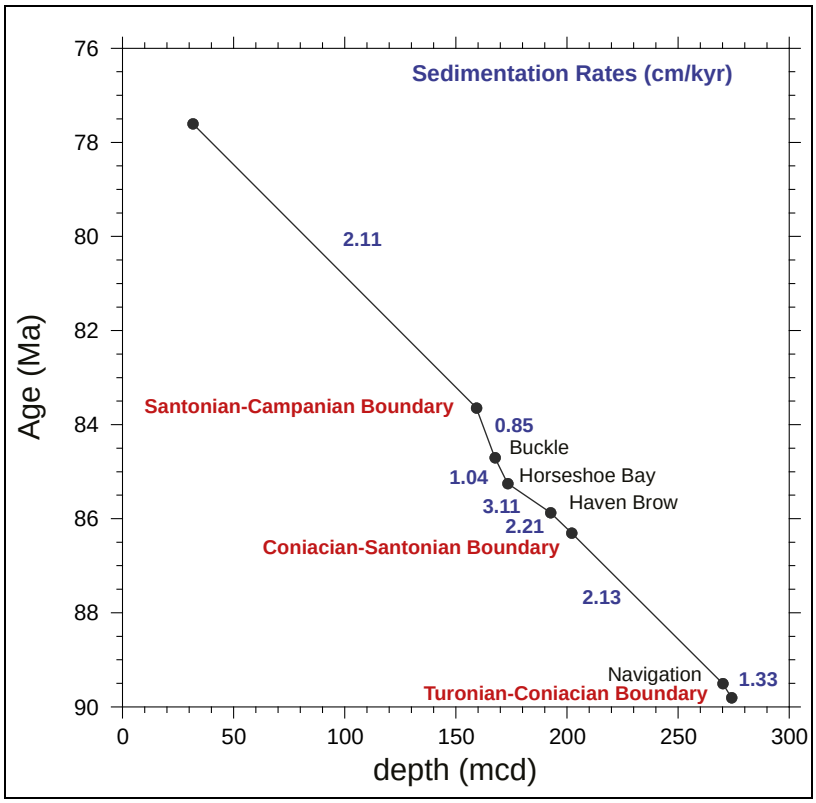

Figure 8: Age-depth plot of main carbon isotope events in the Tarfaya SN°1-2 composite section, following the chronology of Wendler (2013).

5. Conclusion

Two drill holes in the center of the Tarfaya Basin recovered a complete spliced record of 290 m organic rich marlstones of late Turonian to early Campanian age. High resolution XRF-scanner elemental records provide new insights into the sedimentary response of the depositional environment in the Tarfaya Basin to Late Cretaceous climate evolution and sea-level changes. Fluctuations in the abundance of the terrigenous elements Al, Ti, K, Si and Fe, normalized against Ca indicate three major sedimentary cycles of 33.2, 32 and 31 m thickness (286.7 to 253.5 mcd, 253.5 to 221.5 mcd and 221.5 to 190.5 mcd) during the Coniacian to middle Santonian. This time interval is also characterized by recurrent impinging of an expanded oxygen minimum zone onto the Tarfaya shelf, which is expressed by low Mn/S and high V/Ca ratios in the XRF-scanner records. The interval from 158.8 to 190.5 mcd (late Santonian), corresponds to the transition from anoxic to oxic

conditions, which dominate in the early Campanian. An increase of fine-grained carbonate and clay–rich hemipelagic sediment and increased bulk carbonate $\delta^{18}O$ values (indicating cooler conditions) are associated with improved bottom water oxygenation during the early Campanian.

The bulk carbon isotope record of the Tarfaya Basin exhibits strong similarities to the global carbon isotope stack of Wendler (2013). Marked events in the Tarfaya Basin, that are correlative to the English Chalk (Jarvis et al., 2006) and the Niobrara Formation in the US Western Interior Seaway (Locklair et al., 2011) are the Navigation Event in the earliest Coniacian, the Haven Brow, the Horseshoe Bay and the Buckle Events in the Santonian and the Santonian/Campanian Boundary Event. The comparison of the depth/age relationship of the main carbon isotope events indicates an average of sedimentation rate of ~2.1 cm/kyr during the Coniacian, ~1.6 cm/kyr during the Santonian and 2.1 cm/kyr during the early Campanian.

The sea-level record imprinted in the depositional sequences of the Tarfaya Basin is correlative to regional sea-level variations in the New Jersey Margin record (Miller et al., 2004; Mizintseva et al., 2009). In particular, we correlate the major unconformities U1/U2 and U3 in the Tarfaya Basin to the base of the Merchantville III and the base of Magothy III sequence of Miller et al. (2004) and Mizintseva et al. (2009). The unconformities at 253.5 mcd, 221.5 mcd and 190.5 mcd are correlated to the Cheesequake, Merchantville I and Merchantville II Sequences of Miller et al., (2004) and Mizintseva et al. (2009), respectively.

The Santonian/Campanian Boundary Event exhibits a positive carbon isotope excursion of 1.5‰, followed by a long-term cooling trend in the bulk $\delta^{18}O$ through the early Campanian. This climatic change is associated with an increase in terrigenous flux and cooler and drier conditions in the source area (indicated by an increase in the K/Al ratio related to a change from kaolinite to illite-dominated clay mineral assemblages) as a first step in the Campanian-Maastrichtian climate transition towards a cool greenhouse state.

Acknowledgements

This research was funded by RWE-DEA and ONHYM in the framework of the Atlantic Margin Integrated Basin Analysis Project and by the German Research Council (DFG) in the framework of SFB 754, TPA7. We thank Mohammed El Mallali for helping with sawing the cores in Rabat. We thank Dr. Nils Andersen (Leibniz Laboratory for Radiometric Dating and Stable Isotope Research) for stable isotope measurements, Dr. Dieter Garbe-Schönberg for advice with the XRF scanner and Wolfgang Reimers, Samuel Müller and Moritz Kuest for technical help.

Supplementary Material of Chapter III. A complete archive of late Turonian to Campanian sedimentary deposition in newly drilled cores from the Tarfaya Basin, SW Morocco

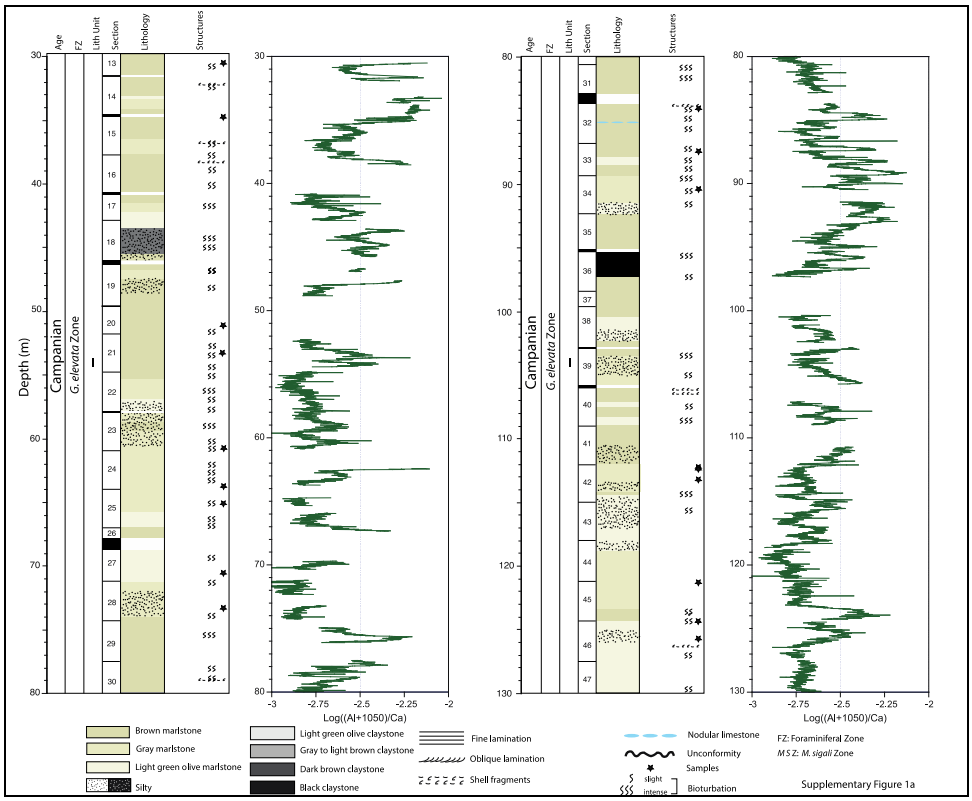

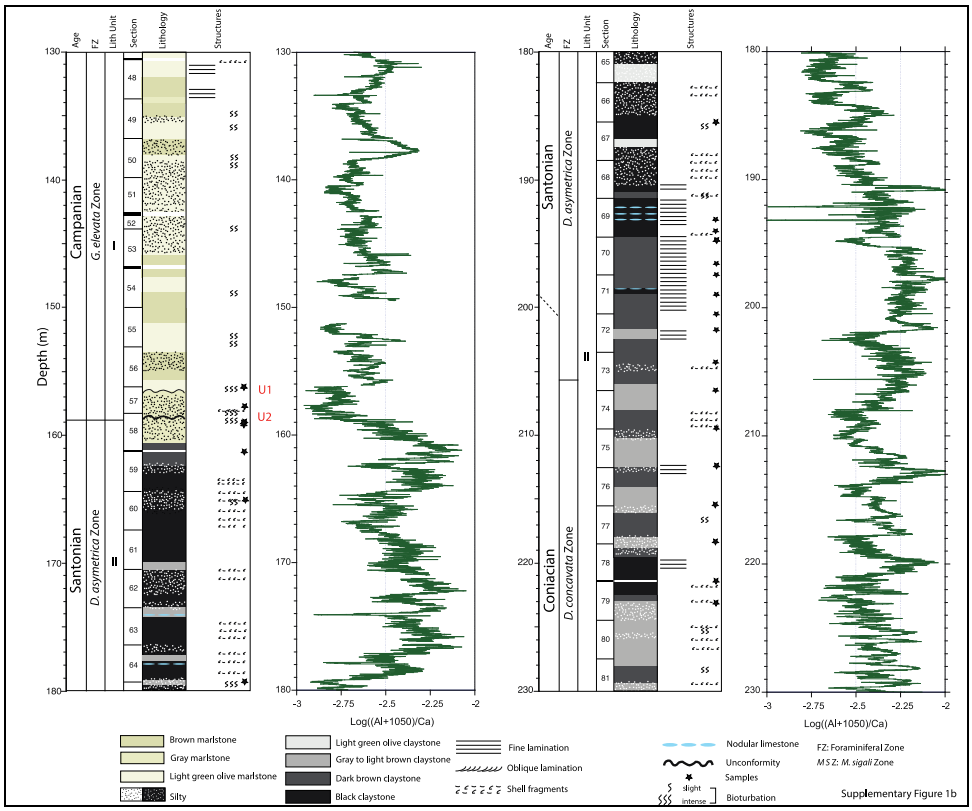

Supplementary Figure 1a and b: Generalized lithostratigraphic units of core Tarfaya SN°2 with the position of studied samples and log(Al+/Ca). Foraminiferal zonation follows Robaszynki and Caron (1995), except for the base of the *G. concavata* Zone due to the later occurrence of *G. concavata* in the Tarfaya Basin.

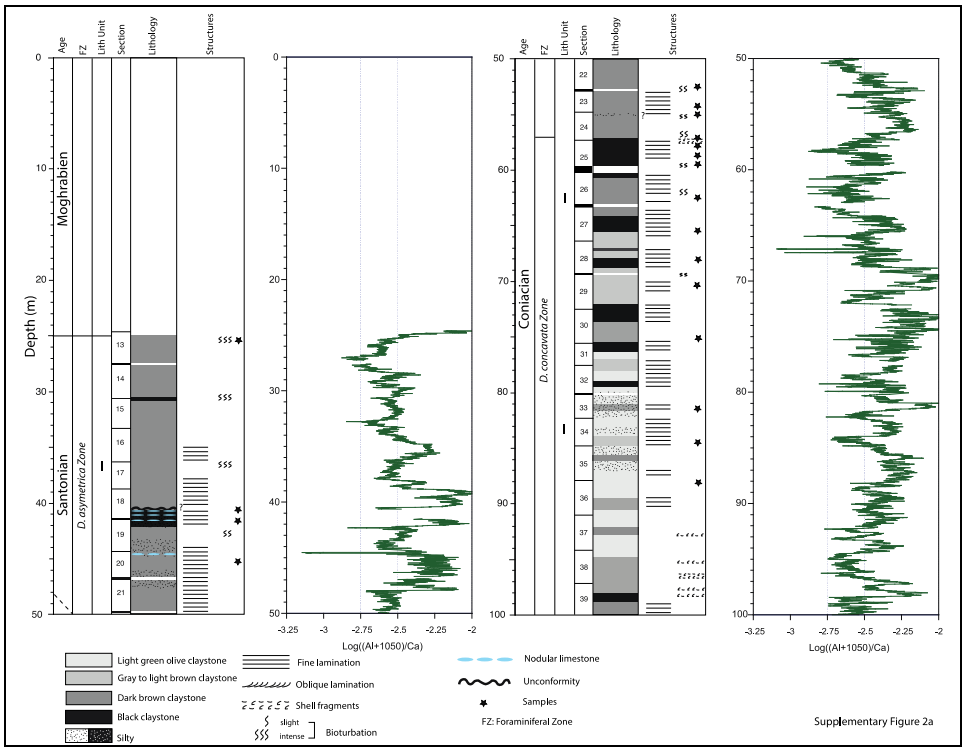

Supplementary Figure 2a

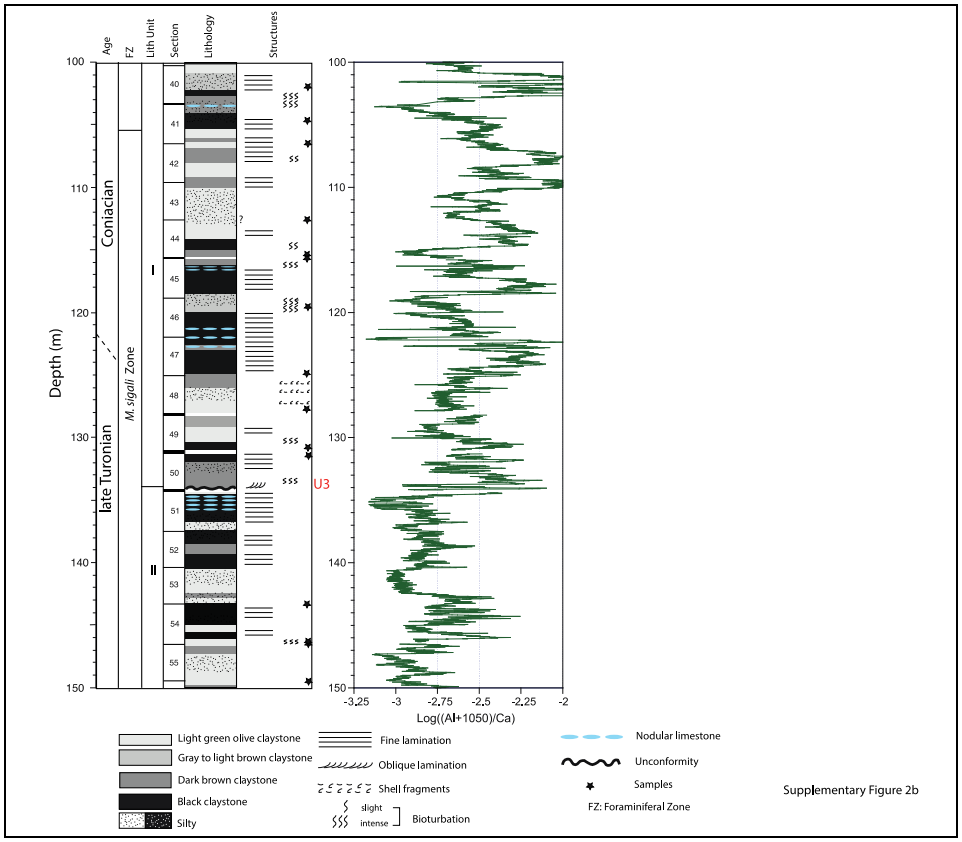

Supplementary Figure 2b

Supplementary Figure 2a and b: Generalized lithostratigraphic units of core Tarfaya SN°1 with the position of studied samples and log(Al/Ca). Foraminiferal zonation follows Robaszynki and Caron (1995), except for the base of the *G. concavata* Zone due to the later occurrence of *G. concavata* in the Tarfaya Basin.

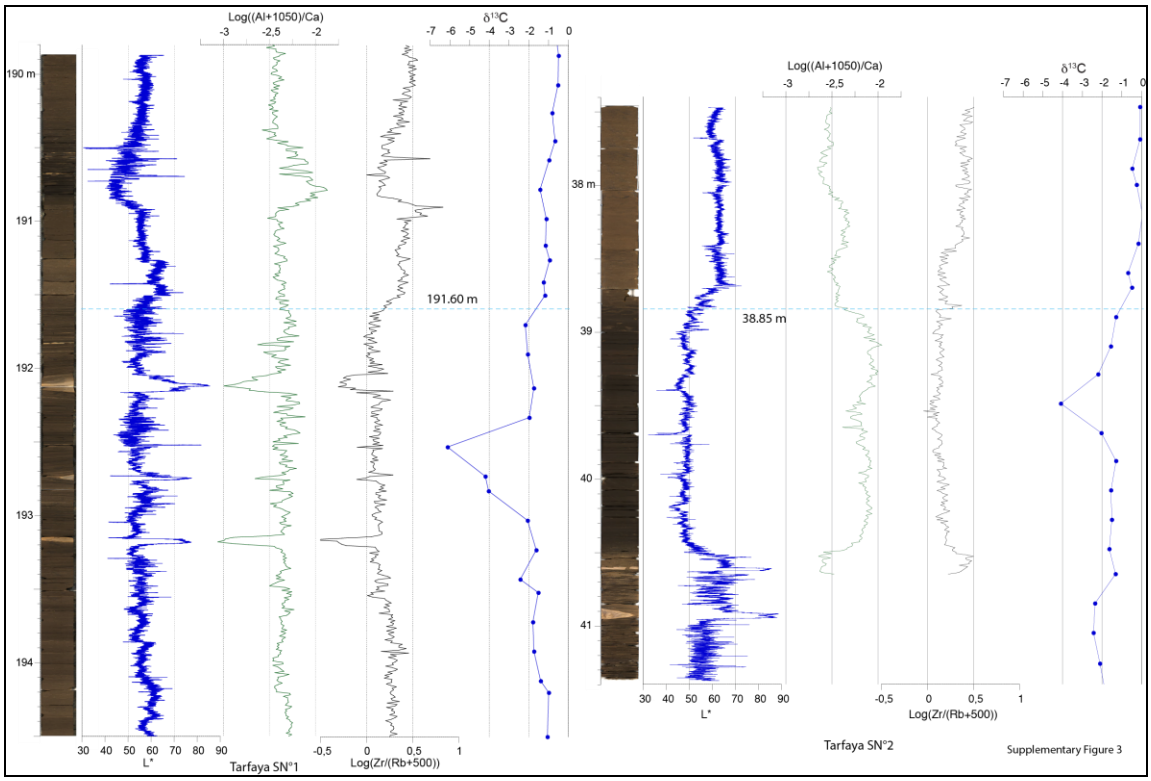

Supplementary Figure 3: Core photograph, line-scan (L*), geochemical (Al/Ca and Zr/Rb) and bulk carbon isotopes ($\delta^{13}C$) records of the correlation interval in the cores Tarfaya SN°1 and 2.

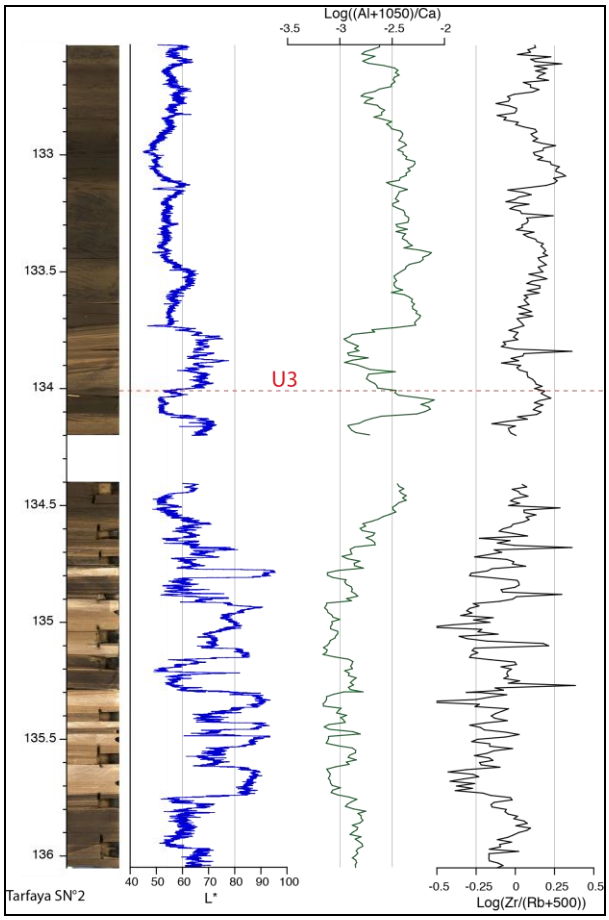

Supplementary Figure 4: Core photograph, line-scan (L*) and composite geochemical (Al/Ca and Zr/Rb) records of the unconformity U3 in the core Tarfaya SN°2.

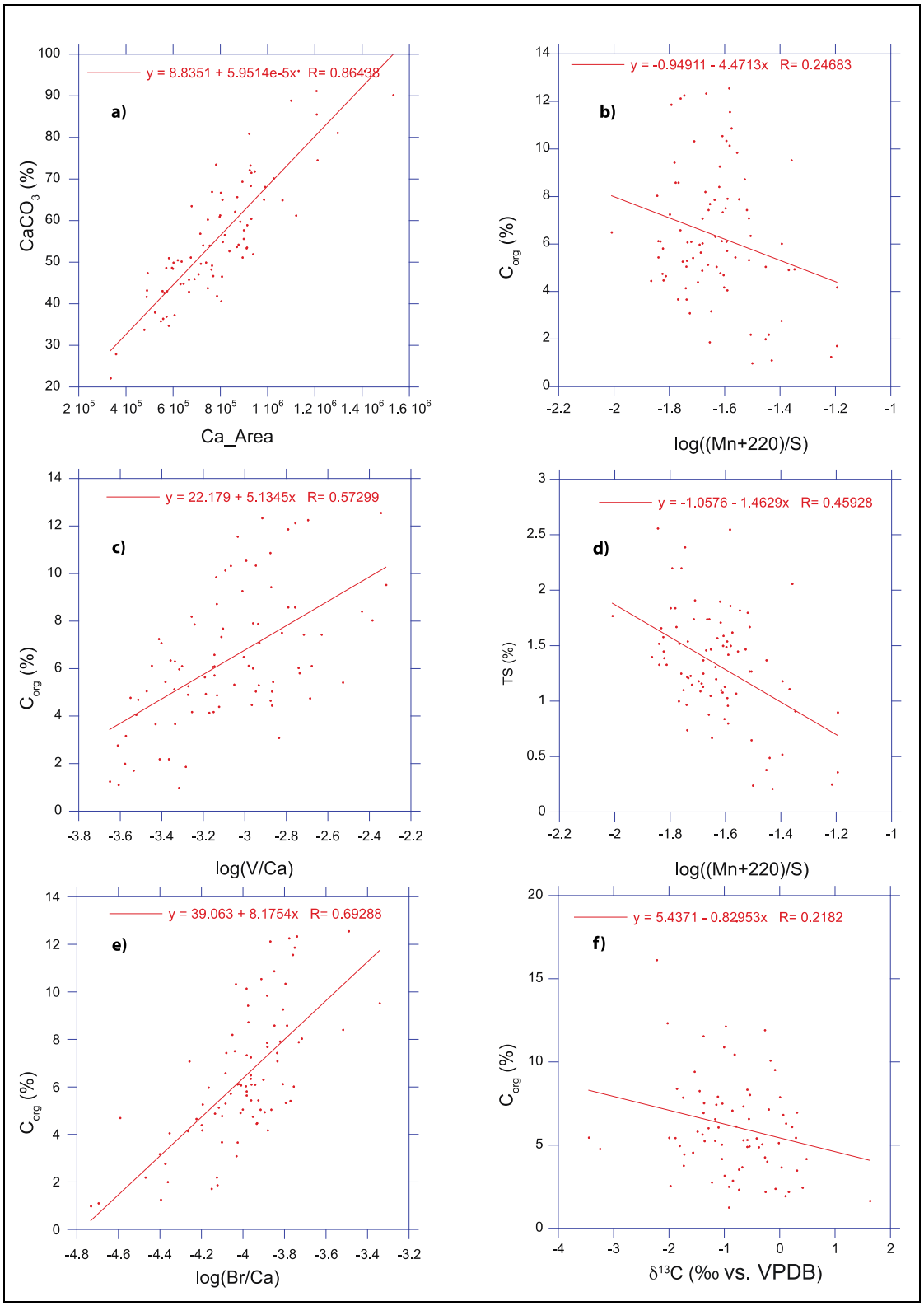

Supplementary Figure 5: Cross-plots of elements in the core Tarfaya SN°2 with linear regression lines. **a)** Cross-plot of $CaCO_3$ content (%) vs. Ca counts (XRF); **b)** Cross-plot of C_{org} (%) vs. log(Mn/S) (XRF); **c)** Cross-plot of C_{org} (%) vs. log(V/Ca) (XRF); **d)** Cross-plot of TS (%) vs. log(Mn/S) (XRF); **e)** Cross-plot of C_{org} (%) vs. log(Ba/Ca) (XRF); **f)** Cross-plot of C_{org} (%) vs. $\delta^{13}C$ (‰ vs. VPDB). $CaCO_3$ content (%), Total Sulfur (%) and Total Organic Carbon (%) are used as reference from Sachse et al. (2012).

Chapter IV. XRF core scanning techniques and its application in the Tarfaya Basin

1. Introduction

High-resolution stratigraphic and environmental information plays a major role in modern palaeoceanographic and sedimentological research. Various geochemical records are used as the basis of climate and environmental interpretation. The acquisition of these geochemical records is generally time consuming and also leads to loss of sediments. In contrast, the X-ray fluorescence (XRF) core scanner offers an economic way to estimate the chemical composition of the rocks and sediments. The XRF core scanner allows non-destructive, near continuous and relatively fast analysis of major and some minor elements from Aluminum (Al) through Uranium (U). The first prototype XRF core scanner was produced by the Netherlands Institute of Sea Research (NIOZ) in 1988 (Jansen et al., 1998). Since then, in many recent scientific publications XRF core scanner records of sediment cores are used to support the interpretation of paleo-environment and paleoclimate (Table 1).

A computer-controlled XRF that is able to perform high-resolution measurements within a short time (few seconds). The system used for the XRF core scanner has important advantages such; a very high resolution can be achieved to produce nearly continuous records, XRF measurements can be carried out rapidly, which can help to adapt coring and sampling programs and provides data about the actual composition of the sediment. Results obtained by XRF core scanner is usually presented in the form of count rates (expressed as counts per unit time per unit area), or intensities of elements (Richter et al., 2006; Rothwell et al., 2006; Thomson et al., 2006).

In this work, we present more result of the XRF core scanner on the cores of Tarfaya SN°1 and 2, and to develop a basic technique to normalize the data for further geochemical study. XRF studies of biogeochemical elements e.g. Ca, Si, Ba, V, Br, P can be used to understand changes in productivity (e.g., Brumsack, 1986, 2006; Scopelliti et al., 2006; Tribovillard et al., 2006; Mayer et al., 2007; Ziegler et al., 2008). XRF scanning measured elements Al, K, Ti and Fe elements which allow to constrain terrigenous input in the basin. Whereas, the elements as Fe, Mn and S can be used to depict the redox environment and oxygenation in the basin. Our objectives in this study are to illustrate changes in elements (Al, Ti, Fe, S, Mn, Ca, Ba, Br, Si, K, Br, P), in carbonate content, in organic carbon total sulfur and to reconstruct the paleo-environment changes during the Upper

Cretaceous in the Tarfaya Basin from the XRF scanning.

Author	Publication date	Scientific objectives	Age of sediments
Peterson et al.	2000	Rapid Changes in the Hydrologic Cycle of the Tropical Atlantic, Fe and Ti proxy of terrigenous input.	Past 90,000 years
Haug et al.	2001	Ti and Fe data from the anoxic Cariaco Basin can be used to infer variations in the hydrological cycle over northern South America.	Holocene
Arz et al.	2003	Influence of Northern Hemisphere climate and global sea level rise on the restricted Red Sea marine environment, Fe and Ti proxy of terrigenous input.	Late Holocene
Jaccard et al.	2005	Glacial/Interglacial Changes in Subarctic North Pacific Stratification, Ba/Al ratio proxy of productivity.	Ice ages
Thomson et al.	2006	A geochemical application of the ITRAX scanner to a sediment core containing eastern Mediterranean sapropel units	
Rothwell et al.	2006	Turbidite emplacement on the southern Balearic Abyssal Plain (western Mediterranean Sea)	Marine Isotope Stages 1–3
Yancheva et al.	2007	Ti content of the sediments of Lake Huguang Maar in coastal southeast China used as proxies for the strength of the winter monsoon winds.	Middle and late Holocene
Löwemark et al.	2008	Arctic Ocean manganese contents and sediment colour cycles	
Diekmann et al.	2008	Variations in the modes and sources of detrital sediment input.	Northwestern Taiwan between 28 and 19.5 ka BP and from East China sources between 19.5 and 11.2 ka BP.
Tjallingii et al.	2010	Infilling and flooding of the Mekong River incised valley during deglacial sea-level rise	
Löwemark et al.	2011	Paleoproxy data from organic-rich lake records	The last 4 ky
Hennekam and de Lange	2012	Paleoclimatic studies	
Ma et al.	2014	Lithogenic, biogenic, and syngenetic-authigenic proxies through the uppermost Lincoln Limestone Member, the Hartland Shale Member, and the Bridge Creek Limestone Member, including oceanic anoxic event 2 (OAE 2)	Cenomanian/Turonain (Upper Cretaceous)

Table 1. Overview of using XRF core scanner records of sediment cores to support the interpretation of paleo-environment and paleoclimate.

2. X-ray fluorescence (XRF)

2.1. XRF analytical technique

The principle of XRF, for the first time, was discussed by Jenkins and De Vries (1970). XRF analysis is based on excitation of electrons by incident X-radiation. Incident X-rays eject an electron from an inner shell of an atom. The resulting vacancy is then filled by an electron from an outer shell (Fig. 1). The electron gives up its surplus energy in the form of electromagnetic radiation. The surplus energy, which is equal to the energy difference between the two electron shells, appears as X-rays. So, each couple of shells produces a characteristic radiation and, therefore, every atom emits its own characteristic energy and wavelength spectra. The detector detected every atom emits and store it as elements intensity indicated by a spectrum. This spectrum (with *.*spe* file or *.*wax* files) is built up by dividing the energy spectrum into discrete bins and counting the number of pulses registered within each energy bin. The radiation is transmitted within a Helium (He) flushed chamber to minimize scatter and absorption of radiation between source and detector. The intensity of the fluorescence from a sample can be used to determine the abundance of different elements. Jenkins et al., 1995 used the theoretical calculations (e.g., the method of fundamental parameters) and/or the known standards to determine the elemental concentrations from the intensities (count rates) of the X rays at each energy level.

The XRF Core Scanner measures the intensity of elements in multiple runs depending on the generator settings; voltage and count rate can be adjusted by changing the power (mA) and or measurement duration (time). Filters are used during high-energy runs (e.g. 30 and 50 kV) to reduce the background, which originates predominately from scatter of the initial radiation. Overview of the recommended settings (kV) for the most common elemental range analyses with the XRF core scanner are presented in Table 2. The optimed source power (mA) can best be found by a test run on the lightest and the darkest part of the sediment core.

Tube voltage (kv)	Filter	Elements analysed
10	None	Al, Si, P, S, Cl, K, Ca, Ti, Mn, Fe, Cu, Zn
20	None	K, Ca, Ti, Mn, Fe, Br, Rb, Sr
30	Pd thick	Br, Rb, Sr, Zr
50	Cu	Ba, Pb, U

Table 2: Instrumental settings of the Avaatech XRF core scanner for specific sets of elements after Richter et al. (2006).

The XRF Core Scanner obtains a spectrum of element unique fluorescence lines at each position. WinBatch is software applies background subtraction, sum- and escape-peak corrections and peak integration. The peak integration procedure uses an iterative least-square fitting procedure of Gaussian functions to approximate the area under the fluorescence lines of the spectrum (yellow area in Figs. 2 and 3). A MS Excel file produced from WinBatch indicates the peak integration results as the initial element intensities (Area) and a goodness of fit parameter (chi-square) that should ideally be < 3. The WinAxil application (package from Canberra Eurisys) allows one to create or modify a processing model. Additional K- and L-line can be add to *.*spe* file or *.*wax* files and can be save as a processing model *.*mod*. The model should identify as much spectral lines as possible and for the Tarfaya Samples we use the Kiel model.

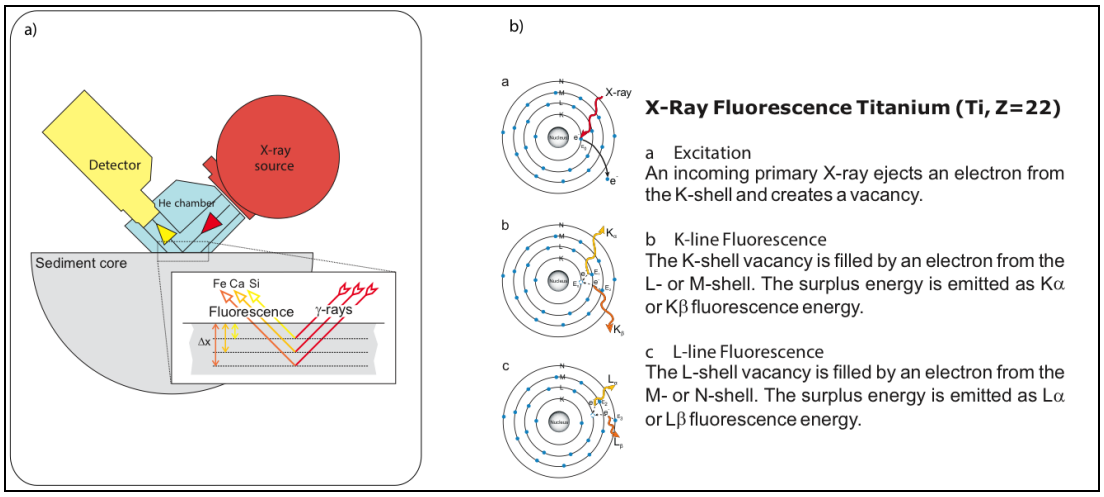

Figure 1: a) Schematic overview of excitation geometry of the X-ray fluorescence analysis of the elements Si, Ca, and Fe by the XRF core scanner after Richter et al., 2006. Elements in the sediment are ionized by the primary X-rays and emit an element-specific fluorescence radiation, which is registered by the detector. **b)** Schematic overview of excitation of atoms by the X-ray fluorescence analysis.

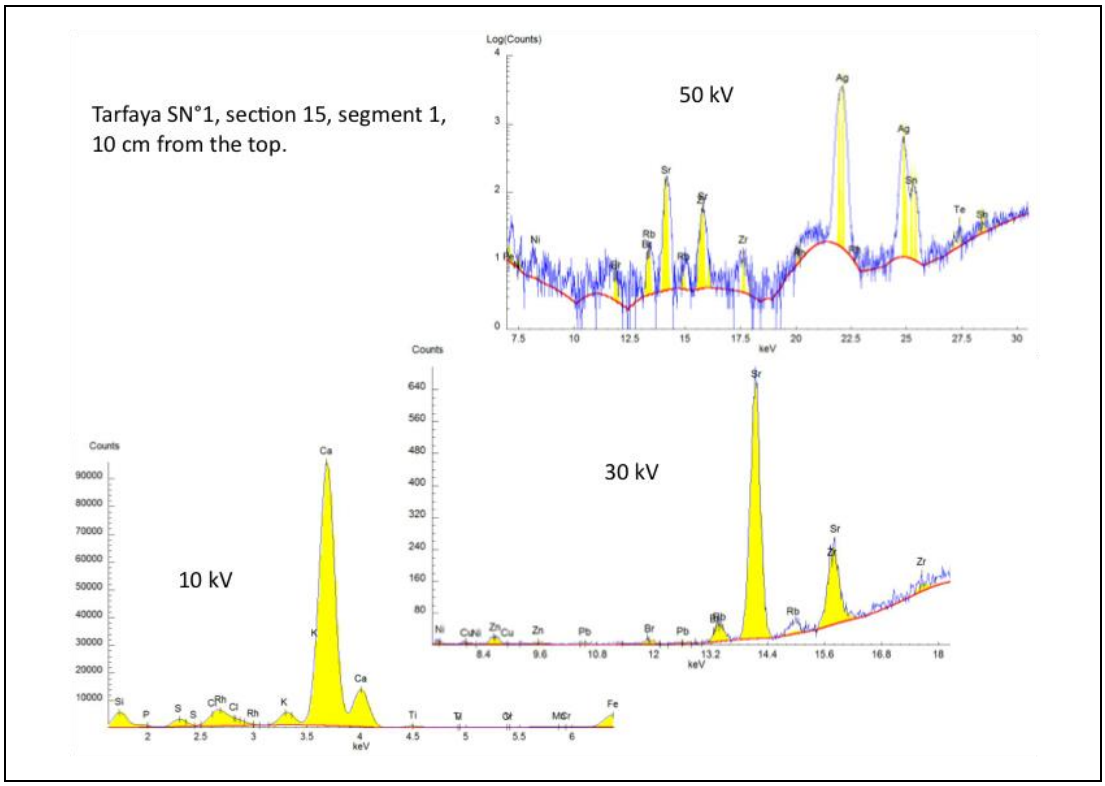

Figure 2: XRF core scanner spectra of 10, 30 and 50 kV run and the element intensities as area in yellow at position 10 cm in section 15 (segment 1) at Tarfaya SN°1.

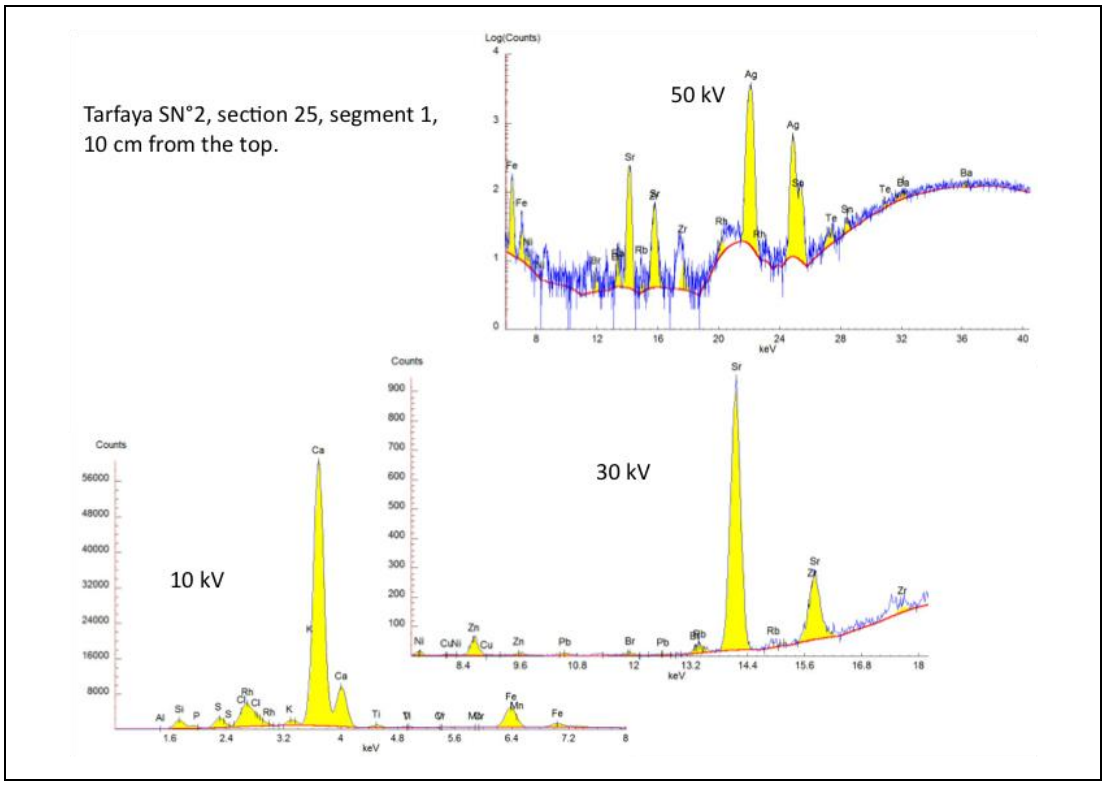

Figure 3: XRF core scanner spectra of 10, 30 and 50 kV run and the element intensities as area in yellow at position 10 cm in section 25 (segment 1) at Tarfaya SN°2.

2.2. Sample preparation

The sediments recovered from two drilled cores Tarfaya SN°1 and 2 were split into two halves with a high precision Kaufmann-Titan diamond rock saw in order to produce a smooth surface for analyses. Sediments were cleaned with normal water before logging. The core surface was covered with 4 μm thickness Ultralene plastic film to avoid contamination and to protect the detector. Measurements were taken continuously over the entire spliced core length at 1 cm intervals with a downcore slit size of 10 mm over a 1 cm^2 area.

2.3. Applicability of XRF scanner derived elemental ratios in cores Tarfaya SN°1 and 2 for paleoenvironmental reconstruction

2.3.1. Iron normalized S, Br and Mn

An enrichment of sulfur in sediments is related to pyrite formation under dysoxic or anoxic bottom or pore water conditions and is associated with enhanced accumulation of organic matter (OM) (e.g., Leventhal, 1983; Arthur and Dean, 1998; Canfield et al., 1996; Raiswell and Canfield, 1998; Anderson and Raiswell, 2004). The OM in the black shales is significantly enriched in sulfur when compared to marine planktonic material due to the reaction of reduced sulfur species with OM during early diagenesis (François, 1987; Aizenshtat et al., 1983, 1995; Passier et al., 1999; Werne et al., 2004). Geochemical analysis of discrete samples from Tarfaya SN°2 indicates that the total sulfur (TS) and total organic carbon (TOC) contents are positively correlated and controlled by the redox status of the environment and the intensity of microbial sulfate reduction during deposition (Sachse et al., 2012). In Tarfaya SN°2, XRF-scanner derived log(S/Ca) and log(S/Fe) exhibit weak correlations with TS (r=0.54 and r=0.10) and TOC (r=0.32 and r=0.11) (Fig. 4) only correlations with $r > 0.5$ are regarded as significant but closely match TOC and TS cyclicity during intervals where intermediate-high resolution discrete measurements are available (i.e. between 135 and 145 m).

The geochemistry of bromine in marine sediments is mainly controlled by the organic fraction of marine sediments and by diagenetic reactions involving organic matter degradation (Bojanowski and Paslawska, 1970; Calvert and Pedersen, 1993). Bromine in the particulate phase of sediments is associated with marine organic matter (Price et al., 1970; Harvey, 1980) since marine primary producers and heterotrophic organisms commonly produce brominated compounds (Fenical, 1975; Gribble, 1998; Van Pée, 1996). The ratio of bromine to TOC is constant in most marine evironments

(i.e. Ten Haven et al., 1987) and thus bromine can be used as a proxy for organic matter accumulation. Recently, Ziegler et al. (2008) demonstrated a strong correlation of XRF-scanner derived bromine values to marine organic carbon content of late Pleistocene organic-rich sediment cores from the Arabian Sea. However, the concentration of bromine in terrestrial organic matter is significantly lower than in the oceans and the ratio of bromine to organic carbon has been even used to distinguish marine from terrigenous organic matter (Mayer et al., 1981 and 2007; Malcolm and Price, 1984; Upstill-Goddard and Elderfield, 1988). In the Late Cretaceous Tarfaya Basin, where the flux of terrestrial organic matter was almost neglible, the ratio of bromine counts and log(Br/Ca) to TOC remained constant (r=0.59 and 0.54, Fig. 4) and XRF-scanner derived bromine provides thus a robust tool for high-resolution estimates of marine organic matter accumulation.

The accumulation of manganese in marine sediments is highly sensitive to fluctuations in bottom water oxygen conditions (Hem, 1972; Dickens et al., 1994; Calvert and Pedersen, 1993; De Lange et al., 1994). Under oxic conditions, Mn precipitates predominantly as insoluble Mn oxyhydroxides with only a relatively small amount present as dissolved Mn^{2+} (Martin and Whitfield, 1983). The solubility of Mn oxyhydroxides largely increases under oxygen deficient bottom water or pore water conditions within oxygen minimum zones (OMZ) (Saager et al., 1989; Johnson et al., 1992; Dickens et al., 1994) and Mn is generally depleted in sediments deposited under OMZ conditions (Hetzel et al., 2009). Surprisingly, in the Tarfaya SN°2 record higher Mn concentrations correlate to intervals of higher S and TOC accumulation during periods of an expanding OMZ. Similar trends of increased Mn accumulation despite decreasing basin oxygenation were observed in other sedimentary environments and have been related to enhanced input of Mn from hydrothermal activity, gas hydrate dissociation, rapid re-oxygenation events at the margins of the OMZ, or redistribution of Mn within the basin during the intensification of the OMZ (Renard et al., 2005; Schenau et al., 2002).

2.3.2. Iron normalized Ba and P

The Ba content in the sediments is a residue from dissolution and oxidation of hard and soft parts of carbonate and siliceous organisms, thus directly related to primary productivity during deposition and can be used as a proxy of paleoproductivity (Dymond et al., 1992). The strong correlation of particulate organic carbon with barium fluxes over broad areas of the modern ocean indicates a connection between barium removal in the oceans and biological processes (Dymond et

al., 1992). It is thus somewhat surprising, that our records from Tarfaya SN°2 indicate no significant correlation of Ba measurements with TOC (Fig. 4). A possible explanation would be early diagenetic remobilization of biogenic barium. Arndt et al. (2006) show in a transport-reaction model that OM degradation and anaerobic oxidation of methane above the black shales of Demerara Rise influence sulfate availability and therefore favor the remobilization of biogenic barium.

Phosphorus (P) is one of the essential elements for life on Earth and plays an important role in the biological productivity in oceans and on continents. The changes in the oceanic P-cycle may considerably affect the chemistry of the oceans and atmosphere throughout geological time (Van Cappellen and Ingall, 1994, 1996). The main input of organic and inorganic P compounds into the oceans is by riverine transport (Benitez-Nelson, 2000). The major part of this input is trapped in estuarine and coastal shelf areas (Ruttenberg, 1993), and the remaining particulate and dissolved P is transported to the deep ocean. During transport, the predominant portion of P, which is associated with organic compounds, is decomposed microbially within the water column (Heggie et al., 1990; Baturin, 2003; Paytan and McLaughlin, 2007). In the Tarfaya Basin, log-ratios of (P+4000)/Ca and (P+4000)/Fe show a good linear correlation with log((Ba+5500)/Ca) and log((Ba+5500)/Fe) (linear correlation factor of $r = 0.856$ and $r = 0.933$, respectively (Fig. 4) indicating that P and Ba accumulations are useful proxies of productivity in the Tarfaya Basin and can be used to evaluate changes in nutrient availability and primary production.

2.3.3. Calcium-normalized Si, Fe, Ti, Al and K

Terrigenous materials are transported into the oceans via fluvial and eolian pathways, which are both sensitive to climate changes (Milliman and Meade, 1983; Miller and Russell, 1992; Rea, 1994) and/or to the variations in sea-level (Milliman et al., 1975). A number of studies used the major element (Fe, Ti and Al) composition of marine sediment cores to trace changes in terrigenous input into the basins (Peterson et al., 2000; Yarincik et al., 2000; Haug et al., 2001; Zabel et al., 2001; Adegbie et al., 2003; Jaeschke et al., 2007; Mulitza et al., 2008; Tisserand et al., 2009). Increases in Fe and Ti can be interpreted as enhanced input of siliciclastic material of fluvial origin (Peterson et al., 2000; Haug et al., 2001). The ratios of Ti/Ca, Al/Ca and Fe/Ca are most commonly used for paleoclimate reconstructions. For instance, Fe/Ca and Ti/Ca ratios have been used to trace changes in terrigenous input of fluvial origin in particularly offshore northeastern Brazil (Arz et al., 1998 and 1999; Jaeschke et al., 2007) and western Africa (Adegbie et al., 2003; Pierau et al., 2010). Ti is

enriched in the coarse sediment fractions of marine sediments (Schütz and Rahn, 1982; Shiller, 1982), while Al is associated with fine-particle clay minerals (Biscaye, 1965). In Tarfaya SN°2, log(Fe/Ca), log(Ti/Ca), log(Al/Ca) as well as log(Si/Ca) and log(K/Ca) (not shown) exhibit similar trends, reflecting changes in riverine terrigenous flux. Biogenic Si and Fe coated eolian grains are present, but do not constitute a significant component of the sediment accumulated during the Late Cretaceous in the Tarfaya Basin (unpublished thin section analysis of outcrop sections).

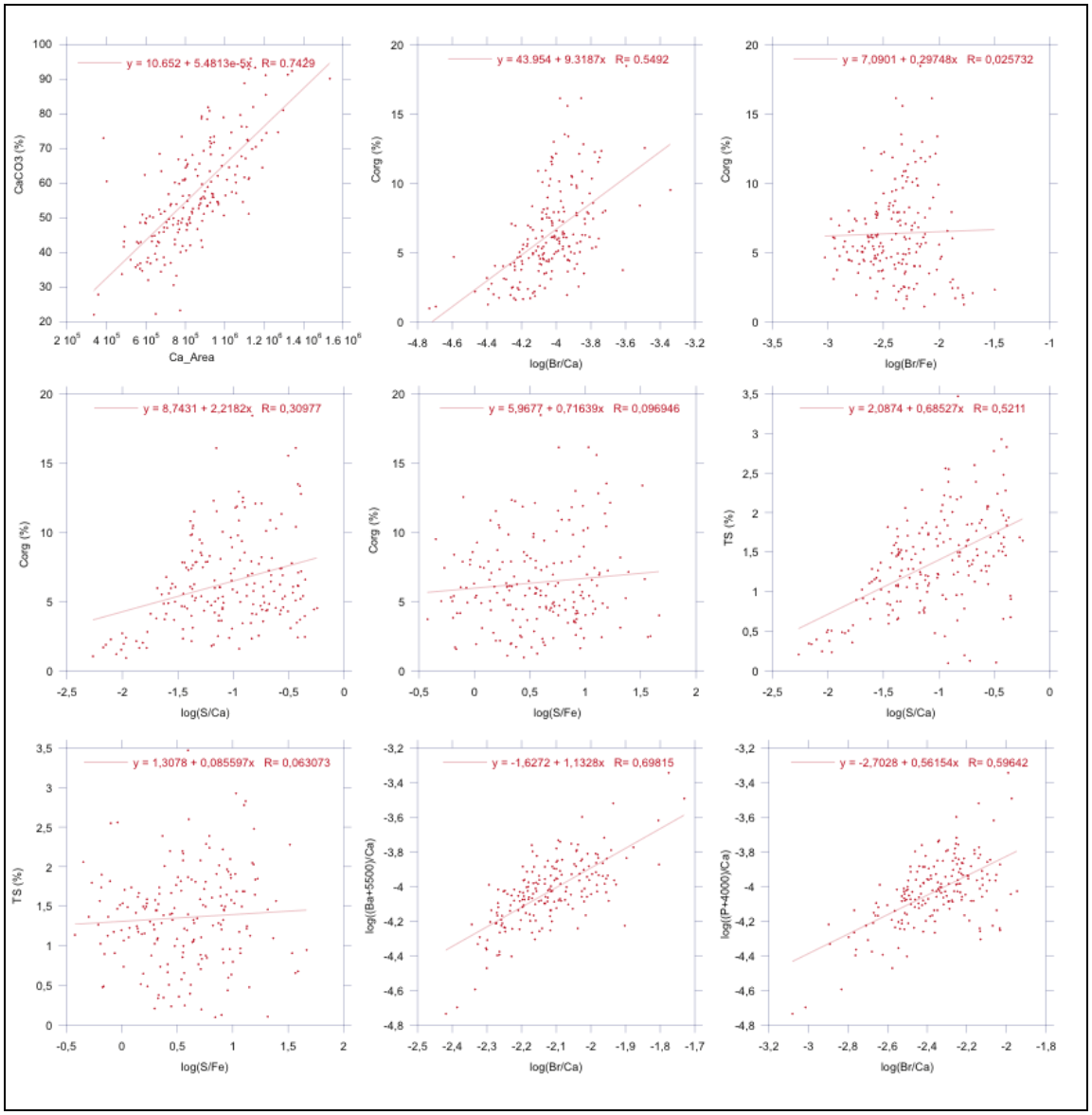

Figure 4: Cross-plots of elements in the Tarfaya SN°2 core with linear trend lines. a) Cross-plot of $CaCO_3$ content (%) vs Ca counts (XRF); b) Cross-plot of Corg (%) vs log((Mn+220)/S) (XRF); c) Cross-plot of Corg (%) vs log(V/Ca) (XRF); d) Cross-plot of TS (%) vs log((Mn+220)/S) (XRF); e) Cross-plot of Corg (%) vs $\delta^{13}C$ (‰ vs. VPDB). $CaCO_3$ content (%), Total Sulfur (%) and Total Organic Carbon (%) are used as reference from Sachse et al. (2012).

2.4. XRF-scanning elemental distribution in cores Tarfaya SN°1 and 2

Although, we presented most significant elemental ratios in the previous chapter. However, in this chapter we will concentrate individual element behavior against Ca and Fe in more detail to display terrigenous sediment flux, oxygenation, and productivity within the basin. In a first approach, we plotted (Figs. 5 and 7) log-ratios of the elements Al and Ti (major components of detrital sediments), Mn and S (oxygenation), Br, P and Ba (productivity) versus Ca (carbonate-rich sediments) to visualize the relationship of these elements with Ca. log(Fe/Ti) ratio was also used which allows to depict source of the iron (terrigenous or marine). Lack of variability in the log(Fe/Ti) curve indicates that both iron and titanium have a similar origin e.g. terrigenous. Therefore in a second approach, we plotted (Figs. 6 and 8) log-ratios of elements (Ti, Mn, S, Ba and P) against Fe to investigate their relative variability, independent from Ca because log-ratios of all elements against Ca, which represents a major element in sediments, show generally a similar trend and also to visualize the other proxy of oxygenation, productivity and productivity in the basin.

The log(Al/Ca) and log(Ti/Ca) curves exhibit similar trend as log((Al+Ti+Fe+K+Si)/Ca) curve, which is a proxy for the terrigenous flux. The log(Mn/Ca) and log(S/Ca) cures show similar trend due to influence of Ca. High Mn related to increased oxygenation. In contrast, high S indicates an increase degree of pyritization, which indicate low oxygenation. Log(Mn/Fe) and log(S/Fe) have same influence of Fe. To solve this issue, we use log(Mn/S) in the previous chapter to illustrate the oxygenation in the basin. The log(Ba/Ca) and log(P/Ca) cores exhibit a similar trend to log(Br/Ca), which are presented in the previous chapter. These log-ratios show good correlation with log(Br/Ca) (linear correlation factor of r = 0.70 and r = 0.60, respectively). The log(Ba/Fe) and log(P/Fe) also exhibit a similar trend to log(Br/Fe). In contrast, similar trend to log(Br/Fe) show a weak correlation to C_{org} (%) (linear correlation factor of r = 0.03) (Fig. 4).

2.4.1. Tarfaya SN°1

The ratios of terrigenous elements Al and Ti against Ca (log(Al/Ca) and log(Ti/Ca)) are relatively higher in the upper Turonian to Santonian interval (158.8-273 m) with mean values of -2.432 and -2.305, respectively (Fig. 5). This interval exhibits also high variability in log(Al/Ca) and log(Ti/Ca) (standard deviation of 0.181 and 0.224). In the lower Campanian (30-158.8 m), log(Al/Ca) and log(Ti/Ca) exhibit a low value (mean values of -2.625 and 2.519 of Al/Ca and Ti/Ca)

and relatively low variability in comparison to the upper Turonian to Santonian interval. The log(Fe/Ti) shows major decrease at 190 m (middle Santonian) with values drop from 1 to 0.7.

The log(Mn/Ca) and log(S/Ca) exhibit a highest values in the upper Turonian to Santonian interval (158.8-273 m) with mean values of -2.868 and -1.375 and lowest in the lower Campanian with mean values of -3.175 and -1.848, respectively. The upper Turonian to Santonian interval is characterized by relative high variability with standard deviation of 0.283 and 0.269 of log(Mn/Ca) and log(S/Ca), respectively. Whereas, log(Mn/Fe) and log(S/Fe) indicate no major change in the core Tarfaya SN°1 (mean values of -1.437 and -0.020), except in the Santonian which the log(Mn/Fe) and log(S/Fe) an increases in trends. The log(Mn/Fe) and log(S/Fe) show a relatively high variability in upper Turonian to Santonian interval (standard deviation of 0.314 and 0.301) than lower Campanian (standard deviation of 0.284 and 0.218, respectively) (Figs. 5 and 6).

The log(Br/Ca), log(Ba/Ca) and log(P/Ca) show a higher values in the Santonian interval (158.8-200 m) (mean values of -3.449, -1.988 and -2.167, respectively) and lowest values in the lower Campanian (30-158.8 m) (mean values of -3.822, -2.176 and -2.390, respectively), lower Conacian (~245 m) and late Turonian (240-273 m) (mean values of 3.434, -2.105 and -2.364, respectively). The upper Turonian to Santonian interval exhibits a high variability with standard deviation of 0.228, 0.125 and 0.141 of the log(Br/Ca), log(Ba/Ca) and log(P/Ca), respectively. The log(Ba/Fe) and log(P/Fe) exhibit relatively lower values in the upper Turonian to lower Santonian interval (200-273 m) (mean values of -1.955 and -0.626) and higher in middle and upper Santonian and in the lower Campanian (mean values of -2.114 and -0.469, respectively). Log(Ba/Fe) and log(P/Fe) exhibit a high variability in the upper Turonian to lower Santonian interval with standard deviation of 0.242 and 0.200, respectively. The log(Br/Fe) shows no major changes in the cores Tarfaya SN°1 (Figs. 5 and 6).

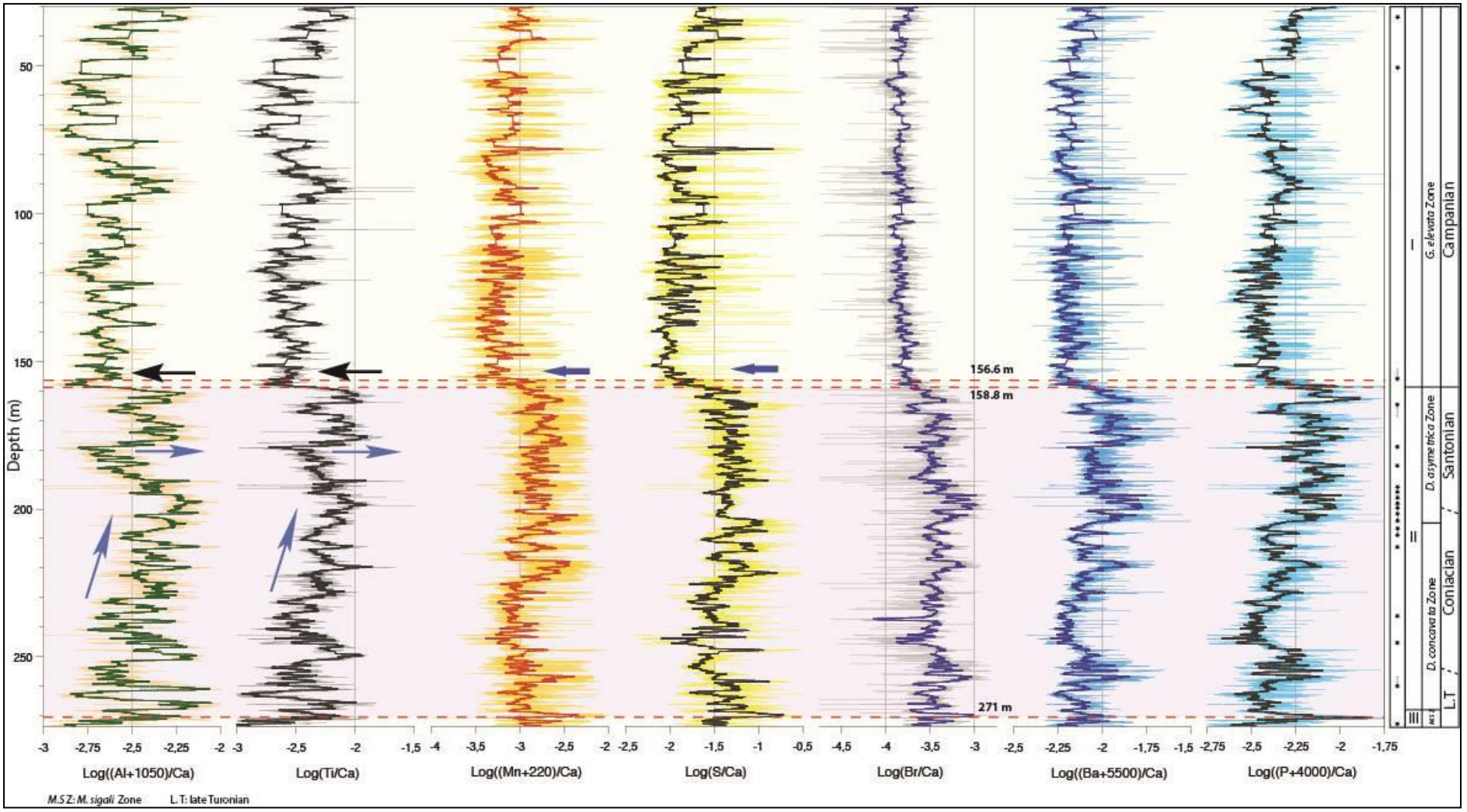

Figure 5: Composite geochemical and paleontological records in newly drilled core Tarfaya SN°1. Log-ratios of elements (Al, Ti, Mn, S, Br, Ba and P against Ca) were derived from X-ray fluorescence scanning. Black arrows indicate decrease in terrigenous flux in the Tarfaya Basin and light blue arrows indicate vice-versa. Dark blue arrows indicate increse in oxygenation in the Tarfaya Basin.

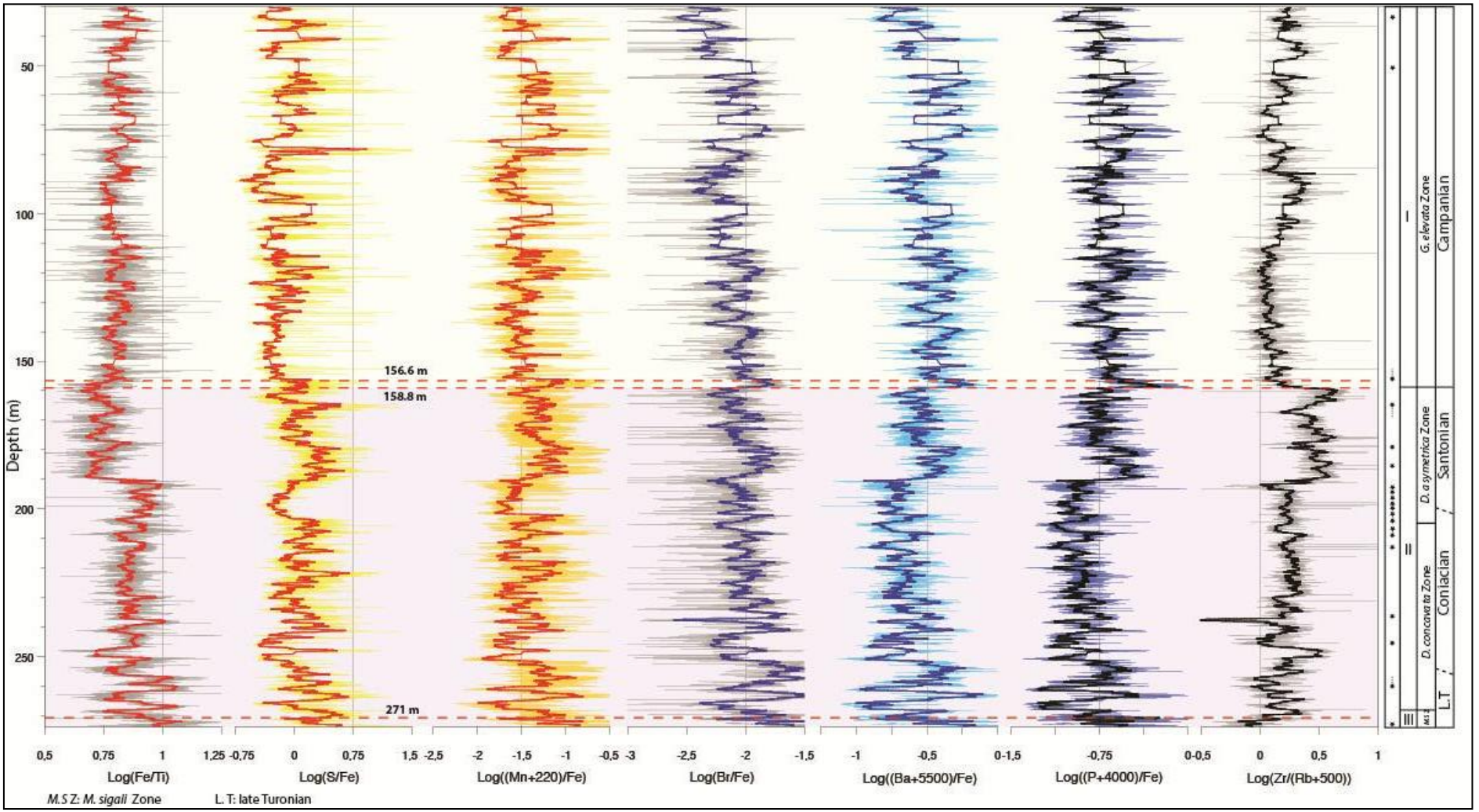

Figure 6: Composite geochemical and paleontological records in newly drilled core Tarfaya SN°1. Log-ratios of elements (Ti, Mn, S, Br, Ba and P against Fe) were derived from X-ray fluorescence scanning.

Tarfaya SN°2

The ratios of terrigenous elements against Ca (log(Al/Ca) and log(Ti/Ca)) are relatively high in the Coniacian to Santonian interval (24-134 m) with the mean of -2.452 and -2.313, respectively. This interval exhibits also a high variability in log(Al/Ca) and log(Ti/Ca) with standard deviation of 0.197 and 0.250, respectively. The upper Turonian (134-190 m) exhibits a low value (mean values of -2.88 and -2.935 of Al/Ca and Ti/Ca) and relatively low variability in comparison to the Coniacian to Santonian interval. The high values of the log(Al/Ca) and log(Ti/Ca) characterized the base of the core Tarfaya SN°2 (190-200 m) with mean values of -2.55 and -2.349 and standard deviation of 0.199 and 0.217, respectively (Fig. 7).

The log(Mn/Ca) and log(S/Ca) exhibit no clear trend in the core Tarfaya SN°2 with mean values of -2.932 and -1.353, respectively. Log(Mn/Ca) and log(S/Ca) exhibits a high variability in the upper Turonian (134-200 m) with standard deviation of 0.393 and 0.508, respectively. In contrast, log(Mn/Fe) and log(S/ Fe) are higher in the upper Turonian (134-190 m) with mean values of -0.845 (±0.276) and 0.745 (±0.319), respectively. These high variation in standard deviations indicate higher variability in log(Mn/Fe) and log(S/ Fe) ratios and hence productivity. On the other hand, lower mean values with less standard deviation during the Coniacian to Santonian suggest low productivity in the Tarfaya basin. These log-ratios exhibit lowest values (mean values of -1.506 and 0.073) and relatively low variability (standard deviation of 0.276 and 0.319) (Figs. 7 and 8).

The log(Ba/Ca) and log(P/Ca) show a lowest values in the upper Turonian interval (134-190 m) (mean values of -2.233 and -2.567) and high values in the upper Turonian (190-200 m) (mean values of -2.059 and -2.263) and Conacian to Santonian (24-134 m) (mean values of -2.074 and -2.341) intervals. The upper Turonian interval (134-190 m) exhibits a high variability in the log(P/Ca) (standard deviation of 0.163) and low variability in the log(Ba/Ca) (standard deviation of 0.092). The log(Br/Ca) exhibits no major change in the core Tarfaya SN°2. In contrast, the log(Br/Fe), log(Ba/Fe) and log(P/Fe) are higher in the upper Turonian interval (134-190 m) (mean values of -2.031, -0.163 and -0-497, respectively) with also high variability (standard deviation of 0.265, 0.276 and 0.219, respectively) and lowest in the Coniacian to Santonian interval (24- ~130 m). The base of the core Tarfaya SN°2 (190-200 m) exhibits intermediate values (mean values of -2.546, -0.585 and -0.789) with relatively low variability (standard deviation of 0.172, 0.176 and 0.232) (Figs. 7 and 8).

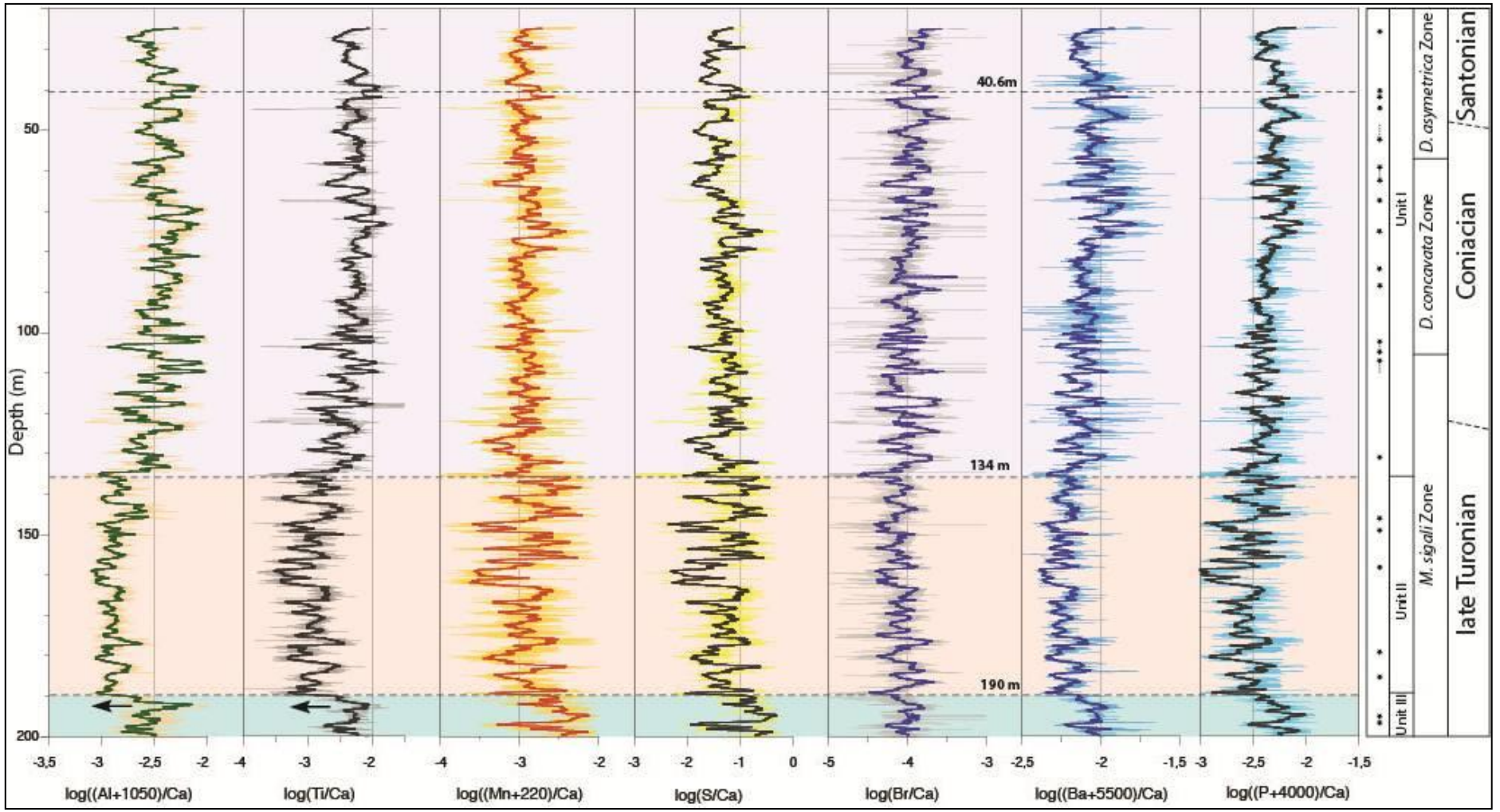

Figure 7: Composite geochemical and paleontological records in newly drilled core Tarfaya SN°2. Log-ratios of elements (Al, Ti, Mn, S, Br, Ba and P against Ca) were derived from X-ray fluorescence scanning. Black arrows indicate decrease in terrigenous flux in the Tarfaya Basin and light blue arrows indicate vice-versa. Dark blue arrows indicate increase in oxygenation in the Tarfaya Basin.

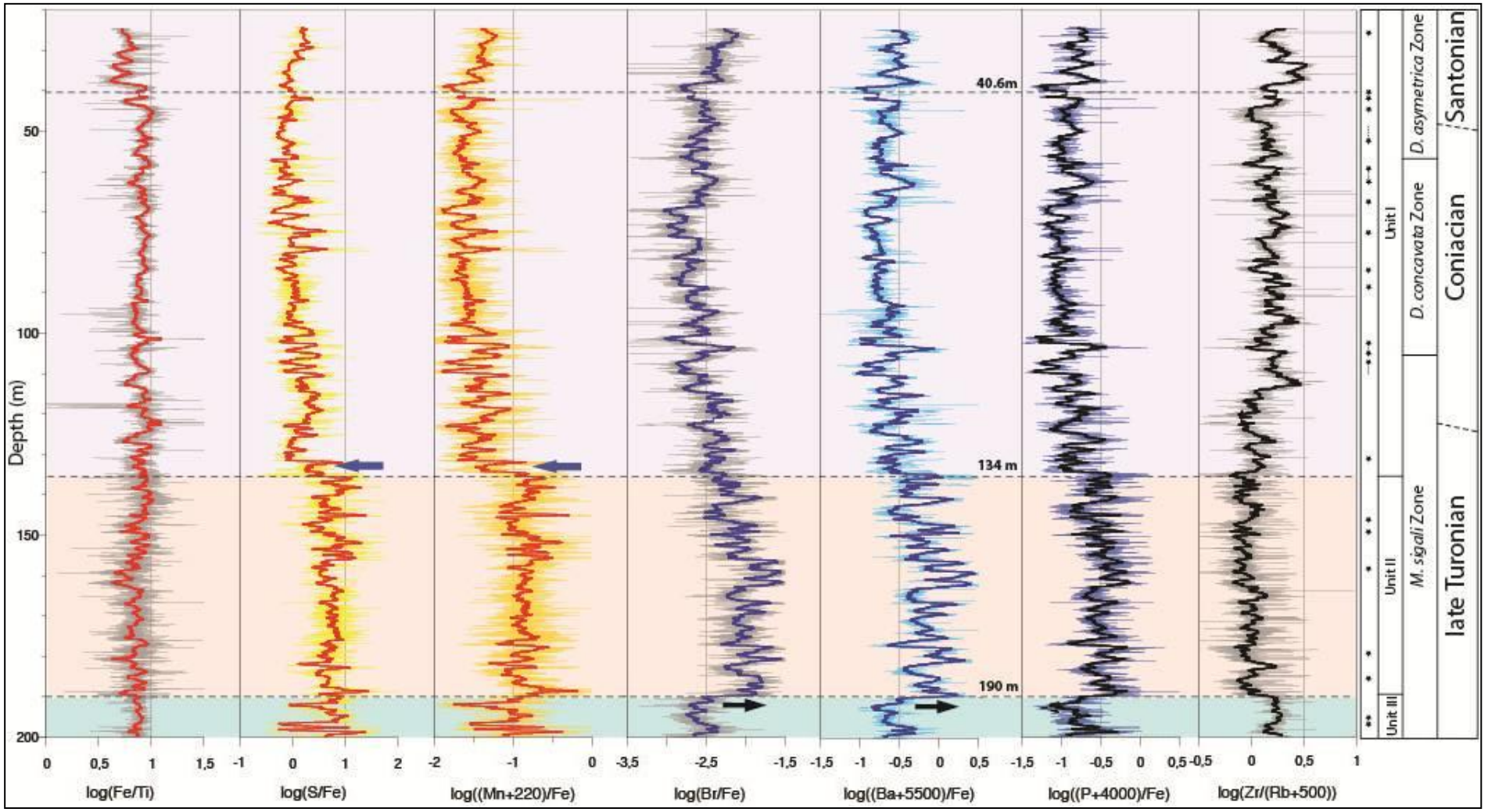

Figure 8: Composite geochemical and paleontological records in newly drilled core Tarfaya SN°2. Log-ratios of elements (Ti, Mn, S, Br, Ba and P against Fe) were derived from X-ray fluorescence scanning.

3. Carbonate content ($CaCO_3$) based on Ca counts

The correlation of cores Tarfaya SN°1 and 2 is defined and presented in the **Chapter III** (Aquit et al., in prep) based on elemental Al/Ca and Zr/Rb ratios (XRF scanning results), lithological descriptions, line-scan records, bulk carbonate stable isotopes and planktonic foraminiferal biostratigraphy. The tie point for correlation is encountered at 191.6 m in Tarfaya SN°1 and at 38.85 m in Tarfaya SN°2. A total composite depth scale is constructed for the two cores by using the following equation:

Composite depth (mcd) = depth in SN°2 (m) - 38.85 m + 191.6 m.

The carbonate content was measured for the core Tarfaya SN°2 (not for core Tarfaya SN°1) by using $CaCO_3=C_{inorg}*8.333$ formula after Sachse et al. (2012). These measurements were taken at ~3 m intervals and over short disturbed intervals at ~30 cm intervals. The carbonate content ($CaCO_3$) shows a good linear correlation with Ca-counts (linear correlation factor of r = 0.7429) in the core Tarfaya SN°2. We further interpolated a new $CaCO_3$ (%) curve for the cores Tarfaya SN°1 and 2 using the mathematical equation of linear correlation:

Y ($CaCO_3$ %) = 10.652 + 5.4813 * 10^{-5} * X (Ca-count)

The carbonate content interpolated for the cores Tarfaya SN°1 and 2 is highest in the upper Turonian interval between 286.7 mcd and 342.7 mcd (mean value of 68.497 and standard deviation of 10.638) and lowest in the Coniancian to Santonian interval of the succession (158.8-286.7 mcd) (mean value of 50.344 and high variability with standard deviation of 10.470) (Fig. 9). This interval also shows three successive decreases trend from 286.7 to 253.5 mcd, 253.5 to 221.5 mcd and 221.5 to 190.5 mcd depth intervals. In the lower Campanian (30-158.8 mcd), $CaCO_3$ indicates relatively intermediate values with mean value of 63.105 and relatively high variability with standard deviation of 8.715. The base of the core Tarfaya SN°2 below 342.7 mcd exhibits a low values with mean value of 51.161 and standard deviation of 8.033 (Fig. 9).

Also we interpolated a new organic carbon C_{org} (%) and Total Sulfur (TS) (%) curves for the cores Tarfaya SN°1 and 2 using the mathematical equations of linear correlations. The C_{org} (%) were measured at Tarfaya SN°1 by Sachse et al. (2014) and at Tarfaya SN°2 by Sachse et al. (2012):

Y (C_{org} %) = -4.1683 - 6.3621 * X (log(Br/Ca))

Y (TS %) = -1.5635 - 1.7617 * X (log((Mn+220)/S)) for core Tarfaya SN°2

Y (TS %) = -1.4052 - 1.5796 * X (log((Mn+220)/S)) for core Tarfaya SN°1

The organic carbon (C_{org}) and Total Sulfur interpolated for the cores Tarfaya SN°1 and 2 are highest in the upper Turonian to middle Santonian (interval between 352 mcd and 190.5 mcd) with mean value of 6.618 and 1.253 and standard deviation of 12.570 and 0.349, respectively, and lowest in the lower Campanian (30-158.8 mcd) with mean value of 3.042 and 0.775 and standard deviation of 0.366 and 0.398, respectively (Fig. 9). In the upper Santonian (158.8-190.5 mcd), the C_{org} and TS exhibit decreases values from highest (upper Turonian) to lowest (lower Campanian).

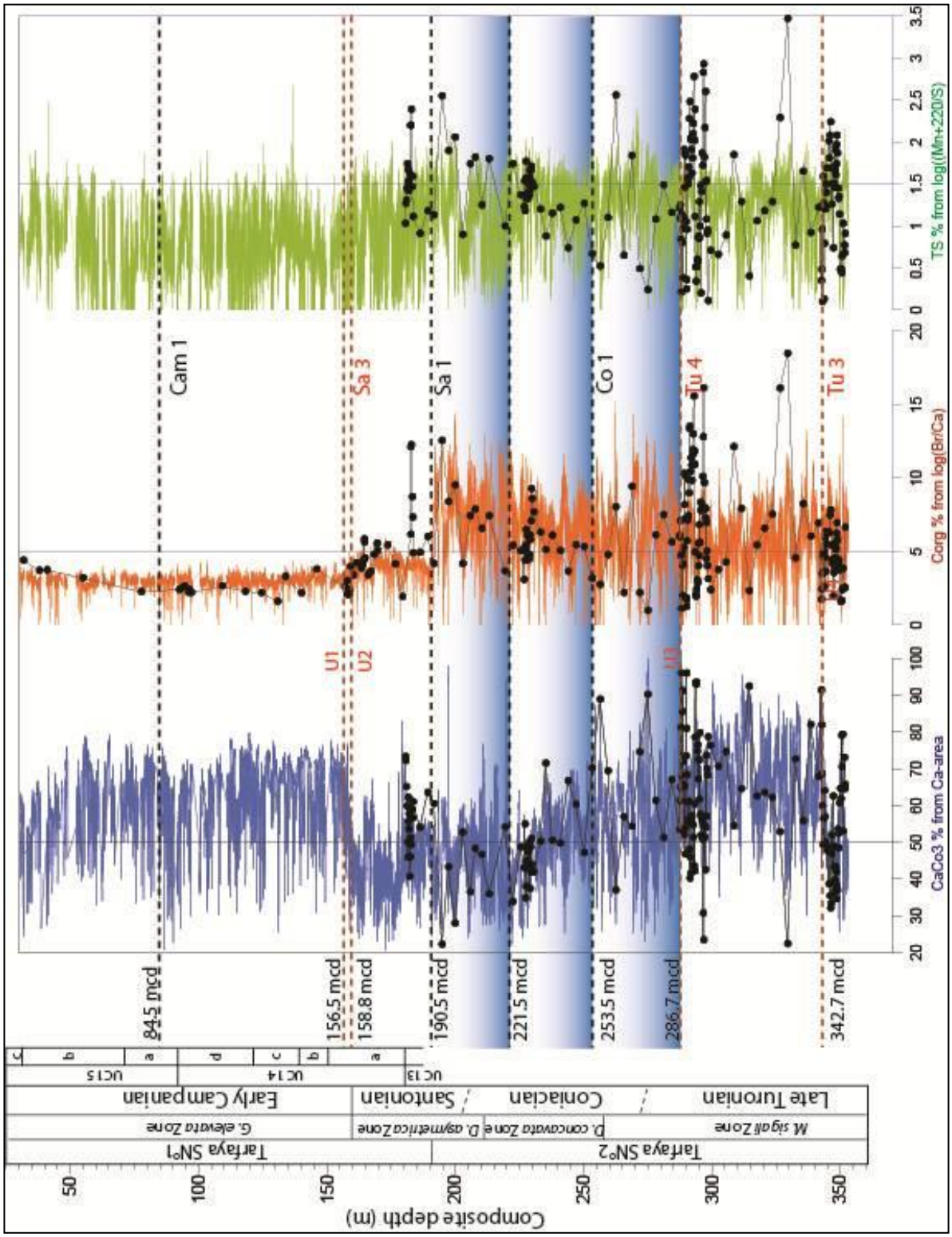

Figure 9. Composite geochemical and paleontological records in newly drilled cores Tarfaya SN°1 and 2 (composite core). $CaCO_3$ content (%), Total Sulfur (%) and Total Organic Carbon (%) were interpolated from Sachse et al. (2012) records.

4. Identification of sequences

The high-resolution XRF-scanning record of Tarfaya SN°2 core reveals several sequences of carbonate-rich intervals with distinct basal contacts, which subsequently grade into organic-rich laminated marlstones. We interpret the onset of carbonate-rich, commonly coarse-grained sedimentation as sequence boundaries above a regressive system tract, which may be truncated and overlies carbonates as lowstand and early trangressive sediments (Fig. 10). The following organic-rich, often laminated sediments, which dominate the Late Cretaceous sedimentation in the Tarfaya Basin were deposited during elevated sea-level, favoring impingement of an upwelling-related Oxygen Minimum Zone (OMZ) onto the shelf (Kolonic et al., 2005; Kuhnt et al., 2004, 2009 etc.). These organic-rich are representing the later part of the transgressive system and the highstand system tracts (Fig. 10).

The major sequences identified in the cores Tarfaya SN°1 and 2 based on changes in the log-ratios of the elements (log(Al/Ca)), Ca-counts, and the lithological evidence, which presented in sediment as erosive horizon and correspond to the unconformities shown in the **Chapter III** (Aquit et al., in prep).

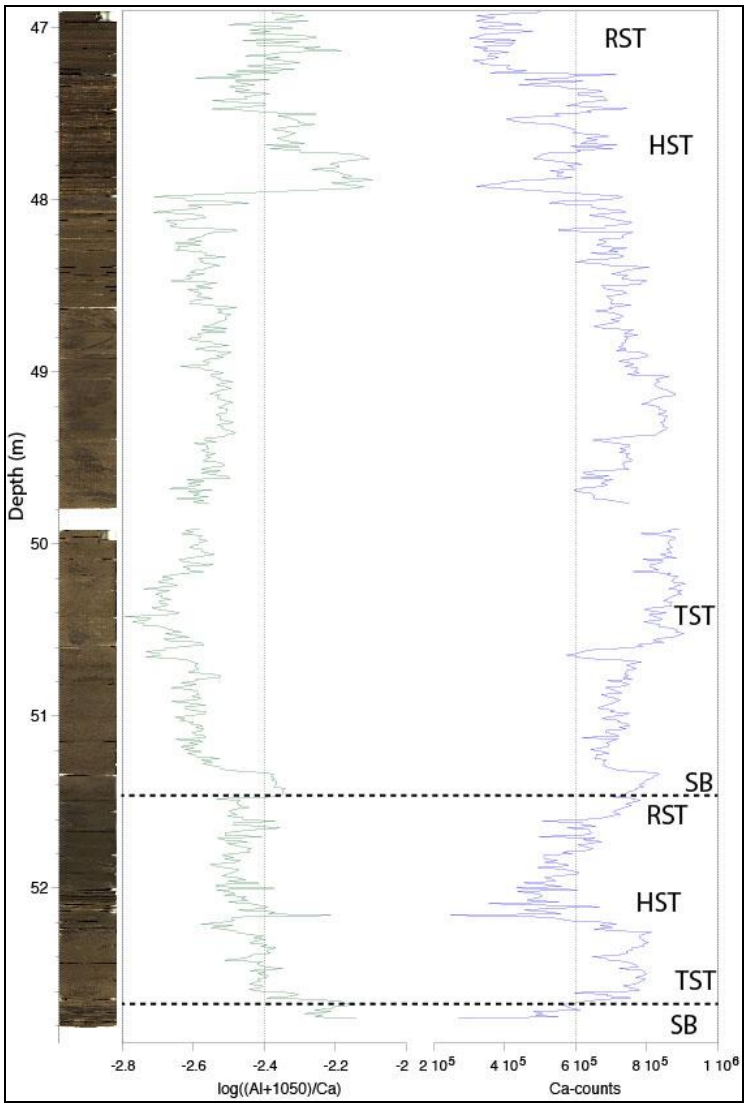

Figure 10: Core photograph and log(Al/Ca) and Ca (counts) of idealized sequence in the Tarfaya cores. LS-lowstand sediments, TST-transgressive systems tract, HST-highstand systems tract, RST-regressive systems tract, SB-sequence boundary (transgressive surface of erosion), although sequence boundaries are still marked by erosional unconformities.

5. Line-scanning and core photography

The sediment colour records are one of sediment properties that can be measured by relatively fast and non-destructive techniques on marine and lacustrine cores. High-resolution colour records are helpful for cross-correlation of overlapping cores (e.g. Kroon et al., 1998), as a proxy for sediment composition (Balsam et al., 1999; Helmke et al., 2002) or for wiggle-matching with other palaeoclimate records (e.g. Hughen et al., 1998).

Line scan measurements and photographs were acquired with a Ja CVL 1073 CCD color line scan camera. Camera resolution is specified as total number of pixels in the final image. A single

pixel in the final image consists of three values, one for each of the three colour channels, red, green and blue. The raw image data are generally processed within the camera before they were transferred to a storage medium.

Original colour data, which are linearly proportional to the amount of light received by the camera, are transformed into a non-linear version of RGB. The most commonly used colour co-ordinate system to describe sediment colour is meanwhile the CIE L*a*b* system (defined by the Commission Internationale de l'Éclairage). L* is lightness, and ranges from 0 to 100 (black to white). The actual colour (hue) is expressed in a* (negative values are red, positive is green) and b* (negative for blue and positive values for yellow). Translation from linear RGB into the L*a*b* system is by definition done via an intermediate step, the XYZ tristimulus system (Nederbragt et al., 2006).

Line scan measurements and photographs were taken with a Ja CVL 1073 CCD color line scan camera with 3 sensors of 2048 pixels and Dichroic RGB beam splitter prism (RGB channels at 630 nm, 535 nm and 450 nm) at the Institute of Geosciences, Kiel University. Scanning was performed (resolution of 143 pixel per 70 micron) on the polished surface of oriented cores. Line scan measurements and photographs were used in the previous chapter to correlate the cores Tarfaya SN°1 and 2 and lithological changes at the unconformities (Fig. 11).

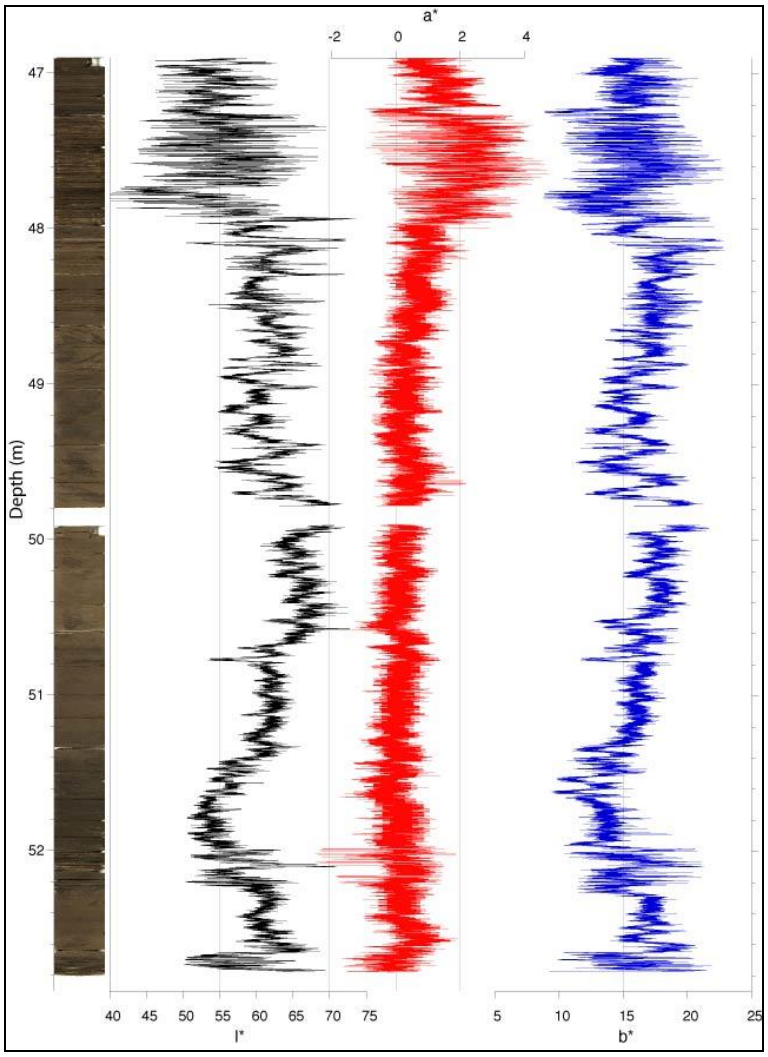

Figure 11: Core photograph and l*, a* and b* from line Scan of idealized sequence in the Tarfaya cores.

Chapter V. Organic geochemical characterization of Santonian to early Campanian organic matter-rich marls (Sondage No 1 cores) as related to OAE3 from the Tarfaya Basin, Morocco

Sachse, V.F.[a]*, Heim, S. [a,b], Jabour, H.[c], Kluth, O.[d], Schümann, T.[d]; Aquit, M.[e], Littke, R.[a]

[a] Institute of Geology and Geochemistry of Petroleum and Coal, Energy and Mineral Resources Group (EMR), RWTH Aachen University, Lochnerstrasse 4-20, 52056 Aachen, Germany

[b]Federal Institute for Geosciences and Natural Resources- BGR, Stilleweg 2, 30655 Hannover, Germany

[c] National Office of Hydrocarbons and Mining, Rabat 10050, Morocco

[d]RWE Dea AG, D-22297 Hamburg, Germany

[e]Institute of Geosciences, Christian-Albrechts-University, Ludewig-Meyn-Str. 14, 24118 Kiel, Germany

*Corresponding author: victoria.sachse@emr.rwth-aachen.de

Abstract

In addition to previously analyzed sediments of Cenomanian to Santonian age in the Tarfaya Sondage No. 2 well, this study presents the results of a stratigraphically younger interval of Santonian to early Campanian age in the adjacent well Tarfaya Sondage No. 1. This interval is part of the oceanic anoxic event 3 (OAE3), which occurred mainly in the Atlantic realm. Due to known high quality source rocks related to OAEs (i.e. Cenomanian-Turonian), the investigated sample section was tested for the quality, quantity and kind of organic matter (OM), describing also the depositional environment. The study was carried out by means of (i) elemental analysis (C_{org}, $CaCO_3$, TS), (ii) Rock-Eval pyrolysis, (iii) vitrinite reflectance measurements, (iv) gas chromatography-flame ionization detection (GC-FID) and (v) GC-mass spectrometry (GC-MS). Total content of organic carbon (C_{org}), values for the hydrogen index (HI) (mainly in the range 500 to 700 mg/g C_{org}) and S_2 values (10 to 40 mg/g rock), support the assumption of a high petroleum generation potential in these Upper Cretaceous sediments. TS/C_{org} ratios as well as pristane/phytane ratios indicate variable oxygen contents during sediment deposition, representing a typical depositional setting for the Late Cretaceous and are in good agreement with previously analyzed data in the Tarfaya Basin. Phyto- and zooplankton were identified as marine sourced. All of the investigated early Campanian and Santonian samples are immature with some tendencies to early maturation. These results are based on vitrinite reflectance (0.3 to 0.4 % VR_r), T_{max} values (409 to 425 °C), production indices (PI; $S_1/(S_1 + S_2) < 0.1$) and *n*-alkane ratios (i.e. carbon preference index). As the deposition of these sediments is time related to OAE3, the depositional environment was characterized by oxygen-deficiency or even anoxic bottom water conditions. This situation was favored during the Cretaceous greenhouse climate by limited oxygen solubility in the then warmer ocean water. Furthermore, local factors related to nutrient supply and primary bioproductivity led to the exceptionally thick, Upper Cretaceous organic matter-rich sedimentary sequence of the Tarfaya Basin.

Keywords: Petroleum source rocks; Tarfaya Basin, Morocco; Late Cretaceous; Depositional environment; Thermal maturity; Kerogen type; Ocean anoxic event

1. Introduction

Oceanic anoxic events (OAEs) have been widely discussed in literature (i.e., Schlanger and Jenkyns, 1976; Hofmann et al., 2003; Sageman et al., 2006; Locklair et al., 2011). Ocean wide anoxia have been considered as key mechanism for organic carbon burial for specific time intervals (Arthur et al., 1990; Wagreich, 2012) and are characterized by the occurrence of organic matter-rich pelagic sediments, such as black shales. Wagreich (2012) noted three factors to qualify for an OAE: (1) organic- rich strata must be widespread, (2) correlation in time to qualify as a supra-regional single event and (3) accompanied by a significant carbon isotope excursion. OAE 3 (Coniacian-Santonian) is known as the last Cretaceous oceanic anoxic event (Arthur et al., 1990). In contrast to the global extents of the early Aptian OAE 1a and the Cenomanian-Turonian OAE 2, Arthur and Schlanger (1979) describe the occurrence of OAE 3 as regionally more restricted.

The influence of oceanic anoxic events (OAEs) and especially of the OAE 2 on the quality and quantity of organic matter and the depositional environment was previously described by Sachse et al. (2012) for the Sondage No.2 (Turonian to Santonian), closely located to the Sondage No.1 (Santonian to early Campanian) presented in this study (Fig. 1). In addition different Cenozoic and Mesozoic sedimentary sequences in the Tarfaya Basin (TB) were tested for their petroleum generation potential (Sachse et al., 2011), focusing mostly on the Cenomanian/Turonian sequence (e.g. Lüning et al., 2004; Kolonic et al., 2002; Kuhnt et al., 2001, 2005b, 2009; Sachse et al., 2012).

The TB in Morocco was highly affected by different phases of OAE, but the possible influence of OAE3 on type, quality and quantity of organic matter is still poorly investigated. Thus, the main objective of this study was to determine conditions of sedimentation based on a geochemical study on a newly drilled core. Indicators which give further insight to the depositional environment are discussed and a detailed overview on organic matter (OM) type, quantity and quality is presented to improve the overall geochemical information available for the Tarfaya Basin. In addition, the relation to the OAE3 can help to improve the knowledge about the extent of this event, its duration and quality with respect to source rock deposition. Furthermore, geochemical analysis can give evidence on the source rock quality of the Santonian and Campanian sediments, which might be of interest for the Moroccan offshore petroleum system.

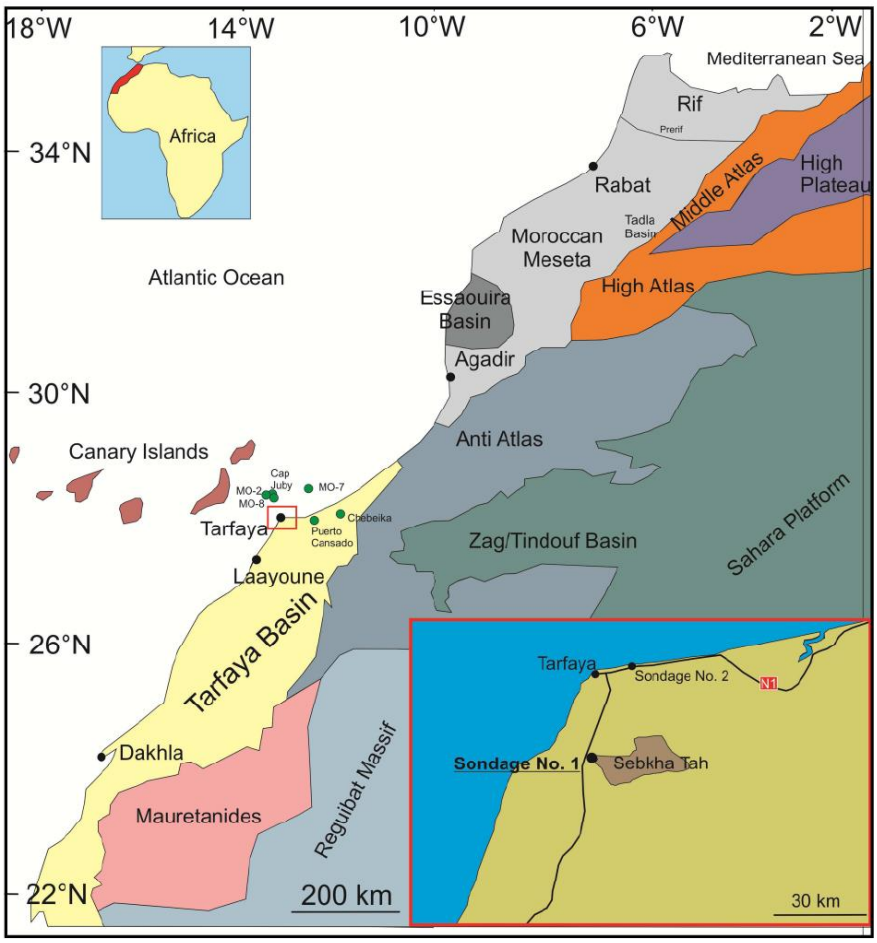

Figure 1: Overview of the geology of Tarfaya Basin and adjacent areas including well Tarfaya Sondage No. 1 and previous investigated well Sondage No. 2 (Sachse et al., 2012). Overview map based on Michard et al. (2008) showing the geological zones of Morocco and its location in Africa (small map in the upper left). Green dots represent key wells with respect to the petroleum system.

1.1. Geological Background

The TB is located in the south of Morocco/Western Sahara and covers an area of 170,000 km² both on- and offshore. The basin is surrounded by the Mauretanides thrust belt in the south, the Precambrian Reguibat Massif in the southeast, and the Paleozoic outcrops of the northern Anti- Atlas as well as the Zag/Tindouf Basin to the northeast (Fig. 1). To the west the East Canary Ridge limits the basin. Northern African basin evolution started with rift phases due to the opening of the North/Central Atlantic during the Permian until the Triassic. During the development of the sag phase the TB showed phases of thermal relaxation and subsidence (Wenke et al., 2011). Open marine sediments were deposited since the Early Jurassic (Davison, 2005) while the Late Jurassic presents carbonate platforms (Michard et al., 2008).

In the Early Cretaceous, the reorganization of the African and South American plates led to changes in the oceanic and atmospheric circulation. The Lower Cretaceous carbonates and clastic were deposited in a mainly deltaic (e.g. the Tan Tan delta, northern margin of the TB) or paralic environment (Kolonic et al., 2002; Lüning et al., 2004). A major reorganization of deep-water circulation culminated in the Late Cretaceous, now circulating equatorward to poleward and thus heat transporting to high latitude oceans (Hay, 1995; Wagner, 2002). Furthermore, the constant opening of the Atlantic close to the Equator led to the establishment of full water exchange, influencing also the sedimentary and geochemical record (i.e. Hay, 1995; Jones et al., 2007; Wagner and Pletsch, 1999).

Late Cretaceous (Cenomanian to Coniacian) sediments are highly influenced by oceanic anoxic events (Thurow et al., 1992) and represented by organic-rich clays and marlstones. Global sea-level rises and transgressional events were detected for the late Aptian, Turonian and Campanian. Especially the Turonian led to the deposition of black shales in the TB (Kolonic et al., 2002; Kuhnt et al., 2009; Sachse et al., 2011, 2012). The Cenomanian to Santonian sediments reach a thickness of approx. 800 m in the TB (Leine, 1986; Kolonic et al., 2002). During Santonian and upper Paleogene a first major unconformity occurred (Davison, 2005), truncating these sediments at the shelf edge. This highly erosive unconformity is related to Atlasian uplift (Michard et al., 2008). During the Cenozoic, the Alpine deformation resulted in inversion of former rift systems as the Atlas Gulf and leading to the formation of the Atlas Mountains (Lüning et al., 2004). Since the late Oligocene, erosion took place mainly in the northern shelf of the TB, representing a second major unconformity. In most parts of the Basin, thin Paleocene-Eocene sediments are overlain by a thick Miocene sequence (Davison, 2005). The geological history is described in more detail by Choubert et al. (1966, 1972), Davison (2005), Michard et al. (2008), Wenke et al. (2011) and Sachse et al. (2011).

1.2. Petroleum Systems in Morocco

Various potential source rocks are assumed to occur in the Tarfaya Basin. The main petroleum system in Morocco is of Jurassic age (Essaouira Basin, Tarfaya Basin, Prerif Basin), but older Paleozoic systems are also known (Morabet et al., 1998). Although Paleozoic sediments are eroded in the northern Tarfaya Basin, these Ordovician/Silurian and Devonian sediments were drilled in the southern Tarfaya area and may have charged Triassic reservoirs in shelf areas (El Mostaine, 1991).

Triassic source rocks were drilled in wells Cap Juby and Chebeika-1, possibly related to lacustrine anoxic settings (El Mostaine, 1991).

Jurassic source rocks (Toarcian; type II/III kerogen), also known from Fuerteventura (Steiner et al., 1998; Davison, 2005) were drilled in wells Cap Juby and Tan Tan and may have charged the MO-2 reservoir (Morabet et al., 1998). Younger Jurassic source rocks (Callovian/Oxfordian) were drilled in well Puerto Cansado, containing type II/III kerogen.

The earliest Cretaceous source rock is of Berriasian age, containing type III kerogen. It was drilled in the Tan Tan Delta. Valanginian to Hauterivian type I kerogen bearing source rocks were drilled in well MO-7 (Ellouz et al., 1998). As described in i.e. Sachse et al. (2011, 2012), younger Cretaceous potential source rocks are outcropping along the Moroccan coast, whilst Cenomanian/Turonian black shales are prominent at Oued Ma Fatma (Kuhnt et al., 2001; Kuhnt et al., 2009). Most of these potential source rocks are immature or in an early stage of maturity (Sachse et al., 2011, 2012). In addition, the thickness of the Cretaceous sediments is highly variable and probably small in the slope and deep offshore areas of the Tarfaya Basin (Arthur et al., 1979). Consequently, source rock thickness poses a high risk for a potential petroleum system.

Several potential reservoirs are assumed for the Tarfaya Basin (i.e. Davison, 2005; Wenke et al., 2011): 1) Triassic sandstones, 2) Early Jurassic sandstones and fractured carbonates, 3) Middle to Late Jurassic shelf reef sequences and dolomitized, fractured shelf units, 4) Berriasian to Valanginian basin floor and lowstand fans, 5) late Valanginian to Aptian stacked mouth bars and channel systems of the Tan Tan and Boujdour delta complexes, and 6) Eocene to Oligocene coarse-grained mass transport complexes.

Possible seals might be Late Triassic/Early Jurassic evaporites, Jurassic impermeable shales, Aptian mud flows, Late Cretaceous marls and shales and late Eocene/larly Oligocene/Miocene shales.

Mature Upper Cretaceous source rocks are not proven in Morocco, but are believed to occur in the Dakhla-Laayoune Basin to charge Maastrichtian carbonate reservoirs (Morabet et al., 1998). Furthermore, mature Cretaceous source rocks might occur in the Agadir-Essaouira offshore basin, in the Tadla Basin and are active in the Prerif (Morabet et al., 1998). Up to now, the petroleum system of the offshore Tarfaya Basin is believed to be charged by Liassic source rocks filling Upper Jurassic reservoirs (Morabet et al., 1998). However, the oil shows in well Cap Juby (offshore Tarfaya Basin) cannot be clearly attributed to a specific source (Morabet et al., 1998).

2. Methods

Tarfaya Sondage No 1 (coordinates: N 27°42`36.6``, W 12°56`39.0``) was drilled in October-December 2009 northwest of the Sebkha Tah to a final depth of 350 m. This well was part of a drilling campaign, with the overall goal to recover the Miocene to Albian sequence. Therefore four wells were drilled, finally revealing four overlapping core sequences. Tarfaya Sondage No.1 covers the uppermost part of the succession. The drilling was successful and core recovery was at nearly 100%. The well is located approx. 25 km southeast of Tarfaya village, approximately 220 m east of the main road to Laayoune, and approximately 30 km from Tarfaya Sondage No. 2 (Sachse et al., 2012). The stratigraphic differentiation is based on planktic foraminiferal biostratigraphy and detailed lithological descriptions (Aquit, Kuhnt and Holbourn, unpub. data; Fig. 2). Pleistocene to Pliocene (Mohgrabien) white/grayish to yellow sandstones and lumachelles occur from the surface down to a depth of 25 m. Lower Campanian sediments *(Globotruncanita elevata* Zone) between 25 and 159.2 m consists of brown marl with intercalations of gray and light green olive marls (generally bioturbated) and silty layers. The Santonian interval *(Dicarinella asymetrica* Zone) between 159.2 and 199-201 m is comprised of laminated black shales with occasional nodular limestones. The Coniacian *(Dicarinella concavata* Zone) between 199-201 and 253 m and the upper Turonian *(Marginotruncana sigali* Zone) from 253 m to the base of the core are characterized by intercalations of laminated black, gray and dark brown shales with silty intervals and nodular limestones.

One hundred and twenty-three fresh core samples were taken from this well, covering only the lower Campanian and Santonian (between 20 and 180 m depth). The lower part of the well (upper Turonian and Coniacian) was not sampled because these intervals were partially covered by samples from Tarfaya Sondage No. 2 (Sachse et al., 2012). The sampling approach was two-fold (Fig. 2A). First, samples were taken approximately every 3 m in the depth range between 22 and 180 m to provide an overview on the evolution of thick black shale sequences within the entire succession. In addition two intervals within black shales were selected for denser sampling (20 - 30 cm) to assess the geochemical variability within black shales. The first of these intervals is located within the upper part of the core (92 to 97 m; lower Campanian; Fig. 2B), while the second interval represents the lower Campanian to Santonian transition (155 to 170 m; Fig. 2C).

Total inorganic carbon (C_{inorg}) and C_{org} were measured on all samples of the Tarfaya Sondage No. 1 using a LECO multiphase C/H/H_2O analyzer (RC-412) via IR absorption in a two stage

measurement process (C_{org} between 350°C and 520°C; C_{inorg} between 520 and 1050°C). With this method C_{org} and C_{inorg} can be determined in a single analytical run without previous removal of carbonates by acid treatment. Total carbon (C_{total}) concentration was determined using $C_{total}=C_{inorg}+C_{org}$. The $CaCO_3$ proportion (%) was calculated using $CaCO_3=C_{inorg}*8.333$. If dolomite is present instead of calcite, this leads to a slight overestimation of carbonate content. Dolomite rhomboeders could indeed be identified in some samples.

Furthermore, total sulfur concentration (TS) was measured using a Leco S 200 sulfur analyzer. For this method precision is <5% and the lower limit of determination is 0.001 %.

Rock-Eval analysis (Espitalié et al., 1985) was performed with a DELSI INC Rock-Eval II instrument on 44 samples that showed C_{org} contents >1.0 %. Parameters determined include hydrogen index [HI, mg hydrocarbon (HC) equivalents per g C_{org}), oxygen index (OI, mg CO_2 per g C_{org}) and T_{max} (temperature of maximum pyrolysis yield). A modified van Krevelen diagram (HI/OI) and a cross plot of S_2 and C_{org} were used for kerogen classification. Production index (PI) was calculated based on S_1 and S_2.

Vitrinite reflectance (VR_r) was measured on samples with C_{org} > 0.5 %. For microscopic studies, samples were embedded in an epoxy resin and a section perpendicular to bedding was polished according to the procedure described by Sachse et al. (2012). The polished blocks were investigated at a magnification of 500x in incident white light and in incident light fluorescence mode, excited by ultraviolet (UV) and violet light. VR_r measurements were obtained using a Zeiss Axioplan incident light microscope at λ=546 nm with a Zeiss Epiplan-NEOFLUAR 50x/0.85 oil objective. An yttrium aluminium garnet (YAG) standard was used, with a reflectance of 0.889% (in oil). For samples rich in vitrinite or solid bitumen particles, at least 50 measurements were made. Mean vitrinite reflectance and standard deviation values were calculated using the DISKUS Fossil software (Technisches Büro Carl H. Hilgers). In total, 27 samples were studied by way of reflected light microscopy.

For aliphatic hydrocarbons aliquots of 10 g were extracted twice, each with 40 mL dichloromethane and hexane, respectively, using ultrasonic treatment. The extracts were fractionated by silica gel-based liquid chromatography into subfractions of (I) aliphatic hydrocarbons (5 mL pentane), (II) aromatic hydrocarbons (5 mL pentane: dichloromethane, 4:6 v:v) and (III) polar compounds (5 mL MeOH). Gas chromatographic analyses of aliphatic hydrocarbons were performed with a Fisons Instruments GC 8000 series equipped with split/splitless injection, using a ZB-1 HT

fused silica capillary column (30 m x 0.25 mm i.d., film thickness 0.25 µm). Detection was done with a flame ionization detector (FID). H_2 was used as carrier gas with 40 mL/s gas velocity. Chromatographic conditions were: 270 °C injector temperature, 1 µL split- splitless injection with a splitless time of 60 s, temperature program: 80°C for 3 min, then programmed at 10°C/min to 300°C and held for 20 min. GC-MS analyses were performed on a Finnigan MAT 95 mass spectrometer linked to a Hewlett Packard Series II 5890 gas chromatograph, equipped with a 30 m x 0.25 mm i.d. (0.25 µm film thickness) Zebron ZB-1 fused silica column. The mass spectrometer was operated in electron ionization (EI^+) mode with ionization energy of 70 eV and a source temperature of 260 °C, scanning from *m/z* 35 to 700 at 1.0 s/decade with an interscan time of 0.1 s. He was used as carrier gas with a gas velocity of 60 mL/s. The analytic procedure started with 3 min isothermal at 80 °C, then programmed from 80 to 310°C at 5°C/min. The identification of hopanes and steranes was based on the comparison of EI^+-mass spectra with reference material such as the comparison with compound identification pattern of i.e. Kolonic et al. (2002), Sachse et al. (2011) and Sachse et al. (2012). All molecular ratios were calculated on the base of integration of peak areas of specific ion chromatograms (i.e. *m/z* 57, 191, 217).

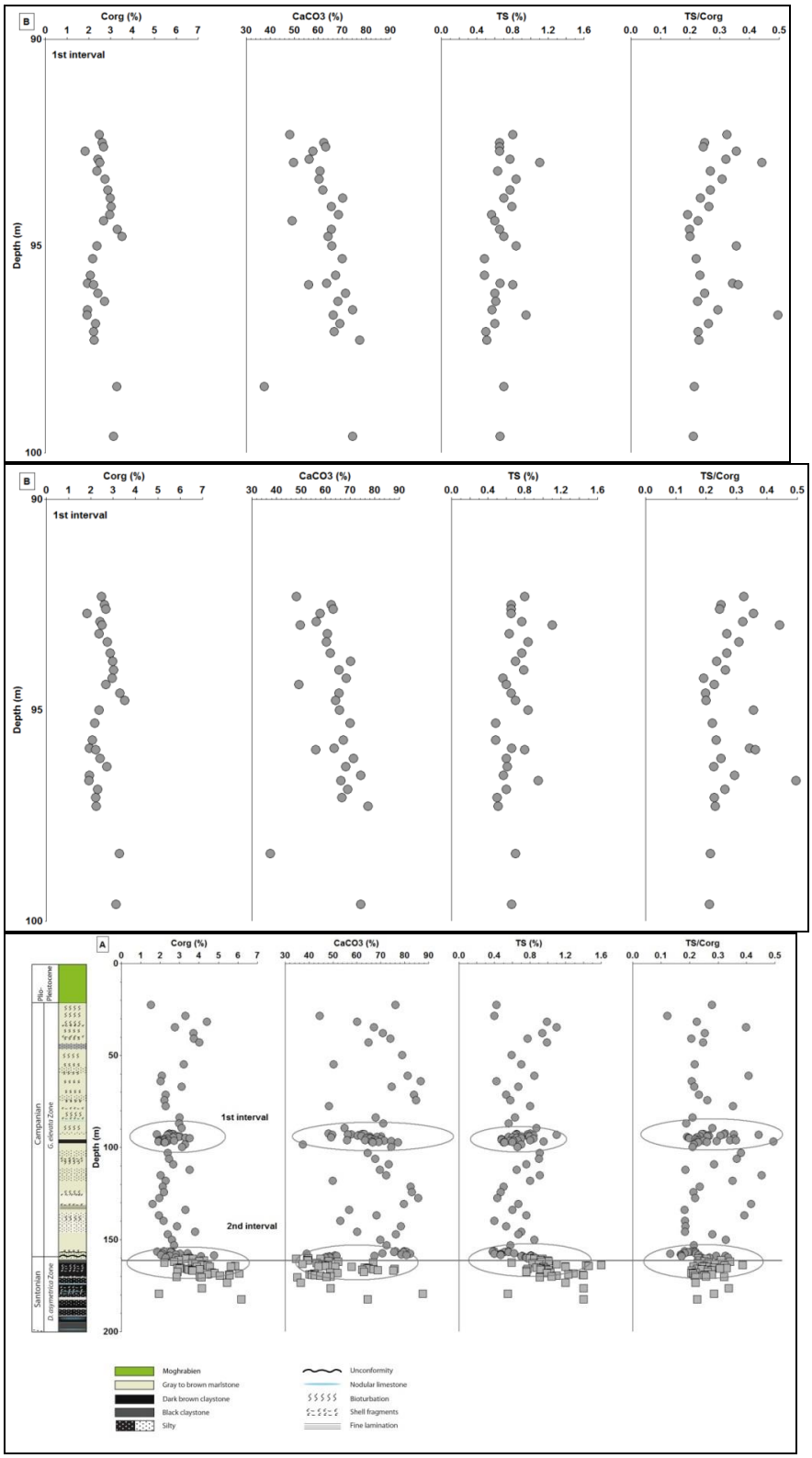

Figure 2: Elemental analysis data of Corg, $CaCO_3$, TS and TS/Corg plotted versus depth for (a) the whole Sondage No. 1; (b) 1st interval (92-97 m) with focus on early Campanian samples and (c) 2nd interval (155-170 m) showing the transition between early Campanian and Santonian samples.

3. Results

3.1. Elemental analysis

Results of the elemental analysis are compiled in the appendix. C_{org} values are high in the entire sample set varying between 1.5 and 5.5% (Fig. 2A). Highest values were measured for the deepest and oldest sediments (approx. 150 to 180 m) and Santonian samples have in general higher C_{org} values than those of the early Campanian. Another pattern is obvious for the total sulfur (TS) content and C_{org} which are positively correlated (Figs. 2, 3). TS values vary between 0.4 and 1.6%. Especially samples from a depth between 150 to 180 m show a high content of TS. Enhanced TS was also measured for sections between 30 to 50 m and 90 to 100 m (Fig. 2A). TS increases with increasing C_{org} in the lowermost section (Fig. 2C; 160 to 180 m), whereas such a correlation is not observed at a depth and 100 m (Fig. 2B). TS/C_{org} ratios vary between 0.17 and 0.46.

In general $CaCO_3$ content shows high values, varying between 37.7 and 86.8% (Fig. 2). A negative correlation exists between $CaCO_3$ and C_{org} and $CaCO_3$ and TS (Fig. 2A).

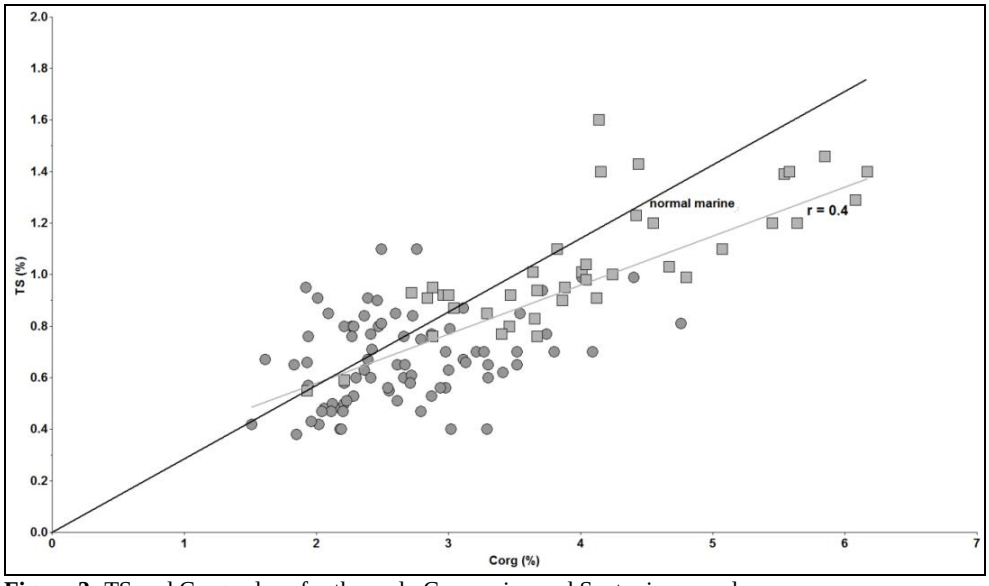

Figure 3: TS and Corg values for the early Campanian and Santonian samples.

3.2. Rock Eval pyrolysis

HI values for the early Campanian vary between 395 and 712 mg HC/g C_{org}, while Santonian samples show constantly high values between 482 and 653 mg HC/g C_{org}. An average value of 578 mg HC/g C_{org} was calculated for both stratigraphic units. T_{max} values are in the range of 409 to 425°C, with PI values < 0.04 for all samples. Highest PI values were calculated for the Santonian

section between 160 and 180 m, but also for one early Campanian sample (depth 46.30 m). S_2 values increase with increasing $C_{org,}$ being in the range of 9 and 38 mg HC/g rock, with highest values for the Santonian. Pyrolysis results are compiled in Figures 4, 5 and in Table 1.

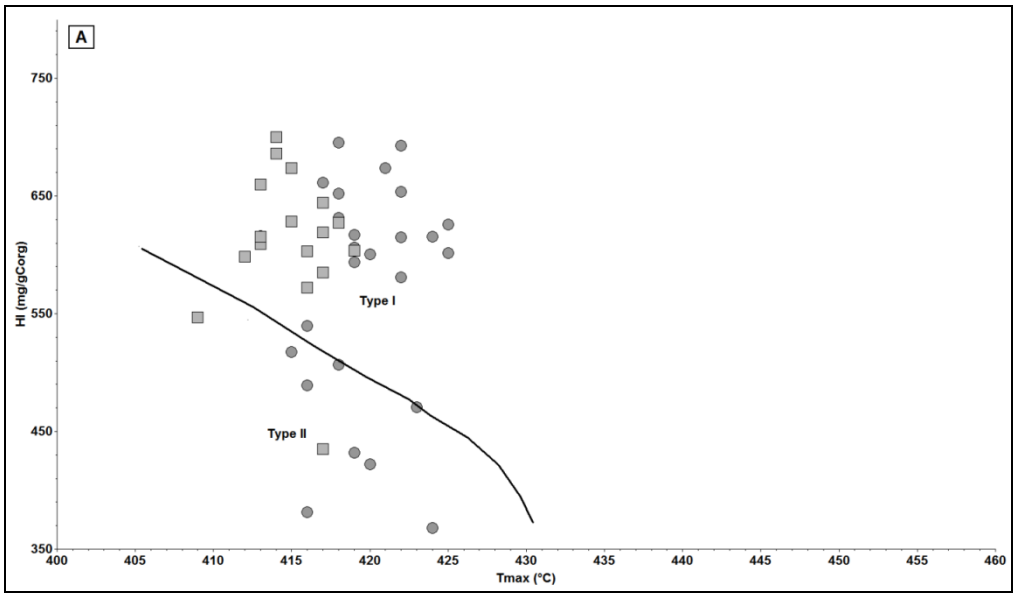

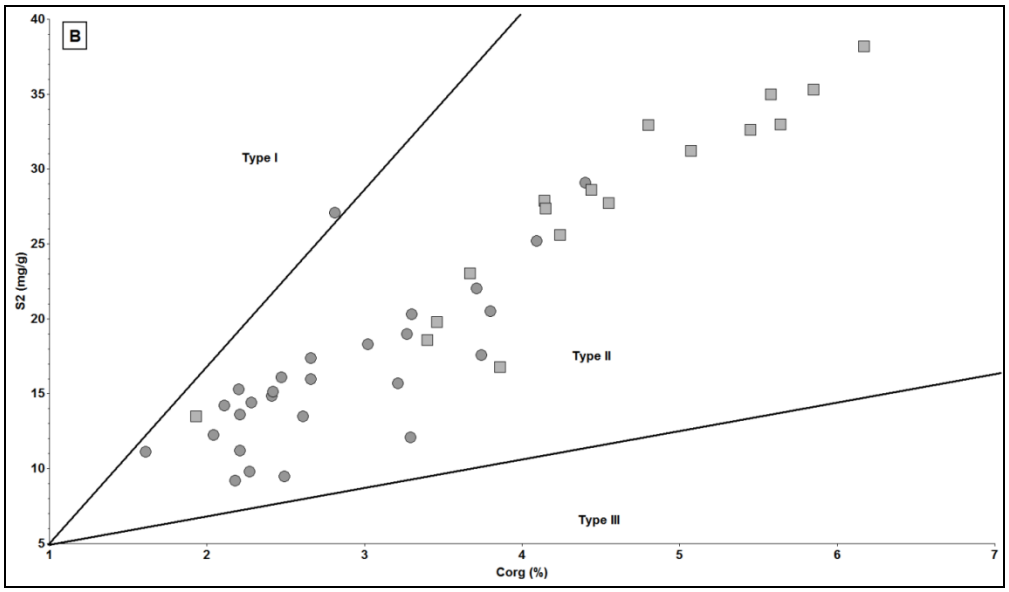

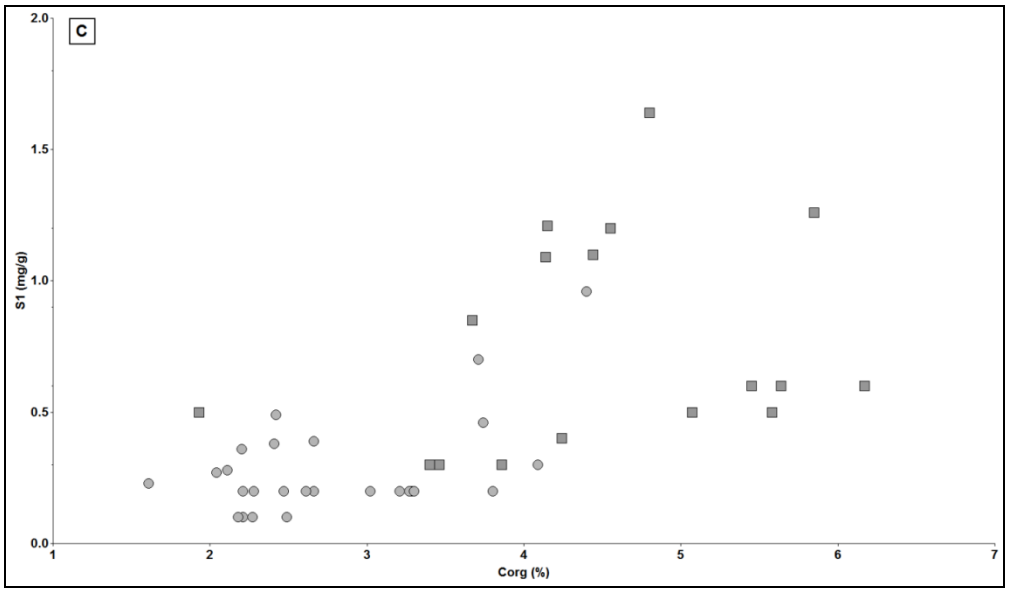

Figure 4: Rock-Eval pyrolysis data for the well samples: (a) HI vs. Tmax, (b) S2 vs. C_{org}, and (c) S1 vs. C_{org}.

3.3. Organic Petrography

An overview on maturity distribution is provided by vitrinite reflectance (VR_r) measurements (Fig. 5), characteristic microscopic observations are shown in Fig. 6. Early Campanian and Santonian samples revealed values between 0.28 and 0.31%VR_r, showing no distinct depth trend. Several samples contain only resedimented vitrinites; resulting in a (much) too high mean value.

Besides vitrinites, also liptinites and inertinites (inertodetrinite) were detected. Liptinite is clearly most abundant with volume percentages of up to 6.2% and percentages of total visible macerals being consistently greater than 90%. The bulk of the OM was classified as fluorescing amorphous OM. Liptinite consists mainly of alginite and alginite fragments (liptodetrinite). In addition sporinite and resinite were rarely observed. Terrestrial derived OM such as vitrinite and inertinite occur in similar, low abundance. High amounts of foraminifera and small pyrites were detected in most samples, as well as dolomite rhomboeders in some samples. It should be noted, that less and smaller pyrites were detected than in Cenomanian/Turonian samples, which is in agreement with lower sulfur contents. Alginite occurs as brightly fluorescing, elongated particles in sections perpendicular to bedding, usually less than 30 µm in length (Fig. 6). Liptodetrinite has a similar fluorescence and small size, but no distinct elongate shape. It is possibly derived from marine plankton, such as alginate. Whereas these types of macerals are common, an even greater part of the OM consists of structureless fluorescing groundmass. Fluorescence is weaker than that of alginate

and liptodetrinite. Such amorphous organic matter occurs commonly in upwelling- related sapropelic marine sediments (Littke and Sachsenhofer, 1994).

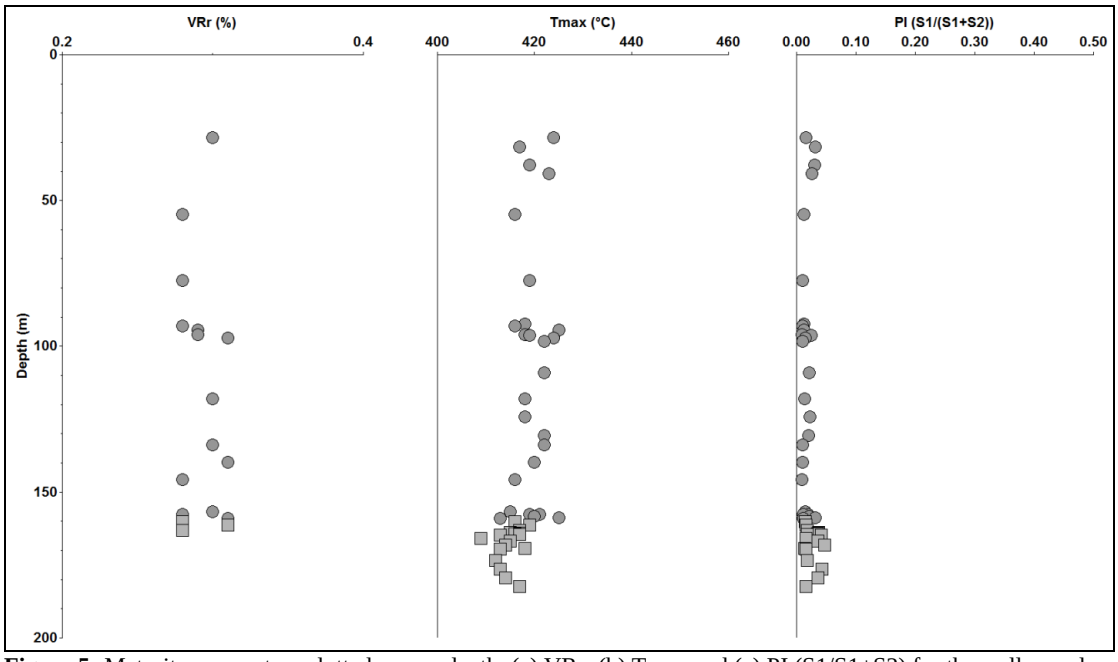

Figure 5: Maturity parameters plotted versus depth: (a) VRr; (b) Tmax and (c) PI (S1/S1+S2) for the well samples.

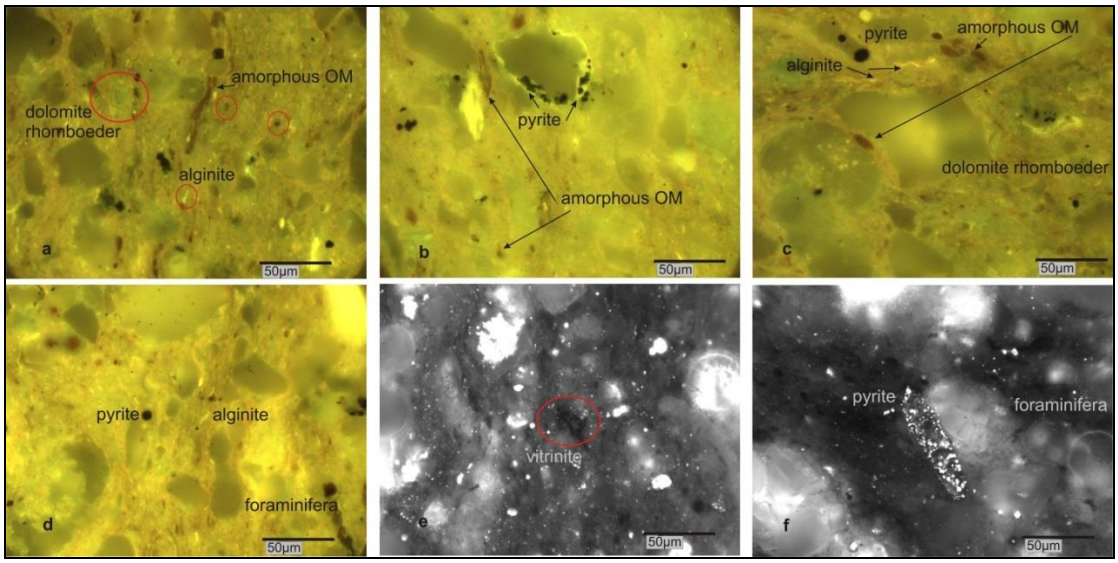

Figure 6: Microscopic observations in incident light fluorescence mode (a-d) and in reflected white light (e, f). Photograph a, c, d and e show a Santonian sample, b and f present the amorphous OM, pyrite and foraminifera in an early Campanian sample.

3.4. Organic Geochemistry

Biomarker ratios were used in order to identify the depositional environment as well as the maturation range of potential source rocks. For the early Campanian and Santonian samples *n*- and

isoalkane patterns revealed a clear dominance of short chain (C_{15} to C_{19}) relative to long chain *n*-alkanes (C_{27}-C_{31}) (Fig. 7).

The ratios of pristane (Pr) and phytane (Ph) over the adjacent *n*-alkanes was moderate to high (Table 2). For the early Campanian samples a dominance of pristane is typical, while Santonian samples show a dominance of phytane. Pr/Ph ratios vary for the early Campanian samples between 0.87 and 1.32 and for Santonian samples between 0.8 and 0.9. A dominance of Pr vs. nC_{17} and of Ph vs. nC_{18} was calculated for all samples, with ratios varying for the early Campanian between 1.74 and 2.92 and for the Santonian samples between 1.76 and 3.05 (Fig. 8). The ratio of nC_{17}/nC_{27} is in most samples >1 except for one sample correlated to early Campanian with a value of 0.96. For the Santonian samples, the ratio is slightly higher (1.99 to 3.91) then for the early Campanian (0.96 to 3.53).

The odd-even predominance (OEP) after Scalan and Smith (1970), calculated with the formula $(nC_{21}+6*nC_{23}+nC_{25})/(4*nC_{22}+4*nC_{24})$, revealed early Campanian ranging between 0.72 and 1.56 and Santonian samples between 0.7 and 2.07. The values of the modified carbon preference index (CPI), calculated after Bray and Evans, (1961) with the formula $(2xnC_{27})/(nC_{26}+nC_{28})$ vary from 0.74 to 2.96, with slightly higher values for the early Campanian (0.84 to 2.96; Santonian 0.74 to 2.37; see Table 2).

Tricyclic and tetracyclic terpanes in the range of C_{21} to C_{29} are detectabel in most samples but under the limit of quantification. Also Pentacyclic terpanes of the hopane series from C_{27} to C_{37} are not quantifiable.

Steranes are much more abundant than hopanes. Relative contributions of cholestane (C_{27}), ergostane (C_{28}) and stigmastane (C_{29}) were quantified (Figs. 9, 10). Cholestane contents are highest in samples of early Campanian and vary between 11.5 and 76.5%, while Santonian samples show ranges in between 11.9 and 57.9%. The ergostane contents are higher in Santonian samples (31.1 to 61.9%; early Campanian 16.2 to 44.8%). Stigmastane shows the lowest contents in both sample series: early Campanian samples vary between 6.9 and 27.2%, Santonian samples between 7.2 and 26.2%.

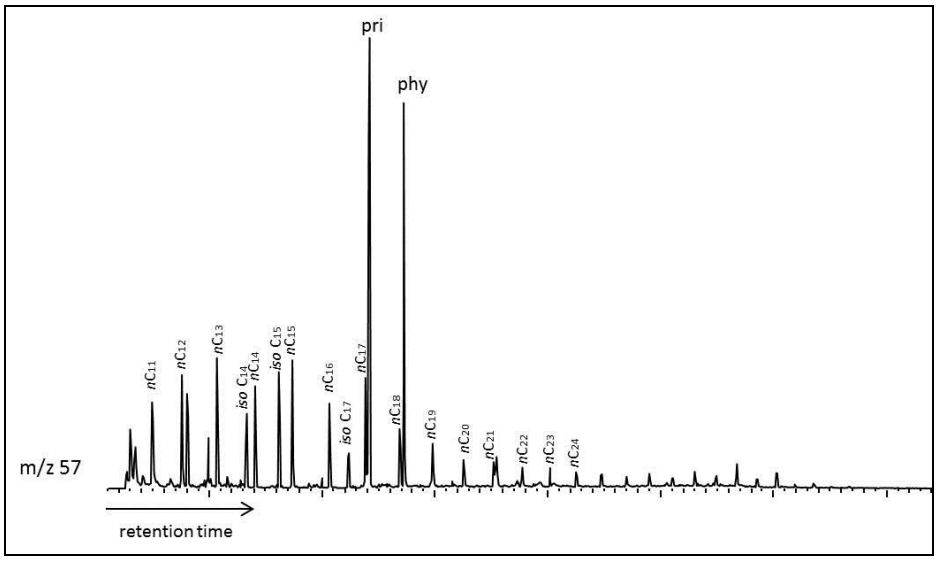

Figure 7: Chromatogram showing distribution of n- and iso- alkanes.

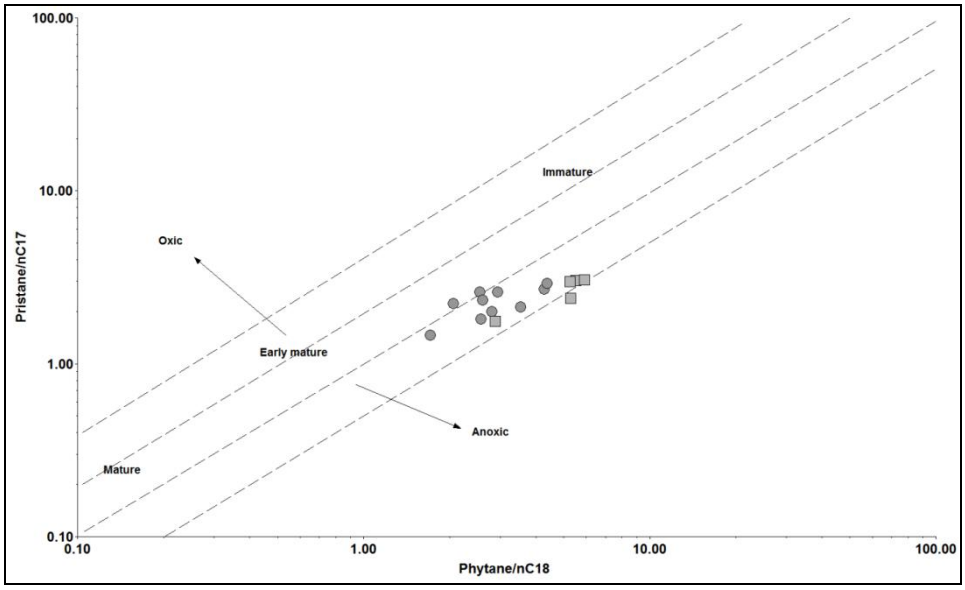

Figure 8: Pr/nC17 vs. Ph/nC18 for well samples indicating oxygen depleted but anoxic environment during deposition (after Shanmugam, 1985).

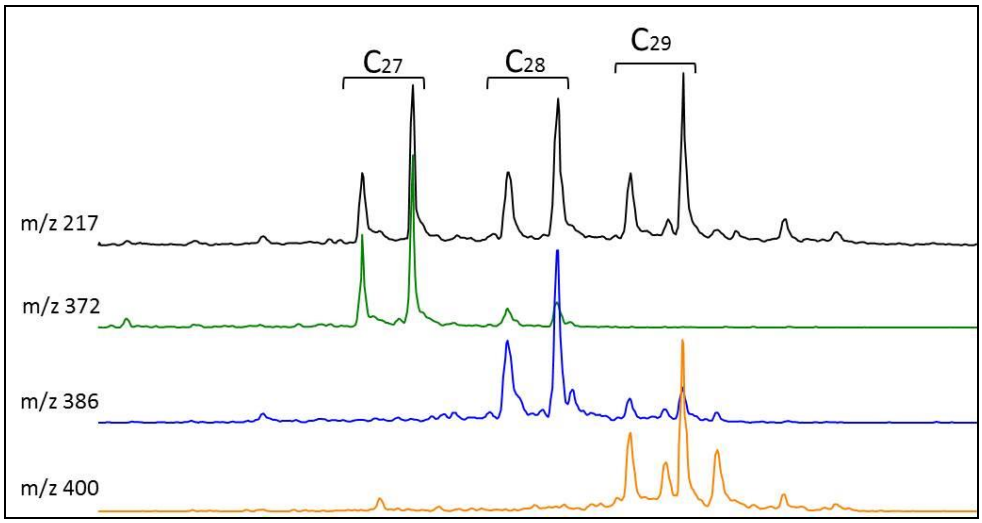

Figure 9: Characteristic ion spectra for steranes.

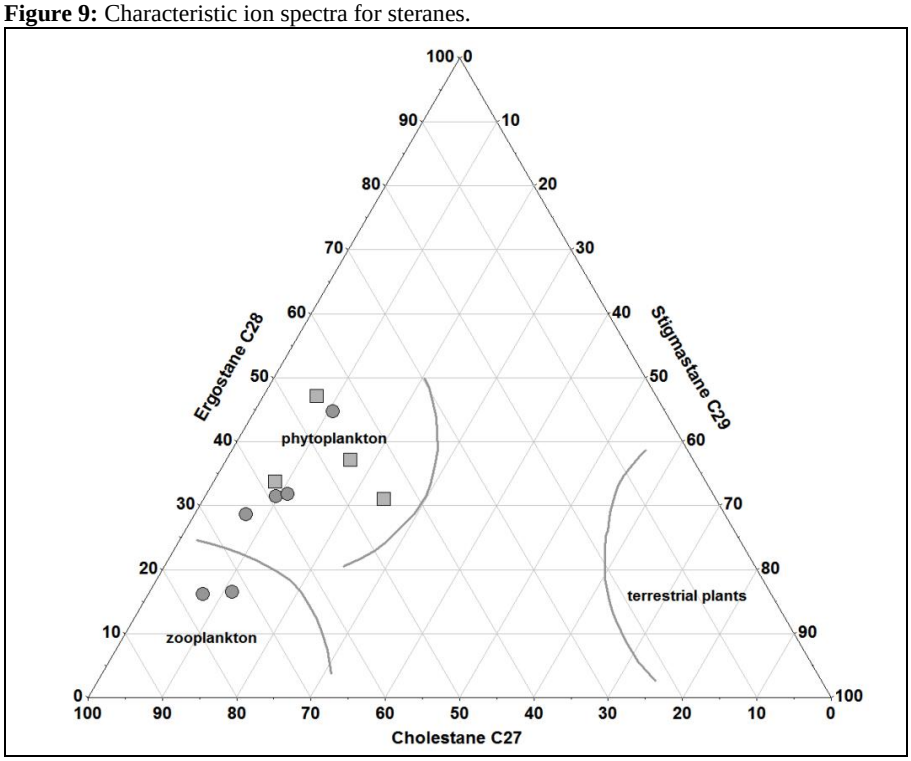

Figure 10: Relative composition of C27, C28 and C29 steranes in early Campanian and Santonian samples.

4. Discussion

4.1. Depositional environment and organic matter preservation

Prominent examples for cyclic black shale deposition during OAE 3 coupled with anoxic to dysoxic conditions were described i.e. offshore Ivory Coast- Ghana (Wagner, 2002; Hofmann et al., 2003), the Demerara Rise offshore Suriname (Friedrich and Erbacher, 2006), the Caribbean, the

Western Interior (Locklair et al., 2011), the Maracaibo Basin (Rey et al., 2004) and northwest Africa (i.e. Rusk, 2001). Although this data indicates a wide distribution of OAE 3 black shales, occurrence is mainly restricted to the Atlantic, possibly as a consequence of the opening of the Equatorial Atlantic Seaway (i.e. Wagner, 2004; Wagreich, 2009; Hofmann and Wagner, 2011), and correlation in time with sites outside the Atlantic is doubtful (Wagreich, 2012). Thus, the impact of local factors is more likely than a global event, controlling the deposition of organic- rich layers (Wagreich, 2012).

The organic-rich sediments on both sides of the Atlantic (Demerara Rise and Ivory Coast-Ghana) were described as more or less continuous succession of cyclic black shales (up to 14% C_{org} on the Demarara Rise), representing precession and eccentricity orbital cycles (Wagner et al., 2004; Friedrich and Erbacher, 2006; Wagreich, 2009) from upper Cenomanian up to upper Santonian or even lower Campanian. It is assumed that anoxic water conditions proceeded from these sites into the Caribbean, the Western Interior and the Maracaibo Basin, depositing organic carbon-rich sediments during Coniacian-Santonian up to the lower Campanian (Locklair et al., 2011; Rey et al., 2004).

Petters and Ekweozor (1982) described black shales of Coniacian to early Santonian in the Benue trough, Nigeria. These fine laminated shales have C_{org} contents up to 1%, but show dominance of terrestrial organic matter. The sediments were deposited under oxygen depleted conditions, based on TS, TS/C_{org} values, and Pr/Ph ratios. The authors assume deposition during global mid-Cretaceous marine transgressions and fed by nutrient-rich, oxygen-depleted waters in the northern parts of the South Atlantic Ocean.

Apart from Atlantic sites, black shales of Coniacian to Santonian age have only limited distribution, but a recent description was carried out for the northern Lebanon. Here, highest C_{org} values were measured for the lower Campanian (up to 6%, type II kerogen; Bou Daher et al., 2014), decreasing through the upper Campanian. The succession consists mainly of lime-mudstones to wackestones. Bou Daher et al., (2014) described variable, dysoxic depositional environments, whilst the study area was only marginally affected by the Santonian phase of transgression. A further compilation of OAE3 related sediments is given by Wagreich (2009).

For the samples of the Tarfaya Sondage No.1, high variations in C_{org}, TS and $CaCO_3$ content are characteristic. For the TB variations in sea-level and upwelling intensity have been proposed (Holbourn et al., 1999), influencing sediment composition and productivity of carbonate and organic matter and thus explaining differences in sedimentary compositions. Based on the relationship

between C_{org} and TS, the original sediment composition before sulfate reduction (silicate, original OM, carbonate) was calculated (Fig. 11). This procedure is based on the fact that (almost all) sulfur in the system is of early diagenetic origin, derived from microbial sulfate reduction under consumption (oxidation) of reactive organic matter. The underlying equations and assumptions are discussed in Littke et al. (1991) for ancient source rock systems and in Lückge et al. (2002) for recent upwelling systems. The depositional system studied here is carbonate dominated (Fig. 11), but a slight increase of OM with an increase of silicate is obvious and probably related to enhanced nutrient supply. This would also point to advanced productivity/preservation and give an explanation for the high OM contents.

Moderate TS/C_{org} ratios are characteristic for nearly all samples. After Berner (1984) high TS/C_{org} values indicate that a high amount of OM was consumed via bacterial sulfate reduction under diagenetic and anoxic marine conditions. In these sediments most sulfur occurs in the form of iron sulfides. Thermochemical sulfate reduction (Michard et al., 2008) did never happen in the TB due to low diagenetic temperature; hence the sulfur is related to bacterial sulfate reduction processes. This is also evident from the presence of pyrite, often as microcrystals of framboidal pyrite. Large pyrite crystals are missing. TS/C_{org} ratios are not uniform within the well, but there are some depth levels, where quite high ratios indicate oxygen-deficiency in bottom waters. Most of the Santonian and early Campanian samples plot below the normal marine line, suggesting an oxygenated water column. In general the data indicate a high bioproductivity and no or only periodically anoxic water column. The pattern of the Santonian samples resembles the one established for Santonian samples of Sondage No. 2 (Sachse et al., 2012) where most samples plot close or below the normal marine line, indicating suboxic conditions and enhanced productivity. TS/C_{org} ratio vs. HI and TS vs. S_2 (Fig. 12) support these conclusions on the depositional environment. High HI values, moderate TS/C_{org} and $(Ph/nC_{18})/(Pr/nC_{17})$ (Figs. 8, 12) ratios indicate preservation of the OM in oxygen-depleted but not anoxic waters. This holds true especially for the Santonian samples.

Organic geochemical results reveal a dominance of short chain *n*-alkanes ($<C_{20}$) which are typical for nearly all samples, and are typical for phytoplankton sources (Cranwell, 1977). Due to low maturity a cracking of long chain hydrocarbons can be ruled out here. Higher abundance of long-chain *n*-alkanes indicates contribution of terrestrial input (Peters et al., 2005), but is not observed here.

The dominance of C_{27} and C_{28} steranes supports the conclusion on predominant marine OM contribution (Figs. 9, 10). The high amounts of ergostane and cholestane point to phytoplankton and zooplankton as source for the OM. The low abundance of hopanes leads to the assumption of a minor bacterial contribution to the organic matter and/or a bad preservation of the precursor bacteriohopanetetrol. Hopanes as minor components were also described, for instance by Kolonic et al. (2002) for black shales of Cenomanian-Turonian age from the TB and by Sachse et al. (2011, 2012) for sediments of various stratigraphic ages in the TB.

The observation of alginite and liptodetrinite supports the marine contribution, while the occurrence of sporinite also shows a minor terrigenous influence. Minor vitrinite and inertinite contents also represent land-derived plant material in the samples. In summary, the high abundance of algae/phytoplankton derived liptinite, the high ratio of short chain over long chain *n*-alkanes and the high concentration of iso-alkanes pristane and phytane indicate phytoplankton (algae) as primary source of OM.

Based on the presented results it can be concluded that during the early Campanian and Santonian the investigated sediments were deposited in a shallow marine nutrient-rich upwelling influenced continental margin basin. The nutrient-rich environment depends on the flooding of the Atlas Gulf resulting in a connection of the Atlantic Ocean with the stagnant/nutrient-rich Tethys during the Cenomanian developing a major upwelling zone along the Central and North African Atlantic margin (Jarvis et al., 1999). Mid-Cretaceous was one of the hottest periods in earth history with elevated sea-levels and shelf areas twice as large as today. During that time, a series of major transgressive cycles caused a widespread flooding and intermittent regressive phases led to sea-level changes with heaving and sinking of the oxygen minimum zone and changing of bottom water conditions (Lüning et al., 2004).

These palaeo sea-level changes coincide with deposition of sediments with high C_{org} content, possibly reflecting strong bioproductivity and a strong oxygen minimum zone. Along modern continental margins, organic matter flux to the seafloor is strongly controlled by intensity, depth and lateral extent of the oxygen minimum zone. As described in Littke et al. (1998) C_{org} and kerogen quality tend to decrease at continental margins from the proximal to the distal (pelagic) realm. However, turbidity currents and mass flows can transport large volumes of organic matter-rich sediment into deep marine areas outside and below the intense oxygen-minimum zone as described in Lückge et al. (1996). In the case of the Cretaceous Tarfaya Basin the zone of intense oxygen

minimum extended far to the proximal parts of the margin or even onto the shelf, leading to exceptionally thick and stratigraphically extended source rocks on the present day coast. The exceptional character of the Tarfaya deposits will be additionally controlled by the paleo-bathymetry along the northwestern African margin. In analogy to sapropel deposition at present-day, organic matter deposition depends not only on bioproductivity (and upwelling intensity), but also on the presence of mini-basins (Reimers and Suess, 1983, Spaulding, 1991).

Moreover, Late Cretaceous oceans were possibly more sensitive than present day oceans, reacting considerably to minor climate or hydrographic chances (Holbourn et al., 1999). These sea-level changes are reflected in the change of the depositional environment, i.e. the variable C_{org}, TS, $CaCO_3$, HI and Pr/Ph values. Transgressive and regressive phases of sea-level changes during the Late Cretaceous can be related to orbital Milankovitch-cycles (Holbourn et al., 1999; Kuhnt et al., 1997). Furthermore the cause of organic matter-rich sedimentation in the Atlantic is not only related to global warming conditions or sea-level changes, but also driven by the configuration of the Atlantic and the shelf basins and continents. Wind-driven upwelling of nutrient rich seawater might be related to an estuarine circulation with respect to the Pacific from where nutrient-rich seawater derived. In this case, the low-latitudinal Atlantic served as a nutrient trap for a prolonged time interval (Wagner, 2002; Trabucho Alexandre et al., 2010) leading to sedimentation and preservation of large amounts of organic matter under oxygen depleted conditions.

Wind-induced upwelling of nutrient rich waters and correlated productivity and preservation were also suggested for the black shale deposits offshore Ivory Coast-Ghana, while cyclicity was explained by fluctuations in preservation and productivity (Hofmann et al., 2003; Beckmann et al., 2005, 2008), coupled with freshwater availability and climate conditions, and thus influencing the water circulation. However, compared to the Demerara Rise, for the Ivory Coast-Ghana a more regional control is assumed. More permanent anoxic conditions were suggested for the Demerara rise (Flögel et al., 2008), where various authors (i.e. Meyers et al., 2006 and citations therein) assume a long-lived upwelling system and thus high primary production. As described by Beckmann et al. (2008), during early to mid Coniacian times stronger oxygenation occurred, while oxygen depleted conditions were present during most times. In contrast, variations in the monsoonal system triggering precipitation, freshwater runoff and nutrient discharge occurred offshore Ivory Coast-Ghana.

It should be noted that organic matter deposition and preservation was much more intense during the Cenomanian and Turonian oceanic anoxic event (OAE 2) than during the Campanian and

Santonian (OAE 3) with C_{org} values more than twice as high (Arthur and Schlanger, 1979; Sachse et al., 2011, 2012). In strong contrast to the widespread OAE 2, OAE 3 may be divided into several short-term events (Arthur et al., 1990), whilst no clear OAE 3 level that applies to most of the sites can be defined (Wagreich, 2012). In addition, the Coniacian-Santonian black shales are more restricted than the Cenomanian-Turonian shales and limitation to shallow water settings and Atlantic and Caribbean regions was noted by Jenkyns (1980). According to calculations from Locklair and Sageman (2008; Western Interior) for Coniacian-Santonian orbital time scale, the duration of the Coniacian (86.3-89.8 Ma) event ranges from 3.26 to 3.50 My, the Santonian (83.6-86.3 Ma) from 2.24 to 2.53 My, giving a total duration for the Coniacian–Santonian event of 5.5 to 6 My. Although this was calculated for an American locality, this is much longer than assumed for the OAE 2, for which a duration of only 0.3 to 0.7 My has been calculated (Sageman et al., 2006) with high-productivity events therein being even of shorter duration (Adams et al, 2010). Meyers et al. (2006) gave a compilation of the duration of the different OAEs, calculating a time span of approx. 300 ky for OAE2 and 2.7 My for OAE3. The absolute age durations are based on Ogg et al. (2004). It should be noted, however, that organic matter-rich sedimentation lasted much longer in the TB (Sachse et al., 2011, 2012). Thus not only the climate changes (seasonal dry wet cyclicity) are responsible for the differences of deposition of OM during OAE 2 and 3, but also ocean circulation.

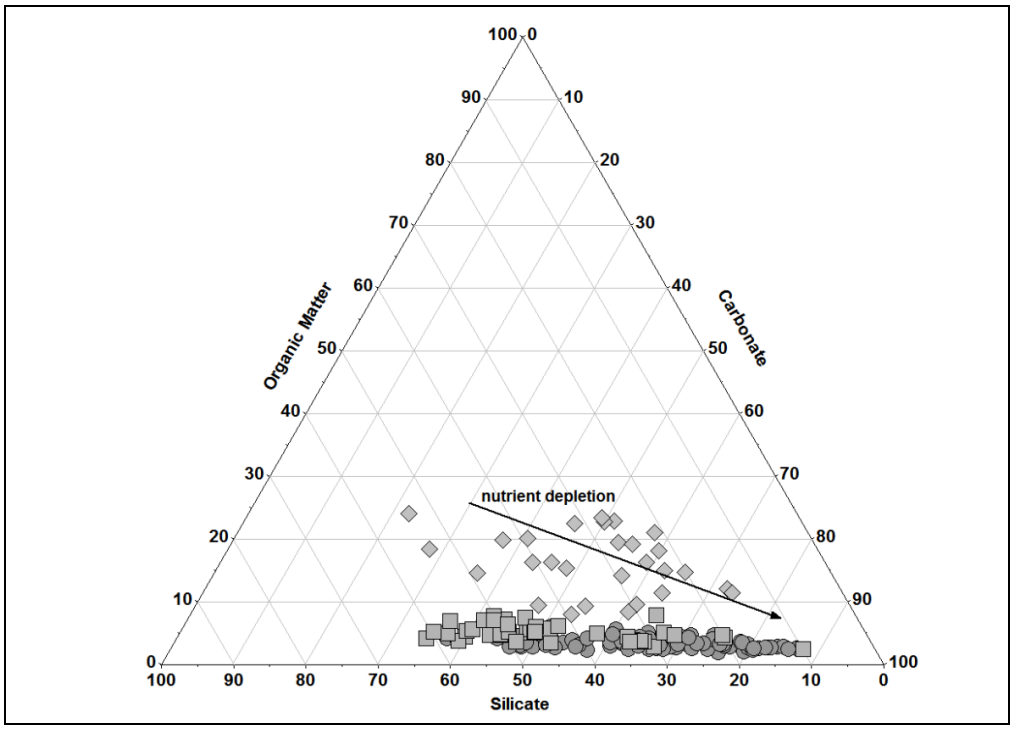

Figure 11: Original sediment compositions of early Campanian and Santonian samples. The lower part of the Santonian drilled in well Sondage No.2 has clearly higher organic matter content than the younger units drilled in well Sondage No.1.

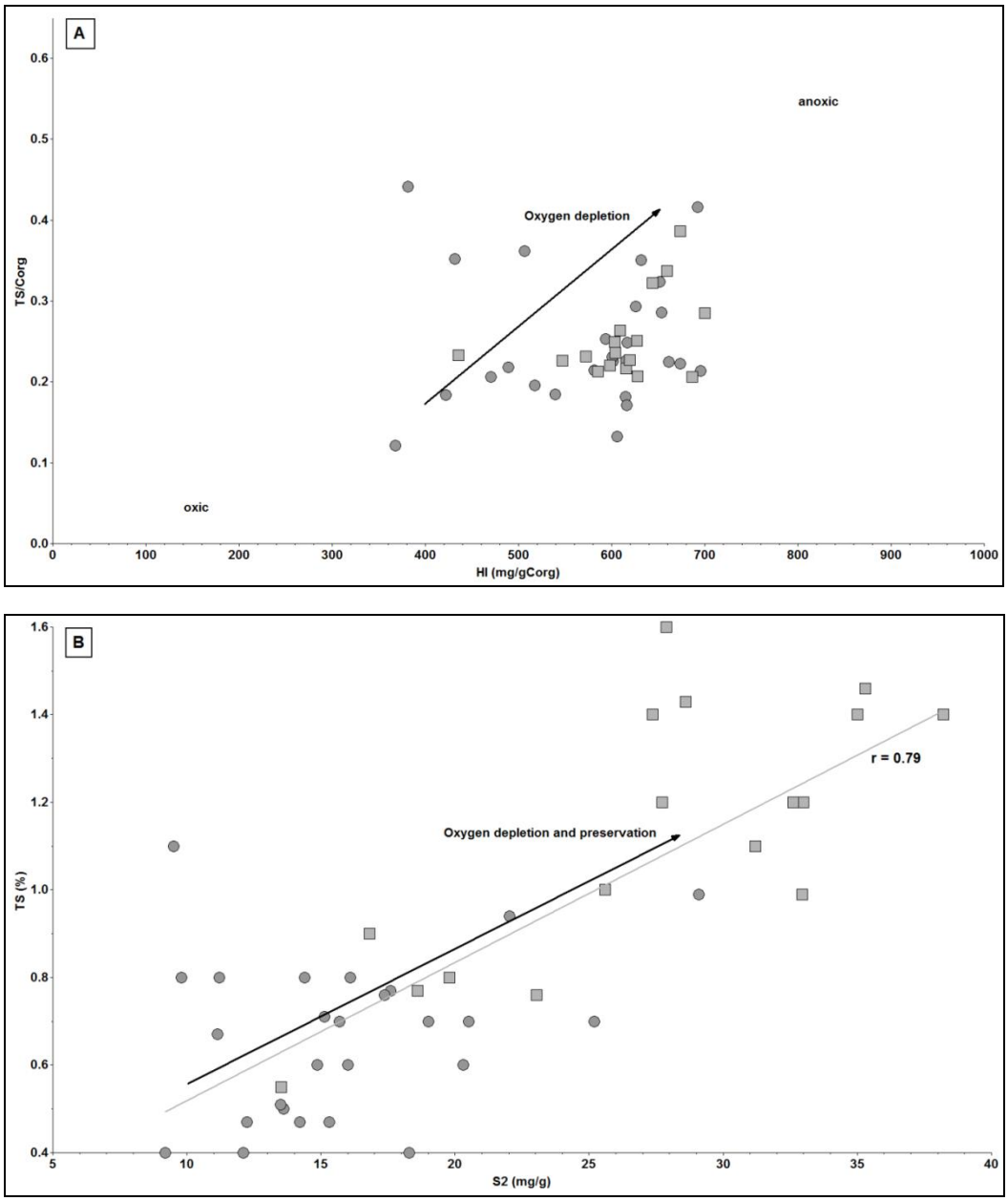

Figure 12: Anoxic parameters: (a) TS/C_{org} ratio vs. HI (mg/g C_{org}) and (b) TS (%) vs. S2 (mg/g rock).

4.2. Petroleum potential and maturity

According to their high HI and S_2 values, the early Campanian and Santonian samples of this 180 m thick sequence have a very high petroleum generation potential (Peters, 1986). Although the different plots used for kerogen classification (Fig. 4 A and B) do not perfectly coincide, a

phytoplankton derived kerogen type II or maybe a mixture of type I/II can be assumed. However, the sediments are at an immature stage, as proven by a variety of parameters, e.g. occurrence of brightly fluorescing particles, low vitrinite reflectance and persistently low T_{max} values.

In this case, the odd-even predominance (OED) does not reflect maturity stages very well. Assuming a thermally mature stage with an OED between 0.9 and 1.3, two samples (sample 575 and 634) represent an immature stage, seven samples even a mature stage and six reach an overmature stage (Table 2). A tendency over depth is not clearly obvious, and this parameter should be handled with care if it does not coincide with other parameters (Hunt, 1995). In contrast, the CPI after Bray & Evans (1961) supports an immature or possibly early mature stage of the samples. Pr/nC$_{17}$ and Ph/nC$_{18}$ ratios also prove an immature to early mature stage (Fig. 8; Table 2). In conclusion, the biomarker ratios based on the *n*-alkanes point to an immature or early mature stage and Rock-Eval parameters and organic petrology indicate an immature stage. Oil generation from these source rocks can only be expected in (offshore) areas, where deeper burial has occurred leading to higher temperatures. In the onshore area, the very thick organic matter-rich Upper Cretaceous sequence might by economically interesting for oil shale retorting purposes in future. However, a Late Cretaceous source rock contribution is unlikely also in offshore areas due to thinning or absence of sediments (Wenke et al., 2011).

5. General discussion and conclusions

Our data confirm the presence of early Campanian and Santonian high quality source rock intervals in the coastal area of the TB. The high C_{org} contents of the early Campanian and especially of the Santonian samples are related to high bio-productivity of marine organisms (algae/phytoplankton) and favorable conditions of preservation. Import or upwelling of nutrient-rich waters during the Late Cretaceous may be one of the key mechanisms for deposition and preservation of organic material, similar as described for the Cenomanian/Turonian sequences. Another important factor seems to be the local hydrographic and topographic situation during the Late Cretaceous explaining the variations between the sample sites (outcrops, Sondage No.1 and No. 2). Small scale variations in primary production and C_{org}-content are also known from recent upwelling areas (Reimers and Suess, 1983) and other prominent examples of Coniacian-Santonian organic-rich deposits. The higher amount of organic matter and its preservation in the Santonian samples in contrast to the early Campanian can be explained by the relative rise of the sea-level (Fig. 13C),

whilst during the early Campanian a slight sea-level fall was noted (Haq et al., 1987; Fig. 13C). In addition, preservation is related to relative high temperatures of the sea water during the Late Cretaceous (Fig. 13B). During the Cenomanian/Turonian, sea surface temperatures reached values of 30°C, followed by a cooling towards the Campanian with still high values of about 23°C. This affects the solubility of oxygen in sea water as shown in Figure 14 as warmer climates have smaller temperature gradients and thus affecting the concentration of water vapor increases with temperature (Pierrehumbert, 2002). High temperatures were typical for the Cretaceous greenhouse climate and especially for the Cenomanian/Turonian period leading to lower oxygen concentration at several hundred meters depth below sea-level and thus to better preservation of organic matter due to more expanded oxygen minimum layers. This situation was present in all oceans during the Mid-Cretaceous, but most pronounced at low latitudes. This might be an explanation for the occurrence of black shales around this time interval, especially in the Atlantic. However, further parameters should also be considered (i.e. continental run off, salinity, water circulation). As shown in Figure 14, oxygen concentration rises with decreasing water temperature leading to a stronger degradation of phytoplankton and other organic material in the oceans. Thus, highest C_{org} contents were measured for times of or close after temperature maxima as for the Cenomanian/Turonian with a maximum at 93 Ma. Santonian and Campanian (85 to 75 Ma) also represent periods of high temperatures, though somewhat lower than during the Cenomanian and Turonian (Friedrich et al., 2012). This fact indicates and supports the assumption of various authors (Wagreich, 2012) that OAE 3 might not be a single short-term event as OAE 2, but distributed over a long-time span. The negative feedback of organic carbon burial and preservation in contrast to Cenomanian/Turonian is thus related to decrease of global hothouse conditions during the Late Cretaceous and the better solubility of O_2. Following this approach, changes in continent/ocean configuration as the opening of the Atlantic, climate, water circulation (as result of Atlantic opening) and sea-level fluctuation (Erbacher et al., 1996; Beckmann et al., 2005; Fig. 13C) ultimately control the production and deposition of organic matter in the Atlantic Ocean.

The presence of oxygen depleted but not completely anoxic conditions is supported by redox parameters such as Pr/Ph ratio and TS/C_{org} and support the assumption of a third widespread oceanic anoxic event of Coniacian to Santonian age (OAE 3) affecting the southern North Atlantic. A comparison with previous investigated samples (outcrops and Sondage No.2) and literature information for the Demerara Rise, the offshore area of the Ivory Coast-Ghana, the Lebanon and

Nigeria shows clearly that not all OAEs record similar depositional conditions as shown here for the temperature dependence of preservation and more regional controls and models should be considered, especially with respect to organic matter productivity and preservation.

Within the TB, the sediments were never deeply buried and organic matter remained immature, as supported by a variety of petrological and geochemical data discussed above. The Upper Cretaceous sequence does not act as active petroleum source rock in this area, but a potential for petroleum generation should be considered in areas of deeper burial and adequate thickness, particularly because the assumed Jurassic oil shows in well Cap Juby are not finally proven.

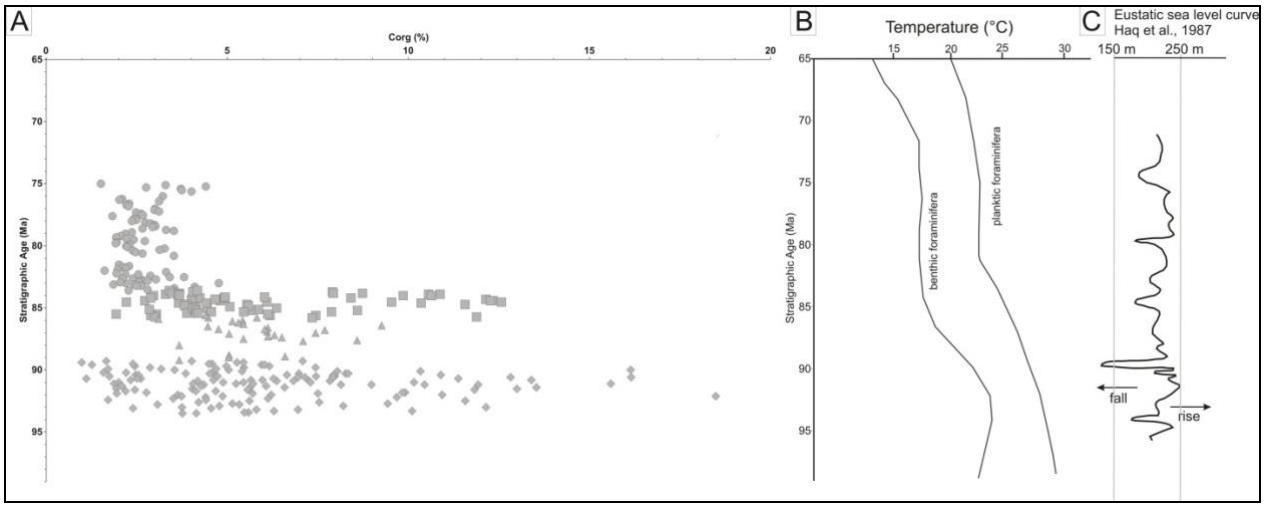

Figure 13: Stratigraphic ages plotted vs (a) Corg content for all samples of Sondage No. 1 and Sondage No. 2 and (b) temperature evolution against stratigraphic age based on Haq et al., 1987 and c) the eustatic sea-level curve (Haq et al., 1987).

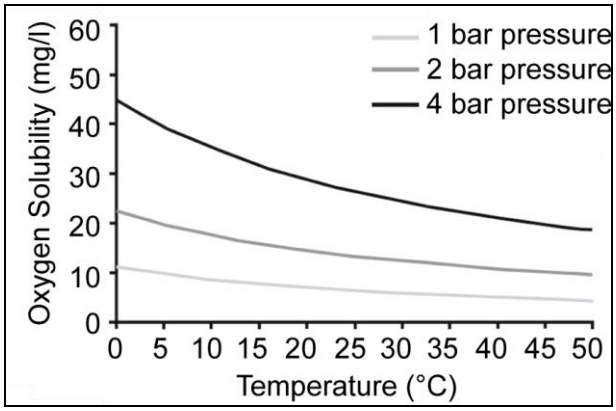

Figure 14: Temperature depending oxygen solubility for different pressure ranges in sea-water, based on Geng and Duan, 2010.

Acknowledgments

We thank RWE Dea AG for financial support. ONHYM, W. Kuhnt, and A. Holbourn (Christian-Albrecht University, Kiel) are gratefully acknowledged for logistic support and sample supply.

Table 1: Overview of Rock-Eval pyrolysis data.

Sample No.	Depth (m)	Stratigraphy	C_{org} (%)	S_1 (mg/g rock)	S_2 (mg/g rock)	T_{max} (°C)	HI (mg/g C_{org})	PI (S_1/S_1+S_2)
513	28.5	Early Campanian	3.29	0.2	12.1	424	367	0.016
514	31.6	Early Campanian	4.4	0.96	29.1	417	661	0.032
516	37.8	Early Campanian	3.71	0.7	22.03	419	593	0.03
517	40.8	Early Campanian	3.74	0.46	17.59	423	470	0.025
519	46.3	Early Campanian	2.81	1.03	27.1	420	964	0.036
522	54.8	Early Campanian	3.21	0.2	15.7	416	489	0.012
530	77.5	Early Campanian	2.27	0.1	9.8	419	431	0.01
535	92.3	Early Campanian	2.4	0.2	16.1	418	651	0.012
539	92.98	Early Campanian	2.49	0.1	9.5	416	381	0.01
547	94.39	Early Campanian	2.66	0.2	16	425	601	0.012
555	95.94	Early Campanian	2.21	0.1	11.2	418	506	0.008
556	96.14	Early Campanian	2.41	0.38	14.87	419	617	0.024
561	97.07	Early Campanian	2.21	0.2	13.6	424	615	0.014
563	98.4	Early Campanian	3.27	0.2	19	422	581	0.01
567	109.0	Early Campanian	2.66	0.39	17.38	422	653	0.021
570	118.0	Early Campanian	2.28	0.2	14.4	418	631	0.013
572	124.3	Early Campanian	2.2	0.36	15.3	418	695	0.022
574	130.6	Early Campanian	1.61	0.23	11.15	422	692	0.02
575	133.7	Early Campanian	3.3	0.2	20.3	422	615	0.009
577	139.8	Early Campanian	2.18	0.1	9.2	420	422	0.01
579	145.8	Early Campanian	3.8	0.2	20.5	416	539	0.009
586	156.67	Early Campanian	2.61	0.2	13.5	415	517	0.014
590	157.58	Early Campanian	2.11	0.28	14.21	421	673	0.019
591	157.72	Early Campanian	3.02	0.2	18.3	419	606	0.01
593	158.3	Early Campanian	2.04	0.27	12.25	420	600	0.021
595	158.69	Early Campanian	2.42	0.49	15.14	425	625	0.031
597	158.99	Early Campanian	4	0.3	25.2	413	616	0.011
601	160.11	Santonian	3.4	0.3	19.8	416	572	0.014
605	161.3	Santonian	4.24	0.4	25.6	419	603	0.015
610	163.12	Santonian	3.86	0.3	16.8	417	435	0.017

612	163.81	Santonian	4.14	1.09	27.88	415	673	0.037
613	164.11	Santonian	4.44	1.1	28.6	417	644	0.037
614	164.32	Santonian	5.85	1.26	35.29	416	603	0.034
615	164.4	Santonian	5.64	0.6	33	417	585	0.017
616	164.63	Santonian	4.55	1.2	27.72	413	609	0.041
621	165.86	Santonian	3.4	0.3	18.6	409	547	0.015
625	166.84	Santonian	3.67	0.85	23.05	415	628	0.035
629	168.11	Santonian	4.8	1.64	32.94	414	686	0.047
633	169.32	Santonian	5.58	0.5	35	418	627	0.014
634	169.54	Santonian	5.07	0.5	31.2	413	615	0.015
638	173.5	Santonian	5.45	0.6	32.6	412	598	0.018
639	176.4	Santonian	4.15	1.21	27.37	413	659	0.042
640	179.3	Santonian	1.93	0.5	13.51	414	700	0.035
641	182.4	Santonian	6.17	0.6	38.2	417	619	0.015

Table 2: n- and isoalkane ratios.

Sample No.	Stratigraphy	Depth (m)	OEP (Scalan&Smith, 1970)	CPI (Bray&Evans, 1961)	Pr/Ph	Pr/nC$_{17}$	Ph/nC$_{18}$	nC$_{17}$/nC$_{27}$
513	Early Campanian	28.5	1.4	3.0	1.0	1.5	1.7	1.0
530	Early Campanian	77.5	1.0	0.8	1.2	2.6	2.5	1.4
539	Early Campanian	92.98	1.4	1.0	1.1	2.6	2.9	1.1
555	Early Campanian	95.94	1.3	0.9	1.2	2.3	2.6	1.5
563	Early Campanian	98.4	1.5	1.9	1.1	2.0	2.8	2.2
570	Early Campanian	118	1.3	1.2	0.9	2.1	3.5	1.5
575	Early Campanian	133.7	0.7	1.0	0.9	2.7	4.3	2.1
579	Early Campanian	145.8	1.6	0.7	1.0	2.9	4.4	3.5
586	Early Campanian	156.67	1.4	1.4	1.3	2.2	2.1	1.1
597	Early Campanian	158.99	1.4	1.8	1.2	1.8	2.6	1.5
605	Santonian	161.3	1.8	0.7	0.8	2.4	5.3	3.6
615	Santonian	164.4	2.1	2.4	0.8	3.0	5.6	3.9
621	Santonian	165.86	1.3	1.5	0.9	3.0	5.3	n.d.
634	Santonian	169.54	0.7	1.0	0.9	3.1	5.9	2.0
641	Santonian	182.4	1.5	1.2	0.8	1.8	2.9	4.3

Chapter VI. General Conclusions

In contrast to previous studies that mainly concentrated on the Cenomanian-Turonian sediments of the Tarfaya basin, this study provides new insights into the late Turonian to Campanian successions of the basin. In this context, the paleoenvironmental evolution and sea-level history are tentatively reconstructed. The study combines outcrop and core records. Outcrops allowed the observation of lateral development of sedimentary features. The oldest sediments occur in the northern part of the basin at Mohammed Plage (Cenomanian) and En Naila section (early Turonian), whereas the youngest sediments are located more to the south at Tisfourine and Tah West sections (early Campanian) due to regional tectonics (uplift events in the Atlas system (Frizon de Lamotte et al., 2009; Ruiz et al., 2010)) which affected the Tarfaya Basin. Core records enabled a high-resolution reconstruction of the depositional variability and thus allowed us to conduct sequence analyses. These cores recovered the organic-rich sediments from the uppermost late Turonian to early Campanian in core Tarfaya SN°1 and from late Turonian to middle Santonian in core Tarfaya SN°2. Planktonic foraminiferal and nannofossil biostratigraphy allowed us to construct the age models of these two cores. The sedimentation rate was calculated in the Tarfaya Basin on the comparison of the depth/age relationship of the main carbon isotope events and indicates an average of sedimentation rate of ~2.1 cm/kyr during the Coniacian, ~1.6 cm/kyr during the Santonian and ~2.1 cm/kyr during the early Campanian. In constract, the end of the Cretaceous sedimentary succession in the Sebkha Tah and Tisfourine sections as well as in core Tarfaya SN°1 was marked by a major hiatus, which comprises the entire latest Cretaceous (middle Campanian-Maastrichtian) and Paleogene.

The depositional environmental in the Tarfaya Basin was reconstructed based on elemental distributions measured by XRF core scanner and benthic foraminifera assemblages. Fluctuations in the abundance of the terrigenous elements Al, Ti, K, Si and Fe, normalized against Ca indicate three major sedimentary cycles of 33.2, 32 and 31 m thickness (286.7 to 253.5 mcd, 253.5 to 221.5 mcd and 221.5 to190.5 mcd) during the Coniacian to middle Santonian. This time interval is also characterized by recurrent impinging of an expanded oxygen minimum zone onto the Tarfaya shelf, which is expressed by low Mn/S and high V/Ca ratios in the XRF-scanner records. These periods of organic matter-rich sedimentation on the Tarfaya shelf correspond in a very broad sense to the Coniacian-Santonian Anoxic Event (OAE-3). The interval from 158.8 to 190.5 mcd (late Santonian), corresponds to the transition from anoxic to oxic conditions, which dominate in the early Campanian.

The early Campanian sedimentary environment is characterized by enhanced accumulation of fine-grained carbonate and clay-rich hemipelagic sediments, which may indicate a major regional climate change towards wetter conditions. This time interval also experienced an improvement of the oxygenation at the sea floor as recorded by an increase in log(Mn/S) and a high diversity and abundance of benthic foraminiferal assemblages in the Tisfourine and Tah West sections.

The benthic foraminiferal assemblages exhibit, during the early Turonian, an installation of an oxygen minimum zone (OMZ) reflected by the absence or low abundance of benthic foraminifera (>250 microns) at the base of El Amra and En Naila sections. This OMZ was linked to the intensification of upwelling along the margin of the Tarfaya Basin. The presence of relatively well-preserved planktonic foraminifera throughout the sections (El Amra and En Naila sections) indicated that the lack of benthic foraminifera does not reflect poor preservation in these intervals. During the middle Turonian, the appearance of shelf benthic foraminifera tolerant of low-oxygen conditions in the El Amra section reflects an improvement in bottom water oxygenation, possibly related to a seaward shift and/or decrease in the intensity of the oxygen minimum zone due to lowering of the sea-level. From the late Turonian to Santonian, the presence of benthic foraminiferal with low diversity in the El Amra, Akhfennir and Tah North sections suggests relatively impoverished oxygenation in bottom water along the shelf. In contrast, lack of benthic foraminifera in the upper part of the Tah North section (late Santonian) reflects again an intensification and/or expansion of the oxygen minimum zone. During the early Campanian, high diversity and abundance of benthic foraminifera at the Tisfourine and Tah West sections indicate an overall improvement in bottom water oxygenation.

Sea-level change reconstructed in the Tarfaya Basin is correlated to regional sea-level variations in the New Jersey Margin record (Miller et al., 2004; Mizintseva et al., 2009). In particular, we correlate the major unconformities U1/U2 and U3 in the Tarfaya Basin to the base of the Merchantville III and the base of Magothy III sequence of Miller et al. (2004) and Mizintseva et al. (2009). The unconformities based on XRF records at 253.5 mcd, 221.5 mcd and 190.5 mcd are correlated to the Cheesequake, Merchantville I and Merchantville II Sequences of Miller et al., (2004) and Mizintseva et al. (2009), respectively.

The Upper Cretaceous (Turonian to Campanian) bulk carbonate isotope records from outcrop sections were tentatively correlated to the English Chalk carbon isotope reference curve of Jarvis et al. (2006) but showed only a few major events (Hitch Wood Event, Navigation Event and the

Santonian/Campanian Boundary Event) due to low resolution sampling and difficulties in correlation of outcrop sections. In contrast, high resolution records from the cores Tarfaya SN°1 and 2 exhibits strong similarities to the global carbon isotope stack of Wendler (2013). Marked events in the Tarfaya Basin, that are correlative to the English Chalk (Jarvis et al., 2006) and the Niobrara Formation in the US Western Interior Seaway (Locklair et al., 2011) are the Navigation Event in the earliest Coniacian, the Haven Brow, the Horseshoe Bay and the Buckle Events in the Santonian and the Santonian/Campanian Boundary Event. The Santonian-Campanian Boundary Event has an overall carbonate isotope ($\delta^{13}C$) amplitude of ~1.5‰ which is higher than in the English chalk (0.6‰) and in the Gubbio Scaglia limestone (0.4‰). The bulk carbonate isotope records ($\delta^{18}O$) exhibit a long-term increasing trend in the early Campanian (following the Santonian-Campanian Boundary Event), which indicates the establishment of cooler intermediate water conditions along the NW African Margin.

Further investigation will focus on a sedimentary core (Tarfaya SN°4), drilled in the Tarfaya Basin, which provides a continuous and expanded record of shelf sedimentation from the Aptian to the Turonian. High resolution XRF core scanning data and bulk stable isotopes will allow to closely track short- and long-term variations in elemental composition and in $\delta^{13}C$ and $\delta^{18}O$, thus providing an essential dataset to better understand the paleoceanographic evolution and the sea-level history of this marginal shelf basin during the early part of the Late Cretaceous. This study will also help to better understand the underlying mechanisms driving the onset and spread of Oceanic Anoxic Event 2.

References

Abou Ali, N., Hafid, M., Chellai, E.H., Nahim, M., Zizi, M., 2005. Structure de socle, sismostratigraphie et héritage structural au cours du rifting au niveau de la marge d´Ifni/Tan-Tan (Maroc sud-occidental). Comptes Rendus Geoscience 337, 1267–1276.

Adams, D.D., Hurtgen, M.T., Sageman, B.B., 2010. Volcanic triggering of a biogeochemical cascade during Oceanic Anoxic Event 2. Nature Geoscience 3, 201–204.

Adegbie, A.T., Schneider, R.R., Röhl, U., Wefer, G., 2003. Glacial millennial-scale fluctuations in central African precipitation recorded in terrigenous sediment supply and freshwater signals offshore Cameroon. Palaeogeography, palaeoclimatology, palaeoecology 197, 323–333.

Aizenshtat, Z., Stoler, A., Cohen, Y., Nielsen, H., 1983. The geochemical sulphur enrichment of recent organic matter by polysulfides in the Solar Lake, in: Bjorøy, M., Albrecht, C., Cornford, C., de Groot, K., Eglinton, G. (Eds.), Advances in Organic Geochemistry, 1981. Proceedings International Meeting on Organic Geochemistry 10, 279–288.

Aizenshtat, Z., Krein, E.B., Vairavamurthy, M.A.A., Goldstein, T.P., 1995. Role of sulfur in the transformations of sedimentary organic matter: A mechanistic overview, in: Vairavamurthy, M.A.A., Schoonen, A. (Eds.), Geochemical Transformation of Sedimentary Sulfur. American Chemical Society, Symposium Series 612, pp. 16–39.

Amédro, F., Bidar, A., Damotte, R., Manivit, H., Robaszynski, F., Sornay, J., 1978. Echelles biostratigraphiques dans le Turonien du Cap Blanc-Nez (Pas-de-Calais, F.). Bulletin d'Information des Géologues du Bassin de Paris 15, 3–20.

Amijaya, H., Littke, R., 2006. Properties of thermally metamorphosed coal from Tanjung Enim area, South Sumatra Basin, Indonesia with special reference to the coalification path of macerals. International Journal of Coal Geology 66, 271–295.

Anderson, T.F., Raiswell, R., 2004. Sources and mechanisms for the enrichment of highly reactive iron in euxinic Black Sea sediments. American Journal of Science 304, 203–233.

Ando, A., Littler, K., Woodard, S.C., Herrmann, S., Evans, H.F., Khim, B., Robinson, S.A., Huber B.T., 2011. Discovery and paleoceanographic significance of unconsolidated Cretaceous sediment cover on northern Tamu Massif, Shatsky Rise (IODP Site U1348). American Geophysical Union, Fall Meeting 2011, San Francisco, abstract V51D-2539.

Aquit, M., Kuhnt, W., Holbourn, A., Chellai, E.H., Stattegger, K., Kluth, O., and Jabour, H., 2013. Late Cretaceous paleoenvironmental evolution of the Tarfaya Atlantic coastal Basin, SW Morocco. Cretaceous Research 45, 288–305.

Arndt, S., Brumsack, H.-J., Wirtz, K.W., 2006. Cretaceous black shales as active bioreactors: a biogeochemical model for the deep biosphere encountered during ODP Leg 207 (Demerara rise). Geochimica et Cosmochimica Acta 70, 408–425.

Arthur, M.A., Schlanger, S.O., 1979. Cretaceous "oceanic anoxic events" as causal factors in development of reef-reservoired giant oil fields. The American Association of Petroleum Geologists Bulletin 63, 870–885.

Arthur, M.A., von Rad, U., Cornford, C., McCoy, F.C., Sarnthein, M., 1979. Evolution and Sedimentary history of the Cape Bojador continental margin, Northwestern Africa, in: Ryan, W.B.F., von Rad, U., et al. (Eds.), Initial Reports of the Deep Sea Drilling Project 47 (1), pp. 773–816.

Arthur, M.A., Dean, W.E., and Pratt, L.M., 1988, Geochemical and climatic effects of increased marine organic carbon burial at the Cenomanian/Turonian boundary: Nature 335, 714–717.

Arthur, M.A., Jenkyns, H.C., Brumsack, H.J., Schlanger, S.O., 1990. Stratigraphy, geochemistry, and paleoceanography of organic carbon-rich Cretaceous sequences, in: Ginsburg, R.N., Beaudoin, B. (Eds.), Cretaceous resources events and rhythms. Dordrecht, Kluwer Academic Publishers, pp. 75–120.

Arthur, M.A., and Sageman, B.B., 1994, Marine black shales: Depositional mechanisms and environments of ancient deposits: Annual Reviews of Earth and Planetary Sciences 22, 499–551.

Arthur M.A., Dean, W.E., 1998. Organic-matter production and preservation and evolution of anoxia in the Holocene Black Sea. Paleoceanography 13, 395–411.

Arz, H.W., Pätzold, J., Wefer., G., 1998. Correlated millennial-scale changes in surface hydrography and terrigenous sediment yield inferred from last-glacial marine deposits off northeastern Brazil. Quaternary Research 50, 157–166.

Arz, H.W., Pätzold, J., Wefer., G., 1999. Climatic changes during the last deglaciation recorded in sediment cores from the northeastern Brazilian Continental Margin. Geo-Marine Letters 19, 209–218.

Arz, H.W., Pätzold, J., Müller, P.J., 2003. Influence of Northern Hemisphere climate and global sea level rise on the restricted Red Sea marine environment during termination I. Paleoceanography 18, doi:10.1029/2002PA000864.

Balsam, W.L., Deation, B.C., Damuth, J.E., 1999. Evaluating optical lightness as a proxy for carbonate content in marine sediment cores. Marine Geology 161, 141–153.

Baudin, T., Marquer, D., Barfety, J.C., Kerckhove, C., Persoz, F., 1995. A new stratigraphical interpretation of the Mesozoic cover of the Tambo and Suretta nappes. Evidence for early thin-skinned tectonics. Comptes Rendus de l´Académie des Sciences de Paris IIa 321, 401–408.

Baturin, G.N., 2003. Phosphorus cycle in the ocean. Lithology and Mineral Resources 38,

Beckmann, B., Flögel, S., Hofmann, P., 2005. Linking Coniacian- Santonian (OAE3) black- shale deposition to African climate variability: a reference section from eastern tropical Atlantic at orbital time scales (ODP site 959, off Ivory Coast and Ghana), in: Harris, N.B. (Ed.), The deposition of organic- Carbon – Rich Sediments: Models, Mechanisms, and Consequences. SEPM Special Publications 82, 125–143.

Beckmann, B., Hofmann, P., März, C., Schouten, S., Sinninghe Damsté, J.S., Wagner, T., 2008. Coniacian- Santonian deep ocean anoxia/euxinia inferred from molecular and inorganic markers: Results from the Demerara Rise (ODP leg 207). Organic Geochemistry 39, 1092– 1096.

Benitez-Nelson, R.C., 2000. The biogeochemical cycling of phosphorus in marine systems. Earth-Science Reviews 51, 109–135.

Bergen, J.A., 1994, Berriasian to early Aptian calcareous nannofossils from the Vocontian trough (SE France) and Deep Sea Drilling Site 534: New nannofossil taxa and a summary of low-latitude biostratigraphic events: Journal of Nannoplankton Research 16, 59–69.

Berger, W.H., Killingley, J.S., 1977. Glacial-Holocene transition in deepsea carbonates: selective dissolution and the stable isotope signal. Science 197, 563–566.

Berner, R.A., 1984. Sedimentary pyrite formation: an update. Geochimica et Cosmochimica Acta 48, 605–615.

Biscaye, P.E., 1965. Mineralogy and sedimentation of recent deep-sea clay in the Atlantic Ocean and adjacent seas and oceans. Geological Society of America Bulletin 76, 803–832.

Bojanowski, R., Paslawska, S., 1970. On the occurence of iodine in bottom sediments and interstitial waters of the southern Baltic Sea. Acta Geophysica Polonica 18, 277–286.

Bou Daher, S., Nader, F.H., Strauss, H., Littke, R., 2014. Depositional environment an source- rock characterisation of organic- matter rich Upper Turonian- Upper Campanian carbonates, Norther Lebanon. Journal of Petroleum Geology 37, 1–20.

Boulila, S., Galbrun, B., Miller, K.G., Pekar, S.F., Browning, J.V., Laskar, J., Wright, J.D., 2011. On the origin of Cenozoic and Mesozoic "third-order" eustatic sequences. Earth-Science Reviews 109, 94–112.

Brachert, T.C., Forst, M.H., Pais, J.J., Legoinha, P., Reijmer, J.J.G., 2003. Lowstand carbonates, highstand sandstones?. Sedimentary Geology 155, 1–12.

Bralower, T.J., Leckie, R.M., Slliter, W.V., Thierstein, H.R., 1995. An integrated Cretaceous microfossil biostratigraphy: In, Berggren, W.A., Kent, D.V., Hardenbol, J. (eds.), Geochronology, Time Scales and Global Stratigraphic Correlations: SEPM Special Publication 54, pp. 65–79.

Bray, E.E., Evans, E.D., 1961. Distribution of n-paraffins as a clue to recognition of source beds. Geochimica et Cosmochimica Acta 22, 2–15.

Browning, J.V., Miller, K.G., Sugarman, P.J., Kominz, M.A., McLaughlin, P.P., Kulpecz, A.A., Feigenson, M.D., 2008. 100 Myr record of sequences, sedimentary facies and sea level change from Ocean Drilling Program onshore coreholes, US Mid-Atlantic coastal plain. Basin Research 20, 227–248.

Brumsack, H.J., 1986. The inorganic geochemistry of Cretaceous black shales (DSDP Leg 41) in comparison to modern upwelling sediments from the Gulf of California, in: Summerhayes, C.P., Shackleton, N.J. (Eds.), North Atlantic Paleoceanography. Geological Society Special Publication 21, London, pp. 447–462.

Brumsack, H.J., 2006. The trace metal content of recent organic carbon-rich sediments: implications for Cretaceous black shale formation. Palaeogeography, Palaeoclimatology, Palaeoecology 232, 344–361.

Burnett, J.A., Gallagher, L.T., Hampton, M.J., 1998, Upper Cretaceous, in Bown, P.R., ed., Calcareous Nannofossil Biostratigraphy: British Micropalaeontological Society, London, Publication Series, Chapman & Hall, p. 132–199.

Butt, A., 1982. Micropaleontological bathymetry of the Cretaceous of Western Morocco. Palaeogeography, Palaeoclimatology, Palaeoecology 37, 235–275.

Calvert, S.E., Pedersen, T.F., 1993. Geochemistry of oxic and anoxic sediments: implications for the geological record. Marine Geology 113, 67–88.

Calvert S.E., Pedersen T.F., 1996. Sedimentary geochemistry of manganese; implications for the environment of formation of manganiferous black shales. Economic Geology 91, 36–47.

Campbell S.N., and Abigail M.S., 1996. Stable oxygen and carbon isotope compositional fields for skeletal and diagenetic components in New Zealand Cenozoic nontropical carbonate sediments and limestones: A synthesis and review. New Zealand Journal of Geology and Geophysics 39, 93-107.

Canfield D.E., Teske A., 1996a. Late Proterozoic rise in atmospheric oxygen concentration inferred from phylogenetic and sulphurisotope studies. Nature 382. 127–132.

Canfield, D.E., Lyons, T.W., Raiswell, R., 1996b. A model for iron deposition to euxinic Black Sea sediments. American Journal of Science 296, 818–834.

Chen, J., Chen, Y., Liu, L., Ji, J., Balsam, W., Sun, Y., Lu, H., 2006. Zr/Rb ratio in the Chinese loess sequences and its implication for changes in the East Asian winter monsoon strength. Geochimica et Cosmochimica Acta 70, 1471–1482.

Choubert, G., Faure Muret, A., Hottinger, L., 1966. Apercu géologique du Bassin côtier de Tarfaya (Stratigraphie), in: Choubert, G., Faure Muret, A., Hottinger, L., Viotti, C. Lecointre, G. (Eds.), Le Bassin côtier de Tarfaya (Maroc Méridional). Notes et Mémoire Service Géologique du Maroc 1751I, pp. 7–106.

Choubert, G., Faure- Muret, A., Hottinger, L., 1972. La série stratigraphique de Tarfaya Maroc sud occidental, et le problème de la naissance de l´Atlantique. Notes et Mémoire du Service Géologique du Maroc 31, 29–40.

Clarke, L.J., Jenkyns, H.C., 1999. New oxygen isotope evidence for long-term Cretaceous climatic change in the Southern Hemisphere. Geology 27, 699–702.

Cranwell, P.A., 1977. Organic geochemistry of Cam Loch (Sutherland) sediments. Chemical Geology 20, 205–221.

Cushman, J.A., 1936. New genera and species of the families Verneuilinidae and Valvulinidae and of the subfamily Virgulinidae. Cushman Laboratory for Foraminiferal Research Special Publication 6, 1–71.

Davison, I., 2005. Central Atlantic margin basins of North West Africa: Geology and hydrocarbon potential (Morocco to Guinea). Journal of African Earth Sciences 43, 254–274.

De Lange, G.J., Van O, B., Pruysers, P.A., Middelburg, J.J., Castradori, D., Van Santvoort, P., Müller, P.J., Eggenkamp, H., Prahl, F.G., 1994. Possible early diagenetic alteration of palaeo proxies, in: Zahn, R., Pedersen, T.F., Kaminski, M.A., Labeyrie, L. (Eds.), Carbon Cycling in the Glacial Ocean. Constraints on the Ocean's Role in Global Change, NATO ASI Series, volume 17, New York, pp. 225 – 258.

den Dulk, M., Reichart, G.J., van Heyst, S., Zachariasse, W.J., Van der Zwaan., G.J., 2000. Benthic foraminifera as proxies of organic matter flux and bottom water oxygenation? A case history from the northern Arabian Sea. Palaeogeography, Palaeoclimatology, Palaeoecology 161, 337–359.

Dewey J.F., Pitman W.C., Ryan W.B.F., Bonin J., 1973. Plate tectonics and the evolution of the Alpine system. Geological Society of America Bulletin 84, 3137–3180.

Dickens, G.R., Owen, R.M., 1994. Late Mioceneearly Pliocene manganese redirection in the central Indian Ocean: Expansion of the intermediate water oxygen minimum zone. Paleoceanography 9, 169–181.

Diekmann, B., Hofmann, J., Henrich, R., Fütterer, D.K., Röhl, U., Wei, K-Y., 2008. Detrital sediment supply in the southern Okinawa Trough and its relation to sea-level and Kuroshio dynamics during the late Quaternary. Marine Geology 255, 83–95.

Dudley, W.C., Blackwelder, P.L., Brand, L.E., Duplessy, J.C., 1986. Stable isotope composition of coccoliths. Marine Micropaleontology 10, 1–8.

Dymond, J., Suess, E., Lyle, M., 1992. Barium in deep-sea sediment: A geochemical proxy for paleoproductivity. Paleoceanography 7, 163–181.

El Albani, A., Kuhnt, W., Luderer, F., Caron, M., 1999a. Palaeoenvironmental evolution of the Late Cretaceous sequence in the Tarfaya Basin (southwest of Morocco), in: Cameron, N.R., Bate, R.H., Clure, V.S. (Eds.), The Oil and Gas Habitats of the south Atlantic. Geological Society Special Publication 153, London, pp. 223–240.

El Albani, A., Vachard, D., Kuhnt, W., Chellai, H., 1999b. Signature of hydrodynamic activity caused by rapid sea level changes in pelagic organic-rich sediments, Tarfaya Basin (southern Morocco). Comptes Rendus de l´Académie des Sciences de Paris II 329, 397–404.

El Albani, A., Vachard, D., Kuhnt, W., Thurow, J., 2001. The role of diagenetic carbonate concretions in the preservation of the original sedimentary record. Sedimentology 48, 875-886.

El Khatib, J., Ruellan, E., El Foughali, A., El Morabet, A., 1995. Évolution de la marge atlantique sud-marocaine: bassin de Tarfaya-Laâyoune. Comptes Rendus de l´Académie des Sciences de Paris IIa 320, 117–124.

El Khatib, J., El Foughali, A., Ruellan, E., El Morabet, A., 1996. Évolution post-rift des secteurs NE et SW du bassin Tarfaya-Laâyoune. Mines, Géologie et Energie 55, 57–72.

El Mostaine, M., 1991. Evaluation du Potentiel Petrolier du Bassin de Tarfaya-Laayoune onshore. ONAREP Internal report 31526, 92 p.

Ellouz, N., Muller, C., Faure, J.L., 1998. Datations et Etude Geochemique des Forages BTS 1 et MO-7 du Bassin de Tarfaya – Maroc. Unpublished report of ifp, EAP and ONAREP, ONAREP 41016, 83 p.

Ennyu, A., Arthur, M.A., and Pagani, M., 2002. Fine-fraction carbonate stable isotopes as indicators of seasonal shallow mixed-layer paleohydrography. Marine Micropaleontology 46, 317–342.

Epstein, S., Buchsbaum, R., Lowenstam, H., Urey, H., 1953. Revised carbonate-water isotopic temperature scale. Geological Society of America Bulletin 64, 1315–1326.

Erbacher, J., Thurow, J., Littke, R., 1996. Evaluation patterns of radiolarian and organic matter variations: a new approach to identify sea-level changes in mid-Cretaceous pelagic environments. Geology 24, 499–502.

Espitalié, J., Deroo, G., Marquis, F., 1985. La pyrolyse Rock-Eval et ses applications. Revue de l`Institut Français du Petrole 40, 563–579.

Fenical, W., 1975. Halogenation in the Rhodophyta: areview. Journal of Phycology 11, 245–259.

Flögel, S., Beckmann, B., Hofmann, P., Bornemann, A., Westerhold, T., Norris, D.R., Dullo, C., Wagner, T., 2008. Evolution of tropical watersheds and continental hydrology during the Late Cretaceous greenhouse; impact on marine carbon burial and possible implications for the future. Earth Planetary Science letters 274, 1–13.

Flögel, S., K.; Wallmann, K., Kuhnt, W., 2011. Cool episodes in the Cretaceous - Exploring the effects of physical forcings on Antarctic snow accumulation. Earth and Planetary Science Letters 307, 279-288.

Fox, S.K., Jr., 1954. Cretaceous Foraminifera from the Greenhorn, Garlile, and Gody Formations, South Dakota, Wyoming. Geological Survey Professional Paper 254-E, 97–124.

François, R., 1987. A study of sulphur enrichment in the humic fraction of marine sediments during early diagenesis. Geochimica et Cosmochimica Acta 51, 17– 27.

Friedrich, O., Erbacher, J., 2006. Benthic foraminifera assemblages from Demerara Rise (ODP Leg 207, western tropical Atlantic): Possible evidence for a progressive opening of the Equatorial Atlantic Gateway. Cretaceous Research 27, 377–397.

Friedrich, O., Norris, R.D., Erbacher, J., 2012. Evolution of middle to Late Cretaceous oceans – A 55 my record of Earth's temperature and carbon cycle. Geology 40, 107–110.

Frizon de Lamotte, D.F., Leturmy, P., Missenard, Y., Khomsi, S., Ruiz, G., Saddiqi, O., Guillocheau, F., Michard, A., 2009. Mesozoic and Cenozoic vertical movements in the Atlas system (Algeria, Morocco, Tunisia): an overview. Tectonophysics 475, 9–28.

Gale, A.S., Montgomery, P., Kennedy, W.J., Hancock, J.M., Burnett, J.A., and McArthur, J.M., 1995. Definition and global correlation of the Santonian-Campanian boundary. Terra Nova, 7, 611-622.

Gautier, D.L., 1987. Isotopic composition of pyrite: relationship to organic matter type and iron availability in some North American Cretaceous shales. Chemical Geology 65, 293–303.

Gebhardt, H., Kuhnt, W., Holbourn, A., 2004. Foraminiferal response to sea level change, organic flux and oxygen deficiency in the Cenomanian of the Tarfaya Basin, Southern Morocco. Marine Micropaleontology 53, 133–157.

Geng, M., Duan, Z., 2010. Prediction of oxygen solubility inpure waters and brines up to high temperatures and pressures. Geochimica and Cosmochimica Acta 74, 5631–5640.

Gertsch, B., Adatte, T., Keller, G., Tantawy, A.A.A.M., Berner, Z., Mort, H.P., Fleitmann, D., 2010. Middle and late Cenomanian oceanic anoxic events in shallow and deeper shelf environments of western Morocco. Sedimentology 57, 1430–1462.

Gooday, A.J., 1994. The biology of deep-sea foraminifera: a review of some advances and their applications in paleoceanography. Palaios 9, 14–31.

Govin, A., Holzwarth, U., Heslop, D., Ford Keeling, L., Zabel, M., Mulitza, S., Collins, J.A., Chiessi, C.M., 2011. Distribution of major elements in Atlantic surface sediments (36°N–49°S): Imprint of terrigenous input and continental weathering. Geochemistry, Geophysics, Geosystems 13, 1525–2027.

Gradstein, M. F., Ogg, J., Schmitz, M., Ogg, G., 2012. The Geologic Time Scale 2012. 2-Volume, first ed. Elsevier, p.1176.

Gribble, G.W., 1998. Naturally Occurring Organohalogen Compounds. Accounts of Chemical Research 31, 141–152.

Hafid, M., Tari, G., Bouhadioui, D., El Moussaid, I., Echarfaoui, H., Ait Salem, A., Nahim, M., Dakki, M., 2008. Atlantic basins, in: Michard, A., Saddique, O., Chalouan, A., Frizon de Lamotte, D. (Eds.), The Atlas System, Continental Evolution, The Geology of Morocco, Springer, Heidelberg, pp 303–328.

Haq, B.U., Hardenbol, J., Vail, P.R., 1987. Chronology of fluctuating sea levels since the Triassic. Science 235, 1156–1167.

Haq, B.U., Hardenbol, J., Vail, P.R., 1988. Mesozoic and Cenozoic chronostratigraphy and cycles of sea-level change, in Wilgus, C.K., Hastings, B.S., Kendall, C.G.St.C., et al. (Eds.), Sea-Level Changes: An Integrated Approach. Economic Paleontologists and Mineralogists, Special Publication Society 42, p. 71–108.

Haq, B., 2014. Cretaceous eustaxy revisited. Global and Planetary Change 113, 44-58.

Hardenbol, J., Thierry, J., Farley, M.B., Jacquin, T., De Graciansky, P.C., Vail, P.R., 1998. Mesozoic and Cenozoic sequence chronostratigraphic framework of European basins, in: Graciansky, P.C., Hardenbol, J., Jacquin, T., Vail, P.R. (Eds.), Mesozoic and Cenozoic sequence stratigraphy of European basins. SEPM Special Publication 60, Tulsa, pp. 3–13.

Harvey, G.R., 1980. A study of the chemistry of iodine and bromine in marine sediments. Marine Chemistry 8, 327–332.

Haug, G.H., Hughen, K.A., Sigman, D.M., Peterson, L.C., Rohl, U., 2001. Southward migration of the Intertropical Convergence Zone through the Holocene. Science 293, 1304–1308.

Hay, W.W., 1995. Cretaceous paleoceanography. Geologica Carpathica 46, 257–266.

Heggie, D.T., Skyring, G.W., O'brien, G.W., Reimers, C., Herczeg, A., Moriarty, D.J.W., Burnett, W.C., Milnes, A.R., 1990. Organic carbon cycling and modern phosphorite formation on the East Australian continental margin, in: Notholt, A.J.G., Jarvis, I. (Eds), Phosphorite Research and Development. Geological Society Special Publication 52, London, pp. 87–117.

Helmke, J.P., Schulz, M., Bauch, H.A., 2002. Sediment-color record from the Northeast Atlantic reveals patterns of millennial-scale climate variability during the past 500,000 years. Quaternary Research 57, 49–57.

Hem, J.D., 1972. Chemical Factors that Influence the Availability of Iron and Manganese in Aqueous Systems. Geological Society of America Bulletin 83, 443–450.

Hennekam, R., de Lange, 2012. G., X-ray fluorescence core scanning of wet marine sediments: methods to improve quality and reproducibility of highresolution paleoenvironmental records. Limnology and Oceanography 10, 991–1003.

Hermanni, F., 1962. Zur Artfassung von Osangularien aus der Oberkreide (Foraminiferen). Neues Jahrbuch für Geologie und Paläontologie, Abhandlungen 115, 279–280.

Hetzel, A., Böttcher, M.E., Wortmann, U.G., Brumsack, H.J., 2009. Paleo-redox conditions during OAE 2 reflected in Demerara Rise sediment geochemistry (ODP Leg 207). Palaeogeography, Palaeoclimatology, Palaeoecology 273, 302–328.

Hofmann, P., Wagner, T., Beckmann, B., 2003. Millenial- to centennial-scale record of African climate variability and organic carbon accumulation in the Coniacian- Santonian eastern tropical Atlantic (Ocean Drilling Program Site 959, off Ivory Coast and Ghana). Geology 31, 135–138.

Hofmann, P., Wagner, T., 2011. ITCZ controls on Late Cretaceous black shale sedimentation in the tropical Atlantic Ocean. Paleoceanography 26, PA4223, doi:10.1029/2011PA002154.

Holbourn, A., Kuhnt, W., El Albani, A., Pletsch, T., Luderer, F., Wagner, T., 1999. Upper Cretaceous palaeoenvironments and benthonic foraminiferal assemblages of potential source rocks from the western African margin, Central Africa. In: Cameron, N.R., Bate, R.H., Clure, V.S. (Eds.) The Oil and Gas Habitats of the South Atlantic. Geological Society, London, Special Publications, 153, 195–222.

Holbourn, A., Kuhnt, W., Soeding, E., 2001. Atlantic paleobathymetry, paleoproductivity and paleocirculation in the late Albian: the benthic foraminiferal record. Palaeogeography, Palaeoclimatology, Palaeoecology 170, 171–196.

Huber, B.T., Norris, R.D., MacLeod, K.G., 2002. Deep-sea paleo-temperature record of extreme warmth during the Cretaceous. Geology 30, 123–126.

Hughen, K.A., Overpeck, J.T., Lehman, S.J., Kashgarian, M., Southon, J., Peterson, L.C., Alley, R., Sigman, D.M., 1998. Deglacial changes in ocean circulation from an extended radiocarbon calibration. Nature 391, 65–68.

Hunt, J.M., 1996. Petroleum Geochemistry and Geology. W.H. Freeman and Company, New York, pp. 743.

Jaccard, S.L., Haug, G.H., Sigman, D.M., Pedersen, T.F., Thierstein, H.R., Röhl, U., 2005. Glacial/Interglacial Changes in Subarctic North Pacific Stratification. Science 308, 1003–1006.

Jaeschke, A., Rühlemann, C., Arz, H., Heil, G., Lohmann, G., 2007. Coupling of millennial-scale changes in sea surface temperature and precipitation off northeastern Brazil with high-latitude climate shifts during the last glacial period. Paleoceanography 22, doi: 10.1029/2006PA001391.

James, N.P., Boreen, T.D., Bone, Y., Feary, D.A., 1994. Holocene carbonate sedimentation on the west Eucla Shelf, Great Australian Bight: a shaved shelf. Sedimentary Geology 90, 161–177.

Jansen, J.H.F., Van Der Gaast, S.J., Koster, B., Vaars, A.J., 1998. CORTEX, a shipboard XRF-scanner for element analyses in split sediment cores. Marine Geology 151, 143–153.

Jarvis, J., Fish, P.,Garwood, T., 1999. Morocco`s Tarfaya deepwater prospects encouraging. Oil and Gas Journal 16, 90–94.

Jarvis, I., Gale, A., Jenkyns, H.C., Pearce, M.A., 2006. Secular variation in Late Cretaceous carbon isotope: a new $\delta^{13}C$ carbonate reference curve for the Cenomanian- Campanian (99.6-70.6 Ma). Geological Magazine 143, 561–608.

Jenkins, R., De Vries, J.L., 1970. Practical X-Ray Spectrometry. 2nd edition. Macmillan, London. Chapter 5, 90–107.

Jenkins, R., Gould, R.W., Gedcke, D., 1995. Quantitative X-Ray Spectrometry. Second Edition, Marcel Dekker, Inc: New York, 439-460.

Jenkyns, H. C., 1980. Cretaceous anoxic events: from continents to oceans. Geological Society of London 137, 171–188.

Johnson, K.S., Berelson, W.M., Coale, K.H., Coley, T.L., Elrod, V.A., Fairey, W.R., Iams, H.D., Kilgore, T.E., Nowicki, J.L., 1992. Manganese Flux from Continental Margin Sediments in a Transect Through the Oxygen Minimum. Science 257, 1242–1245.

Jones, E.J.W., Bigg, G.R., Handoh, I.C., Spathopoulos, F., 2007. Distribution of deep- sea black shales of Cretaceous age in the eastern Equatorial Atlantic from seismic profiling. Paleogeography, Paleoclimate 248, 233–246.

Keller, G., Adatte, T., Berner, Z., Chellai, E.H., Stüben, D., 2008. Oceanic events and biotic effects of the Cenomanian-Turonian anoxic event, Tarfaya Basin, Morocco. Cretaceous Research 29, 976–994.

Kolonic, S., Sinninghe Damsté, J.S., Böttcher, M.E., Kuypers, M.M.M., Kuhnt, W., Beckmann, B., Scheeder, G., Wagner, T., 2002. Geochemical Characterization of Cenomanian/Turonian Black Shales from the Tarfaya Basin (SW Morocco). Journal of Petroleum Geology 25, 325–350.

Kolonic, S., Wagner, T., Firster, A., Sinninghe Damsté, J.S., Walsworth-Bell, B., Erba, E., Turgeon, S., Brumsack, H.J., Chellai, E.H., Tsikos, H., Kuhnt, W., Kuypers, M.M.M., 2005. Black shale deposition on the northwest African Shelf during the Cenomanian-Turonian oceanic anoxic event: Climate coupling and organic carbon burial. Paleoceanography 20, doi:10.1029/2003PA000950.

Kominz, M.A., 1984. Oceanic ridge volumes and sea level change an error analysis, in: Schlee, J. (Ed.), Interregional Unconformities and Hydrocarbon Accumulation. American Association of Petroleum Geologists Memoir 36, Tulsa, pp. 109–127.

Kominz, M. A., Browning, J. V., Miller, K. G., Sugarman, P. J., Mizintsevaw, S., Scotese, C. R., 2008. Late Cretaceous to Miocene sea-level estimates from the New Jersey and Delaware coastal plain coreholes: an error analysis. Basin Research 20, 211–226.

Kroon, D., Norris, R.D., Klaus, A., et al., 1998. Proceedings of the Ocean Drilling Program, Initial Reports, 17lB. Ocean Drilling Program, College Station, TX.

Kuhnt, W., Thurow, J., Wiedmann, J., Herbin, J.P., 1986. Oceanic anoxic conditions around the Cenomanian/Turonian Boundary and the response of the biota, in: Degens, E.T., Meyers, P.A., Brassell, S.C. (Eds.), Biogeochemistry of Black Shales, Mitteilungen aus dem Geologischen Institut der Universität Hamburg 60, Hamburg, pp. 205–246.

Kuhnt, W., Herbin, J.P., Thurow, J., Wiedmann, J., 1990. Distribution of Cenomanian-Turonian Organic Facies in the Western Mediterranean and along the Adjacent Atlantic Margin, in: Huc, A.Y. (Ed.), Deposition of Organic Facies. American Association of Petroleum Geologists Studies in Geology 30, Tulsa, pp. 133–160.

Kuhnt, W., Wiedmann, J., 1995. Cenomanian-Turonian source rocks: paleobiogeography and paleoenvironmental aspects, in: Huc, A.Y. (Ed.), Paleogeography, Paleoclimate and source Rocks. American Association of Petroleum Geologists Studies in Geology 40, Tulsa, pp. 213–232.

Kuhnt, W., Nederbragt, A., Leine, L., 1997. Cyclicity of Cenomanian-Turonian organic-carbon-rich sediments in the Tarfaya Atlantic Coastal Basin (Morocco). Cretaceous Research 18, 587–601.

Kuhnt, W., Chellai, H., Holbourn, A., Luderer, F., Thurow, J., Wagner, T., El Albani, A., Beckmann, B., Herbin, J. P., Kawamura, H., Kolonic, S., Nederbragt, S., Street, C., Ravilious, K., 2001. Morocco Basin's sedimentary record may provide correlations for Cretaceous paleoceanographic events worldwide. Eos, 82, 33, 361–368.

Kuhnt, W., Luderer, F., Nederbragt, S., Thurow, J., Wagner, T., 2004. Orbital-scale record of the late Cenomanian-Turonian oceanic anoxic event (OAE-2) in the Tarfaya Basin (Morocco). International Journal of Earth Sciences 94, 147–159.

Kuhnt, W., Hess, S., Holbourn, A., Paulsen, H., Salomon, B., 2005. The impact of the 1991 Mt. Pinatubo eruption on deep-sea foraminiferal communities: A model for the Cretaceous-Tertiary (K/T) boundary?. Palaeogeography, Palaeoclimatology, Palaeoecology 224, 83–107.

Kuhnt, W., Holbourn, A., Gale, A., Chellai, E.H., Kennedy, W.J., 2009. Cenomanian sequence stratigraphy and sea-level fluctuations in the Tarfaya Basin (SW Morocco). Bulletin of the Geological Society of America 121, 11–12.

Lehman, U., 1966. Dimorphismus bei Ammoniten der Ahrensburger Lias Geschibe.- Ibidem, 40, 1/2, 26-55, Stuttgart.

Leine, L., 1986. Geology of the Tarfaya oil shale deposit, Morocco. Geologie en Mijnbouw 65, 57–74.

Leventhal, J.S., 1983. An interpretation of carbon and sulfur relationships in Black Sea sediments as indicators of environments of deposition. Geochimica et Cosmochimica Acta 47, 133–37.

Lewan, M.D., Maynard, J.B., 1982. Factors controlling enrichment of vanadium and nickel in the bitumen of organic sedimentary rocks. Geochimica et Cosmochimica Acta 46, 2547–2560.

Li, X., Jenkyns, H.C., Wang, C., Hu, X., Chen, X., Wei, Y., Huang, Y., Cui, J., 2006. Upper Cretaceous carbon-and oxygen-isotope stratigraphy of hemipelagic carbonate facies from southern Tibet, China. Journal of the Geological Society 163, 375–382.

Littke, R., Baker, D.R., Leythaeuser, D., Rullkötter, J., 1991. Keys to the depositional history of the Posidonia Shale (Toarcian) in the Hils Syncline, northern Germany. Geological Society Special Publications 58, 311–333.

Littke, R., Sachsenhofer, R.F., 1994. Organic petrology of deep sea sediments: a compilation of results from the Ocean Drilling Program and the Deep Sea Drilling Project. Energy and Fuels 8, 1498–1512.

Littke, R., Lückge A., Wilkes, H., 1998. Organic matter in Neogene sediments of the southern Canary Channel, Canary Islands (Sites 955 and 956), in: Weaver, P.P.E., Schmincke, H.-U., Firth, J.V., Duffield, W. (Eds.), Proceedings of the Ocean Drilling Program. scientific Results 157, pp. 361–372.

Liu, L., Chen, J., Ji, J., Chen, Y., 2004. Comparison of paleoclimatic change from Zr/Rb ratios in Chinese loess with marine isotope records over the 2.6-1.2 Ma BP interval. Geophysical Research Letters 31, 4–7.

Locklair, R.E., Sageman, B.B., 2008. Cyclostratigraphy of the Upper Cretaceous Niobrara Formation, western interior, USA: a Coniacian–Santonian orbital timescale. Earth and Planetary Science Letters 269, 540–553.

Locklair, R., Sageman, B., Lerman, A., 2011. Marine carbon burial flux and the carbon isotope record of Late Cretaceous (Coniacian–Santonian) Oceanic Anoxic Event III. Sedimentary Geology 235, 38–49.

Löwemark, L., Jakobsson, M., Mörth, M., Backman, J., 2008. Arctic Ocean manganese contents and sediment colour cycles. Polar Research 27, 105–113.

Löwemark, L., Chen, H.F., Yang, T.N., Kylander, M., Yu, E.F., Hsu, Y.W., Lee, T.Q., Song, S.R., Jarvis, S., 2011. Normalizing XRF-scanner data: A cautionary note on the interpretation of high-resolution records from organic-rich lakes. Journal of Asian Earth Sciences 40, 1250–1256.

Lückge, A., Boussafir M., Lallier-Vergès, Littke, R., 1996. Comparative study of organic matter preservation in immature sediments along the continental margins of Peru and Oman. Organic Geochemistry 24, 437–451.

Lückge, A., Horsfield, B., Littke, R., Scheeder, G., 2002. Organic matter preservation and sulfur uptake in sediments from the continental margin off Pakistan. Organic Geochemistry 33, 477–488.

Lüning, S., Kolonic, S., Belhadj, E.M., Belhadj, Z., Cota, L., Baric, G., Wagner, T., 2004. Integrated depositional model for the Cenomanian-Turonian organic-rich strata in North Africa. Earth-Science Reviews 64, 51–117.

Ly, A., Kuhnt, W., 1994. Late Cretaceous benthic foraminiferal assemblages of the Casamance Shelf (Senegal, NW Africa)-indication of a late Cretaceous oxygen minimum zone. Revue de Micropaléontologie 37, 49–74.

Ma, C., Meyers, S.R., Sageman, B.B., Singer, B.S., Jicha, B.R., 2014. Testing the astronomical time scale for oceanic anoxic event 2, and its extension into Cenomanian strata of the Western Interior Basin (USA). Geological Society of America Bulletin, doi:10.1130/B30922.1.

MacLeod, K.G., 2006. Data report: stable isotopic ratios in bulk carbonate from upper Campanian and Maastrichtian samples (Demerara Rise, western tropical North Atlantic), in: Mosher, D.C., Erbacher, J., and Malone, M.J., (Eds.), ODP Scientific Results, v. 207, College Station, TX (Ocean Drilling Program), 1–9. doi:10.2973/odp.proc.sr.207.110.2006.

Malcolm, S.J., Price, N.B., 1984. The behaviour of iodine and bromine in estuarine surface sediments. Marine Chemistry 15, 263–271.

Martin, J.M., Whitfield, M., 1983. The significance of the river input of chemical elements to the oceans, in: Wong, C.S., Boyle, E., Binland, K.W., Burton, J.D., Goldberg, E.D. (Eds), Trace Metals in Sea Water. Plenum Press, New York, pp. 265–296.

Matthews, R.K., 1984. Dynamic Stratigraphy. 2nd Edition. Prentice-Hall, Englewood Cliffs, New Jersey, p. 489.

Mayer, L.M., Macko, S.A., Mook, W.H., Murray, S.M., 1981. The distribution of bromine in coastal sediments and its use as a source indicator for organic matter. Organic Geochemistry 3, 37–42.

Meyers , P.A., Bernasconi, S.M., Forster, A., 2006. Origins and accumulation of organic matter in expanded Albian to Santonian black shale sequences on the Demerara Rise, South American margin. Organic Geochemistry 37, 1816–1830.

Mayer, L.M., Schick, L.L., Allison, M.A., Ruttenberg, K.C., Bentley, S.J., 2007. Marine vs. terrigenous organic matter in Louisiana coastal sediments: The uses of bromine:organic carbon ratios. Marine Chemistry 107, 244–254.

Miall, A.D., 2009. Correlation of Sequences and the Global Eustasy Paradigm: A Review of Current Data. AAPG Search and Discovery Article #90171 CSPG/CSEG/CWLS GeoConvention 2009, Calgary, Alberta, Canada, May 4-8, 2009.

Michard, A., Saddiqi, O., Chalouan, A., Frizon de Lamotte, D., 2008. Continental Evolution: The Geology of Morocco. Structure, Stratigraphy, and Tectonics of the Africa-Atlantic-Mediterranean Triple Junction. Lecture Notes in Earth Sciences, Springer-Verlag, Berlin, Heidelberg, 424 pp.

Miller, J.R., Russell, G.L., 1992. The impact of global warming on river runoff. Journal of Geophysical Research 97, 2757–2764.

Miller, K.G., Sugarman, P.J., Browning, J.V., Kominz, M.A., Hernández, J.C., Olsson, R.K., Wright, J.D., Feigenson, M.D., Van Sickel, W., 2003. Late Cretaceous chronology of large, rapid sea level changes: Glacioeustasy during the greenhouse world. Geology 31, 585–588.

Miller, K.G., Sugarman, P. J., Browning, J. V., Kominz, M. A., Olsson, R. K., Feigenson, M. D., Hernández, J. C., 2004. Upper Cretaceous sequences and sea-level history, New Jersey coastal plain. Geological Society of America Bulletin 116, 368–393.

Miller, K.G., Wright, J.D., Browning, J.V., 2005. Visions of ice sheets in a greenhouse world. Marine Geology 217, 215–231.

Milliman, J.D., Summerhayes, C.P., Barretto, H.T., 1975. Quaternary Sedimentation on the Amazon Continental Margin: A Model. Geological Society of America Bulletin 86, 610–614.

Milliman, J.D., Meade, R.H., 1983. World-wide delivery of river sediment to the oceans. Journal of Geology 91, 1–21.

Mizintseva, S. F., Browning, J. V., Miller, K. G., Olsson, R. K., Wright, J.D., 2009. Integrated Late Santonian-Early Campanian sequence stratigraphy, New Jersey Coastal Plain: Implications for global sea-level studies. Stratigraphy 6, 45–60.

Morabet, A. M., Bouchta, R., Jabour, H. 1998. An overview of the petroleum systems of Morocco, in: Mac- Gregor, D. S., Moody, R. T. J., Clark-Lowes, D. D. (Eds.), 1998. Petroleum Geology of North Africa. Geological Society, London, Special Publication 132, pp. 283–296.

Mort, H.P., Adatte, T., Foellmi, K.B., Keller, G., Steinmann, P., Matera, V., Berner, Z. Stueben, D., 2007. Phosphorus and the roles of productivity and nutrient recycling during Oceanic Event 2. Geology 35, 483–486.

Mort, H.P., Adatte, T., Keller, G., Bartels, D., Follmi, K.B., Steinmann, P., Berner, Z. Chellai, E.H., 2008. Organic carbon deposition and phosphorus accumulation during Oceanic Anoxic Event 2 in Tarfaya, Morocco. Cretaceous Research 29, 1008–1023.

Mulitza, S., Prange, M., Stuut, J.B.W., Zabel, M., von Dobeneck, T., Itambi, A.C., Nizou, J., Schulz, M., Wefer, G., 2008. Sahel megadroughts triggered by glacial slowdowns of Atlantic meridional overturning. Paleoceanography 23, doi: 10.1029/2008PA001637.

Müller, R. D., Sdrolias, M., Gaina, C., Steinberger, B., Heine, C., 2008. Long-Term Sea-Level Fluctuations Driven by Ocean Basin Dynamics. American Association for the Advancement of Science 319, 1357–1362.

Nederbragt, A.J., Dunbar, R.B., Osborn, A.T., Palmer, A., Thurow, J.W., Wagner, T., 2006. Sediment colour analysis from digital images and correlation with sediment composition, in: Rothwell, R.G. (Ed.), New Techniques 01 Sediment Core Analysis. Geological Society, London, Special Publications, 267, 113–128.

Niebuhr, B., 2005. Geochemistry and time-series analyses of orbitally forced Upper Cretaceous marl–limestone rhythmites (Lehrte West Syncline, northern Germany). Geological Magazine 142, 31–55.

Nzoussi-Mbassani, P., Khamli, N., Disnar, J.R., Laggoun-Défarge, F., Boussafir, M., 2005. Cenomanian–Turonian organic sedimentation in North-West Africa: A comparison between the Tarfaya (Morocco) and Senegal basins. Sedimentary Geology 177, 271–295.

Ogg, J.G., Agterberg, F.P., Gradstein, F.M., 2004. The Cretaceous Period, in: Gradstein, F.M., Agterberg, F.P., Smith, A.G. (Eds.), A Geological Time Scale 2004. Cambridge University Press, Cambridge, pp. 344–383.

Olsen, P.E., 1999. Giant lava flows, mass extinctions, and mantle plumes, Science 284, 604–605.

Passier, H.F., Bosch, H., Lourens, L.J., Böttcher, M.E., Leenders, A., Damste, J.S.S., de Lange, G.J., de Leeuw, J.W., 1999. Sulfidic Mediterranean surface waters during Pliocene sapropel formation. Nature 397, 146–149.

Paytan, A., McLaughlin, K., 2007. The oceanic phosphorus cycle. Chemical Review 107, 563–576.

Perner. J., 1892. Foraminifery Ceskeh Cenomanu, Trida 2. Ceska Akademie Cisare Frantiska Josefa, Paleontographica Bohemiae, Praha.

Peters, K.E., 1986. Guidelines for evaluating petroleum source rocks using programmed pyrolysis. The American Association of Petroleum Geologists Bulletin 70, 318–329.

Peters, K.E., Walters, C.C., Moldowan, J.M., 2005. The Biomarker Guide, Volume 2 Biomarkers and Isotopes in Petroleum Exploration and Earth History, 2nd ed., Cambridge University Press, Cambridge.

Peterson, L.C., Haug, G.H., Hughen, K.A., Rohl, U., 2000. Rapid changes in the hydrologic cycle of the tropical Atlantic during the last glacial. Science 290, 1947–1951.

Peterson, L.C., Haug, G.H., Hughen, K.A., Rohl, U., 2000. Rapid changes in the hydrologic cycle of the tropical Atlantic during the last glacial. Science 290, 1947–1951.

Petters, S.W., Ekweozor, C.M., 1982. Petroleum Geology of Benue Trough and Southeastern Chad Basin, Nigeria. AAPG Bulletin, 66, 1141–1149.

Pierau, R., Hanebuth, T.J.J., Krastel, S., Henrich R., 2010. Late Quaternary climatic events and sea-level changes recorded by turbidite activity, Dakar Canyon, NW Africa. Quaternary Research 73, 385–392.

Pierrehumbert, R.T. 2002. The Hydrologic Cycle in Deep Time Climate Problems. Nature 419, 191–198.

Prange, A., Kremling, K., 1985. Distribution of dissolved molybdenum, uranium and vanadium in Baltic Sea waters. Marine Chemistry 16, 259–274.

Price, N.B., Calvert, S.E., Jones, P.G.W., 1970. The distribution of iodine and bromine in the sediments of the South Western Barents Sea. Journal of Marine Research 28, 22–34.

Rachold, V., Brumsack, H.J., 2001. Inorganic geochemistry of Albian sediments from the Lower Saxony basin, NW German: paleoenvironmental constraints and orbital cycles. Palaeogeography, Palaeoclimatology, Palaeoecology 174, 123–144 .

Raiswell, R., Canfield, D. E., 1998. Sources of iron for pyrite formation. American Journal of Science 298, 219–245.

Rank, U., Von Rad, U., Wissman, G., 1982. Stratigraphy, facies and tectonic development of the On- and Offshore Aaiun-Tarfaya Basin, in: von Rad, U., Hinz, K., Sarnthein, M., Seibold, E. (Eds.), Geology of the Northwest African Continental Margin. Springer, Heidelberg, pp. 87–105.

Ratschiller, L.K., 1970. Lithostratigraphy of the northern Spanish Sahara. Memorie Museo Tridentino Sci Trento 18, 1–18.

Rea, D.K., 1994. The paleoclimatic record provided by eolian deposition in the deep sea: The geologic history of wind. Reviews of Geophysics 32, 159–195.

Reimers, C.E., Suess, E., 1983. Spatial and temporal patterns of organic matter accumulation on the Peru continental margin, in: Thiede, J. and Suess, E. (Eds.), Coastal Upwelling. Part B: Sedimentary records of ancient coastal upwelling, New York, Plenum Press, pp. 311-346.

Renard, M., Rafélis de, M., Emmanuel, L., Moullade, M., Masse, J.P., Kuhnt, W., Bergen, J.A., Tronchetti, G., 2005. Early Aptian $\delta^{13}C$ and manganese anomalies from the historical Cassis-La Bédoule stratotype sections (S.E. France):

relationship with a methane hydrate dissociation event and stratigraphic implications. Notebooks on Geology, CG2005_A04.

Reuss, A.E., 1844. Geognostische Skizzen aus Böhmen. II-Die Kreidgebilde des Westlichen Böhmens, ein monographischer Versuch, Prague: C. W. Medau, p.214.

Reuss, A.E., 1863. Die Foraminiferen des norddeutschen Hils und Gault. Sitzungberichte der Mathematische-Naturwissenschaftliche Klasse der Kayserliche Akademie der Wissenschaften in Wien 46, 5–100.

Rey, O., Simo, J.A., Lorente, M.A., 2004. A record of long- and short- term environmental and climatic change during OAE3: La Luna Formation, Late Cretaceous (Santonian- early Campanian), Venezuela. Sedimentary Geology 170, 85–105.

Richter, T.O., Van Der Gaast, S., Koster, B., Vaars, A., Gieles, R., De Stigter, H.O., De Haas, H., Van Weering, T.C.E., 2006. The Avaatech XRF Core Scanner: technical description and applications to NE Atlantic sediments, in: Rothwell, R.G. (Ed.), New Techniques in Sediment Core Analysis. Geological Society Special Publication 267, London, pp. 39–50.

Robaszynski, F., Caron, M., 1995. Foraminifères planctoniques du Crétacé: commentaire de la zonation Europe-Méditerranée. Bulletin de la Société Géologique de France 166, 681–692.

Rothwell, R.G., Hoogakker, B., Thomson, J., Croudace, I.W., Frenz. M., 2006. Turbidite emplacement on the southern Balearic Abyssal Plain (western Mediterranean Sea) during Marine Isotope Stages 1–3: an application of ITRAX XRF scanning of sediment cores to lithostratigraphic analysis. In R.G. Rothwell (ed.), New techniques in sediment core analysis. Geological Society Special Publication, p. 39-50.

Ruiz, G., Sebti, S., Negro, F., Saddiqi, O., Frizon de Lamotte, D., Stockli, D., Foeken, J., Stuart, F., Barbarand, J., Schaer, J.P., 2010. From central Atlantic continental rift to Neogene uplift – western Anti-Atlas (Morocco). Terra Nova 23, 35–41.

Rusk, D.C., 2001. Lybia: petroleum potential of the underexplored basin centers- a twenty- first- century challenge, in: Downey, M.W., Threet, J.C., Morgan, W.A. (Eds.), Petroleum provinces of the twenty-First-Century. AAPG Memoirs 74, pp. 429–452.

Ruttenberg, K.C., 1993. Reassessment of the oceanic residence time of phosphorus. Chemical Geology 104, 405–409.

Saager, P.M., De Baar, H.J.W., Burkill, P.H., 1989. Manganese and iron in Indian Ocean waters. Geochimica et Cosmochimica Acta 53, 2259– 2267.

Sachse, V.F., Littke, R., Heim, S., Kluth, O., Schober, J., Boutib, L., Jabour, H., Perssen, F., Sindern, S., 2011. Petroleum source rocks of the Tarfaya Basin and adjacent areas, Morocco. Organic Geochemistry 42, 209–227.

Sachse V.F., Littke, R., Jabour, H., Schümann, T., Kluth, O., 2012. Late Cretaceous (Late Turonian, Coniacian and Santonian) petroleum source rocks as part of an OAE, Tarfaya Basin, Morocco. Marine and Petroleum Geology 29, 35–49.

Sageman, B.B., Meyers, S.R., Arthur, M.A., 2006. Orbital time scale and new C-isotope record for Cenomanian-Turonian boundary stratotype. Geology 34, 125–128.

Sahagian, D., Pinous, O., Olferiev, A., Zakaharov, V., and Beisel, A., 1996. Eustatic curve for the middle Jurassic-Cretaceous based on Russian platform and Siberian stratigraphy: Zonal resolution. American Association of Petroleum Geologists Bulletin 80, 1433–1458.

Scalan, R.S, Smith, J.E., 1970. An improved measure of the odd-to-even predominance in the normal alkanes of sediment extracts and petroleum. Geochimica et Cosmochimica Acta 34, 611–620.

Schenau, S.J., Reichart, G.J., De Lange, G.J., 2002. Oxygen minimum zone controlled Mn redistribution in Arabian Sea sediments during the late Quaternary. Paleoceanography 17, doi: 10.1029/2000PA000621.

Schlanger, S.O., Jenkyns, H.C., 1976. Cretaceous anoxic events: Causes and consequences. Geologie en Mijnbouw 55, 179–184.

Scholle, RA., Arthur, M.A., 1980. Carbon isotope fluctuations in Cretaceous pelagic limestones: potential stratigraphic and petroleum exploration tool. American Association of Petroleum Geologists bulltian Bulletin 64, 67–87.

Schütz, L., Rahn K.A., 1982. Trace-element concentrations in erodible soils. Atmospheric Environment 16, 171–176.

Scopelliti, G., Bellanca, A., Neri, R., Baudin, F., Coccioni, R., 2006. Comparative high-resolution chemostratigraphy of the Bonarelli Level from the reference Bottaccione section (Umbria–Marche Apennines) and from an equivalent section in NW Sicily: Consistent and contrasting responses to the OAE2. Chemical Geology 228, 266 – 285.

Shackleton, N.J., Kennett, J.P., 1975. Paleotemperature history of the Cenozoic and the initiation of Antarctic glaciation: Oxygen and carbon isotope analyses in DSDP Sites 277, 279 and 281, in, Kennett, J.P., Houtz, R.E., et al., Init. Repts. DSDP, 29. Washington (U.S. Govt. Pr int ing Office), 801–808.

Shanmungam, G., 1985. Significance of coniferous rain forests and related organic matter in generating commercial quantities of oil, Gippsland Basin, Australia. The American Association of Petroleum Geologists Bulletin 69, 1241–1254.

Shannon, C.E., Weaver, W., 1949. The Mathematical Theory of Communication. University of Illinois Press, 1-125.

Shaw, T.J., Gieskes, J.M., Jahnke, R.A., 1990. Early diagenesis in differing depositional environments: the response of transition metals in pore water. Geochimica et Cosmochimica Acta 54, 1233–1246.

Shiller, A.M., 1982. The geochemistry of particulate major elements in Santa Barbara Basin and observations on the calcium carbonate-carbon dioxide system in the ocean. PhD thesis, pp. 197, University of California, San Diego.

Spaulding, S., 1991. Neogene nannofossi biostratigraphy of Sites 723 through 730, Oman continental margin; northwestern Arabian Sea, in: Prell, W.L., Niitsuma, N., et al. (Eds.), proceedings of the Ocean Drilling Program, Scientific Results 117, 5–36.

Stoll, H.M., Schrag, D., 2000. High-resolution stable isotope records from the Upper Cretaceous rocks of Italy and Spain: Glacial episodes in a greenhouse planet?. Geological Society of America Bulletin 112, 308–319.

Taylor, G.H., Teichmüller, M., Davis, A., Diessel, C.F.K., Littke, R., Robert, P., 1998. Organic Petrology. Borntraeger, Stuttgart.

Ten Haven H.L., De Leeuw, J.W., Schenck, P.A., Klaver, G.T., 1987. Geochemistry of Mediterranean sediments. Bromine/organic carbon and uranium/organic carbon ratios as indicators for different sources of input and post-depositionai oxidation, respectively. Organic Geochemistry 13, 255–261.

Thomson, J., Croudace, I.W., Rothwell, R.G., 2006. A geochemical application of the ITRAX scanner to a sediment core containing eastern Mediterranean sapropel units, in: Rothwell, R.G. (Ed.), New Techniques in Sediment Core Analysis. Geological Society, London, Special Publications, 267, pp. 65–77.

Thurow, J., Brumsack, H.J., Littke, R., Meyers, P., Rullkötter, J., 1992. The Cenomanian/Turonian boundary event in the Indian Ocean – a key to understand the global picture. Geophysical Monograph 70, 253–273.

Tisserand, A., Malaizé, B., Jullien, E., Zaragosi, S., Charlier, K., Grousset F., 2009. African monsoon enhancement during the penultimate glacial period (MIS 6.5-170 ka) and its atmospheric impact. Paleoceanography 24, doi: 10.1029/2008PA001630.

Tjallingii, R., Stattegger, K., Wetzel, A., Van Phach P., 2010. Infilling and flooding of the Mekong River incised valley during deglacial sea-level rise. Quaternary Science Reviews 29, 1432–1444.

Trabucho Alexandre, J., Tuenter, E., Henstra, G.A., van der Zwan, K.J., van de Wal, R.S.W., Dijkstra, H.A., de Boer, P.L., 2010. The mid-Cretaceous North Atlantic nutrient trap: Black shales and OAEs. Paleoceanography 25, PA4201, doi:10.1029/2010PA001925.

Tribovillard, N., Algeo, T.J., Lyons, T., Riboulleau, A., 2006. Trace metals as paleoredox and paleoproductivity proxies: an update. Chemical Geology 232, 12–32.

Upstill-Goddard, R.C., Elderfield, H., 1988. The role of diagenesis in the estuarine budgets of iodine and bromine. Continental Shelf Research 8, 405–430.

Vail, P.R., MItchum, J.R.M., Thompson, S., 1977. Global cycles of relative changes of sea level, in: Vail, P.R. et al. (Eds.), Seismic Stratigraphy and global changes of sea level. American Association of Petroleum Geology Memoir 26, 83–98.

Van Bentum, E.C., Reichart, G.-J., Forster, A., Sinninghe Damste, J.S., 2012. Latitudinal differences in the amplitude of the OAE-2 carbon isotopic excursion: pCO2 and paleo productivity. Biogeosciences 9, 717–731.

Van Cappellen, P., Ingall, E.D., 1994. Benthic phosphorus regeneration, net primary production, and ocean anoxia: A model of the coupled marine biogeochemical cycles of carbon and phosphorus. Paleoceanography 9, 677–692.

Van Cappellen, P., Ingall, E.D., 1996. Redox stabilizations of the atmosphere and oceans by phosphorus-limited marine productivity. Science 271, 493–496.

van der Zwaan, G.J., Duijnstee, I.A.P., den Dulk, M., Ernst, S.R., Jannink, N.T., Kouwenhoven, T.J., 1999. Benthic foraminifers: proxies or problems? A review of paleocological concepts. Earth-Science Reviews 46, 213–236.

Van Pée, K.H., 1996. Biosynthesis of halogenated metabolites by bacteria. Annual Review of Microbiology 50. 375–399.

Van Sickel, W.A, Kominz, M.A., Miller, K.G., Browning, J.V., 2004. Late Cretaceous and Cenozoic sea-level estimates backstripping analysis of borehole data, onshore New Jersey. Basin research 16, 451–465.

Wagner, T., 2002. Late Cretaceous to early Quaternary organic sedimentation in the eastern equatorial Atlantic. Palaeogeography, Palaeoclimatology, Palaeoecology 179, 113–147.

Wagner, T., Pletsch, T., 1999. Tectono- sedimentary controls on Cretaceous black shale deposition along the opening Equatorial Atlanttic Gateway (ODP Leg 159), in: Cameron, N.R., Bate, R.H., Clure, V.S. (Eds.), The Oil and Gas Habitats of the South Atlantic. Geological Society, Special Publication 153, London, pp. 241–265.

Wagner, T., Sinninghe Damsté, J., Hofmann P., Beckmann, B., 2004. Euxinia and primary production in Late Cretaceous eastern equatorial Atlantic surface waters fostered orbitally driven formation of marine black shales. Paleoceanography 19, doi: 10.1029/2003PA000898.

Wagreich, M., 2009. Coniacian- santonian oceanic red beds and their link to Oceanic Anoxic Event 3, in: Hu, X., Wang, C., Scott, R.W., Wagreich, M., Jansa, L. (Eds.), Cretaceous Oceanic Red Beds: Stratigraphy, Composition, Origins, and Paleoceanographic and Paleoclimatic Significance. SEPM Special Publications 91, pp. 235–242.

Wagreich, M., 2012a. " OAE 3"–a low-to mid-latitude Atlantic oceanic event during the Coniacian-Santonian. Climate of the Past Discussions 8, 1209–1227.

Wagreich, M., 2012b. “OAE 3” regional Atlantic organic carbon burial during the Coniacian- Santonian. Climate of the Past 8, 1447–1455.

Weltje, G.J., Tjallingii, R., 2008. Calibration of XRF core scanners for quantitative geochemical logging of sediment cores: Theory and application. Earth and Planetary Science Letters 274, 423–438.

Wendler, I., 2013. A critical evaluation of carbon isotope stratigraphy and biostratigraphic implications for Late Cretaceous global correlation. Earth-Science Reviews 126, 116–146.

Wendler, I., Wendler, J., Gräfe, K.-U., Lehmann, J., Willems, H., 2009. Turonian to Santonian carbon isotope data from the Tethys Himalaya, southern Tibet. Cretaceous Research 30, 961–979.

Wenke, A., Zühlke, R., Jabour, H., Kluth, O., 2011. High-resolution sequence stratigraphy in basin reconnaissance: example from the Tarfaya Basin, Morocco. First break 29, 85–96.

Werne, J.P., Hollander, D.J., Lyons, T.W., Sinninghe Damsté, J.S., 2004. Organic sulfur biogeochemistry: recent advances and future research directions, in: Amend, J., Edwards, K., Lyons, T. (Eds.), Sulfur Biogeochemistry: Past and Present. Geological Society of America, Special Paper 379, pp. 135–150.

Wiedmann, J., Butt, A., Einsele, G., 1978. Vergleich von marokkanischen Kreide-Küstenaufschlüssen und Tiefseebohrungen (DSDP): Stratigraphie, Paläoenvironment und Subsidenz an einem passiven Kontinentalrand. Geologische Rundschau 67, 454–508.

Wiedmann, J., Butt, A., Einsele, G., 1982. Cretaceous Stratigraphy, Environment, and Subsidence History at the Moroccan Continental Margin, in: von Rad, U., Hinz, K., Sarnthein, M., Seibold, E. (Eds.), Geology of the Northwest African Continental Margin. Springer, Berlin, pp. 366–395.

Wiedmann, J., Kuhnt, W., 1996. Biostratigraphy of Cenomanin/Turonian organic carbon-rich sediments in the Tarfaya Atlantic coastal basin (Morocco). Berichte-Reports, Geologisch-Paläontologisches Institut Kiel 76, 195–200.

Wonders, A.A.H., 1980. Middle and Late Cretaceous planktonic foraminifera of the Western Mediterranean area. Bulletin of Utrecht Micropaleontology 24, 1–157.

Yancheva, G., Nowaczyk, N.R., Mingram, J., Dulski, P., Schettler, G., Negendank, J.F.W., Liu, J., Sigman, D.M., Peterson, L.C., Haug, G.H., 2007. Influence of the intertropical convergence zone on the East Asian monsoon. Nature 445, doi:10.1038.

Yarincik, K.M., Murray, R.W., Peterson L.C., 2000. Climatically sensitive eolian and hemipelagic deposition in the Cariaco Basin, Venezuela, over the past 578,000 years: Results from Al/Ti and K/Al. Paleoceanography 15, doi: 10.1029/1999PA900048.

Zabel, M., Schneider, R.R., Wagner, T., Adegbie, A.T., de Vries, U. Kolonic, S., 2001. Late Quaternary climate changes in Central Africa as inferred from terrigenous input to the Niger Fan. Quaternary Research 56, 207–217.

Ziegler, M., Jilbert, T., De Lange, G.J., Lourens, L.J., Reichart, G.J., 2008. Bromine counts from XRF scanning as an estimate of the marine organic carbon content of sediment cores. Geochemistry, Geophysics, Geosystems 9, 1525–2027.

Appendices

Appendix 1. Depth scale adopted for the core Tarfaya SN1.

		Lithological description depth				XRF depth				Final depth			
Section	Segment	Segment length (cm)	Section depth (bottom m)	Segment depth (top m)	Bottom section depth discrepancy (cm) to ONHYM depth	Segment length by XRF (cm)	Section depth by XRF (bottom m)	Segment depth by XRF (top m)	Segment length discrepancy (cm) Lithological description - XRF	Section depth ONHYM (top m)	Final section depth (bottom m)	Segment length for XRF plot (cm)	Final Isotope and XRF plot segment (Top m)
12	3	60											
	4	69				69			0			69	
	5	55				55						55	
13	1	66		28.5		66		28.5		28.5		66	28.5
	2	63		29.16		63		29.16				63	29.16
	3	72		29.79		72		29.79				72	29.79
	4	71		30.51		70		30.51	1			70	30.51
	5	23	31.45	31.22	15	23	31.44	31.21	0		31.45	23	31.22
14	1	77		31.6		35		31.6	42	31.6		35	31.6
	2	70		32.37		70		31.95				70	31.95
	3	54		33.07		54		32.65				54	32.65
	4	65		33.61		64		33.19	1			64	33.19
	5	40		34.26		33		33.83	7			33	33.83
	6	37	35.03	34.66	-33	37	34.53	34.16	0		34.53	37	34.16
15	1	67		34.7		67		34.7	0	34.7		67	34.7
	2	62		35.37		61		35.37	1			61	35.37
	3	67.5		35.99		67		35.98	0.5			67	35.98
	4	67.5		36.665		66		36.65	1.5			66	36.65
	5	49	37.83	37.34	-3	49	37.8	37.31	0		37.8	49	37.31
16	1	75		37.8		75		37.8	0	37.8		75	37.8
	2	59		38.55		59		38.55	0			59	38.55
	3	69		39.14		69		39.14	0			69	39.14
	4	77	40.6	39.83	20	77	40.6	39.83	0		40.6	77	39.83
17	1	81.5		40.8		80		40.8	1.5	40.8		77	40.8
	2	71		41.615		70		41.6	1			67	41.57
	3	83	43.155	42.325	-25.5	69	42.99	42.3	14		43.89	66	42.24
18	1	65.5		42.9		65.5		42.9	0	42.9		65.5	42.9
	2	79		43.555		79		43.555	0			79	43.555
	3	75		44.345		75		44.345	0			75	44.345
	4	67		45.095		67		45.095	0			67	45.095
	5	13		45.765		13		45.765	0			13	45.765
	6	10	45.995	45.895	30.5	10	45.995	45.895	0		45.995	40.5	45.895
19	1	18		46.3		18		46.3	0	46.3		18	46.3
	2	19		46.48		19		46.48	0			19	46.48
	3	18.5		46.67		28		46.67	-9.5			28	46.67
	4	66		46.855		66		46.95	0			66	46.95
	5	62.5		47.515		62		47.61	0.5			62	47.61
	6	62		48.14		61		48.23	1			61	48.23
	7	71	49.47	48.76	13	71	49.55	48.84	0		49.55	76	48.84
20	1	52		49.6				49.6		49.6		47	49.6
	2	41		50.12								35	50.07
	3	71		50.53								66	50.42
	4	76	52	51.24	-5200		49.6				51.76	68	51.08
21	1	58		52								52	51.76
	2	78		52.58		77			1			77	52.28
	3	70.5		53.36		69			1.5			69	53.05
	4	71		54.065		70			1			70	53.74
	5	36	55.14	54.775	-34						54.8	36	54.44
22	1	79		54.8		78		54.8	1	54.8		79	54.8
	2	65		55.59		64		55.58	1			65	55.59
	3	73.5		56.24		70		56.22	3.5			73.5	56.24
	4	63.5		56.975		61		56.92	2.5			63.5	56.975
	5	23.5	57.845	57.61	5.5	24	57.77	57.53	-0.5		57.845	24	57.61
23	1	77		57.9		78		57.9	-1	57.9		77	57.9
	2	79		58.67		79		58.68	0			79	58.67
	3	78		59.46		75		59.47	3			78	59.46
	4	66	60.9	60.24	10	65	60.87	60.22	1		60.9	76	60.24
24	1	62		61		62		61	0	61		62	61
	2	78		61.62		78		61.62	0			78	61.62
	3	81		62.4		70		62.4	11			81	62.4
	4	64		63.21		54		63.1	10			64	63.21
	5	25	64.1	63.85	-10	25	63.89	63.64	0		64	25	63.85
25	1	71		64		71		64	0	64		71	64
	2	71		64.71		63		64.71	8			71	64.71
	3	54		65.42		54		65.34	0			50	65.42
	4	69		65.96		69		65.88	0			69	65.92
	5	38.5	67.035	66.65	-3.5	38	66.95	66.57	0.5		67	39	66.61
26	1	73	67.73	67	97	37	67.37	67	36	67	67.73	67	67
27	1	69		68.7		60		68.7	9	68.7		60	68.7
	2	45		69.39		38		69.3	7			38	69.3
	3	27		69.84		26		69.68	1			26	69.68
	4	44		70.11		42		69.94	2			42	69.94
	5	19		70.55		14		70.36	5			14	70.36
	6	74		70.74		64		70.5	10			64	70.5
	7	11	71.59	71.48	-39	6	71.2	71.14	5		71.2	6	71.14
28	1	72		71.2		72		71.2	0	71.2		72	71.2

	2	61		71.92		41		71.92	20			61	71.92
	3	69		72.53		69		72.33	0			67	72.53
	4	58		73.22		57		73.02	1			58	73.2
	5	51	74.31	73.8	-1	50	74.09	73.59	1		74.31	52	73.78
29	1	62		74.3		62		74.3	0	74.3		62	74.3
	2	45		74.92		39		74.92	6			45	74.92
	3	79.5		75.37		77		75.31	2.5			77	75.37
	4	58		76.165		53		76.08	5			53	76.14
	5	54		76.745		49		76.61	5			49	76.67
	6	38	77.665	77.285	-16.5	34	77.44	77.1	4		77.5	34	77.16
30	1	56		77.5		55		77.5	1	77.5		56	77.5
	2	75		78.06		75		78.05	0			75	78.06
	3	71		78.81		72		78.8	-1			71	78.81
	4	71		79.52		70		79.52	1			71	79.52
	5	32	80.55	80.23	5	30	80.52	80.22	2		80.55	37	80.23
31	1	74		80.6		73		80.6	1	80.6		74	80.6
	2	68		81.34		67		81.33	1			68	81.34
	3	69		82.02		68		82	1			69	82.02
	4	16	82.87	82.71	83	16	82.84	82.68	0		82.87	16	82.71
32	1	77.5		83.7		74		83.7	3.5	83.7		74	83.7
	2	69.5		84.475		58		84.44	11.5			58	84.44
	3	75		85.17		75		85.02	0			75	85.02
	4	75		85.92		73		85.77	2			73	85.77
	5	17.5	86.845	86.67	-4.5	26	86.76	86.5	-8.5		86.845	26	86.5
33	1	61		86.8		60		86.8	1	86.8		60	86.8
	2	71		87.41		53		87.4	18			53	87.4
	3	81		88.12		81		87.93	0			81	87.93
	4	76		88.93		54		88.74	22			54	88.74
	5	16	89.85	89.69	-55	16	89.44	89.28	0		89.44	0	
34	1	70		89.3		66		89.3	4	89.3		70	89.3
	2	76		90		50		89.96	26			76	90
	3	73		90.76		69		90.46	4			68	90.76
	4	47		91.49		46		91.15	1			47	91.44
	5	38	92.34	91.96	-4	38	91.99	91.61	0		92.34	39	91.91
35	1	67.5		92.3		67		92.3	0.5	92.3		67.5	92.3
	2	66		92.975		64		92.97	2			66	92.975
	3	75		93.635		72		93.61	3			75	93.635
	4	73	95.115	94.385	18.5	72	95.05	94.33	1		95.115	73	94.385
36	1	64		95.3		63		95.3	1	95.3		64	95.3
	2	72.5		95.94		71		95.93	1.5			72.5	95.94
	3	69.5		96.665		69		96.64	0.5			69.5	96.665
	4	72		97.36		67		97.33	5			67	97.36
	5	40	98.48	98.08	-8	37	98.37	98	3		98.48	37	98.03
37	1	60		98.4		55		98.4	5	98.4		55	98.4
	2	72	99.72	99	-12	65	99.6	98.95	7		99.72	65	98.95
38	1	76		99.6		76		99.6	0	99.6		76	99.6
	2	76		100.36		42			34			76	100.36
	3	42		101.12		41			1			42	101.12
	4	75		101.54		75			0			75	101.54
	5	48	102.77	102.29	13	22	102.16		26		102.77	48	102.29
39	1	13		102.9		13		102.9	0	102.9		13	102.9
	2	72		103.03		50		103.03	22			72	103.03
	3	71		103.75		69		103.53	2			71	103.75
	4	64		104.46		63		104.22	1			64	104.46
	5	69	105.79	105.1	21	68	105.53	104.85	1		105.79	69	105.1
40	1	70		106		60		106	10	106		60	106
	2	66		106.7		54		106.6	12			54	106.6
	3	77		107.36		76		107.14	1			76	107.14
	4	73		108.13		59		107.9	14			59	107.9
	5	50	109.36	108.86	-36	50	108.99	108.49	0		108.99	51	108.49
41	1	71		109		63		109	8	109		63	109
	2	69		109.71		62		109.63	7			62	109.63
	3	54		110.4		46		110.25	8			46	110.25
	4	75		110.94		75		110.71	0			75	110.71
	5	57	112.26	111.69	-26	55	112.01	111.46	2		112.01	56	111.44
42	1	14		112		14		112	0	112		13	112
	2	67		112.14		67		112.14	0			62	112.13
	3	83		112.81		82		112.81	1			77	112.75
	4	78		113.64		77		113.63	1			72	113.52
	5	81	115.23	114.42	-23	81	115.21	114.4	0		115	76	114.24
43	1	54		115		53		115	1	115		54	115
	2	66		115.54		65		115.53	1			66	115.54
	3	65		116.2		64		116.18	1			65	116.2
	4	67		116.85		66		116.82	1			67	116.85
	5	46	117.98	117.52	2	46	117.94	117.48	0		117.98	48	117.52
44	1	79		118		79		118	0	118		79	118
	2	77		118.79		76		118.79	1			77	118.79
	3	75		119.56		75		119.55	0			75	119.56
	4	75.5		120.31		75		120.3	0.5			75.5	120.31
	5	12	121.185	121.065	1.5	12	121.17	121.05	0		121.185	12	121.065
45	1	74		121.2		50		121.2	24	121.2		50	121.2
	2	50		121.94		74		121.7	-24			74	121.7
	3	77		122.44		75		122.44	2			75	122.44
	4	77		123.21		77		123.19	0			77	123.19
	5	33	124.31	123.98	-1	33	124.29	123.96	0		124.29	33	123.96
46	1	18		124.3		18		124.3	0	124.3		18	124.3
	2	70		124.48		70		124.48	0			70	124.48
	3	70		125.18		70		125.18	0			70	125.18
	4	81		125.88		64		125.88	17			81	125.88
	5	75	127.44	126.69	6	63	127.15	126.52	12		127.44	75	126.69

47	1	66		127.5		66		127.5	0	127.5		66	127.5
	2	71		128.16		70		128.16	1			71	128.16
	3	76.5		128.87		76		128.86	0.5			76.5	128.87
	4	81	130.445	129.635	15.5	80	130.42	129.62	1		130.445	81	129.635
48	1	58		130.6		58		130.6	0	130.6		58	130.6
	2	76		131.18		76		131.18	0			76	131.18
	3	75		131.94		73		131.94	2			75	131.94
	4	72		132.69		72		132.67	0			72	132.69
	5	30	133.71	133.41	-1	30	133.69	133.39	0		133.71	29	133.41
49	1	31		133.7		31		133.7	0	133.7		31	133.7
	2	80		134.01		82		134.01	-2			80	134.01
	3	70		134.81		74		134.83	-4			70	134.81
	4	71		135.51		70		135.57	1			71	135.51
	5	51	136.73	136.22	7	51	136.78	136.27	0		136.73	51	136.22
50	1	78		136.8		78		136.8	0	136.8		78	136.8
	2	77		137.58		77		137.58	0			77	137.58
	3	71		138.35		71		138.35	0			71	138.35
	4	73	139.79	139.06	1	72	139.78	139.06	1		139.79	73	139.06
51	1	67		139.8		67		139.8	0	139.8		67	139.8
	2	67.5		140.47		67		140.47	0.5			67.5	140.47
	3	61.5		141.145		61		141.14	0.5			61.5	141.145
	4	75.5	142.515	141.76	28.5	75	142.5	141.75	0.5		142.515	75.5	141.76
52	1	73		142.8		73		142.8	0	142.8		73	142.8
	2	28	143.81	143.53	-1	22	143.75	143.53	6		143.81	27	143.53
53	1	77		143.8		76		143.8	1	143.8		77	143.8
	2	74.5		144.57		63		144.56	11.5			75	144.57
	3	62		145.315		62		145.19	0			62	145.32
	4	61		145.935		60		145.81	1			60.5	145.94
	5	22	146.765	146.545	23.5	28	146.69	146.41	-6		146.765	28	146.545
54	1	66		147		66		147	0	147		66	147
	2	71		147.66		71		147.66	0			71	147.66
	3	50		148.37		50		148.37	0			50	148.37
	4	62	149.49	148.87	61	62	149.49	148.87	0		149.49	62	148.87
55	1 _ 4	68		150.1		55		150.1	13	150.1		55	150.1
	5 _ 8	71		150.78		61		150.65	10			61	150.65
	9	82.5		151.49		82		151.26	0.5			82	151.26
	10	58		152.315		58		152.08	0			58	152.08
	11	44	153.335	152.895	-23.5	44	153.1	152.66	0		153.1	44	152.66
56	1	13		153.1		13		153.1		153.1		13	153.1
	2	15		153.23		15		153.23				15	153.23
	3	74.5		153.38		74		153.38	0.5			74.5	153.38
	4	77		154.125		76		154.12	1			77	154.125
	5	79		154.895		78		154.88	1			79	154.895
	6	43		155.685		42		155.66	1			43	155.685
	7	8	156.195	156.115	0.5	8	156.16	156.08	0		156.195	8	156.115
57	1	76.5		156.2		76		156.2	0.5	156.2		76.5	156.2
	2	75.5		156.965		75		156.96	0.5			75.5	156.965
	3	55.5	158.275	157.72	2.5	55	158.26	157.71	0.5		158.275	55.5	157.72
58	1	69		158.3		68		158.3	1	158.3		69	158.3
	2	73.5		158.99		73		158.98	0.5			73.5	158.99
	3	75		159.725		74		159.71	1			75	159.725
	4	74	161.215	160.475	8.5	74	161.19	160.45	0		161.215	74	160.475
59	1	73		161.3		72		161.3	1	161.3		72	161.3
	2	70		162.03		70		162.02	0			70	162.02
	3	71		162.73		69		162.72	2			69	162.72
	4	71		163.44		70		163.41	1			70	163.41
	5	29	164.44	164.15	-4	29	164.4	164.11	0		164.4	29	164.11
60	1	74		164.4		73		164.4	1	164.4		74	164.4
	2	71.5		165.14		71		165.13	0.5			71.5	165.14
	3	80.5		165.855		69		165.84	11.5			80.5	165.855
	4	75	167.41	166.66	-1	74	167.27	166.53	1		167.41	74	166.66
61	1	70.5		167.4		70		167.4	0.5	167.4		70.5	167.4
	2	71.5		168.105		71		168.1	0.5			71.5	168.105
	3	72		168.82		72		168.81	0			72	168.82
	4	66		169.54		65		169.53	1			65	169.54
	5	33	170.53	170.2	-3	31	170.49	170.18	2		170.49	31	170.19
62	1	81.5		170.5		80		170.5	1.5	170.5		74	170.5
	2	64		171.315		64		171.3	0			60	171.24
	3	71.5		171.955		71		171.94	0.5			66	171.84
	4	76.5		172.67		76		172.65	0.5			70	172.55
	5	22	173.655	173.435	-15.5	22	173.63	173.41	0		173.5	20	173.2
63	1	69.5		173.5		69		173.5	0.5	173.5		69.5	173.5
	2	70.5		174.195		70		174.19	0.5			70.5	174.195
	3	73		174.9		73		174.89	0			73	174.9
	4	57.5	176.205	175.63	19.5	57	176.19	175.62	0.5		176.205	57.5	175.63
64	1	78		176.4		77		176.4	1	176.4		76	176.4
	2	78		177.18		77		177.17	1			75	177.16
	3	70		177.96		69		177.94	1			67	177.91
	4	75	179.41	178.66	-11	74	179.37	178.63	1		179.3	72	178.58
65	1	19.5		179.3		19		179.3	0.5	179.3		19	179.3
	2	74		179.495		73		179.49	1			73	179.49
	3	70		180.235		69		180.22	1			69	180.22
	4	73.5		180.935		73		180.91	0.5			73	180.91
	5	77	182.44	181.67	-4	76	182.4	181.64	1		182.4	76	181.64
66	1	67		182.4		67		182.4	0	182.4		67	182.4
	2	58.5		183.07		58		183.07	0.5			58.5	183.07
	3	59		183.655		59		183.65	0			59	183.655
	4	75		184.245		74		184.24	1			75	184.245
	5	50	185.495	184.995	0.5	50	185.48	184.98	0		185.495	50	184.995
67	1	63.5		185.5		63		185.5	0.5	185.5		63.5	185.5

	2	69		186.135		69		186.13	0			69	186.135
	3	64.5		186.825		65		186.82	-0.5			64.5	186.825
	4	71		187.47		66		187.47	5			71	187.47
	5	29.5	188.475	188.18	2.5	29	188.42	188.13	0.5		188.475	29.5	188.18
68	1	71		188.5		71		188.5	0	188.5		69	188.5
	2	70		189.21		70		189.21	0			68	189.19
	3	73.5		189.91		73		189.91	0.5			71	189.87
	4	71		190.645		70		190.64	1			68	190.58
	5	25.5	191.61	191.355	-11	25	191.59	191.34	0.5		191.5	24	191.26
69	1	63.5		191.5		63		191.5	0.5	191.5		63	191.5
	2	70		192.135		70		192.13	0			70	192.13
	3	69		192.835		69		192.83				69	192.83
	4	68		193.525		68		193.52				68	193.52
	5	32	194.525	194.205	-2.5	32	194.52	194.2			192.52	30	194.2
70	1	76		194.5		76		194.5		194.5		76	194.5
	2	80		195.26		80		195.26				80	195.26
	3	71.5		196.06		71.5		196.06				71.5	196.06
	4	71	197.485	196.775	1.5	71	197.485	196.775			197.485	71	196.775
71	1	76		197.5		76		197.5		197.5		73	197.5
	2	79.5		198.26		79.5		198.26				76	198.23
	3	75		199.055		75		199.055				72	198.99
	4	82.5	200.63	199.805	-13	82.5	200.63	199.805				79	199.71
72	1	74		200.5		74		200.5		200.5		72	200.5
	2	69.5		201.24		69.5		201.24				67	201.22
	3	84		201.935		84		201.935				82	201.89
	4	81	203.585	202.775	-8.5	80	203.575	202.775	1			78	202.71
73	1	75.5		203.5		75		203.5	0.5	203.5		74	203.5
	2	76		204.255		76		204.25	0			75	204.24
	3	77.5		205.015		77		205.01	0.5			75	204.99
	4	78.5	206.575	205.79	-7.5	78	206.56	205.78	0.5		206.5	76	205.74
74	1	78.5		206.5		78		206.5	0.5	206.5		78	206.5
	2	76.5		207.285		76		207.28	0.5			76	207.28
	3	76.5		208.05		76		208.04	0.5			76	208.04
	4	71.5	209.53	208.815	-3	71	209.51	208.8	0.5		209.53	70	208.8
75	1	76		209.5		75		209.5	1	209.5		75	209.5
	2	76		210.26		75		210.25	1			75	210.25
	3	77		211.02		76		211	1			76	211
	4	75	212.54	211.79	-4	74	212.5	211.76	1		212.5	74	211.76
76	1	74.5		212.5		74		212.5	0.5	212.5		74.5	212.5
	2	76.5		213.245		76		213.24	0.5			76.5	213.245
	3	74.5		214.01		74		214	0.5			74.5	214.01
	4	72	215.475	214.755	2.5	71	215.45	214.74	1		215.475	72	214.755
77	1	77		215.5		77		215.5	0	215.5		75	215.5
	2	76		216.27		75		216.27	1			73	216.25
	3	78		217.03		77		217.02	1			74	216.98
	4	81.5	218.625	217.81	-12.5	81	218.6	217.79	0.5		218.5	78	217.72
78	1	75		218.5		74		218.5	1	218.5		75	218.5
	2	74.5		219.25		74		219.24	0.5			74.5	219.25
	3	72		219.995		72		219.98	0			72	219.995
	4	67	221.385	220.715	11.5	67	221.37	220.7	0		221.385	67	220.715
79	1	80		221.5		82		221.5	-2	221.5		81	221.5
	2	78		222.3		78		222.32	0			78	222.31
	3	81.5		223.08		81		223.1	0.5			81	223.09
	4	60.5	224.5	223.895	0	60	224.51	223.91	0.5		224.5	60	223.9
80	1	80		224.5		79		224.5	1	224.5		78	224.5
	2	76		225.3		75		225.29	1			74	225.28
	3	72		226.06		71		226.04	1			71	226.02
	4	79	227.57	226.78	-7	78	227.53	226.75	1		227.5	77	226.73
81	1	74		227.5		73		227.5	1	227.5		73	227.5
	2	74.5		228.24		74		228.23	0.5			74	228.23
	3	71.5		228.985		71		228.97	0.5			71	228.97
	4	77.5		229.7		77		229.68	0.5			77	229.68
	5	6	230.535	230.475	-3.5	5	230.5	230.45	1		230.5	5	230.45
82	1	72.5		230.5		72		230.5	0.5	230.5		72.5	230.5
	2	81.5		231.225		81		231.22	0.5			81.5	231.225
	3	69		232.04		68		232.03	1			69	232.04
	4	76	233.49	232.73	1	76	233.47	232.71	0		233.49	76	232.73
83	1	78		233.5		77		233.5	1	233.5		77	233.5
	2	29		234.28		28		234.27	1			28	234.27
	3	70.5		234.57		70		234.55	0.5			70	234.55
	4	75.5		235.275		75		235.25	0.5			75	235.25
	5	49.5	236.525	236.03	-2.5	49	236.49	236	0.5		236.49	49.5	236
84	1	76		236.5		75		236.5	1	236.5		75	236.5
	2	75.5		237.26		75		237.25	0.5			75	237.25
	3	78		238.015		77		238	1			77	238
	4	78	239.575	238.795	-7.5	70	239.47	238.77	8		239.47	73	238.77
85	1	76		239.5		76		239.5	0	239.5		76	239.5
	2	78		240.26		78		240.26	0			78	240.26
	3	77		241.04		56		241.04	21			73	241.04
	4	73	242.54	241.81	-4	72	242.32	241.6	1		242.5	73	241.77
86	1	67.5		242.5		67		242.5	0.5	242.5		67.5	242.5
	2	63.5		243.175		63		243.17	0.5			63.5	243.175
	3	65.5		243.81		65		243.8	0.5			65.5	243.81
	4	71.5		244.465		71		244.45	0.5			71.5	244.465
	5	24.5	245.425	245.18	7.5	24	245.4	245.16	0.5		245.425	24.5	245.18
87	1	76		245.5		75		245.5	1	245.5		75	245.5
	2	76.5		246.26		76		246.25	0.5			76	246.25
	3	75.5		247.025		75		247.01	0.5			75	247.01
	4	74	248.52	247.78	-2	73	248.49	247.76	1		248.49	74	247.76
88	1	72		248.5				248.5		248.5			248.5

	2	74		249.22		73			1			73	249.22
	3	77.5		249.96		76			1.5			77.5	249.96
	4	76.5	251.5	250.735	0	76	250.75		0.5		250.78	76.5	250.735
89	1	66		251.5		66		251.5	0	251.5		62	251.5
	2	83.5		252.16		83		252.16	0.5			78	252.12
	3	83		252.995		83		252.99	0			78	252.9
	4	82.5		253.825		83		253.82	-0.5			78	253.68
	5	6	254.71	254.65	-21	4	254.69	254.65	2		254.5	4	254.46
90	1	66		254.5		65		254.5	1	254.5		65	254.5
	2	78		255.16		77		255.15	1			77	255.15
	3	76.5		255.94		76		255.92	0.5			76	255.92
	4	83	257.535	256.705	-3.5	82	257.5	256.68	1		257.5	82	256.68
91	1	68		257.5		67		257.5	1	257.5		68	257.5
	2	72		258.18		71		258.17	1			72	258.18
	3	79		258.9		78		258.88	1			79	258.9
	4	73	260.42	259.69	8	76	260.42	259.66	-3		260.42	76	259.69
92	1	69		260.5		68		260.5	1	260.5		69	260.5
	2	69		261.19		68		261.18	1			69	261.19
	3	79		261.88		78		261.86	1			79	261.88
	4	78	263.45	262.67	5	77	263.41	262.64	1		263.45	78	262.67
93	1	70.5		263.5		70		263.5	0.5	263.5		70.5	263.5
	2	70		264.205		69		264.2	1			70	264.205
	3	80		264.905		79		264.89	1			80	264.905
	4	79	266.495	265.705	0.5	78	266.46	265.68	1		266.495	79	265.705
94	1	74		266.5		74		266.5	0	266.5		74	266.5
	2	80		267.24		79		267.24	1			80	267.24
	3	73		268.04		75		268.03	-2			73	268.04
	4	73	269.5	268.77	0	73	269.51	268.78	0		269.5	73	268.77
95	1	72		269.5		72		269.5	0	269.5		72	269.5
	2	79		270.22		78		270.22	1			79	270.22
	3	72.5		271.01		72		271	0.5			72.5	271.01
	4	70	272.435	271.735	6.5	60	272.32	271.72	10		272.435	70	271.735
96	1	72.5		272.5		72		272.5	0.5	272.5		72.5	272.5
	2	56.5		273.225		55		273.22	1.5				273.225
	3							273.77					
	4												
	5		273.79				273.77				273.79		

Depth(m) given by ONHYM for the top of each section

Final depth(m) for the top of each section

Appendix 2. Depth scale adopted for the core Tarfaya SN2.

		Lithological description depth				XRF depth				Final depth			
Section	Segment	Segment length (cm)	Section depth (bottom m)	Segment depth (top m)	Bottom section depth discrepancy (cm) to ONHYM depth	Segment length by XRF (cm)	Section depth by XRF (bottom m)	Segment depth by XRF (top m)	Segment length discrepancy (cm) Lithological description - XRF	Section depth ONHYM (top m)	Final section depth (bottom m)	Segment length for XRF plot (cm)	Final Isotope and XRF plot segment (Top m)
13	1	77		24.6		75		24.6	2	24.6		77	24.6
	2	70		25.37		70		25.35	0			70	25.37
	3	73		26.07		73		26.05	0			73	26.07
	4	62	27.42	26.8	-18	46	27.24	26.78	16		27.42	62	26.8
14	1	76		27.6		76		27.6	0	27.6		76	27.6
	2	74		28.36		74		28.36	0			74	28.36
	3	64.5		29.095		64		29.1	0.5			64.5	29.095
	4	81	30.555	29.74	-4.5	81	30.55	29.74	0		30.555	81	29.74
15	1	68		30.6		68		30.6	0	30.6		68	30.6
	2	67.5		31.28		67		31.28	0.5			67.5	31.28
	3	68.5		31.955		68		31.95	0.5			68.5	31.955
	4	62	33.26	32.64	-4	62	33.25	32.63	0		33.26	62	32.64
16	1	76		33.3		76		33.3	0	33.3		76	33.3
	2	75		34.06		74		34.06	1			75	34.06
	3	78		34.81		79		34.8	-1			78	34.81
	4	78	36.37	35.59	7	78	36.37	35.59	0		36.37	78	35.59
17	1	49		36.3		49		36.3	0	36.3		49	36.3
	2	34		36.79		34		36.79	0			34	36.79
	3	34		37.13		34		37.13	0			34	37.13
	4	22		37.47		21		37.47	1			22	37.47
	5	31		37.69		31		37.68	0			31	37.69
	6	69	38.69	38	-1	69	38.68	37.99	0		38.69	69	38
18	1	59		38.7		59		38.7	0	38.7		59	38.7
	2	59		39.29		59		39.29	0			59	39.29
	3	77		39.88		77		39.88	0			77	39.88
	4	74	41.39	40.65	-11		40.65	40.65	74		41.39	74	40.65
19	1	65.5		41.5		64		41.5	1.5	41.5		65.5	41.5
	2	55.5		42.155		55		42.14	0.5			55.5	42.155

	3	77		42.71		77		42.69	0			77	42.71
	4	78.8		43.48		78		43.46	0.8			78.8	43.48
	5	8	44.348	44.268	-5.2		44.24	44.24	8		44.348	8	44.268
20	1	60.8		44.4		59		44.4	1.8	44.4		60.8	44.4
	2	76		45.008		75		44.99	1			76	45.008
	3	62.5		45.768		62		45.74	0.5			62.5	45.768
	4	30	46.693	46.393	-20.7	31	46.67	46.36	-1		46.693	30	46.393
21	1	36		46.9		36		46.9	0	46.9		36	46.9
	2	71		47.26		70		47.26	1			71	47.26
	3	64.5		47.97		64		47.96	0.5			64.5	47.97
	4	76		48.615		76		48.6	0			76	48.615
	5	40	49.775	49.375	-12.5	40	49.76	49.36	0		49.775	40	49.375
22	1	67.5		49.9		67		49.9	0.5	49.9		67.5	49.9
	2	74.5		50.575		74		50.57	0.5			74.5	50.575
	3	77.8		51.32		77		51.31	0.8			77.8	51.32
	4	66.6	52.764	52.098	-13.6	66	52.74	52.08	0.6		52.764	66.6	52.098
23	1	71		52.9		71		52.90	0	52.90		71	52.9
	2	69		53.61		69		53.61	0			69	53.61
	3	53.5	54.835	54.3	3.5	53	54.83	54.3	0.5		54.83	53	54.3
24	1	15		54.8		15		54.80	0	54.80		15	54.8
	2	78		54.95		78		54.95	0			78	54.95
	3	75		55.73		75		55.73	0			75	55.73
	4	70.5		56.48		70		56.48	0.5			70	56.48
	5	21.2	57.397	57.185	9.7	21	57.39	57.18	0.2		57.39	21	57.18
25	1	57		57.3		57		57.30	0	57.30		57	57.3
	2	70		57.87		70		57.87	0			70	57.87
	3	62		58.57		62		58.57	0			62	58.57
	4	44	59.63	59.19	-57	44	59.63	59.19	0		59.63	44	59.19
26	1	71		60.2		71		60.20	0	60.20		71	60.2
	2	75		60.91		75		60.91	0			75	60.91
	3	75		61.66		73		61.66	2			73	61.66
	4	63.5	63.045	62.41	-25.5	69	63.08	62.39	-5.5		63.08	69	62.39
27	1	77.5		63.3		75		63.30	2.5	63.30		77.5	63.3
	2	70		64.075		60		64.05	10			70	64.075
	3	80.5		64.775		81		64.65	-0.5			80.5	64.775
	4	71		65.58		71		65.46	0			71	65.58
	5	10	66.39	66.29	-1		66.17	66.17	10		66.39	10	66.29
28	1	76		66.4		77		66.40	-1	66.40		76	66.4
	2	63		67.16		64		67.17	-1			63	67.16
	3	70		67.79		69		67.81	1			70	67.79
	4	77.5	69.265	68.49	-13.5	76	69.26	68.5	1.5		69.265	77.5	68.49
29	1	72		69.4		72		69.40	0	69.40		72	69.4
	2	71		70.12		70		70.12	1			71	70.12
	3	73		70.83		72		70.82	1			73	70.83
	4	87		71.56		61		71.54	26			87	71.56
	5	39	72.82	72.43	32		72.15	72.15	39		72.82	39	72.43
30	1	71		72.5		71		72.50	0	72.50		71	72.5
	2	61		73.21		60		73.21	1			60	73.21
	3	74		73.82		74		73.81	0			74	73.81
	4	79.5		74.56		79		74.55	0.5			79	74.55
	5	26	75.615	75.355	1.5	26	75.6	75.34	0		75.6	26	75.34
31	1	55		75.6		55		75.60	0	75.60		55	75.6
	2	67		76.15		67		76.15	0			67	76.15
	3	77.5	77.595	76.82	-0.5	41	77.23	76.82	36.5		77.595	77.5	76.82
32	1	59.5		77.6		59		77.60	0.5	77.60		59.5	77.6
	2	72		78.195		70		78.19	2			72	78.195
	3	30.5		78.915		30		78.89	0.5			30.5	78.915
	4	84	80.06	79.22	-14	84	80.03	79.19	0		80.06	84	79.22
33	1	76.5		80.2		76		80.20	0.5	80.20		76.5	80.2
	2	67		80.965		67		80.96	0			67	80.965
	3	66	82.295	81.635	-0.5	67	82.3	81.63	-1		82.3	66	81.635
34	1	82		82.3		81		82.30	1	82.30		81	82.3
	2	80		83.12		78		83.11	2			78	83.11
	3	64.5		83.92		64		83.89	0.5			64	83.89
	4	28	84.845	84.565	4.5	27	84.8	84.53	1		84.8	27	84.53
35	1	76		84.8		77		84.80	-1	84.80		76	84.8
	2	71		85.56		71		85.57	0			71	85.56
	3	79		86.27		72		86.28	7			79	86.27
	4	83	87.89	87.06	-1	83	87.83	87	0		87.89	83	87.06
36	1	77		87.9		77		87.90	0	87.90		77	87.9
	2	72.5		88.67		72		88.67	0.5			72.5	88.67
	3	81		89.395		80		89.39	1			81	89.395
	4	79	90.995	90.205	-0.5	79	90.98	90.19	0		90.995	79	90.205
37	1	80.5		91		80		91.00	0.5	91.00		80.5	91
	2	80		91.805		80		91.8	0			80	91.805
	3	71		92.605		70		92.6	1			71	92.605
	4	75.5	94.07	93.315	-3	75	94.05	93.3	0.5		94.07	75.5	93.315
38	1	75		94.1		72		94.10	3	94.10		75	94.1
	2	76.5		94.85		76		94.82	0.5			76.5	94.85
	3	77		95.615		77		95.58	0			77	95.615
	4	76.5	97.15	96.385	-5	76	97.11	96.35	0.5		97.15	76.5	96.385
39	1	81		97.2		81		97.20	0	97.20		81	97.2
	2	73.7		98.01		73		98.01	0.7			73.7	98.01
	3	74		98.747		73		98.74	1			74	98.747
	4	77	100.257	99.487	-4.3	76	100.23	99.47	1		100.257	77	99.487
40	1	77.5		100.3		78		100.30	-0.5	100.30		77.5	100.3
	2	75		101.075		75		101.08	0			75	101.075
	3	71		101.825		71		101.83	0			71	101.825
	4	77	103.305	102.535	-9.5	64	103.18	102.54	13		103.305	77	102.535

41	1	76		103.4		75		103.40	1	103.40		75	103.4
	2	75		104.16		75		104.15	0			75	104.15
	3	54.5		104.91		54		104.9	0.5			54	104.9
	4	56.5		105.455		56		105.44	0.5			56	105.44
	5	56	106.58	106.02	8	56	106.56	106	0		106.56	56	106
42	1	82		106.5		80		106.50	2	106.50		82	106.5
	2	81		107.32		81		107.3	0			81	107.32
	3	74		108.13		74		108.11	0			74	108.13
	4	69.5	109.565	108.87	-3.5	70	109.55	108.85	-0.5		109.565	69.5	108.87
43	1	75		109.6		72		109.60	3	109.60		75	109.6
	2	78.5		110.35		78		110.32	0.5			78.5	110.35
	3	76.5		111.135		76		111.1	0.5			76.5	111.135
	4	80	112.7	111.9	0	79	112.65	111.86	1		112.7	80	111.9
44	1	74		112.7		74		112.70	0	112.70		74	112.7
	2	76.5		113.44		76		113.44	0.5			76.5	113.44
	3	71		114.205		71		114.2	0			71	114.205
	4	75	115.665	114.915	-13.5	75	115.66	114.91	0		115.665	75	114.915
45	1	74		115.8		77		115.80	-3	115.80		77	115.8
	2	78		116.54		78		116.57	0			78	116.57
	3	71		117.32		71		117.35	0			71	117.35
	4	78	118.81	118.03	-9	78	118.84	118.06	0		118.84	78	118.06
46	1	77		118.9		77		118.90	0	118.90		77	118.9
	2	74		119.67		76		119.67	-2			74	119.67
	3	76.5		120.41		76		120.43	0.5			76.5	120.41
	4	78	121.955	121.175	-4.5	78	121.97	121.19	0		121.97	78	121.175
47	1	80.8		122		80		122.00	0.8	122.00		80.8	122
	2	75		122.808		75		122.8	0			75	122.808
	3	75.5		123.558		75		123.55	0.5			75.5	123.558
	4	78	125.093	124.313	-0.7	78	125.08	124.3	0		125.093	78	124.313
48	1	75		125.1		75		125.10	0	125.10		75	125.1
	2	72		125.85		72		125.85	0			72	125.85
	3	53		126.57		64		126.57	-11			53	126.57
	4	78		127.1		78		127.21	0			78	127.1
	5	14	128.02	127.88	-18		127.99	127.99	14		128.02	14	127.88
49	1	70		128.2		70		128.20	0	128.20		70	128.2
	2	57		128.9		57		128.9	0			57	128.9
	3	62		129.47		62		129.47	0			62	129.47
	4	42.5		130.09		42		130.09	0.5			42.5	130.09
	5	48.5	131	130.515	-30	52	131.03	130.51	-3.5		131.03	48.5	130.515
50	1	52.5		131.3		52		131.30	0.5	131.30		52.5	131.3
	2	11		131.825		12		131.82	-1			11	131.825
	3	59.5		131.935		59		131.94	0.5			59.5	131.935
	4	61		132.53		60		132.53	1			61	132.53
	5	50		133.14		50		133.13	0			50	133.14
	6	57	134.21	133.64	-19	56	134.19	133.63	1		134.21	57	133.64
51	1	36		134.4		36		134.40	0	134.40		36	134.4
	2	53		134.76		54		134.76	-1			54	134.76
	3	76.5		135.29		77		135.3	-0.5			77	135.29
	4	70		136.055		70		136.07	0			70	136.055
	5	72	137.475	136.755	-2.5	72	137.49	136.77	0		137.49	72	136.755
52	1	61		137.5		61		137.50	0	137.50		61	137.5
	2	55		138.11		55		138.11	0			55	138.11
	3	71		138.66		71		138.66	0			71	138.66
	4	65		139.37		65		139.37	0			65	139.37
	5	46	140.48	140.02	8	46	140.48	140.02	0		140.48	46	140.02
53	1	68		140.4		68		140.40	0	140.40		68	140.4
	2	76		141.08		75		141.08	1			76	141.08
	3	74		141.84		74		141.83	0			74	141.84
	4	70	143.28	142.58	-12	70	143.27	142.57	0		143.28	70	142.58
54	1	74		143.4		74		143.40	0	143.40		74	143.4
	2	75		144.14		75		144.14	0			75	144.14
	3	75.5		144.89		75		144.89	0.5			75.5	144.89
	4	68	146.325	145.645	-17.5	68	146.32	145.64	0		146.325	68	145.645
55	1	78		146.5		78		146.50	0	146.50		78	146.5
	2	73		147.28		73		147.28	0			73	147.28
	3	74		148.01		73		148.01	1			74	148.01
	4	71	149.46	148.75	-4	71	149.45	148.74	0		149.46	71	148.75
56	1	75		149.5		75		149.50	0	149.50		75	149.5
	2	79		150.25		79		150.25	0			79	150.25
	3	78		151.04		78		151.04	0			78	151.04
	4	66	152.48	151.82	-2	66	152.48	151.82	0		152.48	66	151.82
57	1	78		152.5		78		152.50	0	152.50		78	152.5
	2	78		153.28		79		153.28	-1			78	153.28
	3	72		154.06		72		154.07	0			72	154.06
	4	74.5	155.525	154.78	2.5	74	155.53	154.79	0.5		155.525	74.5	154.78
58	1	74.5		155.5		74		155.50	0.5	155.50		74.5	155.5
	2	77		156.245		77		156.24	0			77	156.245
	3	75.5		157.015		76		157.01	-0.5			75.5	157.015
	4	67.5	158.445	157.77	-5.5	67	158.44	157.77	0.5		158.445	67.5	157.77
59	1	80.5		158.5		80		158.50	0.5	158.50		80	158.5
	2	69		159.305		69		159.3	0			69	159.3
	3	71		159.995		71		159.99	0			71	159.99
	4	81	161.515	160.705	1.5	80	161.5	160.7	1		161.5	80	160.7
60	1	73		161.5		73		161.50	0	161.50		73	161.5
	2	69		162.23		69		162.23	0			69	162.23
	3	76		162.92		76		162.92	0			76	162.92
	4	73		163.68		73		163.68	0			73	163.68
	5	13	164.54	164.41	4	13	164.54	164.41	0		164.54	13	164.41
61	1	64		164.5		64		164.50	0	164.50		64	164.5

	2	70		165.14		70		165.14	0			70	165.14
	3	81.5		165.84		76		165.84	5.5			76	165.84
	4	72.5		166.655		72		166.6	0.5			72	166.6
	5	16	167.54	167.38	4	16	167.48	167.32	0		167.48	16	167.32
62	1	46		167.5		46		167.50	0	167.50		46	167.5
	2	70		167.96		70		167.96	0			70	167.96
	3	74		168.66		74		168.66	0			74	168.66
	4	66		169.4		66		169.4	0			66	169.4
	5	36	170.42	170.06	-8	36	170.42	170.06	0		170.42	36	170.06
63	1	78		170.5		78		170.50	0	170.50		78	170.5
	2	75		171.28		75		171.28	0			75	171.28
	3	75		172.03		75		172.03	0			75	172.03
	4	70	173.48	172.78	-2	70	173.48	172.78	0		173.48	70	172.78
64	1	76		173.5		76		173.50	0	173.50		76	173.5
	2	74		174.26		74		174.26	0			74	174.26
	3	75		175		75		175	0			75	175
	4	68	176.43	175.75	-7	67	176.42	175.75	1		176.43	68	175.75
65	1	77		176.5		77		176.50	0	176.50		77	176.5
	2	76		177.27		76		177.27	0			76	177.27
	3	68		178.03		68		178.03	0			68	178.03
	4	70	179.41	178.71	-9	70	179.41	178.71	0		179.41	70	178.71
66	1	70		179.5		70		179.50	0	179.50		70	179.5
	2	75		180.2		75		180.2	0			75	180.2
	3	74.7		180.95		74		180.95	0.7			74.7	180.95
	4	72	182.417	181.697	-8.3	61	182.3	181.69	11		182.417	72	181.697
67	1	78		182.5		78		182.50	0	182.50		78	182.5
	2	66		183.28		66		183.28	0			66	183.28
	3	73		183.94		73		183.94	0			73	183.94
	4	59.5	185.265	184.67	-23.5	59	185.26	184.67	0.5		185.265	59.5	184.67
68	1	36		185.5		36		185.50	0	185.50		36	185.5
	2	51		185.86		51		185.86	0			51	185.86
	3	78		186.37		78		186.37	0			78	186.37
	4	70		187.15		70		187.15	0			70	187.15
	5	67	188.52	187.85	2	66	188.51	187.85	1		188.51	66	187.85
69	1	64		188.5		63		188.50	1	188.50		64	188.5
	2	49		189.14		44		189.13	5			49	189.14
	3	74		189.63		74		189.57	0			74	189.63
	4	68		190.37		68		190.31	0			68	190.37
	5	44	191.49	191.05	-1	43	191.42	190.99	1		191.49	44	191.05
70	1	32		191.5		32		191.50	0	191.50		32	191.5
	2	68		191.82		68		191.82	0			68	191.82
	3	68.5		192.5		68		192.5	0.5			68.5	192.5
	4	58		193.185		58		193.18	0			58	193.185
	5	70	194.465	193.765	-3.5	47	194.23	193.76	23		194.465	70	193.765
71	1	70		194.5		69		194.50	1	194.50		69	194.5
	2	67		195.2		64		195.19	3			64	195.19
	3	75		195.87		73		195.83	2			73	195.83
	4	71.5		196.62		70		196.56	1.5			70	196.56
	5	21	197.545	197.335	4.5	20	197.46	197.26	1		197.46	20	197.26
72	1	52		197.5		51		197.50	1	197.50		52	197.5
	2	57		198.02		56		198.01	1			57	198.02
	3	69		198.59		69		198.57	0			69	198.59
	4	82	200.1	199.28		81	200.07	199.26	1		200.1	82	199.28

Depth(m) given by ONHYM for the top of each section

Final depth(m) for the top of each section

Appendix 3. Core photograph of some selected interval in the core Tarfaya SN1.

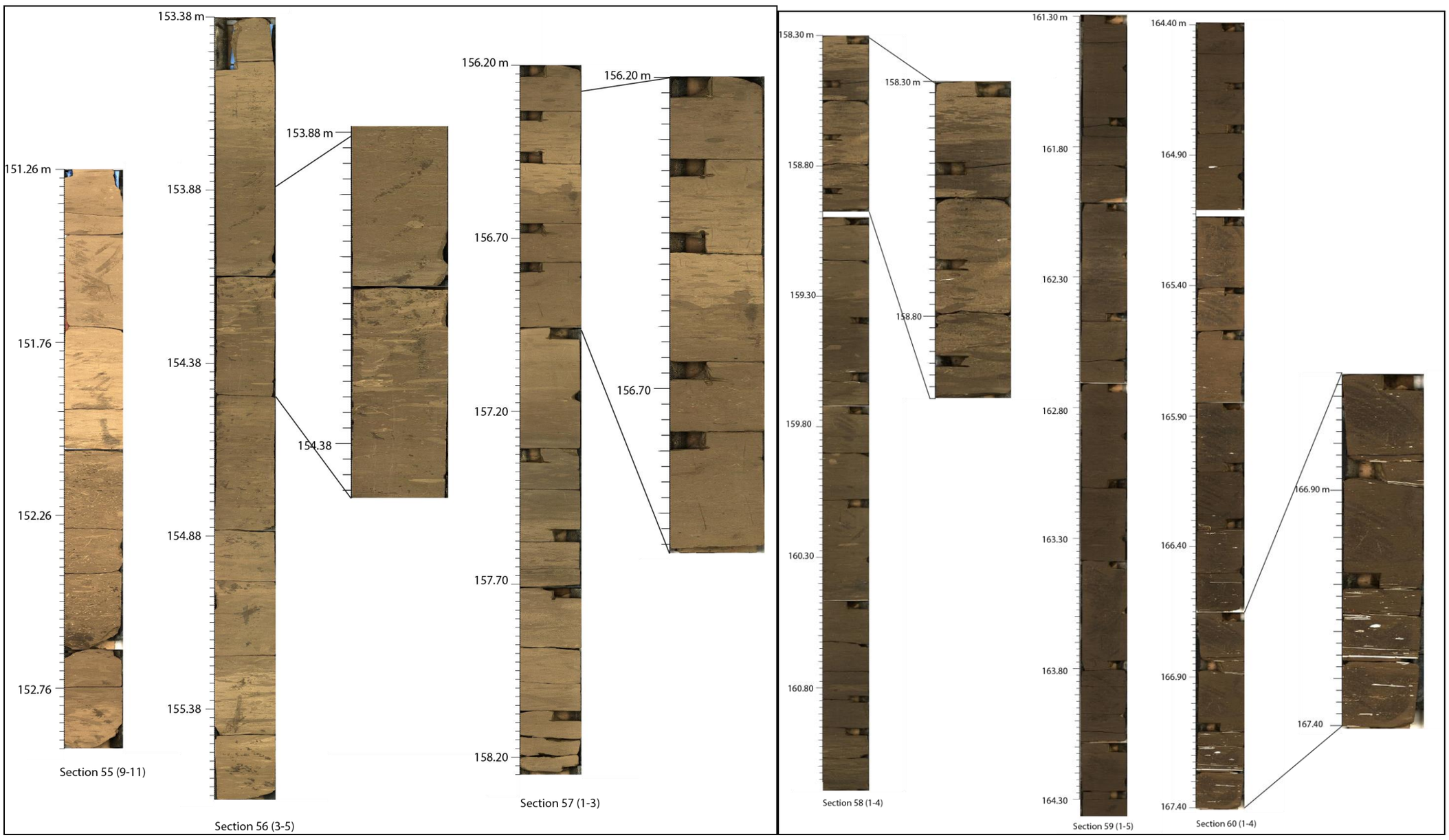

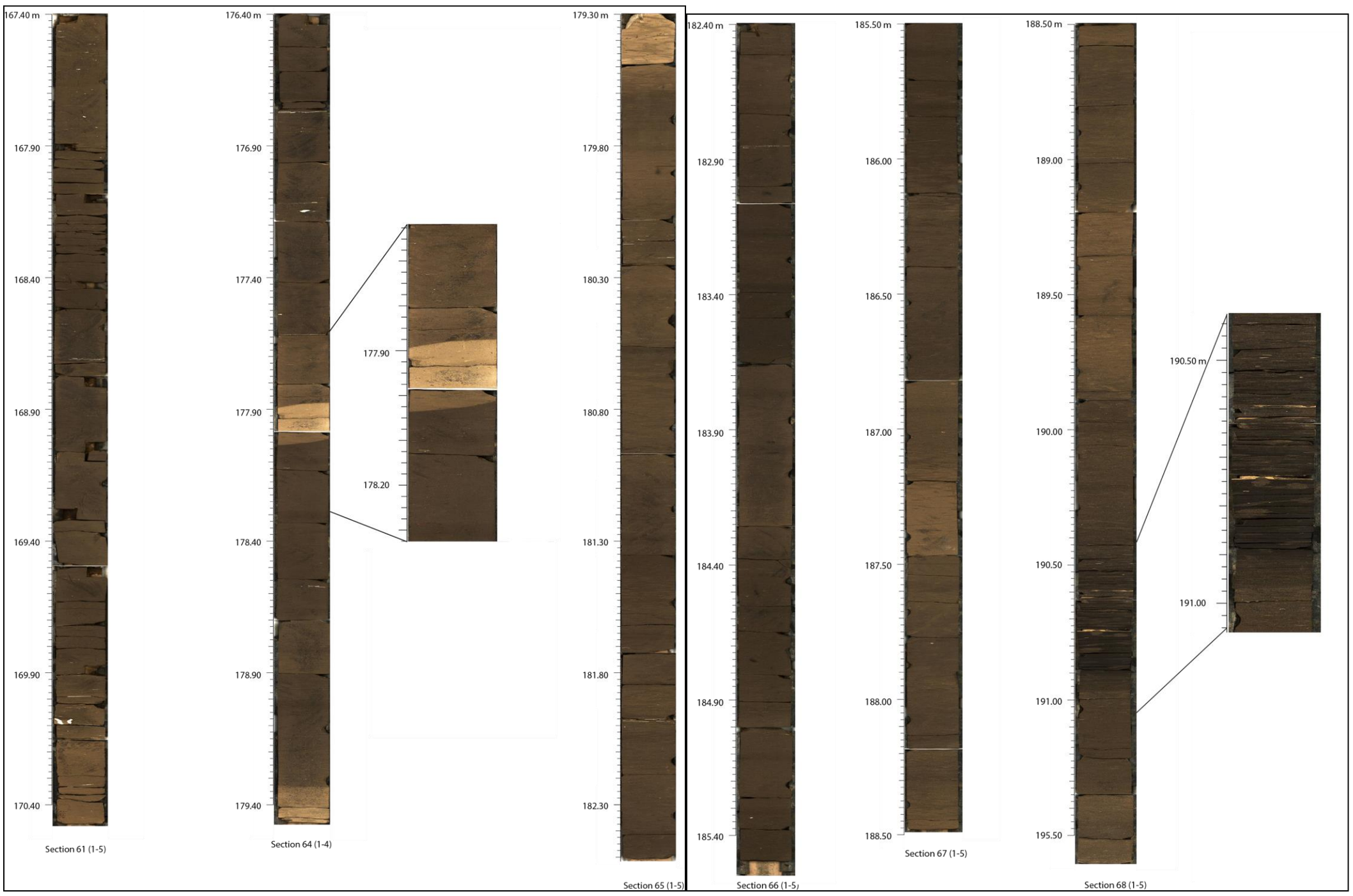

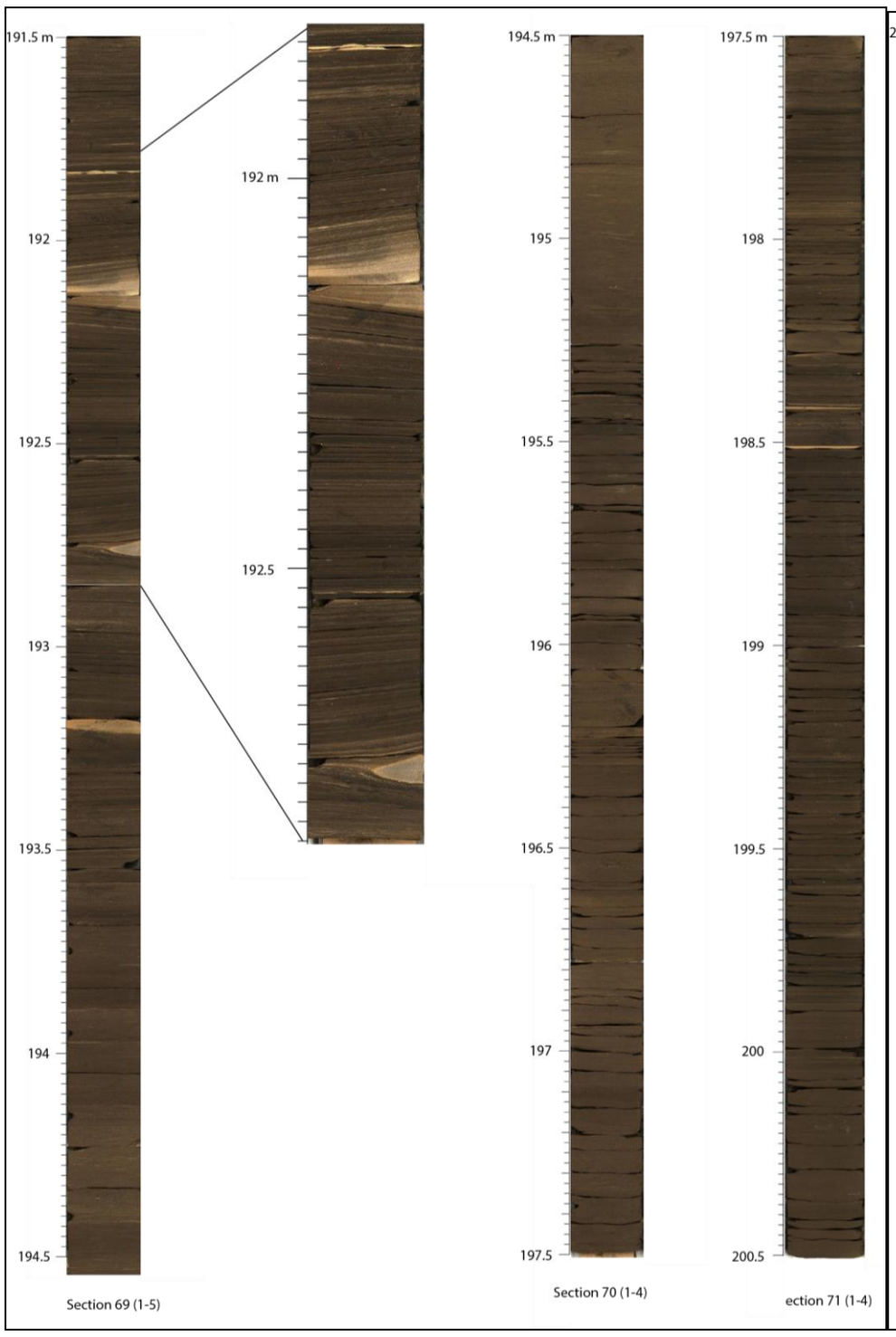
191.5 m
192
192.5
193
193.5
194
194.5
192 m
192.5
Section 69 (1-5)
194.5 m
195
195.5
196
196.5
197
197.5
Section 70 (1-4)
197.5 m
198
198.5
199
199.5
200
200.5
ection 71 (1-4)

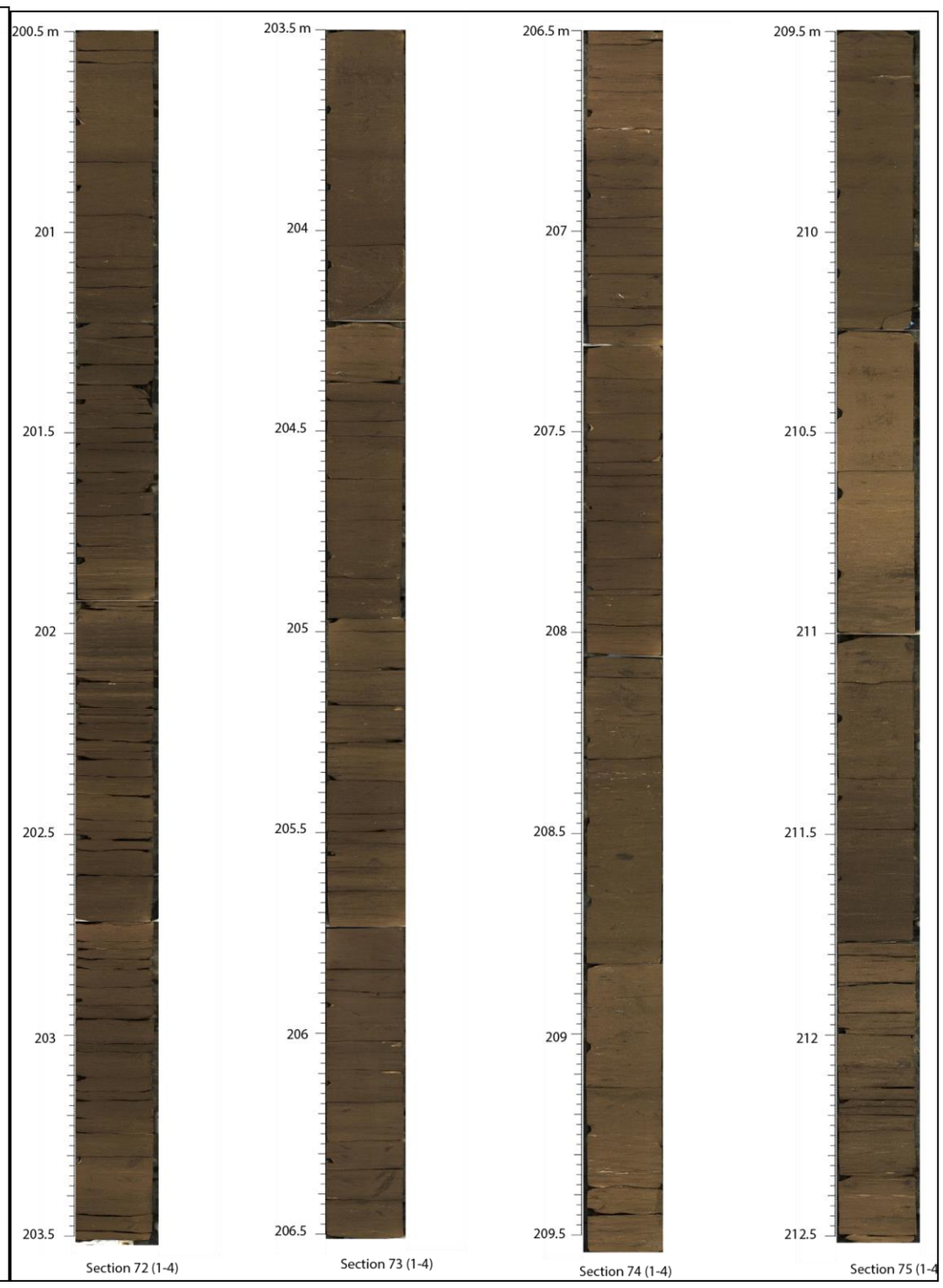
200.5 m
201
201.5
202
202.5
203
203.5
Section 72 (1-4)
203.5 m
204
204.5
205
205.5
206
206.5
Section 73 (1-4)
206.5 m
207
207.5
208
208.5
209
209.5
Section 74 (1-4)
209.5 m
210
210.5
211
211.5
212
212.5
Section 75 (1-4

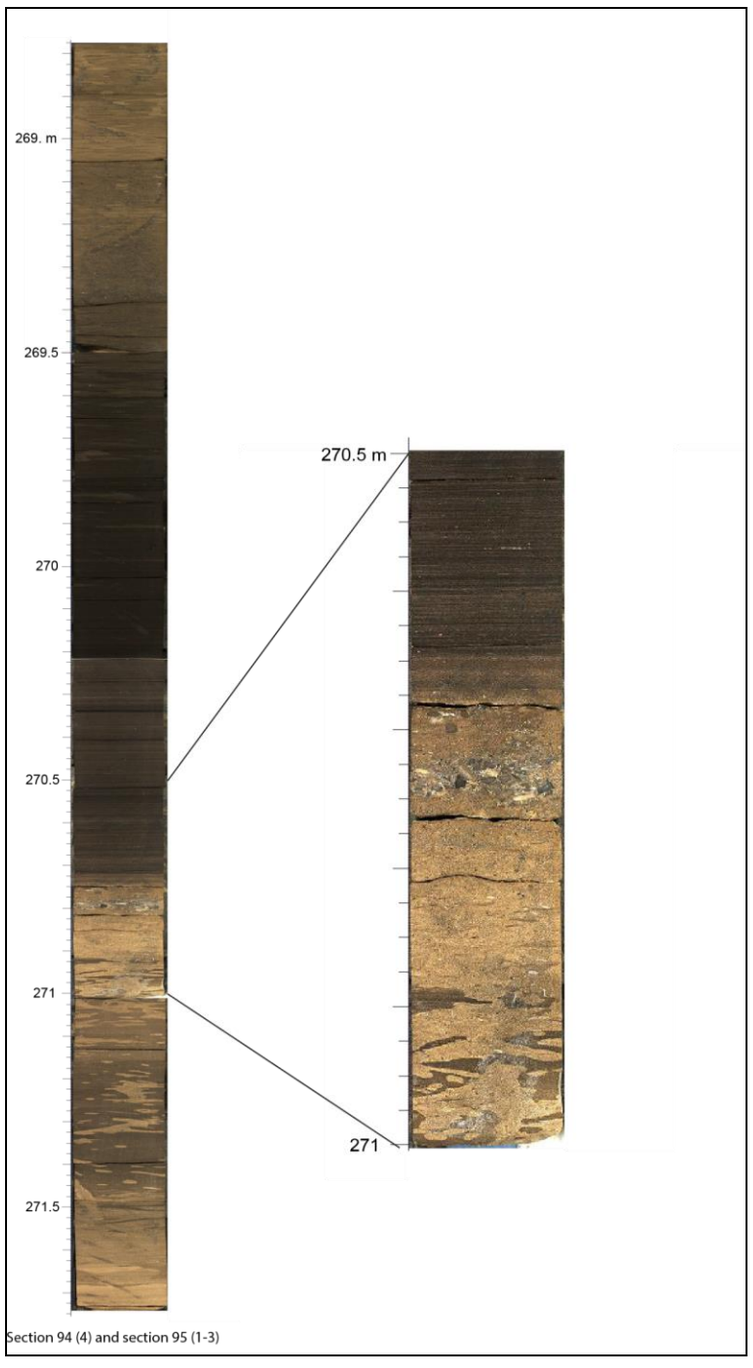
269. m
269.5
270
270.5
271
271.5
270.5 m
271
Section 94 (4) and section 95 (1-3)

Appendix 4. Core photograph of some selected interval in the core Tarfaya SN2.

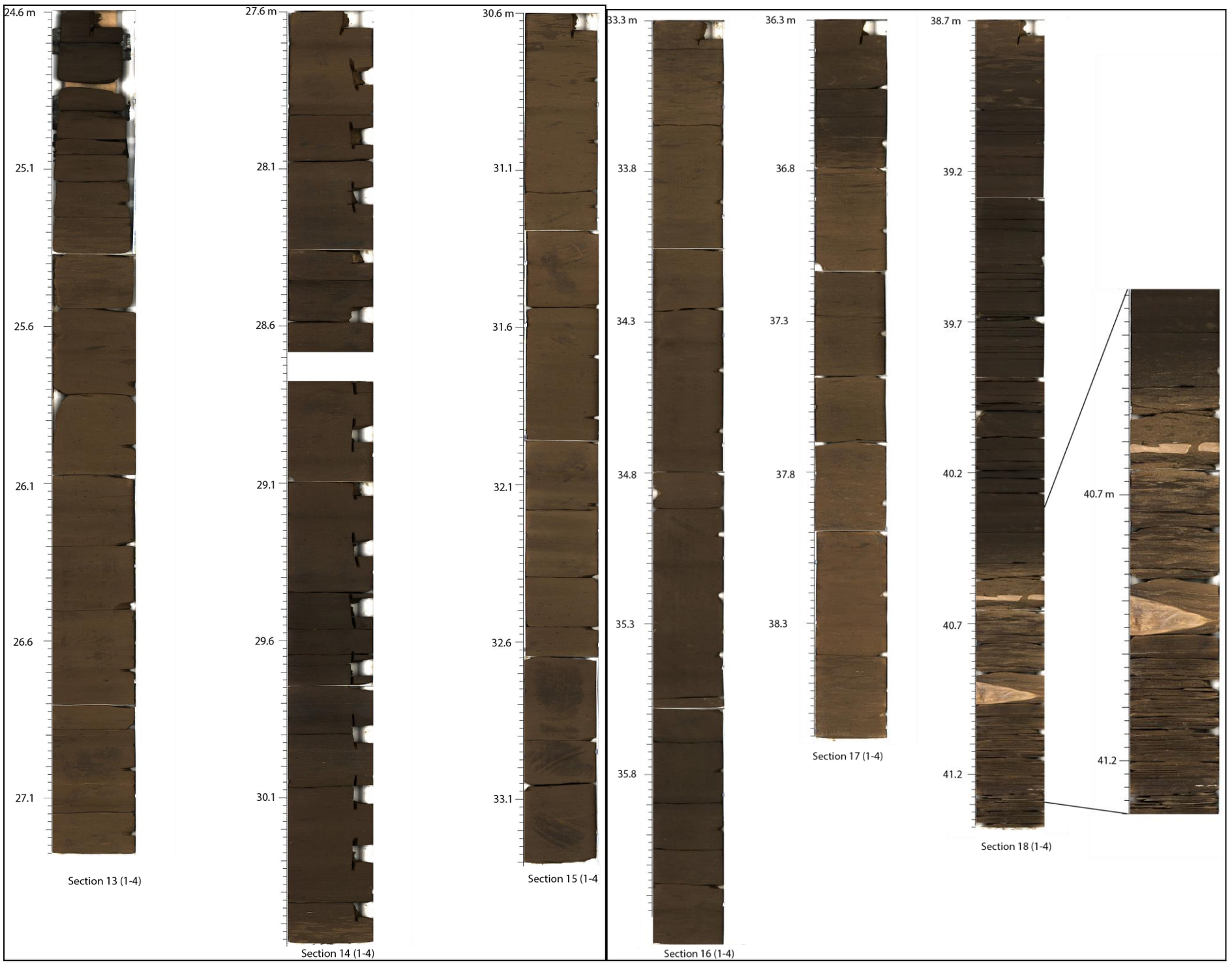

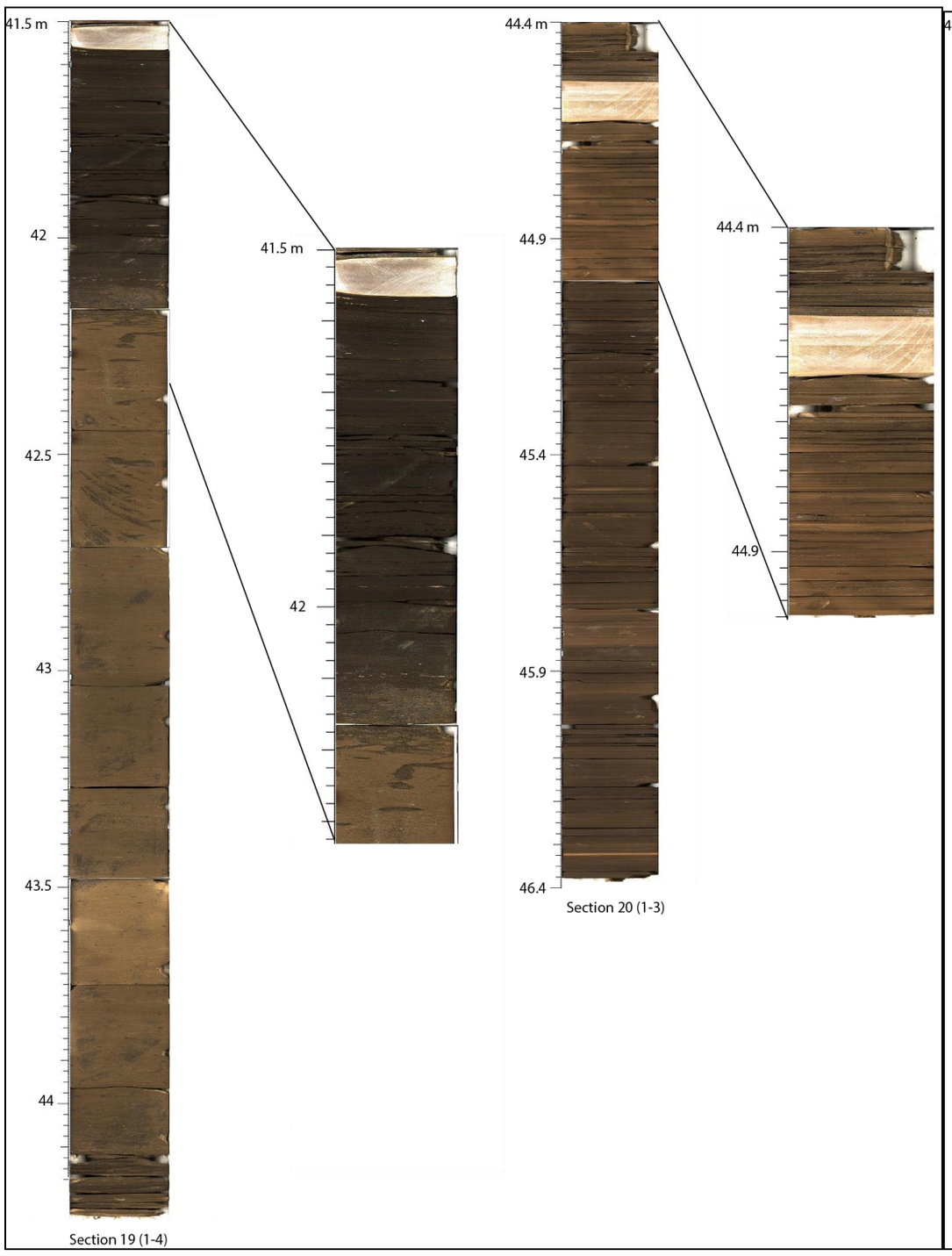

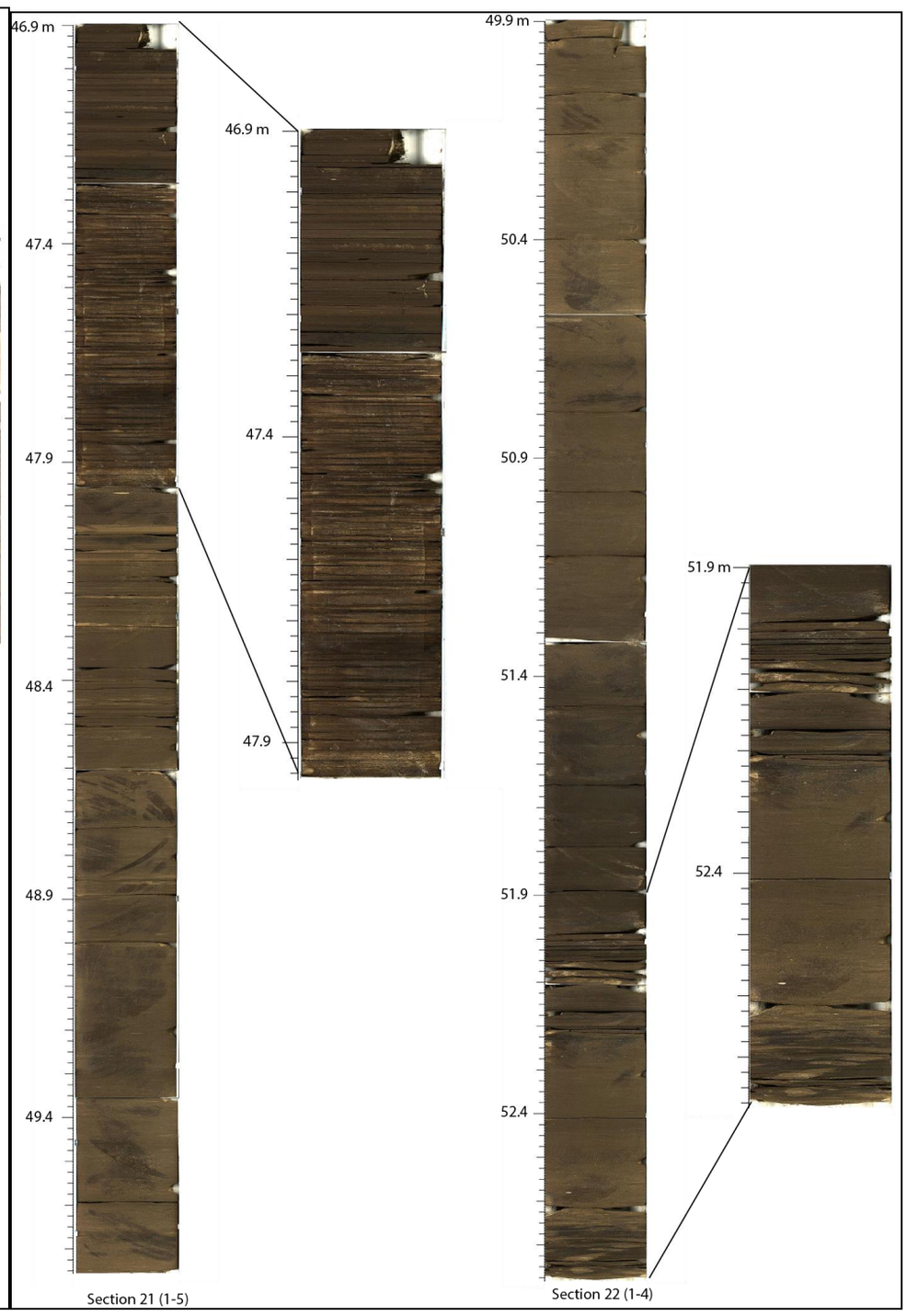

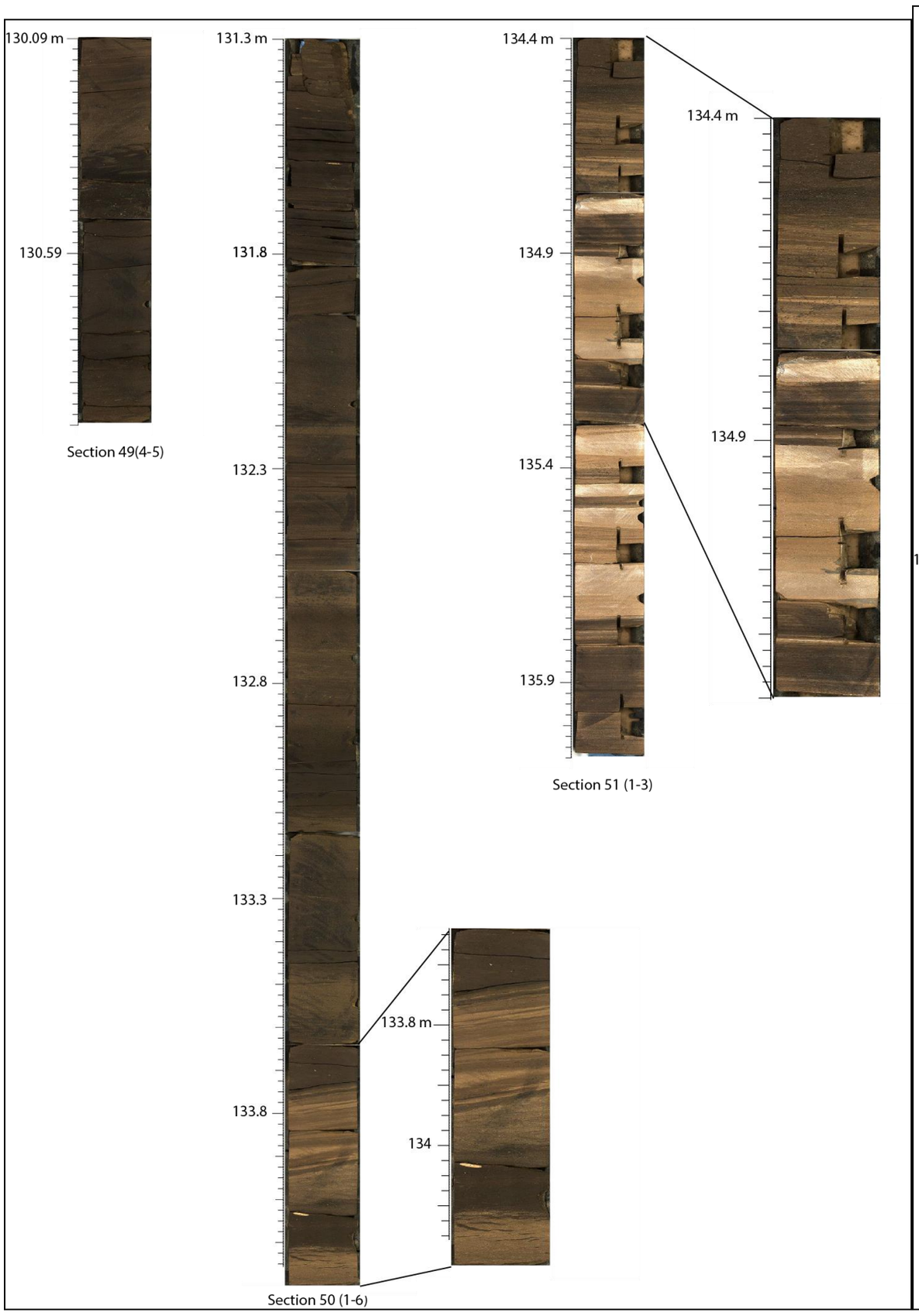
130.09 m
130.59
Section 49(4-5)
131.3 m
131.8
132.3
132.8
133.3
133.8
133.8 m
134
Section 50 (1-6)
134.4 m
134.9
135.4
135.9
134.4 m
134.9
Section 51 (1-3)
188.5 m
189
189.5
190
190.5
191
189.7 m
190
190.5
191
190.5 m
191
Section 69 (1-5)